



Universitat Autònoma de Barcelona

**ADVERTIMENT.** L'accés als continguts d'aquesta tesi queda condicionat a l'acceptació de les condicions d'ús establertes per la següent llicència Creative Commons:  [http://cat.creativecommons.org/?page\\_id=184](http://cat.creativecommons.org/?page_id=184)

**ADVERTENCIA.** El acceso a los contenidos de esta tesis queda condicionado a la aceptación de las condiciones de uso establecidas por la siguiente licencia Creative Commons:  <http://es.creativecommons.org/blog/licencias/>

**WARNING.** The access to the contents of this doctoral thesis it is limited to the acceptance of the use conditions set by the following Creative Commons license:  <https://creativecommons.org/licenses/?lang=en>

Departament de Bioquímica i Biologia Molecular

Facultat de Biociències UAB

Doctorat en Bioquímica, Biologia Molecular i Biomedicina

# **Antioxidant nanoparticles for the treatment of Age-related Macular Degeneration: preclinical studies in the DKOrd8 mouse model**

## **Nanopartícules antioxidants pel tractament de la Degeneració Macular Associada a l'Edat: estudis preclínic en el model de ratolí DKOrd8**

**Tesis doctoral presentada per**

**Anna Badia Pérez**

Treball realitzat sota la direcció del Dr. Jose Garcia Arumí i la Dra. Laura Fontrodona Montals al grup d'investigació en Oftalmologia de l'Institut de Recerca de la Vall d'Hebron (VHIR) Barcelona, 2019

Laura Fontrodona Montals  
(Directora)

José Garcia Arumí  
(Director)

Anna Badia Pérez  
(Doctoranda)





## TABLE OF CONTENTS

|  |     |
|--|-----|
| TABLE OF CONTENTS.....   | i   |
| FIGURE INDEX.....  | v   |
| TABLE INDEX.....   | vii |
| ABBREVIATIONS .....  | ix  |
| <br>   |     |
| INTRODUCTION.....  | 1   |
| 1. The visual system: structure and function .....   | 3   |
| 1.1. The retina .....  | 4   |
| 1.2. Retinal pigment epithelium.....   | 6   |
| 1.3. Retinal vascular supply.....  | 7   |
| 2. Age-Related Macular Degeneration: an emerging problem in ageing populations .....               | 9   |
| 2.1. Epidemiology and risk factors of Age-Related Macular Degeneration .....                       | 9   |
| 2.2. Pathological and clinical features of Age-related Macular Degeneration .....                  | 10  |
| 2.3. Key pathogenic pathways involved in AMD.....  | 12  |
| 2.3.1 Oxidative stress .....   | 12  |
| 2.3.2 Autophagy .....  | 13  |
| 2.3.3 Immune regulation.....   | 13  |
| 2.3.3.1 The role of chemokines .....   | 15  |
| 2.3.4 Cross talk between pathways in advanced AMD .....  | 16  |
| 3. Current treatments and novel approaches.....  | 19  |
| 3.1. AMD current treatments.....   | 19  |
| 3.2. CeO <sub>2</sub> NPs and their antioxidant function .....                                     | 20  |
| 3.2.1. CeO <sub>2</sub> NPs in retinal degenerative pathologies .....                              | 21  |
| 3.3. Drug delivery to the retina .....   | 22  |
| 4. Mouse models for AMD .....  | 24  |
| 4.1. Models for choroidal neovascularization.....  | 24  |
| 4.2. Models with oxidative damage .....  | 26  |
| 4.3. Models with abnormalities in the complement factor pathway .....                              | 27  |
| 4.4. Models with dysregulation in lipid metabolism.....  | 27  |
| 4.5. Models with dysregulation in chemokine pathways .....   | 28  |
| 4.5.1. <i>Ccl2</i> <sup>-/-</sup> ; <i>Cx3cr1</i> <sup>-/-</sup> mice as a model for dry AMD ..... | 28  |

|   |    |
|---|----|
| AIMS .....  | 31 |
| <br>  |    |
| MATERIALS AND METHODS .....                                   | 35 |
| 1. In vivo animal experimentation .....                       | 37 |
| 1.1. Generation of the <i>DKOrd8</i> mice.....                | 37 |
| 1.2. Genotyping.....  | 38 |
| 1.2.1. DNA extraction .....                                   | 38 |
| 1.2.2. Polymerase chain reaction (PCR) and sequencing .....   | 38 |
| 1.3. Eye fundus imaging .....                                 | 40 |
| 1.4. Optical Coherence Tomography .....                       | 40 |
| 1.5. Ganzfeld Electroretinography .....                       | 42 |
| 1.6. AOxNPs synthesis and administration .....                | 44 |
| 1.6.1 Biodistribution experiments.....                        | 44 |
| 1.6.1.1. Intravitreal injection.....                          | 44 |
| 1.6.1.2. Topical administration.....                          | 45 |
| 1.6.2. Treatment of the <i>DKOrd8</i> model .....             | 45 |
| 2. Post-mortem animal experimentation.....                    | 46 |
| 2.1. Tissue processing and histology.....                     | 46 |
| 2.1.1. Hematoxylin and eosin staining .....                   | 46 |
| 2.1.2. Immunofluorescence in paraffin-embedded slides .....   | 46 |
| 2.1.3. Immunofluorescence in flat-mounted RPE and retina..... | 48 |
| 2.2. Gene expression analysis .....                           | 50 |
| 2.2.1. RNA extraction .....                                   | 50 |
| 2.2.2. Microarrays .....                                      | 50 |
| 2.2.3. Bioinformatic analyses .....                           | 51 |
| 2.3. ICP-MS analysis.....                                     | 51 |
| 2.3.1. Tissue obtainment.....                                 | 51 |
| 2.3.2. Tissue digestion and ICP-MS analysis.....              | 52 |
| 3. Cell culture .....   | 53 |
| 3.1. Cell maintenance.....                                    | 53 |
| 3.2. Cell viability assay.....                                | 53 |
| 3.3. Intracellular ROS measurement .....                      | 55 |
| 3.4. Gene expression analyses .....                           | 56 |
| 3.4.1. RNA extraction and retrotranscription .....            | 56 |
| 3.4.2. Quantitative Polymerase Chain Reaction (qPCR).....     | 57 |

|  |     |
|--|-----|
| RESULTS.....   | 59  |
| Chapter 1. Generation and characterization of the <i>DKOrd8</i> mouse.....   | 61  |
| 1. The <i>DKOrd8</i> mouse is generated by crossing three different mouse strains .....                                  | 63  |
| 2. The <i>DKOrd8</i> mouse presents early eye fundus alterations and a progressive thinning of the inferior retina ..... | 66  |
| 3. Retinal function alterations arise in young <i>DKOrd8</i> mice and are maintained upon ageing .....                   | 71  |
| 4. <i>DKOrd8</i> mice present an age-dependent increase of microglia in the subretinal space .....                       | 75  |
| 5. <i>DKOrd8</i> retinas present focal lesions with disruption of the photoreceptors layer.....                          | 79  |
| 6. <i>DKOrd8</i> retinas present an increased gliosis, microglia infiltration and oxidative stress .....                 | 83  |
| 7. <i>DKOrd8</i> mice eyes present an altered gene expression pattern .....  | 87  |
| Chapter 2. Evaluation of AOxNPs for the treatment of age-related macular degeneration .....                              | 93  |
| 1. Evaluation of AOxNPs safety and efficacy in vitro .....   | 95  |
| 1.1. AOxNPs are non-toxic in ARPE19 cell cultures.....   | 95  |
| 1.2. AOxNPs scavenge intracellular ROS and induce SOD2 upregulation.....   | 96  |
| 2. Biodistribution of AOxNPs.....  | 99  |
| 2.1. AOx reaches mice retina after topical administration .....  | 99  |
| 3. Evaluation of AOxNPs topical treatment efficacy in <i>DKOrd8</i> mice .....   | 102 |
| 3.1. Retinal thinning is partially prevented with AOxNPs treatment.....  | 102 |
| 3.2. AOxNPs treatment does not ameliorate retinal function in <i>DKOrd8</i> mice.....                                    | 104 |
| 3.3. AOxNPs reduce microglia infiltration in <i>DKOrd8</i> mice retinas.....   | 105 |
| 3.4. AOxNPs topical treatment reverts the altered gene expression pattern of <i>DKOrd8</i> mice .....                    | 106 |
| DISCUSSION.....  | 113 |
| 1. The use of murine models to study AMD .....   | 115 |
| 1.1. Limitations of mice to model AMD .....  | 115 |
| 1.2. The importance of the genetic background.....   | 117 |
| 2. A close look into the pathological features of the <i>DKOrd8</i> mice .....   | 119 |
| 2.1. Location of the retinal lesions .....   | 119 |
| 2.2. Altered retinal function: age-related or a feature of the model?.....   | 121 |
| 2.3. Histological alterations and compensative mechanisms .....  | 122 |
| 2.4. The role of microglia in retinal degeneration .....   | 125 |
| 2.5. The gene expression profile as an AMD-like feature .....  | 126 |

|  |     |
|--|-----|
| 3. Choosing the right therapy for AMD.....                                   | 130 |
| 4. Topical delivery as a route of administration to the posterior pole ..... | 132 |
| 5. The efficacy of AOxNPs as a treatment for AMD .....                       | 135 |
| 5.1. Reversion of the differential expression pattern .....                  | 135 |
| 5.2. AOxNPs effect on retinal thickness and microglial activation .....      | 137 |
| 5.3. Finding the right dosage.....   | 138 |
| 6. Future prospects for the management of AMD.....                           | 139 |
| <br>   |     |
| CONCLUSIONS .....  | 141 |
| REFERENCES .....   | 145 |

## FIGURE INDEX

### INTRODUCTION

|  |    |
|--|----|
| Figure I.1. Anatomy of the eye.....  | 3  |
| Figure I.2. Retinal layers.....  | 4  |
| Figure I.3. Macula and fovea.....  | 5  |
| Figure I.4. Summary of RPE functions.....  | 7  |
| Figure I.5. Retinal vasculature.....   | 7  |
| Figure I.6. Clinical presentation of AMD .....   | 10 |
| Figure I.7. Representation of retinas with advanced AMD.....   | 11 |
| Figure I.8. Integrated models of AMD pathogenesis, with the key pathways involved .....              | 18 |
| Figure I.9. ROS scavenging activity and surface regeneration properties of CeO <sub>2</sub> NPs..... | 20 |
| Figure I.10. Drug administration routes to the retina.....   | 22 |

### MATERIALS AND METHODS

|   |    |
|---|----|
| Figure MM.1. OCT visualization and quantification of the retinal layers .....                   | 41 |
| Figure MM.2. Components and representative responses of a mouse ERG .....                       | 42 |
| Figure MM.3. Representative diagram of the eye dissection and the RPE/retina flatmounting ..... | 48 |
| Figure MM.4. DCF fluorescent formation .....  | 55 |

### RESULTS

|  |    |
|--|----|
| Figure R.1. Genotyping of <i>Cx3cr1</i> and <i>Ccl2</i> genes.....   | 63 |
| Figure R.2. Genotyping of <i>rd8</i> allele.....   | 64 |
| Figure R.3. Diagram of the DK <i>Ord8</i> mouse generation .....   | 65 |
| Figure R.4. In vivo assessment of retinal status in DK <i>Ord8</i> and C57BL/6N mice with funduscopy .....   | 66 |
| Figure R.5. OCT evaluation of the retina status in DK <i>Ord8</i> and C57BL/6N mice.....                     | 67 |
| Figure R.6. Quantification of the retinal layers.....  | 68 |
| Figure R.7. Progression of retinal thickness.....  | 69 |
| Figure R.8. Comparison of the inferior and superior hemisphere of DK <i>Ord8</i> and C57BL/6N mice eyes..... | 70 |
| Figure R.9. Electroretinographic response of DK <i>Ord8</i> and C57BL/6N mice .....                          | 72 |
| Figure R.10. Representative ERG waveforms of DK <i>Ord8</i> and C57BL/6N mice .....                          | 73 |
| Figure R.11. Oscillatory potentials (OPs) evaluation of DK <i>Ord8</i> and C57BL/6N mice .....               | 74 |



|   |     |
|---|-----|
| Figure R.12. Fluorescent funduscopy evaluation of DK <i>Ord8</i> mice .....                                       | 76  |
| Figure R.13. Microglia quantification in RPE flatmounts .....   | 77  |
| Figure R.14. Microglia quantification in retinal flatmounts.....  | 78  |
| Figure R.15. Histological evaluation of DK <i>Ord8</i> and 6N mice eye sections .....                             | 80  |
| Figure R.16. Evaluation of retinal focal lesions in DK <i>Ord8</i> mice retinas.....                              | 81  |
| Figure R.17. Evaluation of photoreceptors pigments in DK <i>Ord8</i> mice .....                                   | 82  |
| Figure R.18. Evaluation of retinal gliosis in DK <i>Ord8</i> mice.....  | 84  |
| Figure R.19. Evaluation of microglia infiltration in focal retinal lesions .....                                  | 85  |
| Figure R.20. Evaluation of oxidative stress in DK <i>Ord8</i> mice retinas .....                                  | 86  |
| Figure R.21. Differential gene expression in DK <i>Ord8</i> mice .....  | 87  |
| Figure R.22. Heatmap comparing the expression pattern of 3-months old DK <i>Ord8</i> and 6N mice.....             | 88  |
| Figure R.23. Gene enrichment analysis.....  | 92  |
| Figure R.24. Evaluation of the cytotoxic effect of AOxNPs .....   | 95  |
| Figure R.25. Antioxidant capacity of AOxNPs in in vitro cultures .....  | 96  |
| Figure R.26. Changes in <i>SOD2</i> expression after AOxNPs treatment.....  | 97  |
| Figure R.27. Changes in mRNA levels of genes related with the oxidative stress response. ....                     | 98  |
| Figure R.28. AOx concentration in different tissues after ocular administration.....                              | 100 |
| Figure R.29. Evaluation of the retinal status and quantification of the different retinal layers .....            | 103 |
| Figure R.30. Electroretinographic responses of DK <i>Ord8</i> mice after AOxNPs treatment....                     | 104 |
| Figure R.31. Microglia quantification in RPE and retinal flatmounts.....  | 106 |
| Figure R.32. Differential gene expression in DK <i>Ord8</i> mice after the AOxNPs treatment... ..                 | 107 |
| Figure R.33. Heatmap comparing the expression pattern of DK <i>Ord8</i> mice after the treatment with AOxNPs..... | 108 |
| Figure R.34. AOxNPs-treated mice share most of the differentially expressed genes .....                           | 109 |
| Figure R.35. Gene enrichment analysis.....  | 112 |

## DISCUSSION

|   |     |
|---|-----|
| Figure D.1. Scheme followed for the generation of a backcross .....   | 118 |
| Figure D.2. In vivo assessment of eye fundus and retinal status of two different lines of DK <i>Ord8</i> mice ..... | 120 |
| Figure D.3. Schematic cross-sections of a human and a mouse eye .....   | 133 |

## TABLE INDEX

### INTRODUCTION

|  |    |
|--|----|
| Table I.1. Age-Related Eye Disease Study (AREDS) classification .....                    | 11 |
| Table I.2. Main mouse models that mimic phenotypic characteristics observed in AMD ..... | 25 |

### MATERIALS AND METHODS

|  |    |
|--|----|
| Table MM.1. Primers used for genotyping .....                        | 39 |
| Table MM.2. List of antibodies used .....                            | 47 |
| Table MM.3. List of antibodies used for the flatmounts .....         | 49 |
| Table MM.4. Primers used for in vitro gene expression analyses ..... | 58 |

### RESULTS

|  |     |
|--|-----|
| Table R.1. List of relevant genes upregulated in <i>DKOrd8</i> mice .....  | 89  |
| Table R.2. List of relevant genes downregulated in <i>DKOrd8</i> mice .....  | 90  |
| Table R.3. List of genes associated with AMD .....   | 91  |
| Table R.4. Percentage of AOx detected in different tissues after diverse administration routes and schedules ..... | 100 |
| Table R.5. List of relevant downregulated genes in <i>DKOrd8</i> mice after AOxNPs treatment                       | 109 |
| Table R.6. List of relevant upregulated genes in <i>DKOrd8</i> mice after AOxNPs treatment .....                   | 110 |
| Table R.7. List of genes associated with AMD .....   | 111 |



## ABBREVIATIONS

|                                   |  |
|-----------------------------------|--|
| <b>8-OHdG</b>                     | 8-Oxo-2'-deoxyguanosine                                      |
| <b>A2E</b>                        | N-retinylidene-N-retinylethanol-amine                        |
| <b>AMD</b>                        | Age-related Macular Degeneration                             |
| <b>AOxNPs</b>                     | Antioxidant Nanoparticles                                    |
| <b>APO</b>                        | Apolipoprotein   |
| <b>APP</b>                        | Amyloid Precursor Protein                                    |
| <b>ARPE19</b>                     | Adult Retinal Pigment Epithelial 19                          |
| <b>A<math>\beta</math></b>        | Amyloid- $\beta$   |
| <b>AU</b>                         | Arbitrary Units  |
| <b>bp</b>                         | base pairs   |
| <b>BRB</b>                        | Blood Retinal Barrier  |
| <b>C3</b>                         | Complement Factor 3  |
| <b>CCL2</b>                       | C-C Motif Chemokine Ligand 2                                 |
| <b>CCR2</b>                       | C-C Motif Chemokine Receptor 2                               |
| <b>cDNA</b>                       | complementary DNA  |
| <b>CeO<sub>2</sub>NPs</b>         | Cerium Oxide Nanoparticles                                   |
| <b>CEP</b>                        | Carboxyethylpyrrole  |
| <b>CFH</b>                        | Complement Factor H  |
| <b>CNV</b>                        | Choroidal Neovascularization                                 |
| <b>CX3CL1</b>                     | C-X3-C Motif Chemokine Ligand 1                              |
| <b>CX3CR1</b>                     | C-X3-C Motif Chemokine Receptor 1                            |
| <b>DAPI</b>                       | 4',6-diamidino-2-phenylindol                                 |
| <b>DKO</b>                        | Double Knockout  |
| <b>ERG</b>                        | Electroretinography  |
| <b>GCL</b>                        | Ganglion Cell Layer  |
| <b>GFAP</b>                       | Glial Fibrillary Acidic Protein                              |
| <b>GFP</b>                        | Green Fluorescent Protein                                    |
| <b>GO</b>                         | Gene Ontology  |
| <b>H<sub>2</sub>O<sub>2</sub></b> | Hydrogen peroxide  |
| <b>Iba1</b>                       | Ionized calcium Binding Adapter molecule 1                   |
| <b>ICP-MS</b>                     | Inductively Coupled Plasma Mass Spectrometry                 |
| <b>IL</b>                         | Interleukin  |
| <b>INL</b>                        | Inner Nuclear Layer  |
| <b>IPL</b>                        | Inner Plexiform Layer  |
| <b>iPSCs</b>                      | induced Pluripotent Stem Cells                               |
| <b>mETC</b>                       | mitochondrial Electron Transport Chain                       |
| <b>mRNA</b>                       | messenger RNA  |
| <b>MTT</b>                        | 3-(4,5-dimethylthiazol-2-yl)-2,5-diphenyltetrazolium bromide |
| <b>Nrf2</b>                       | Nuclear factor erythroid 2-related factor 2                  |
| <b>O<sub>2</sub><sup>-</sup></b>  | Superoxide radical   |
| <b>OCT</b>                        | Optical Coherence Tomography                                 |
| <b>ONL</b>                        | Outer Nuclear Layer  |

|              |  |
|--------------|--|
| <b>OPL</b>   | Outer Plexiform Layer                    |
| <b>OPs</b>   | Oscillatory Potentials                   |
| <b>PDGF</b>  | Platelet-Derived Growth Factor           |
| <b>PEDF</b>  | Pigment Epithelium-derived Growth Factor |
| <b>PhIS</b>  | Photoreceptor inner segments             |
| <b>PhOS</b>  | Photoreceptor outer segments             |
| <b>PUFAs</b> | Polyunsaturated fatty acids              |
| <b>ROS</b>   | Reactive Oxygen Species                  |
| <b>RPE</b>   | Retinal Pigment Epithelium               |
| <b>RT</b>    | Room Temperature                         |
| <b>SD</b>    | Standard Deviation                       |
| <b>SEM</b>   | Standard Error of the Mean               |
| <b>SNP</b>   | Single Nucleotide Polymorphism           |
| <b>SOD</b>   | Superoxide Dismutase                     |
| <b>tBH</b>   | tert-Butyl Hydroperoxide                 |
| <b>VEGF</b>  | Vascular Endothelial Growth Factor       |
| <b>VLDLR</b> | Very Low Density Lipoprotein Receptor    |
| <b>Wt</b>    | Wild Type                                |

The background is a complex watercolor composition. It features a dense network of thin, black, branching lines that resemble a neural network or a web. These lines are set against a wash of warm, earthy tones, including shades of tan, beige, and light brown. Scattered throughout the composition are various organic, blotchy shapes in dark charcoal, black, and muted blue-grey. Some of these shapes are elongated and vertical, while others are more rounded or irregular. The overall effect is one of intricate, organic complexity.

# INTRODUCTION



## 1. The visual system: structure and function

Humans rely on vision more than on any other sense, constituting up to 80% of our perception and with the eyes being the most sensitive organ we have.

The eye is the primary organ of vision. It contains three different coats: (1) the outer fibrous layer, which includes the cornea and the sclera; (2) the middle vascular layer, which contains the choroid and the iris; (3) and the inner nervous layer, formed by the retina (Figure I.1) (Galloway and Amoaku 1999).

Light enters the eye through the cornea, which helps with refraction. At the center of the iris, the pupil modifies its size regulating the amount of light entering the eye. The lens further focuses light on the retina, with muscles controlling its shape to differentially focus objects based on the distance from the eye. Between the lens and the retina, the vitreous humor gives the eye its spherical shape and keeps the retina in place (Teutsch et al. 2017).

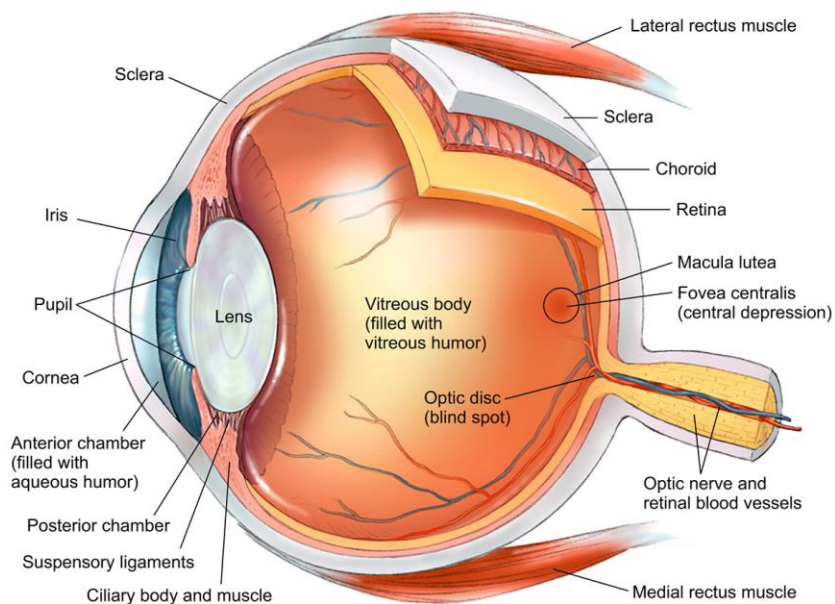


**Figure I.1. Anatomy of the eye.** Sagittal cross section of a human eye with its major components labeled. Image from Dave Carlson©.



## 1.1. The retina

The retina is the most specialized part of the eye, being responsible for converting light into electrical energy and for transmitting it to the brain through the optic nerve. Six classes of neurons and glial support cells are distributed throughout three different nuclear layers, forming the neurosensory retina, which lies on a pigmented cell layer named retinal pigment epithelium (RPE) (Figure 1.2).

The three nuclear layers of the neurosensory retina are known as: (i) outer nuclear layer (ONL), which contains the nuclei of cones and rods photoreceptors, responsible for phototransduction; (ii) inner nuclear layer (INL), containing the nuclei of horizontal, bipolar, amacrine cells and Müller glia, which transmit and modify the synaptic signal; and (iii) ganglion cell layer (GCL) formed by retinal ganglion cells, whose axons constitute the optic nerve (Kolb 2013).

Two other synaptic or plexiform layers separate these three nuclear layers: (i) the inner plexiform layer (IPL) is located between the GCL and the INL and contains the synapses ganglion cells form with the INL neurons; whereas (ii) the outer plexiform layer (OPL), located between the INL and the ONL, contains synaptic connections of photoreceptor cells (Willoughby et al. 2010).

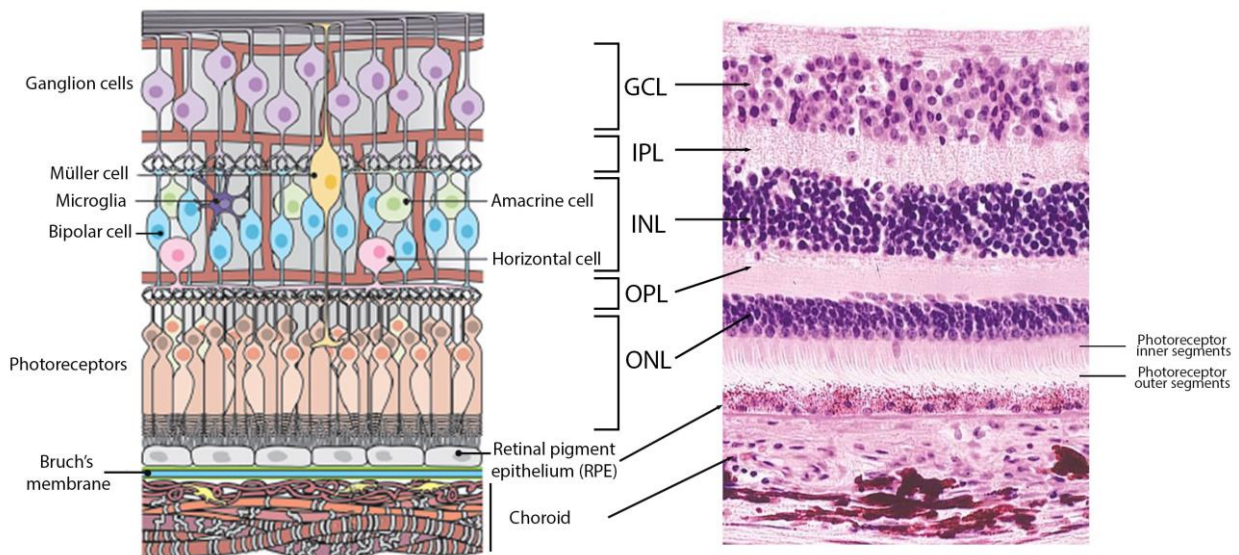


**Figure 1.2. Retinal layers.** Distribution of the distinct layers of the retina and choroid in a drawing (left) and a histological section of a human eye stained with hematoxylin & eosin (right). The different cell types composing the retina are also specified. (GCL, ganglion cell layer; IPL, inner plexiform layer; INL, inner nuclear layer; OPL, outer plexiform layer; ONL, outer nuclear layer). Diagram modified from van Lookeren Campagne et al. 2014; and retinal section from Mescher 2016.

The retina converts photons of light into signals describing visual information and sends them to the brain. This function starts in the outer segments of the photoreceptors, composed of stacked and flattened membranous discs containing abundant light-sensitive photopigments, specialized to different wavelengths. These pigments undergo chemical changes in response to light bringing photoreceptors into a hyperpolarization state that ultimately leads to the generation of action potentials. In a very simplistic view, bipolar cells connect photoreceptors to the ganglion cells providing a vertical transmission to the brain. In addition to this direct pathway, horizontal cells receive information from photoreceptors and transmit it to a number of surrounding bipolar cells. Amacrine cells in turn, receive inputs from bipolar cells and activate ganglion cells in their vicinity, integrating the response (Grossniklaus et al. 2015).

The mammalian retina contains two types of photoreceptors: rods and cones. Rods account for 95% of all photoreceptors and are specialized for high sensitivity under dark conditions. Cones make up only 5% of total photoreceptors but provide high-acuity color vision in daylight conditions. The density of photoreceptors in humans is not equal in the entire retina, as 50% of all retinal cones are located in the eye fundus' temporal area called macula. The center of the macula has an even higher density of cone photoreceptors composing the fovea, responsible for central vision and high visual acuity (Gregg et al. 2012) (Figure I.3).

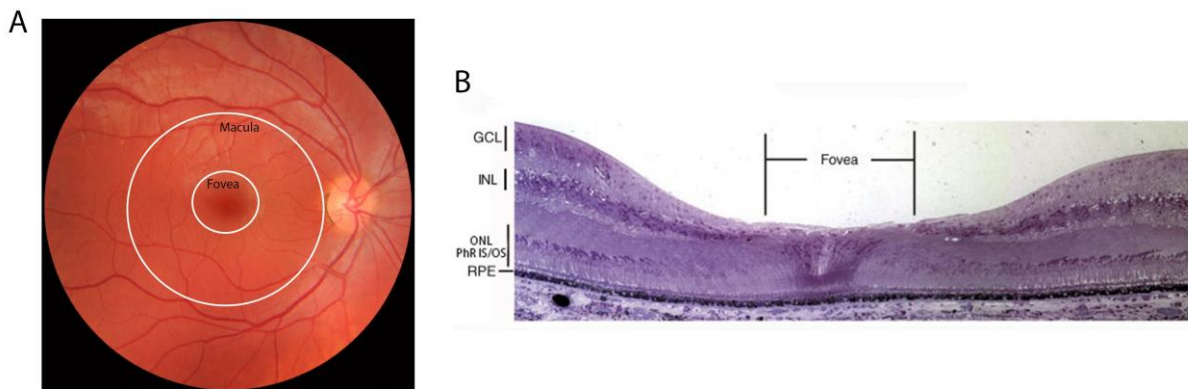


**Figure I.3. Macula and fovea. (A)** Image of a human eye fundus, with the macula and the fovea circled and the optic nerve at the right side. **(B)** Histological section of a human eye showing the macula and fovea with the different retinal layers. The fovea appears as a depression of the retina and contains only cone photoreceptors. Ganglion cell layer (GCL) and inner nuclear layer (INL) are reduced to achieve maximum sensibility and acuity. Image from Marmorstein & Marmorstein 2007.

## 1.2. Retinal pigment epithelium

The other component of the retina, fundamental for the maintenance of photoreceptors, is the retinal pigment epithelium. RPE is a monolayer of pigmented cells whose apical membrane faces the photoreceptor outer segments and its basolateral membrane faces the Bruch's membrane, a collagen-rich extracellular matrix that regulates and restricts the exchange of products between the RPE and the fenestrated choroidal capillaries (Guymer et al. 1999). The main functions of the RPE are shown in figure I.4 and detailed below:

- Epithelial transport: RPE transports ions, water and metabolic end products from the subretinal space to the blood, and takes nutrients and oxygen from the choroid to deliver them to photoreceptors (Figure I.4) (Strauss 2005).
- Light absorption: the retina is constantly exposed to light, allowing photo-oxidation and subsequent oxidative damage. RPE contains pigments, such as melanin and lipofuscin, which are specialized to detect different light wavelengths. These pigments absorb the excess of scattered light and defend photoreceptors from possible damage (Beatty et al. 1999).
- Visual cycle: RPE cells re-isomerize the chromophore all-*trans*-retinal produced by photoreceptors during light absorption back into 11-*cis*-retinal (Chen et al. 2017).
- Spatial buffering of ions (glia): although Müller glia cells enable a major part of the spatial buffering, RPE cells also contribute to stabilizing the ion composition of the subretinal space, essential for the maintenance of photoreceptor excitability.
- Phagocytosis: another function in the maintenance of photoreceptor excitability is the phagocytosis of shed photoreceptor outer segments (PhOS). RPE cells digest PhOS and recycle essential substances to rebuild new PhOS (Mazzoni et al. 2014).
- Secretion: RPE cells secrete diverse growth factors to the retina, such as Vascular Endothelial Growth Factor A (VEGFA) and Pigment Epithelium-Derived Factor (PEDF), maintaining its structural integrity and producing immunosuppressive factors to sustain the immune privilege of the eye.

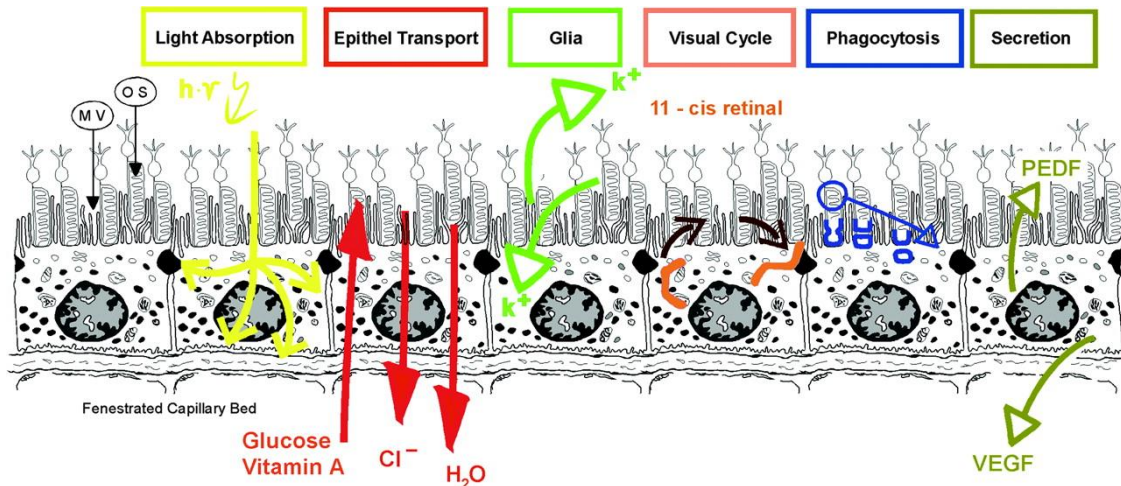


**Figure I.4. Summary of RPE functions.** Main function of the retinal pigment epithelial cells. MV, microvilli; OS, outer segments. Image from Strauss et al. 2004.

### 1.3. Retinal vascular supply

The retina is the most metabolically active tissue in the body, consuming oxygen more rapidly than the brain (Wangsa-Wirawan et al. 2003). Therefore, a continuous oxygen supply is essential. Retina possesses two vascular circulations, although some variations between species exist. In humans, choroidal capillaries supply oxygen to RPE cells and photoreceptors up to the outer two-thirds of the ONL. The layers above, which include the INL, the GCL and the inner one-third of the ONL, receive their oxygen supply from the retinal vasculature (Figure I.5A). All vessels of the retinal vasculature derive from the central retina artery, which runs through the optic nerve and branches into four principal intra-retinal arteries that end up constituting the superficial and deep capillary plexus (Figure I.5B) (Kur et al. 2012).

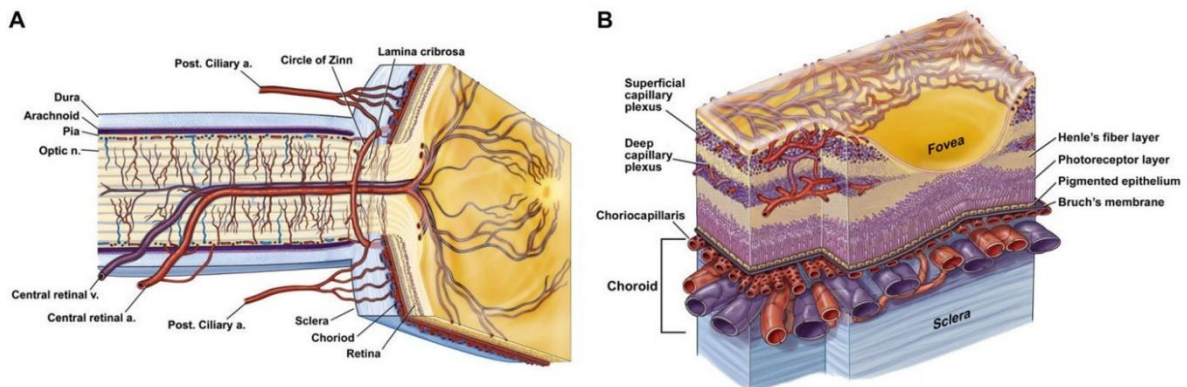


**Figure I.5. Retinal vasculature.** (A) Drawing of a transversal cut of a human eye through the optic nerve, showing the vascular supply to the retina and choroid. (B) Drawing showing the vasculature of the retina and the choroid. (a, artery; v, vein; n, nerve). Image modified from Kur et al. 2012.

In turn, the retina is highly protected from toxins and infectious agents circulating in the bloodstream by the blood-retinal barrier (BRB). The BRB consists in two different barriers: (i) the outer BRB, formed by endothelial cells lining the choroidal vasculature and tight junctions of RPE cells; and (ii) the inner BRB, formed by tight junctions of endothelial cells, pericytes, astrocytes and Müller glia cells (Himawan et al. 2019). This well-developed complex between endothelium and specialized retinal cells allows the neural retina to establish and maintain the appropriate environment necessary for its correct function (Runkle and Antonetti 2011).

## **2. Age-Related Macular Degeneration: an emerging problem in ageing populations**

The retina is a complex structure with a strict regulation to ensure its correct function. Damage or dysfunction of any part of the visual system can lead to retinal degeneration and severe vision impairment. There are hundreds of diseases, conditions and injuries that negatively affect vision, including various rare diseases with a genetic component. However, most cases of vision impairment are attributable to a small number of causes, being age-related macular degeneration one of the most common.

### **2.1. Epidemiology and risk factors of Age-Related Macular Degeneration**

Age-related Macular Degeneration (AMD) is a degenerative and multifactorial late-onset disease that affects the central retina and causes progressive vision impairment. The late stages of the disease lead to severe and permanent visual impairment and to legal blindness, being the major cause of blindness in developed countries (Al-Zamil and Yassin 2017). The typical onset strikes up around 50 and 60 years of age and its prevalence increases with ageing, with an overall prevalence of 8.7% (Wong et al. 2014) and an estimated incidence of almost 300.000 new cases per year in the USA (Rudnicka et al. 2015). Furthermore, its prevalence is expected to increase in coming years as a consequence of ageing populations. The total number of cases estimated by 2020 is 196 million, rising to 288 million people affected by 2040.

AMD is a complex disorder with several associated risk factors. Advanced age is the main risk factor, as shown by epidemiologic data. Environmental factors also play an important role in AMD. From all, smoking is the most consistently associated factor, typically resulting in a two-fold increased risk of developing advanced AMD and at an earlier onset (Myers et al. 2014). Cardiovascular disease risk factors such as hypertension or atherosclerosis have been associated with AMD risk too, although with a lower consistency (Pennington et al. 2016; Kabasawa et al. 2011). Besides these factors, what has gained more relevance in recent years is the genetic component. The discovery of loci associated with AMD was one of the major successes to come from genome-wide association studies. The identification of a major locus in the Complement Factor H (*CFH*) gene was the first genetic locus associated with AMD in 2005 (Klein et al. 2005; Edwards et al. 2005). Since then, 52 variants at 34 genetic loci have been identified to be associated with late AMD (Fritsche et al. 2016). Other complement-related genes such as *CF1*, *C2*, *CFB* and *C3* have been linked to AMD and another locus in the *CFH* gene was found associated to AMD. Common risk variants in TIMP metallopeptidase inhibitor 3 (*TIMP3*) and age-related

susceptibility 2 (*ARMS2*) genes have also been correlated with AMD risk, although the role of these genes in the development of macular degeneration have not been established yet.

## 2.2. Pathological and clinical features of Age-related Macular Degeneration

The first signs of AMD comprise the thickening of Bruch's membrane, pigmentary abnormalities in the macula and accumulation of lipid-rich extracellular deposits between the RPE and its vascular supply, the choroid capillaries' network. These deposits are called drusen and are seen as yellowish subretinal spots in eye fundus imaging (Figure I.6A). Since they can be usually observed when patients are still asymptomatic, drusen have become the main clinical hallmark to identify the disease and grade its progression (Lim et al. 2012).



**Figure I.6. Clinical presentation of AMD.** Human eye fundus images with (A) soft drusen (B) geographic atrophy and (C) subretinal hemorrhage from neovascular AMD. The black circle in A indicates the macula. Image modified from McHarg et al. 2015.

According to the Age-Related Eye Disease Study (AREDS) classification, early and intermediate stages are distinguished mainly by the size of the drusen observed in the eye fundus (Table I.1) (Kassoff et al. 2001). In the advanced stages, AMD presents two different phenotypes: dry AMD, characterized by geographic atrophy; and wet or neovascular AMD, characterized by choroidal neovascularization (CNV) (Figure I.6B, C). These two phenotypes are not excluding and one patient can present the dry form in one eye and the wet in the other (Kaszubski et al. 2016).

**Table I.1. Age-Related Eye Disease Study (AREDS) classification.**

|                                     |   |
|-------------------------------------|---|
| No AMD (AREDS category 1)           | None or a few small drusen (<63µm in diameter).   |
| Early AMD (AREDS category 2)        | Multiple small drusen, few intermediate drusen (63-124µm in diameter) or RPE abnormalities.                                   |
| Intermediate AMD (AREDS category 3) | Extensive intermediate drusen, at least one large drusen (≥125µm in diameter) and geographic atrophy not involving the fovea. |
| Advanced AMD (AREDS category 4)     | Geographic atrophy involving the fovea or any of the features of neovascular AMD.   |

Geographic atrophy consists in a progressive atrophy of the retinal pigment epithelium and the photoreceptors as a result of drusen accumulation in the center of the macula. This accumulation hampers the function of RPE cells, initiating inflammatory and apoptotic processes that lead to photoreceptors' degeneration. Choroidal neovascularization is the hallmark of wet AMD and consists in the growth of new blood vessels from the choroid penetrating into Bruch's membrane and the subretinal space. These blood vessels are leaky and produce subretinal hemorrhage, fluid exudation, lipid deposition and detachment of the RPE from the choroid

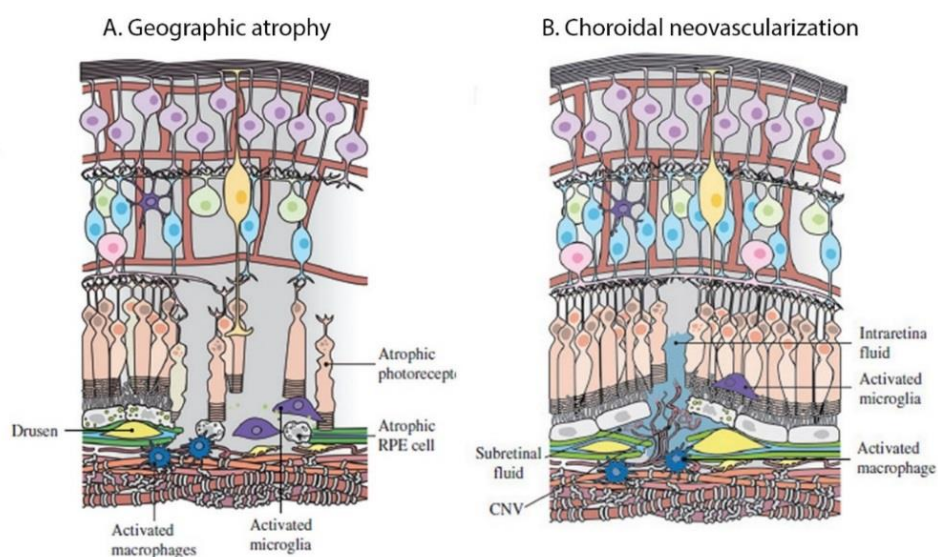


**Figure I.7. Representation of retinas with advanced AMD. (A)** Diagram of a retina with geographic atrophy. Bruch's membrane is severely disrupted, RPE and photoreceptor cell atrophy and loss are pronounced together with the loss of other retinal cell types. The choriocapillaries is poorly perfused and microglia and macrophages are abundant in the degenerated area. **(B)** Diagram of a retina with choroidal neovascularization. Bruch's membrane and RPE are disrupted by neovessels growing from the choroid, which advance into photoreceptors layer. Fluid from the leaky vessels is accumulated in the subretinal and intraretinal space and RPE and photoreceptors are atrophic. Figures modified from Van Lookeren et al. 2014.



resulting, eventually, in the appearance of fibrotic scars that compromise vision severely (Jager et al. 2008) (Figure 1.7).

In early AMD visual loss is generally mild and asymptomatic in most of the cases, emphasizing the need for early detection and prevention. The most characteristic clinical symptoms include blurred vision, visual scotomas (partial alterations in the visual field), decreased contrast sensitivity, abnormal dark adaptation, need for brighter light and additional magnification to read. In advanced AMD, patients with geographic atrophy suffer a gradual visual loss usually over the course of months to years whereas patients with neovascular AMD can have sudden and profound visual loss within days to weeks as a result of subretinal hemorrhage or fluid accumulation (Jager et al. 2008). Although most people with AMD do not become completely blind, visual loss often reduces quality of life and is associated with disability and clinical depression in up to one third of the patients, making the disease more difficult to manage (Inan et al. 2019; Slakter and Stur 2005).

### **2.3. Key pathogenic pathways involved in AMD**

The exact molecular causes of AMD are still being elucidated, although several processes have been postulated to play an important role in the pathogenesis of the disease, including oxidative stress, autophagy and the immune system. What is indeed accepted is that RPE cells are the first cells that become dysfunctional in AMD.

#### **2.3.1 Oxidative stress**

Photoreceptors are exposed to intense levels of light that lead to the accumulation of photo-damaged proteins and lipids in the outer segments, where light absorption occurs. Photoreceptors outer segments (PhOS) are rich in polyunsaturated fatty acids (PUFAs), which are very sensitive to the action of reactive oxygen species (ROS). The oxidation of PUFAs, known as lipid peroxidation, involves the production of more ROS, which can react with other fatty acids, initiating a free radical reaction cascade and dramatically increasing the oxidative damage of the cellular components (Evans et al. 2004).

To maintain the correct function of photoreceptors and avoid a chronic oxidative stress, apical PhOS undergo a constant renewal process with the help of RPE cells that phagocyte these shed PhOS (Sparrow et al. 2010). Oxidized PUFAs are commonly digested in the lysosomes of RPE cells, but with ageing, lysosomes lose efficacy and PUFAs become deposited in the form of

lipofuscin (Nowak 2014). Lipofuscin's major component is A2E (N-retinylidene-N-retinylethanolamine), a harmful fluorophore able to provoke photochemical damage in the retina and RPE cells under light exposure (Blasiak et al. 2014).

These processes take place in the entire retina, but occur with greater presence in the macula. Being the retinal area with the highest density of photoreceptors, the macula is constantly exposed to a high metabolic rate and high levels of oxidative stress. RPE cells and photoreceptors in this area, experience localized peaks of oxidative stress, making the macula the most vulnerable region of the eye for the onset of AMD (Booij et al. 2010).

### **2.3.2 Autophagy**

Increased ROS levels induce genomic and mitochondrial DNA damage and alter mitochondrial activity, which lead cells into senescence. Senescence prevents the proliferation of damaged cells but also induces the secretion of pro-inflammatory cytokines, chemokines and growth factors and regulates autophagy (van Deursen 2014; Kang and Elledge 2016).

Autophagy is involved in the removal of defective structures in the cell and contributes to the equilibrium between the production of proteins and organelles and their clearance (Liu et al. 2010). In the retina, autophagy protects RPE cells from the death induced by oxidative stress (Baek et al. 2017). It is generally accepted that autophagy declines with ageing, resulting in the accumulation of cellular debris, and therefore enhancing the formation and growth of drusen. The accumulation of amyloid- $\beta$  (A $\beta$ ) in drusen is a common feature of AMD patients (Isas et al. 2010). A $\beta$  is generated by the cleavage of the amyloid precursor protein (APP), secreted by RPE cells. But decreased autophagy due to ageing disturbs the balance between its production and clearance and favors its accumulation (Lynn et al. 2017). Lipofuscin cannot be digested either, hence it accumulates in RPE lysosomes. Increased levels of ROS positively regulate autophagy, but chronic oxidative stress declines this cellular function. Moreover, A2E, the main component of lipofuscin has the capacity to inhibit lysosomal activity, decreasing autophagy even more (Shamsi and Boulton 2001; Hyttinen et al. 2017; Saadat et al. 2014).

### **2.3.3 Immune regulation**

Retinal function depends on the fine structure of its retinal neurons, which makes it strongly vulnerable to internal and external insults (Chen et al. 2019). The ocular compartment has evolved to become an immune privileged site, principally maintained by the blood-retinal barrier

and the neuronal production of immunosuppressive factors (Caspi 2006). However, the introduction of specific foreign or endogenous inflammatory signals in the retina evokes innate immune responses.

Proteomic analyses to study drusen composition have revealed the presence of immune associated molecules such as immunoglobulins, class II antigens, A $\beta$  deposits, components of the complement system and molecules with immunogenic properties, which act as foci of chronic inflammation (Crabb et al. 2002; Bergen et al. 2019).

When cells are exposed to stress insults, the local immune network triggers transient inflammatory responses known as parainflammation. Normal parainflammation exists in the ageing retina under physiological conditions, as a protective response against noxious waste products accumulation, which allows for the maintenance of retinal homeostasis. However, prolonged exposition to these insults such as oxidative stress, elevated protein aggregation and lipofuscin accumulation, lead to dysregulated parainflammation that evolves into a chronic inflammatory response through the activation of the inflammasome (Nita et al. 2014).

The inflammasome is a protein complex that culminates in the production of the pro-inflammatory cytokines interleukin-1 $\beta$  (IL-1 $\beta$ ) and IL-18, and ultimately, in caspase1-mediated apoptosis. In normal circumstances, autophagy controls the activation of the inflammasome by degrading its components. But declined autophagy, drusen or A2E can contribute to its activation (Kaarniranta et al. 2013; Gao et al. 2015).

The inflammasome can also be activated by the non-coding *Alu* RNA transcripts. These repetitive transcripts are usually degraded by the RNase DICER1. However, AMD patients with geographic atrophy present a reduced expression of DICER1 in RPE cells and suffer an accumulation of *Alu* RNA transcripts (Kaneko et al. 2011), which act as activating signals for the inflammasome (Tarallo et al. 2012). Deposition of A $\beta$  in drusen has also been associated with inflammasome activation and RPE damage through the upregulation of IL-1 $\beta$  and IL-18 (Prasad et al. 2017).

The complement system is also involved in the chronification of the inflammatory response. It consists of three separate pathways, each activated by different factors: antigen antibody complexes (classical complement pathway), polysaccharides on microorganisms (lectin complement pathway) and pathogen cell surfaces (alternative complement pathway). All pathways converge with the cleavage of complement factor 3 (C3) into C3a and C3b, which induce inflammation and opsonize cells for phagocytosis, respectively (Boyer et al. 2017). Under physiological conditions, retinal cells (microglia and RPE mainly) express high levels of complement regulators, such as CFH, and low levels of complement proteins, including C3 and

C5 (Luo et al. 2011). But with ageing, oxidative stress and low levels of inflammation reverse this balance promoting the clearance of debris and dead cells by phagocytosis (Chen et al. 2019). In AMD, chronic or sustained pathological stimulation, together with genetic polymorphisms in complement-related genes, generate undesirable amounts of activated complement factors inducing RPE damage (Gao et al. 2015).

The resident inflammatory cells in the retina are the microglia. These cells normally reside in the proximity of retinal blood vessels in the inner layers of the neuronal retina and their main functions are to phagocytize cellular debris and to act as antigen-presenting cells (Li et al. 2015). Subretinal migration of microglia is also necessary to eliminate visual by-products (Ma et al. 2009). Pathogens or damage-associated molecular patterns (such as ROS, oxidized lipoproteins or immunogenic drusen proteins) activate microglia, which can either induce the death of further immune cells (macrophages and dendritic cells) infiltrating the retina or convert them into immunosuppressive cells to reduce immunopathology and maintain neuronal function. With age, migration of microglia to the site of damage is reduced, together with their plasticity to change from a pro-inflammatory to an anti-inflammatory phenotype (Ma and Wong 2016; Harry 2013). Aged microglia also display insufficient phagocytic activity towards apoptotic bodies, protein aggregates and myelin, further contributing to the gradual accumulation of potentially toxic compounds in the retina (Safaiyan et al. 2016).

#### 2.3.3.1 The role of chemokines

Microglial activation and migration is regulated by various signals from retinal neurons such as nerve growth factor, transforming growth factor or several chemokines. Chemokines are a diverse set of small molecular weight proteins that mediate the recruitment and migration of inflammatory cells to a target site (Luster 1998). From all chemokines, CCL2 signaling through CCR2 and CX3CL1 through CX3CR1 have become a major focus in ophthalmological research because of their proposed role in AMD.

CX3CR1 (C-X3-C Motif Chemokine Receptor 1) is constitutively expressed by the microglia and its ligand CX3CL1 (C-X3-C Motif Chemokine Ligand 1) is expressed by the neurons as a transmembrane protein (Harrison et al. 1998). CX3CL1-CX3CR1 signaling regulates the communication between the microglia and the neurons and the glia in the nervous system (and therefore also in the retina) to limit microglia-mediated neurotoxicity (Cardona et al. 2006). During ageing, CX3CR1 expression is reduced, which induces microglia accumulation in the

photoreceptor layers and subretinal space and increased microglial activation (Mecca et al. 2018).

CCL2 (C-C Motif Chemokine Ligand 2) expression in the retinal neurons and the RPE, and CCR2 (C-C Motif Chemokine Receptor 2) expression in the microglia is very low in physiological conditions but increases in acute inflammation, with ageing and under oxidative stress.

In the degenerative retina, atrophic photoreceptors express CCL2 to activate and attract the microglia to the injured site, which in turn secrete CCL2 to amplify and accelerate the neuroinflammatory cascade. This, together with the age-induced accumulation of microglia, leads to a dysregulated inflammatory response that evolves into a chronic state of inflammation, detrimental to RPE and photoreceptor survival (Feng et al. 2017).

#### **2.3.4 Cross talk between pathways in advanced AMD**

The onset and progression of age-related macular degeneration is a collection of events. Although oxidative stress is the first and main process involved, accumulation of lipofuscin, dysregulated autophagy, presence of drusen and chronic inflammatory responses must take place in conjunction to create a prone environment for RPE cells atrophy and photoreceptors death, which are the hallmarks for geographic atrophy (Figure I.8).

Advanced AMD can also present a wet phenotype, characterized by choroidal neovascularization (CNV). Although the exact mechanisms involved are not clear yet, CNV is likely a secondary reaction instigated by previous alterations, such as dysregulated immune response, degenerative changes in the choroidal vasculature or increased expression of Vascular Endothelial Growth Factor A (VEGFA).

Ageing and early AMD are both associated with a decreased density of choriocapillaries (Moreira-Neto et al. 2018) and increased thickness of Bruch's membrane. Bruch's membrane thickens due to the accumulation of cholesterol-enriched lipoproteins and the remodeling of its extracellular matrix components; which results in an impaired transport across Bruch's membrane and an isolation of RPE cells (Curcio and Johnson 2012). These changes may lead to hypoxia, which induces RPE cells to upregulate VEGFA and other pro-angiogenic factors, providing the required stimuli for neovascular disease (Seddon et al. 2016).

Dysregulated immune response in early AMD is also involved in the development of CNV. Drusen contain activated complement proteins, such as C3a and C5a (Anderson et al. 2002). These small

proteins induce the complement cascade resulting in the formation of the membrane attack complex (MAC) (McHarg et al. 2015). Accumulation of MAC in the choriocapillaris induces tissue remodeling and causes inflammation and angiogenesis (Kumar-Singh 2019). In addition, C3a and C5a are potent chemotactic agents that mediate the recruitment of macrophages and dendritic cells to the choroid. Invading macrophages secrete some factors with anti-angiogenic activity, such as IL-10 and CXCL10, but they produce a higher amount of pro-angiogenic factors, including IL-1 $\beta$ , IL-6 or TNF $\alpha$ , inducing VEGFA synthesis and exacerbating choroidal vessels invasion (Nozaki et al. 2006; Skeie and Mullins 2009). Dysfunctional RPE cells also modulate macrophage responses, driving further cell death and promoting angiogenesis in the eye (Liu et al. 2016).

How the new vessels growing from the choroid end up disrupting Bruch's membrane is not fully understood although the age-related changes of structural elements like the lack of collagen fibrils and the severe inflammation of the tissue, seems the most plausible explanation.

Altogether, the conjunction of these chronic processes culminates in retinal degeneration and irreversible vision loss.

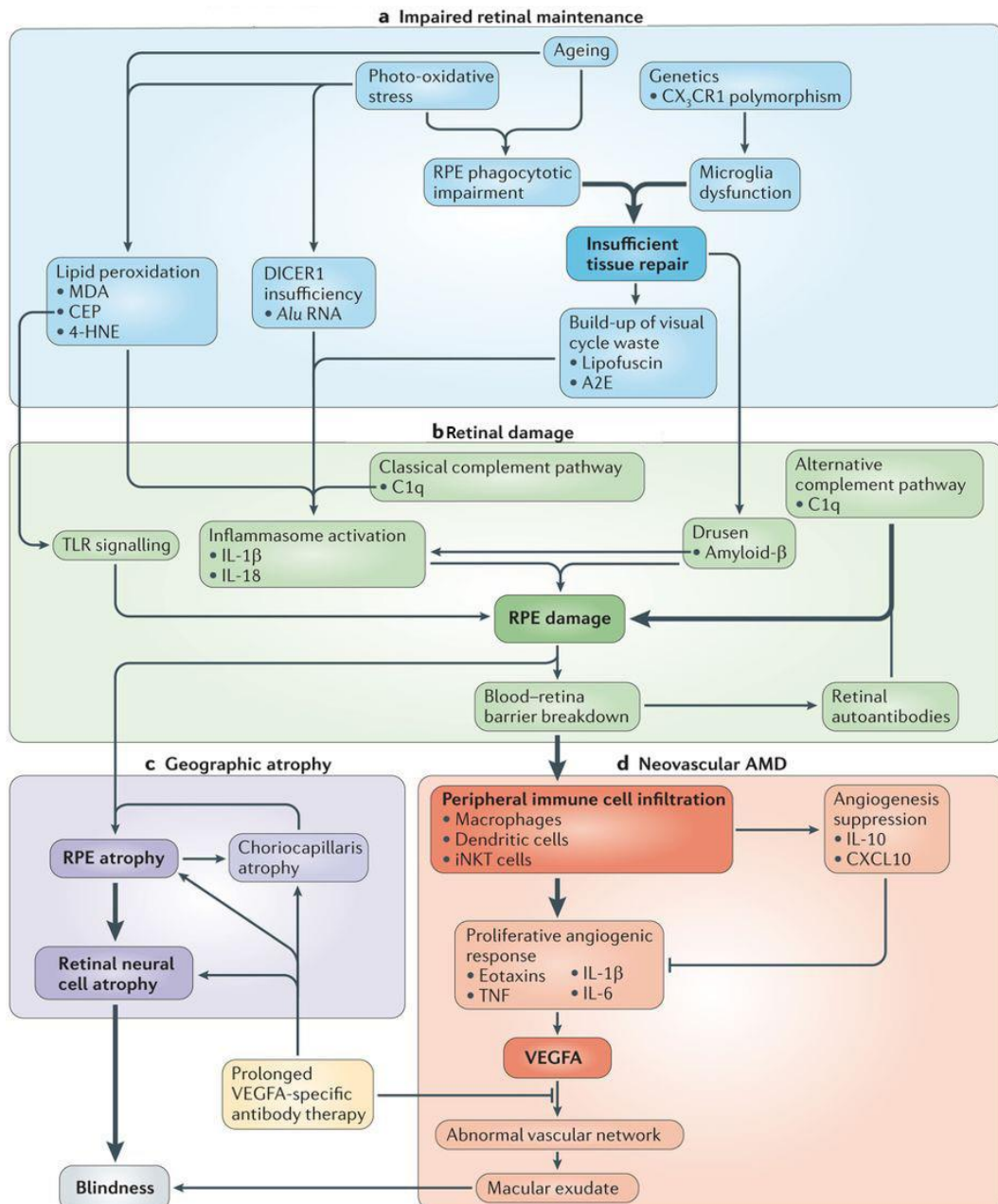


**Figure 1.8. Integrated model of AMD pathogenesis, with the key pathways involved. (a)** The earliest steps in AMD pathogenesis reflect a reduced capacity to manage the metabolic demands of the retina that lead to the accumulation of toxic elements. **(b)** The toxic content of the retina induce the activation of diverse immune pathways, including the inflammasome and the complement. Ultimately, the sustained activation of these pro-inflammatory and damaging pathways leads to advanced AMD (c and d). **(c)** In the case of geographic atrophy, sustained damage to RPE leads to the degeneration of these cells, the choriocapillaris and ultimately, retinal neurons causing blindness. **(d)** In neovascular AMD, the breakdown of the blood-retina barrier results in immune trafficking into the retina which drives a VEGFA-dependent neovascularization causing blindness. Figure from Ambati et al. 2013.

### **3. Current treatments and novel approaches**

#### **3.1. AMD current treatments**

Age-related macular degeneration is a complex disease with no effective treatment available to stop or revert its progression. Considerable advances have been made in the last decade in the management of choroidal neovascularization but geographic atrophy still has no therapy approved.

Effective treatments for neovascular AMD have been long established and are based on the inhibition of VEGFA. Monthly intravitreal injections of ranibizumab and bevacizumab, two antibodies that bind all isoforms of VEGFA have shown similar efficacy in stabilizing the areas of CNV and delaying further neovascularization (Solomon et al. 2016). Aflibercept, a recombinant protein that blocks all VEGFA isoforms, VEGFA receptors 1 and 2, and placental growth factor, has been able to extend the dosing to 2-monthly injections while achieving the same efficacy than monthly therapies (Heier et al. 2012).

Although preventing the hyper-permeability of developing CNV lesions, anti-VEGFA therapies do not promote the regression of these lesions and can ultimately lead to fibrotic scarring (Campbell and Doyle 2019). Moreover, it should be taken into account that a significant proportion of AMD patients (20-30%) are initially refractory to anti-VEGFA therapies, and an even a greater proportion develops resistance to treatment (Rofagha et al. 2013; Yang et al. 2016). Combined with the associated complications that present repeated intravitreal injections, the need of alternative anti-angiogenic therapies is coming to the fore.

The situation for dry AMD is even less favorable. Geographic atrophy affects the majority of patients with advanced AMD. However, there is still no treatment for it. The major outcome until today has been the treatment with lampalizumab, a drug that targets the complement pathway. The first clinical trial consisted in the intravitreal injection of lampalizumab every month during 18 months and led to a 20% reduction of geographic atrophy (Yaspan et al. 2017). However, a larger phase III trial did not show any reduction of geographic atrophy during the 12 months of treatment (Holz et al. 2018), leaving this promising treatment on the air.

With this scenario, therapies to delay the progression from early to late stages are emerging as the first approach to reduce vision loss. In the multicenter and controlled clinical trial AREDS, a combined oral supplement containing high doses of antioxidants (vitamin C and E,  $\beta$ -carotene, copper and zinc) slowed the progression of AMD in patients with an early phenotype by 25%



after a 6 years follow-up (Kassoff et al. 2001). AREDS2 clinical trial added zeaxanthin and replaced  $\beta$ -carotene with lutein (which is normally absorbed from blood into the macula), achieving an 18% reduced risk of progression to advanced AMD (Chew et al. 2014).

### 3.2. CeO<sub>2</sub>NPs and their antioxidant function

Given the benefits oral antioxidant supplementation provide in the progression of dry AMD, preventive therapies focusing on the reduction of ROS formation during the visual cycle should be further explored.

In this context, cerium oxide nanoparticles (CeO<sub>2</sub>NPs) have received much attention in recent years because of their excellent catalytic redox properties. When synthesized at the nanoscale, CeO<sub>2</sub>NPs show unique regenerative antioxidant activity due to their low reduction potential and the coexistence of both Ce<sup>3+</sup> and Ce<sup>4+</sup> on its surface, acting as electron donors or acceptors (Karakoti et al. 2009). Ce<sup>3+</sup> is able to scavenge superoxide radicals, exhibiting a superoxide dismutase (SOD) enzyme mimetic activity. During this reaction, Ce<sup>3+</sup> becomes Ce<sup>4+</sup>, which is able to scavenge hydrogen peroxide while regenerating its surface mimicking catalase activity (Heckert et al. 2008; Pirmohamed et al. 2010) (Figure I.9).

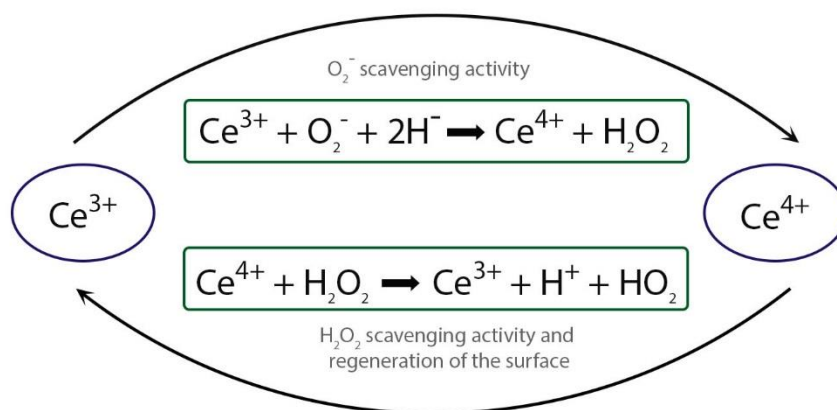


**Figure I.9. ROS scavenging activity and surface regeneration properties of CeO<sub>2</sub>NPs.** Ce<sup>3+</sup> scavenges superoxide radicals (O<sub>2</sub><sup>-</sup>). The reaction produces hydrogen peroxide (H<sub>2</sub>O<sub>2</sub>) and Ce<sup>3+</sup> becomes Ce<sup>4+</sup>. In turn, Ce<sup>4+</sup> scavenges H<sub>2</sub>O<sub>2</sub> regenerating its surface into Ce<sup>3+</sup> again.

These multi-enzyme mimetic properties have raised CeO<sub>2</sub>NPs as a therapeutic option for a wide variety of oxidative stress-related diseases, with a great impact in neurodegenerative diseases. Like the retina, the brain and the central nervous system present high levels of oxygen consumption, which makes them particularly susceptible to increased oxidative stress and free

radical production (Naz et al. 2017). Several studies have examined the in vitro effect of CeO<sub>2</sub>NPs in Alzheimer disease, showing a protection of neuronal cells against cell death and a reduction of A $\beta$  aggregation (Dowding et al. 2014; Cimini et al. 2012). Studies with Parkinson's disease and ischemic stroke mouse models have also shown a reduction of neuronal cell damage after administering CeO<sub>2</sub>NPs by intravenous injection, highlighting the capacity of CeO<sub>2</sub>NPs to cross the brain barrier (Dillon et al. 2011; Kim et al. 2012).

### 3.2.1. CeO<sub>2</sub>NPs in retinal degenerative pathologies

The first evidence showing a beneficial effect of CeO<sub>2</sub>NPs in a retinal degenerative pathology was in 2006. Chen et al. demonstrated a reduction of ROS in primary rat retinal neurons in vitro after the induction of oxidative stress with H<sub>2</sub>O<sub>2</sub>. More importantly, they also showed that a single intravitreal injection of CeO<sub>2</sub>NPs was able to inhibit photoreceptors cell death in the light-damage retinal degeneration rat model, a model with severe retinal degeneration (Chen et al. 2006).

Since then, the efficacy of CeO<sub>2</sub>NPs has been further analyzed in other models through intravitreal administration. CeO<sub>2</sub>NPs conferred protection against photoreceptor degeneration in the *tubby* mouse model (with a spontaneous splicing mutation in the *Tub* gene, codifying for a cell signaling protein associated with neuronal differentiation) and in the P23H rat (an autosomal dominant retinitis pigmentosa rat model), both with early and severe photoreceptor degeneration (Cai et al. 2012; Wong et al. 2015). In addition, in the light-damage rat model, CeO<sub>2</sub>NPs also reduced microglia activation while reducing photoreceptor death (Fiorani et al. 2015).

CeO<sub>2</sub>NPs have also shown a neovascular inhibitory capacity. An intravitreal injection of CeO<sub>2</sub>NPs was able to regress pathological retinal neovascularization by inhibiting the expression of genes associated with inflammation and angiogenesis in the *Vldlr* knockout mouse model (Zhou et al. 2011; Kyosseva et al. 2013); and to inhibit CNV by reducing VEGFA expression in the laser-induced CNV mouse model (Mitra et al. 2017).

The effect of a long-term presence of CeO<sub>2</sub>NPs in murine eyes has also been addressed to discard any cytotoxic response. Wild type rats receiving an intravitreal injection of CeO<sub>2</sub>NPs have been assessed 120 days after administration without any changes observed in their retina structure and function. Moreover, cerium was retained in their retinas during all that period, with a 69% of the injected cerium present after 120 days (Wong et al. 2013). Wild type mice have also been

followed up until 30 days post-intravitreal injection of CeO<sub>2</sub>NPs at different concentrations, with the same outcome (Cai et al. 2016).

Taken together, these results showed an antioxidant, neuroprotective and antiangiogenic effect of CeO<sub>2</sub>NPs, reinforcing their use as a therapy for retinal degenerative diseases.

### 3.3. Drug delivery to the retina

An efficient delivery of any drug implies its availability to the targeted site in sufficient amount and for a sufficient period. Delivery of drugs to the retina and RPE is challenging given its posterior location in the eye and the presence of the blood-retinal barrier, whose permeability hampers the influx from systemic delivery and facilitates the clearance from the vitreous cavity (del Amo et al. 2017).

The main routes of administration used to reach the retina are intravitreal, subretinal, suprachoroidal, topical and systemic; each one with its pros and cons (Himawan et al. 2019) (Figure I.10).

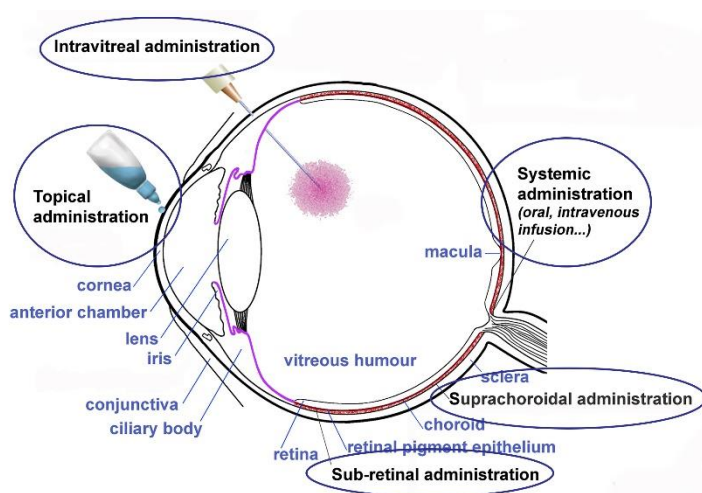


**Figure I.10. Drug administration routes to the retina.** Main drug administration routes into the retina. Intravitreal, subretinal and suprachoroidal administrations are mediated by an injection to the targeted site. Topical administration consists in the application of a drop in the cornea and systemic administration uses the bloodstream to reach the ocular compartment. Image from del Amo et al. 2017.

Intravitreal injection is the current method of choice for most retinal diseases as it provides a direct delivery to the retina producing an immediate and increased therapeutic effect. It is the established route to deliver anti-VEGFA therapies for the treatment of AMD (Lanzetta and Loewenstein 2017). For gene and cell therapies, the route of choice is the subretinal injection as it allows an easy delivery of the material to both RPE cells and photoreceptors. This procedure generates a bleb between RPE cells and photoreceptors that inherently result in retinal detachment. Although the bleb is later absorbed, the detachment produced can be detrimental

to retinal viability (Peng et al. 2017). The newest ocular route explored is the suprachoroidal injection, not used in clinics yet. With this administration, drugs diffuse slowly to the choroid and retina, minimizing the potential systemic side effects and not interfering with the optical path (Rai et al. 2015).

All these injection-mediated administrations need the assistance of an ophthalmologist, and despite reaching the targeted site in sufficient amount, their use in chronic diseases is detrimental. Repeated drug administration is needed in chronic and progressive diseases, what increases the risk of injection-derived side effects (Falavarjani et al. 2013). Endophthalmitis, intraocular inflammation, retinal detachment or intraocular hemorrhages are the main associated complications to injection-mediated administrations, with a prevalence of 1% per injection, but the recurring injections needed for these pathologies increase their risk (Jager et al. 2004).

Topical administration with eye drops is the less invasive route and the most convenient, as patients can apply it themselves. It is commonly used to treat disorders of the anterior part of the eye, given the easy delivery of small molecular weight drugs into the anterior chamber. However, the availability in the posterior part of the eye varies among molecules. In general, about 4% of the dose applied reaches the posterior part of the eye (Djebli et al. 2017). Hence, several clinical trials are exploring topical treatments for retinal pathologies, but none of them are available yet.

Systemic administration is also used in some cases, such as the oral supplementation of antioxidants for AMD. Although less invasive than other intraocular routes, it is limited by the fact that only small molecules can cross the blood-retinal barrier. Overall, the amount of dose reaching the ocular tissue is very poor, even negligible in some cases (Srirangam et al. 2012).

## **4. Mouse models for AMD**

AMD pathogenesis starts in the macula, a region identified in the retina of primates but not in other mammals or vertebrates. Lower simian primates, such as macaque and rhesus monkeys, present pigmentary abnormalities and drusen with ageing, with a similar composition of the one reported in humans. However, there is no evidence of advanced AMD in their retinas (Gouras et al. 2008; Umeda et al. 2005). Moreover, the inherent difficulties associated with the use of these species as animal models, does not make them suitable for the study of AMD.

Despite their absence of macula and fovea, mouse models offer the possibility to dissect distinct characteristics of complex human diseases and investigate contributions of individual components to the complete phenotype (Swaroop et al. 2009).

Regarding the complex pathogenesis of AMD, different models have been developed to mimic the progression to geographic atrophy, usually focusing in one of the main processes involved. Thus, the different models can be categorized according to whether they present abnormalities in the complement factor, metabolism, chemokine pathways or oxidative damage. Models recapitulating the neovascular phenotype of the disease have also been developed. Despite not recreating completely the characteristics of AMD, all models helped to gain insight into the pathogenesis of the disease. Table 1.2 summarizes the most relevant models so far, with their main AMD-related characteristics.

### **4.1. Models for choroidal neovascularization**

The main models for wet AMD rely either on laser or on mechanical disruption of Bruch's membrane (Pennesi et al. 2012). From all of them, the laser-induced choroidal neovascularization model is the most widely used.

This model was first generated in mice in 1998 (Tobe et al. 1998), achieving a high ratio of CNV in lesions where the laser burn disrupted Bruch's membrane. Similar to the CNV in humans, laser-induced CNV follows three stages of development: early membrane formation, establishment of mature fibrovascular network and involution (Miller et al. 1990). However, this model is unable to recapitulate the complex sequence of events that lead to CNV in AMD, as it is a model of acute injury and inflammation rather than a result of chronic inflammation and progressive degeneration (Pennesi et al. 2012).

Despite that, its lower cost, ability to efficiently generate high number of CNV lesions and its short time course, turned it into the standard model to study CNV, greatly contributing to the understanding of the pathogenesis of CNV at a molecular level and to the establishment of anti-VEGFA treatments (Liu et al. 2017).

**Table I.2. Main mouse models that mimic phenotypic characteristics observed in AMD.**

BM: Bruch's membrane; RPE: retinal pigment epithelium; CNV: choroidal neovascularization; CEP: carboxyethylpyrrole; m: months; w: weeks; AV: adenovirus

|  | Increased autofluorescence | Increased autofluorescence | Immune cell accumulation | Photoreceptor atrophy | Reduced retinal function | Retinal fibrosis | Retinal fibrosis | Appearance of the phenotype |
|--|----------------------------|----------------------------|--------------------------|-----------------------|--------------------------|------------------|------------------|-----------------------------|
|  | Thickened BM               | Drusen-like deposits       | RPE atrophy              | Complement deposition | Photoreceptor atrophy    | Retinal fibrosis | CNV              |                             |
| <b>Oxidative damage</b>  |                            |                            |                          |                       |                          |                  |                  |                             |
| <i>Sod1</i> <sup>-/-</sup> mice                                | x                          | x                          | x                        |                       |                          |                  | x                | 7 months                    |
| <i>Sod2</i> knockdown mice                                     | x                          |                            | x                        | x                     | x                        |                  | x                | 2m post AV injection        |
| <i>Nrf2</i> <sup>-/-</sup> mice                                | x                          | x                          | x                        | x                     |                          | x                | x                | 12 months                   |
| Cigarette smoke exposition                                     | x                          | x                          |                          |                       |                          |                  |                  | 16 months                   |
| Hydroquinone exposition  | x                          |                            |                          |                       |                          |                  |                  | 16 months                   |
| Immunization with CEP  | x                          | x                          | x                        |                       | x                        | x                | x                | 9 months                    |
| <b>Complement factor</b>                                       |                            |                            |                          |                       |                          |                  |                  |                             |
| <i>Cfh</i> <sup>-/-</sup> mice                                 |                            |                            |                          | x                     |                          | x                | x                | 12 months                   |
| <i>Cfh</i> <sup>Y402H</sup> mice                               | x                          | x                          |                          |                       | x                        | x                |                  | 24 months                   |
| C3 overexpression mice   |                            |                            | x                        |                       |                          | x                | x                | 2w post AV injection        |
| <b>Lipid metabolism</b>  |                            |                            |                          |                       |                          |                  |                  |                             |
| <i>ApoE</i> <sup>-/-</sup> mice                                | x                          | x                          |                          |                       |                          |                  |                  | from 2 to 8 months          |
| APOE3-Leiden mice  | x                          | x                          | x                        |                       |                          |                  |                  | 9 months                    |
| APOE knock-in mice   | x                          | x                          | x                        |                       |                          |                  |                  | from 9 to 18 months         |
| <i>CD36</i> <sup>-/-</sup> mice                                | x                          | x                          |                          |                       |                          |                  |                  | 12 months                   |
| <i>CD36</i> <sup>-/-</sup> ; <i>ApoE</i> <sup>-/-</sup> mice   | x                          | x                          |                          |                       |                          |                  |                  | 4 months                    |
| <i>Vldlr</i> <sup>-/-</sup> mice                               |                            |                            |                          |                       |                          |                  | x                | 6 weeks                     |
| <b>Chemokine pathways</b>                                      |                            |                            |                          |                       |                          |                  |                  |                             |
| <i>Cx3cr1</i> <sup>-/-</sup> mice                              |                            | x                          |                          |                       | x                        | x                | x                | 12 months                   |
| <i>Ccl2</i> <sup>-/-</sup> mice                                |                            | x                          |                          |                       | x                        | x                |                  | 20 months                   |
| <i>Ccr2</i> <sup>-/-</sup> mice                                |                            | x                          | x                        |                       | x                        | x                |                  | 20 months                   |
| <i>Ccl2</i> <sup>-/-</sup> ; <i>Cx3cr1</i> <sup>-/-</sup> mice | x                          | x                          | x                        |                       | x                        | x                |                  | 6 weeks                     |
| <b>Choroidal Neovascularization</b>                            |                            |                            |                          |                       |                          |                  |                  |                             |
| Laser-induced CNV  |                            |                            |                          |                       |                          | x                | x                | 3 days post-laser           |

## 4.2. Models with oxidative damage

Oxidative stress is considered the first inducer of AMD pathogenesis. Animal models lacking intrinsic antioxidant mechanisms, or those in which additional oxidative stress is applied, show various features of AMD.

Super oxide dismutase (SOD) is a powerful antioxidant enzyme. It has three isoenzymes, all of them expressed in the retina: SOD1, found in the cytosol; SOD2 expressed in the mitochondria; and SOD3, found in the extracellular matrix (Behndig et al. 1998). *Sod1*<sup>-/-</sup> mice start displaying AMD-like characteristics at 7 months of age. They present yellowish drusen-like deposits between the RPE and the Bruch's membrane, oxidative damage in RPE cells, and thickening of Bruch's membrane. They also undergo cell death in the INL and present a reduction of visual function at an advanced age (Imamura et al. 2006). *Sod2* knockdown mice also present AMD-like features such as increased autofluorescence and increased markers of oxidative damage. These features begin 2 months after the adenovirus-mediated transfection with a ribozyme that degrades SOD2. *Sod2* knockdown mice also present a severe atrophy of photoreceptors and degeneration of RPE cells, making it a suitable model for the study of severe retinal degenerative diseases (Justilien et al. 2007).

Another relevant gene in the antioxidant response is *Nrf2* (Nuclear factor erythroid 2-related factor 2). *Nrf2* is a transcription factor considered the master of anti-oxidation, as it regulates several genes involved in the antioxidant response such as *Sod* genes, catalase, or glutathione reductase among many others (Ma 2013). *Nrf2*<sup>-/-</sup> mice develop age-dependent degeneration of the RPE and choroidal capillaries, and present sub-RPE deposits of inflammatory proteins. As in other similar models, the onset of this phenotype starts at one year of age (Zhao et al. 2011).

Besides genetic models, induced models have also been developed. Exposition to cigarette smoke or hydroquinone (one of the pro-oxidant substance of cigarette smoke) in mice diet causes the thickening of Bruch's membrane and an increase of basal laminar deposits in 16-months old mice (Espinosa-Heidmann et al. 2006).

Another induced model is the mouse immunized with carboxyethylpyrrole (CEP), which was developed to study the inflammatory response derived from oxidative damage. CEP is a product of the oxidation of docosahexaenoic acid (DHA), one of the most prevalent fatty acids in the retina. Mice immunized with CEP gradually lose RPE cells, develop sub-RPE deposits, accumulate C3 protein in the subretinal space, and present an increased number of immune cells in the subretinal space. These data highlight the fact that an immune response against an oxidative

stress-derived product can lead to the development of some signs of AMD (Hollyfield et al. 2008).

#### **4.3. Models with abnormalities in the complement factor pathway**

The presence of complement cascade components in drusen, and the increased risk of AMD that confers polymorphisms in *CFH* gene (a negative regulator of the complement cascade) place the complement system as a key player in AMD pathogenesis. To investigate the role of CFH, a knockout mice (*Cfh*<sup>-/-</sup>) and a knock-in mice (*Cfh*<sup>Y402H</sup>) that express the human Y402H polymorphism in RPE upon the *ApoE* promoter have been developed. These mice present deposition of the complement 3 (C3) protein and accumulation of macrophages and immune cells in the subretinal space, starting at two and one years of age respectively (Coffey et al. 2007; Ufret-Vincenty et al. 2010).

Mice injected with C3-expressing adenovirus have also been generated. Subretinal delivery of C3 to murine RPE increases vascular permeability, induces RPE atrophy, loss of photoreceptor outer segments and a reduced retinal function (Cashman et al. 2011).

#### **4.4. Models with dysregulation in lipid metabolism**

The association between cardiovascular diseases, such as atherosclerosis, and AMD is still under discussion. Lipids and cholesterol are known to accumulate within Bruch's membrane with advancing age, and are thought to interfere with the transport of metabolites between the RPE and the choroid capillaries (Curcio et al. 2001). Genetic polymorphisms in apolipoproteins (APO), which mediate lipid transport, have also been postulated in the risk of AMD (Xiyang et al. 2017). This is why the relationship between lipid metabolism and AMD pathogenesis has also been studied using several mouse models.

A variety of mice with a genetically modified expression of *ApoE* have been developed. *ApoE*<sup>-/-</sup> mice exhibits increased serum levels of triglycerides and cholesterol and develop thickened Bruch's membrane, as well as accumulation of lipid deposits between RPE and Bruch's membrane (Dithmar et al. 2000). *ApoE3*-Leiden mice, which express a dysfunctional form of human APOE3, develop similar changes in Bruch's membrane as *ApoE*<sup>-/-</sup> mice, which are worsened with a high fat diet (Kliffen et al. 2000). Knock-in mice expressing the human APOE2, APOE3 or APOE4 proteins under the control of endogenous mouse *ApoE* promoter also develop



thickening of Bruch's membrane and sub-RPE deposits when fed with high-fat diet (Malek et al. 2005).

CD36 is a scavenger receptor for oxidized low-density lipoproteins expressed in RPE cells (Endemann et al. 1993). *CD36*<sup>-/-</sup> mice develop thickening of Bruch's membrane and subretinal deposits, with a worsened phenotype in the *CD36*<sup>-/-</sup>; *ApoE*<sup>-/-</sup> double knockout mouse (Picard et al. 2010).

Another genetic model with impaired lipid metabolism is the *Vldlr*<sup>-/-</sup> mouse. The very low-density lipoprotein receptor (VLDLR) knockout mice display retinal and choroidal neovascularization in advanced ages, resembling retinal angiomatous proliferation diseases more than AMD (Chen et al. 2007).

#### **4.5. Models with dysregulation in chemokine pathways**

Chemotactic cytokines or chemokines are a diverse set of small molecular weight proteins that mediate the recruitment and migration of inflammatory cells to a target site (Luster 1998). In AMD, activated microglia results in the migration of these cells towards the subretinal space, with CCL2/CCR2 and CX3CL1/CX3CR1 axes being implicated. Genetic mouse models with alterations in these genes resulted in mice with many features of AMD.

*Cx3cr1*<sup>-/-</sup> mice present drusen-like deposits composed of an accumulation of subretinal microglia at 12 months of age. At 18 months, they also show a 40% retinal thinning, highlighting the importance of microglia regulation. Additionally, laser-induced choroidal neovascularization (CNV) in *Cx3cr1*<sup>-/-</sup> mice retinas produce bigger neovascular areas than in control mice (Combadière et al. 2007).

The role of CCL2/CCR2 axis in microglia mobilization has also been studied with the generation of both *Ccl2*<sup>-/-</sup> and *Ccr2*<sup>-/-</sup> mice. These mice present accumulation of macrophages in the subretinal space with increased lipofuscin granules observed in aged mice (at 20 months of age), and age-related RPE atrophy (Luhmann et al. 2009).

##### **4.5.1. *Ccl2*<sup>-/-</sup>; *Cx3cr1*<sup>-/-</sup> mice as a model for dry AMD**

*Ccl2*<sup>-/-</sup> and *Cx3cr1*<sup>-/-</sup> single knockout mice exhibit many features of AMD, but in a very advanced age (20 and 18 months respectively) and with incomplete penetrance. To determine if the loss of both CCL2 and CX3CR1 might have a synergistic effect, *Ccl2*<sup>-/-</sup> and *Cx3cr1*<sup>-/-</sup> double knockout

mice were generated (Tuo et al. 2007). These mice presented retinal changes as early as 6 weeks, providing a more convenient model to study AMD. By 9 weeks of age, *Ccl2*<sup>-/-</sup>; *Cx3cr1*<sup>-/-</sup> mice displayed drusen-like deposits and pigment alterations with a high penetrance. Photoreceptors atrophy was also observed around 3 months of age.

However, two independently generated *Ccl2*<sup>-/-</sup>; *Cx3cr1*<sup>-/-</sup> mice did not exhibit severe features and were not so phenotypically different from *Ccl2*<sup>-/-</sup> or *Cx3cr1*<sup>-/-</sup> single knockout mice (Raoul et al. 2010; Vessey et al. 2012). To understand these phenotypic discrepancies, further studies were conducted in which the *Crb1*<sup>rd8/rd8</sup> mutation was established as a third independent mutation responsible for the earlier onset of the AMD-like phenotype in those mice (Luhmann et al. 2012).

This naturally occurring *rd8* mutation is a single nucleotide deletion of a cytosine in the *Crb1* gene that causes a frame shift and premature stop codon. CRB1 is expressed in Müller cells in the retina and is crucially involved in the formation of the outer limiting membrane, located between the nuclei and photoreceptor segments (Mehalow et al. 2003). The presence of the *rd8* mutation has been identified in all vendor lines of C57BL/6N mice substrain, widely used to produce transgenic and knockout mice (Mattapallil et al. 2012).

Therefore, the background in which the *Ccl2*<sup>-/-</sup>; *Cx3cr1*<sup>-/-</sup> mice are generated, determines the appearance of their phenotype. Given that *Ccl2*<sup>-/-</sup>; *Cx3cr1*<sup>-/-</sup> mice with 6J background (without the *rd8* mutation) begin to present AMD-related characteristics as early as 9 months of age, it was established that the early retinal degeneration observed in the *Ccl2*<sup>-/-</sup>; *Cx3cr1*<sup>-/-</sup> mice with 6N background (already at one month of age) was due to the unnoticed mutation present in their genetic background (Chen et al. 2013).

Further characterization of the *Ccl2*<sup>-/-</sup>; *Cx3cr1*<sup>-/-</sup>; *Crb1*<sup>rd8/rd8</sup> mice revealed that the early retinal lesions are localized in the inferior retina, starting in the outer nuclear layer. Microglia is recruited to these primary lesions (Luhmann et al. 2012), which enlarge with ageing until a complete degeneration of photoreceptors layers by 16 months of age is reached (Zhou et al. 2011). *Ccl2*<sup>-/-</sup>; *Cx3cr1*<sup>-/-</sup>; *Crb1*<sup>rd8/rd8</sup> mice retinas also display a thickening of Bruch's membrane, lipofuscin accumulation observed already at 6 weeks of age (Zhang et al. 2013), and increased complement expression (Ross et al. 2008). RPE cells in these mice also show increased expression of apoptotic proteins Fas and FasL (Wang et al. 2012), lipid accumulation and degenerative mitochondria (Wang et al. 2016).

With all these characteristics, the *Ccl2*<sup>-/-</sup>; *Cx3cr1*<sup>-/-</sup> on the C57BL/6N [*Crb1*<sup>rd8</sup>] genetic background has been established as a mouse model of progressive and focal retinal degeneration, mimicking certain features of human AMD.

Different therapies have already been tested in *Ccl2*<sup>-/-</sup>; *Cx3cr1*<sup>-/-</sup>; *Crb1*<sup>rd8/rd8</sup> mice. Following AREDS and AREDS2 clinical trials, their results pointed out that an oral intake of antioxidant rich supplements slowed the progression of AMD, *DKOrd8* mice were treated with a high omega-3 polyunsaturated fatty acids diet. After eight months of treatment, mice showed a slower progression of retinal lesions, and decreased pro-inflammatory derivatives (Tuo et al. 2009). *DKOrd8* mice treated with lutein and zeaxanthin (antioxidants added in the AREDS2 study) for three months also showed a greater regression of their retinal lesions and lower levels of A2E, the main lipofuscin component (Ramkumar et al. 2013a).

The effect of the anti-inflammatory tumor necrosis factor-inducible gene 6 protein (TSG-6) (Tuo et al. 2012) and the neuroprotective factors Pigment Epithelium Derived Factor (PEDF) and Platelet-Derived Growth Factor (PDGF) have also been assessed individually in *Ccl2*<sup>-/-</sup>; *Cx3cr1*<sup>-/-</sup>; *Crb1*<sup>rd8/rd8</sup> mice in different studies, after a single intravitreal injection (Wang et al. 2013; Wang et al. 2014). In all cases, the intravitreal administration slowed the progression of the focal retinal lesions and decreased the expression of inflammatory factors such as TNF $\alpha$  and IL-17a.

An abstract watercolor artwork featuring a dense network of thin, black, branching lines that resemble a neural network or a complex web. The background is a textured wash of warm, earthy tones, including shades of beige, tan, and light brown. Interspersed among the black lines are various organic, dark shapes in shades of black, dark blue, and dark brown, some resembling small, dark, rounded forms. The overall composition is intricate and layered, with the black lines and shapes appearing to be overlaid on the textured background. The word "AIMS" is centered in the upper-middle portion of the image in a bold, black, sans-serif font.

**AIMS**



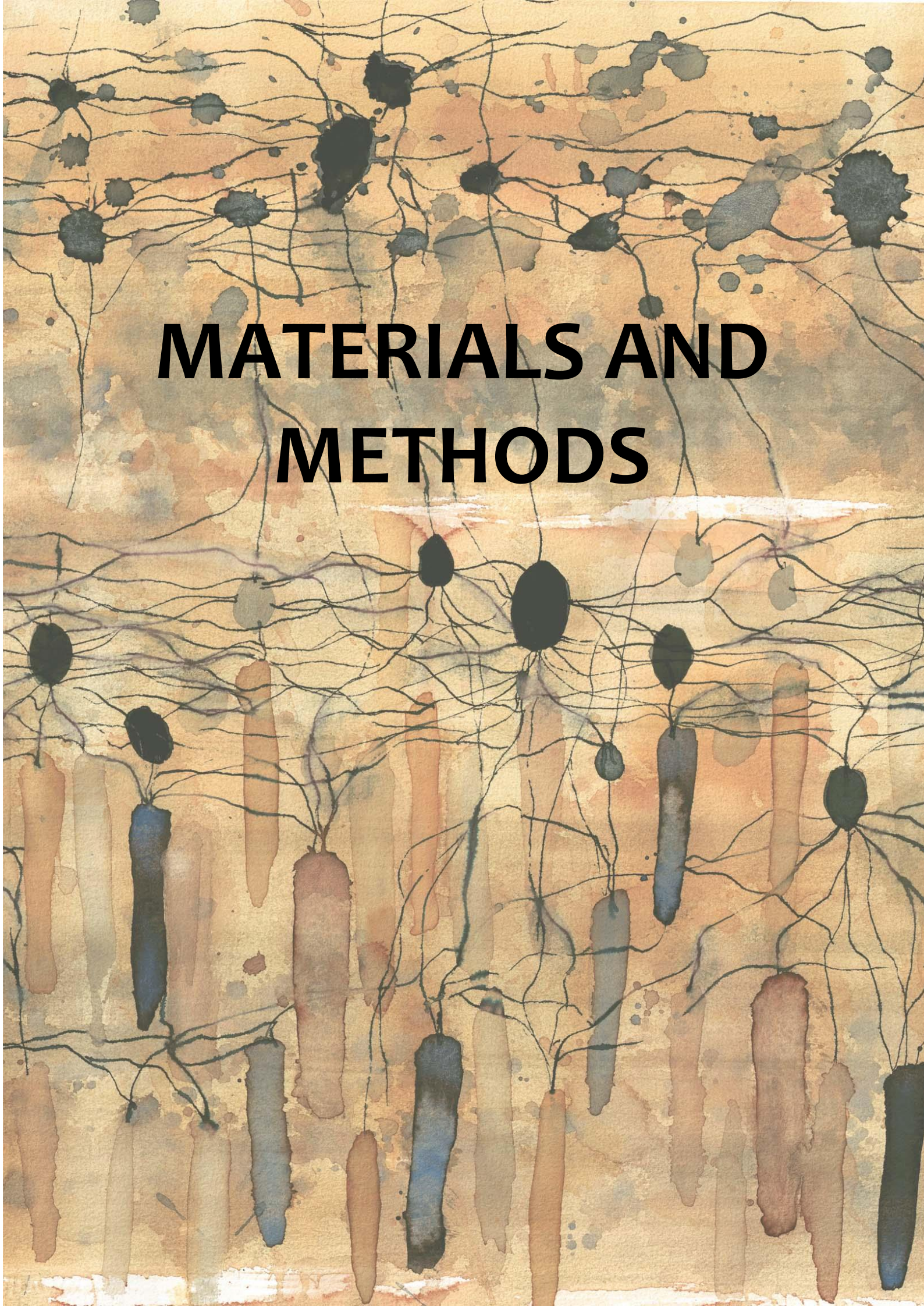
Age-related macular degeneration is a multifactorial disease with a complex pathogenesis. To this day, no effective therapies to revert or stop its progression have been developed. In the last years, CeO<sub>2</sub>NPs and other antioxidant therapies have emerged as a possible treatment for neurodegenerative diseases because of their high and auto-regenerative capacity to reduce ROS levels.

Given the major role oxidative stress plays in the onset and development of AMD, the development of NPs with high antioxidant capacity could become an effective treatment for this pathology.

Under this premise, the general aims of this thesis are:

- To generate the *Ccl2*<sup>-/-</sup>; *Cx3cr1*<sup>-/-</sup>; *Crb1*<sup>rd8/rd8</sup> mouse, a murine model for AMD. Once generated, to characterize the resulting mouse model through an in vivo monitoring of the retinal status and function, and a post-mortem evaluation of the retinal histology and gene expression profile.
- To develop a nanoparticles-based antioxidant therapy by performing preliminary studies to (i) assess in vitro the antioxidant effect and toxicity of AOxNPs, (ii) compare the biodistribution through different delivery routes, and (iii) test the efficacy of the AOxNPs treatment in the *DKO<sup>rd8</sup>* mouse model.



The background is an abstract watercolor composition. It features a dense network of thin, black, branching lines that resemble a neural network or a complex web. These lines are set against a warm, textured background of watercolor washes in shades of beige, tan, and light brown. Interspersed among the lines are various organic, blotchy shapes in dark charcoal, black, and muted blue-grey tones. Some of these shapes are elongated and vertical, while others are more rounded or irregular. The overall effect is one of intricate, organic complexity.

# **MATERIALS AND METHODS**





## 1. In vivo animal experimentation

### 1.1. Generation of the DKOrd8 mice

The *Ccl2* and *Cx3cr1* double knockout (DKO) mice in C57BL/6N background (with presence of the *rd8* mutation) were generated from the single *Ccl2*<sup>-/-</sup> [B6.129S4-Ccl2<sup>tm1Roi</sup>/J] and *Cx3cr1*<sup>-/-</sup> [B6.129P-Cx3cr1<sup>tm1Litt</sup>/J] knockout mice, from Jackson Laboratories and from C57BL/6N mice (referred to as 6N mice) purchased at Charles River.

- *Ccl2*<sup>-/-</sup> [B6.129S4-Ccl2<sup>tm1Roi</sup>/J] mice were originally generated in C57BL/6J background. They present a small deletion and an in frame stop codon in exon 1 of *Ccl2* gene. The secreted protein is not detected in stimulated macrophages, what indicates the impaired recruitment of monocytes in this model (Lu et al. 1998).
- *Cx3cr1*<sup>-/-</sup> [B6.129P-Cx3cr1<sup>tm1Litt</sup>/J] mice were originally generated in C57BL/6J background. They present a disruption in the endogenous locus of *Cx3cr1* gene caused by the insertion of the sequence encoding green fluorescent protein (*GFP*), which replaces the firsts 390 bp of the second coding exon of the gene. *GFP* is expressed instead of the endogenous protein in homozygous mutant mice (Jung et al. 2000).
- C57BL/6N is the most common inbred strain used for animal research and its background is widely used for genetically modified mice. It was originally developed as the C57BL/6 strain by C.C. Little in 1921 and transferred to Jackson Laboratories in 1948 (referred to as C57BL/6J). A subline was separated from the Jackson Labs to the NIH in 1951 giving rise to C57BL/6N mice. Between 1951 and 1961, a spontaneous single base mutation in the *Crb1*<sup>rd8</sup> gene occurred, although it was not detected until 2012. This mutation has been found in homozygosis in all the strains of C57BL/6N mice, but not in any C57BL/6J subline (Charles River Website 2019).

The detailed description of the generation of these mice is reported in the Results section (page 63). In brief, *Ccl2* single knockout mice were crossed with C57BL/6N mice to ensure the presence of the *rd8* mutation. The initial *Ccl2*<sup>+/-</sup>; *Crb1*<sup>+/rd8</sup> double heterozygous mice were intercrossed to obtain the *Ccl2*<sup>-/-</sup>; *Crb1*<sup>rd8/rd8</sup> double homozygous mice. Distinctly, *Cx3cr1*<sup>-/-</sup> mice already presented the *rd8* mutation in their genetic background. Once generated and confirmed their genotype, *Ccl2*<sup>-/-</sup>; *Crb1*<sup>rd8/rd8</sup> and *Cx3cr1*<sup>-/-</sup>; *Crb1*<sup>rd8/rd8</sup> mice were intercrossed to generate mice with the *rd8* allele in homozygosis and the *Ccl2* and *Cx3cr1* alleles in heterozygosis (*Ccl2*<sup>+/-</sup>; *Cx3cr1*<sup>+/-</sup>; *Crb1*<sup>rd8/rd8</sup>). These mice were intercrossed again to generate mice with the *Ccl2*<sup>-/-</sup>;

*Cx3cr1*<sup>-/-</sup>; *Crb1*<sup>rd8/rd8</sup> genotype; hereafter called *DKOrd8* mice. Once obtained, the colony was maintained by setting periodic crossings between *DKOrd8* mice.

For all the experiments, mice aged between one and nine months were used. Mice were housed at Vall d'Hebron Research Institute animal facility under standard cyclic light conditions (12/12 hours light/darkness), free access to filtered water and ad libitum food. All experiments were performed according to the Association for Research in Vision and Ophthalmology (ARVO) statement for the use of animals in vision and ophthalmic research and approved by the Vall d'Hebron Research Institute Ethical Committee for Animal Research (VHIR-CEEA) and local governmental authorities.

## **1.2. Genotyping**

### **1.2.1. DNA extraction**

All mice obtained from the different crosses were genotyped after weaning. For this purpose, collected ear punches from each mice were digested overnight at 55°C with 100 µl of a DNA digestion buffer containing SDS and proteinase K (50 mM TRIS-HCl pH 8.0, 100 mM EDTA pH 8.0, 100 mM NaCl, 1% SDS, 0.5 mg/ml proteinase K) and DNA was extracted the following day using a phenol/chloroform protocol. In brief, 140 µl of neutralized phenol/chloroform/isoamyl alcohol (Sigma, Ref. P2069) were added to each tube and were mixed vigorously. Samples were centrifuged at 16.000 *g* for 15 minutes at 4°C. The aqueous phase was transferred into a new tube, 200 µl of ethanol 100% at room temperature (RT) were added and tubes were inverted until a DNA precipitate was formed. Next, samples were centrifuged at 16.000 *g* for 10 minutes at 4°C, and the supernatant was carefully discarded. The DNA pellet was washed with 100 µl of 70% ethanol at -20°C and samples were centrifuged again at 16.000 *g* for 5 minutes. The supernatant was discarded and the pellet was air-dried at RT before being resuspended in 50 µl of distilled water (dH<sub>2</sub>O). DNA quantity and quality were determined by taking spectrophotometric readings (Nanodrop™, Thermo Scientific).

### **1.2.2. Polymerase chain reaction (PCR) and sequencing**

Evaluation of *Ccl2* and *Cx3cr1* genotype was carried out with standard PCR using MyTaq Red Mix Kit (Bioline, Ref. BIO-25044). The sequence of specific forward primers to distinguish wild type (wt) and knockout alleles, and the sequence of a common reverse primer are shown in table MM.1. In each PCR reaction 1 µl of DNA was used as a template. For *Ccl2*, the three primers

were added together in each reaction. For *Cx3cr1*, each forward primer (the wt and the mutant) were placed separately in an independent reaction, together with the reverse primer. Melting temperatures for each primer set are also indicated in Table MM.1.

The genotype was confirmed by running the samples in a 1% agarose gel electrophoresis and analyzing the different band sizes. For *Ccl2*, the mutant band had 179 base pairs (bp) whereas the wt band had 287 bp. Band sizes for *Cx3cr1* were 937 bp and 698 bp respectively.

For the *rd8* genotyping, we designed primers flanking the *rd8* point mutation to amplify the region of interest by standard PCR. The resulting PCR product, with a length of 357 bp, was cleaned with the ATP™Gel/PCR DNA Fragment Extraction Kit (ATP Biotech Inc. Ref. APF100) following manufacturer's instructions. The cleaned DNA was mixed again with specific primers for sequencing, a procedure that was externalized and performed by Macrogen Inc. After Sanger sequencing, we verified the deletion of a cytosine in the nucleotide 3481 of the *Crb1* gene using the FinchTV Software (Geospiza Inc.).

**Table MM.1. Primers used for genotyping.**

| <b><i>Ccl2</i> primers</b>               |                            |          |
|--|----------------------------|----------|
| Forward (wt band)                        | 5'-TGACAGTCCCCAGAGTCACA-3' |          |
| Forward (mutant band)                    | 5'-GCCAGAGGCCACTTGTGTAG-3' | Tm= 60°C |
| Reverse common                           | 5'-TCATTGGGATCATCTTGCTG-3' |          |
| <b><i>Cx3cr1</i> primers</b>             |                            |          |
| Forward (wt band)                        | 5'-CAGTGTTTTCTCCCGCTTGC-3' |          |
| Forward (mutant band)                    | 5'-ACGACGGCAACTACAAGACC-3' | Tm= 59°C |
| Reverse common                           | 5'-TGGGGTGACGCCACTAAGAT-3' |          |
| <b><i>Crb1<sup>rd8</sup></i> primers</b> |                            |          |
| Forward                                  | 5'-GCACAATAGAGATTGGAGGC-3' |          |
| Reverse                                  | 5'-TGTCTACATCCACCTCACAG-3' | Tm= 55°C |

### **1.3. Eye fundus imaging**

The visualization of the eye fundus or funduscopy is a quick and non-invasive technique that allows for the visualization of the interior surface of the eye. Hence, it can be used to detect and evaluate several eye conditions in vivo. For *DKOrd8* mice characterization, the eye fundus of *DKOrd8* and 6N mice were visualized with the Micron III Retinal Imaging Microscope (Phoenix Research Labs), an imaging platform created for performing funduscopies in rodents.

Mice were anesthetized with 2% inhaled Isoflurane (Aerrane<sup>®</sup>. Baxter laboratories) and pupils were dilated with 1% tropicamide eye drops (Alcon Laboratories). Mice were kept under anesthesia during the whole procedure using a mask attached to the imaging platform. Anesthetized mice were placed on a heating pad integrated into the imaging platform to maintain their body temperature during the eye fundus exploration. The cornea was coupled to the objective lens using Methocel 2% (Omnivision GmbH) and the retina was focused.

The eye fundus was imaged with the Micron III Retinal Imaging Microscope and bright field images were captured with the Micron Discover V1.0 software (Phoenix Research Labs). Micron III microscope also possesses a fluorescent imaging modality for the visualization of green fluorescence, which was used to observe GFP expression in *DKOrd8* mice eyes' fundus and to capture images for further analyses.

### **1.4. Optical Coherence Tomography**

Optical coherence tomography (OCT) is a non-invasive technique that allows for the in vivo imaging of the retina. It uses low-coherence light to produce cross-sectional images of the retina, allowing for the visualization of all the retina layers given the differences in their reflectance. OCT images can be used to determine which are the layers affected by a specific pathology and to quantify retinal thickness, among other applications.

This technique was performed in *DKOrd8* and C57BL/6N mice with the image-guided OCT system from Phoenix Research Labs, which can be integrated into the Micron III Retinal Imaging Microscope. Mice were anesthetized and pupils were dilated as explained above and were kept under anesthesia during the whole procedure. Next, one by one each animal was placed on a heating pad integrated into the imaging platform, and the cornea was coupled to the objective lens using Methocel 2%. OCT imaging was performed with the InEye Software (Voxeleron LLC). Several images from the inferior and superior retina were taken and subsequently analyzed.

For all the experiments, the thickness of different retinal layers was quantified from OCT images of the same mice at different time points, by delineating the layers using the InSight Software (Voxeleron LLC). Specifically, we quantified the thickness of the inner plexiform layer (IPL), inner nuclear layer (INL), outer nuclear layer (ONL), including the outer plexiform layer, the inner and outer segments layer (IS/OS) and total retinal thickness. In all cases, the quantified retinal sections were taken at the same distance from the optic nerve to reduce variability (Figure MM.1)

Statistical analyses comparing the thickness of each retinal layer in a minimum of 20 6N and 20 *DKOrd8* mice were performed applying a two-way ANOVA with a Sidak's multiple comparison test, using the GraphPad Prism 8 Software. Significant differences were established when P-values were inferior than 0.05.

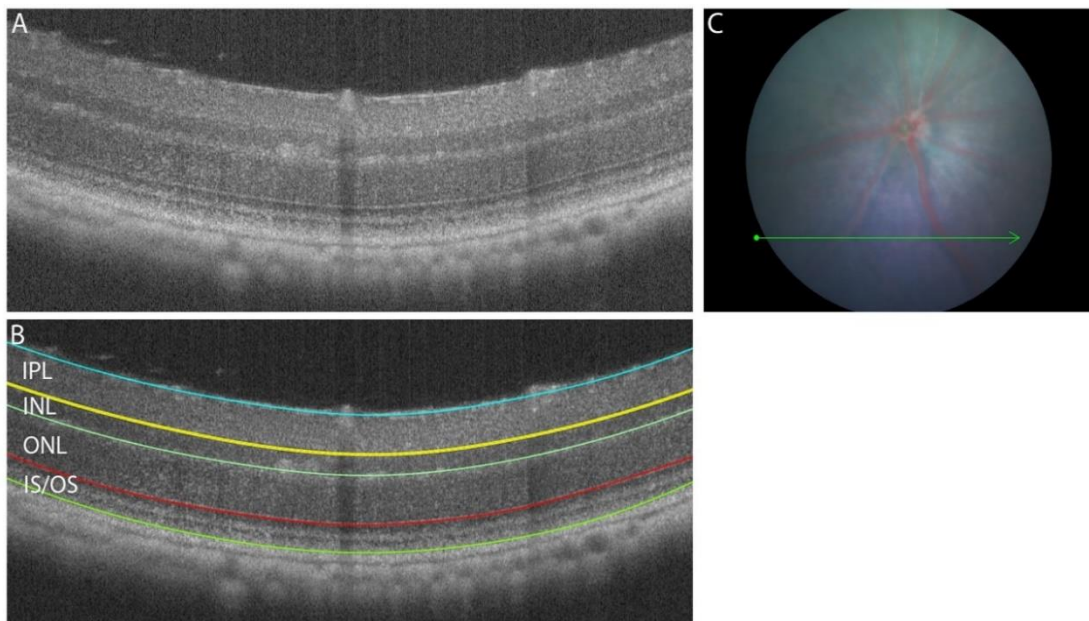


**Figure MM.1. OCT visualization and quantification of the retinal layers. (A)** OCT image of the inferior retina of a mice. **(B)** Inner plexiform layer (IPL), inner nuclear layer (INL), outer nuclear layer (ONL) and inner and outer segments layer (IS/OS) are delineated and later quantified using the OCT equipment's software. **(C)** Visualization of the eye fundus with a horizontal arrow indicating the area where the retina is being imaged.

## 1.5. Ganzfeld Electroretinography

Ganzfeld electroretinography (ERG) is a technique that measures the electrical activity generated in the whole retina in response to a light stimulus. Thus, it is the standard technique used to evaluate retinal function. When a flash or light stimulus is applied to the mouse eye, it evokes a biphasic waveform that can be recorded by placing an electrode on the cornea. The two components of the waveform are the a-wave, a first negative component, followed by the b-wave, which is positive and larger in amplitude. The time elapsing between the emission of the light pulse and the peak of either the a and the b-waves are also measured. These times are referred to as implicit times (Figure MM.2A). The a-wave reflects the activity of photoreceptors whereas the b-wave shows the activity of the inner layers of the retina, including the bipolar and Müller cells (Frishman and Wang 2011).

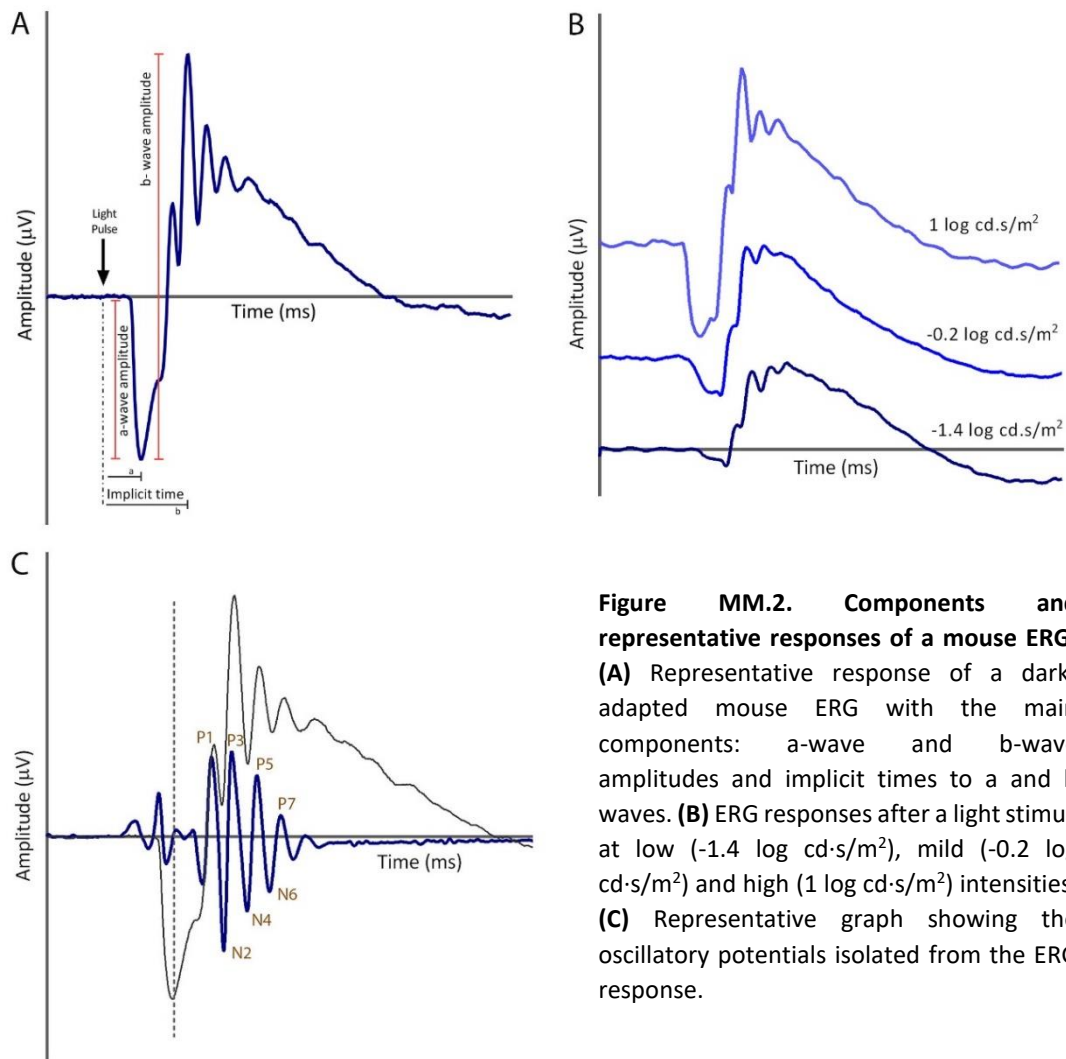


**Figure MM.2. Components and representative responses of a mouse ERG.** (A) Representative response of a dark-adapted mouse ERG with the main components: a-wave and b-wave amplitudes and implicit times to a and b waves. (B) ERG responses after a light stimuli at low (-1.4 log cd.s/m<sup>2</sup>), mild (-0.2 log cd.s/m<sup>2</sup>) and high (1 log cd.s/m<sup>2</sup>) intensities. (C) Representative graph showing the oscillatory potentials isolated from the ERG response.

At lower flash intensities, a normal ERG response presents a small a-wave amplitude and an already prominent b-wave. As the light stimuli intensity is increased, the response of retinal neurons increases, concomitantly with an enlargement of a-wave and b-wave amplitudes (Figure MM.2B).

On the rising phase of the b-wave, low amplitude oscillating waves can be observed, known as Oscillatory Potentials (OPs). This group of wavelets can be isolated using a band-pass filter to quantitatively assess their amplitude. Although the exact origin of the OPs is unclear, it is commonly accepted that they are generated by neural interactions among bipolar, amacrine and ganglion cells (Lei et al. 2006). Therefore, they provide additional information regarding retinal function. As the amplitude of these wavelets is quite low, they are usually evaluated as the summation of the different observed peaks (Figure MM.2C).

Ganzfeld electroretinography recordings in *DKOrd8* and 6N mice were measured using the Ganzfeld ERG system from Micron III (Phoenix Research Labs). As the main photoreceptors in the retina are rods, which are specialized for high sensitivity under dark conditions, mice must be dark-adapted to record the response of the entire retina.

Mice were dark-adapted overnight and the whole procedure was performed in an adapted room under dim red light. Mice were anesthetized with inhaled 2% isoflurane and pupils were dilated with 1% tropicamide before placing them on a heating pad to maintain body temperature. A reference electrode was placed subcutaneously in the head; a ground electrode in the tail and the recording electrode was connected to a gold-plate objective lens, which was coupled to the mouse cornea. One drop of Methocel was applied to ensure complete contact with the lens and to avoid the cornea to dry.

ERG responses were recorded with the LabScribe-3 ERG Software (iWorx Systems, Inc.) after a light stimulation at 7 different intensities (-1.7, -1.4, -0.8, -0.2, 0.4, 1 and 1.6 log cd·s/m<sup>2</sup>), from low to high. The duration of the stimulus was set in 1 millisecond (ms), and 6 to 10 swipes for each intensity were recorded. A progressive interval of time between intensities was set to allow the recovery of the retina.

The analysis of the recordings was performed with the same software, extracting the main components of the ERG (amplitude of a- and b-waves and their implicit times) and the oscillatory potentials (amplitudes and implicit times for each peak).

The ERG amplitude and implicit times of *DKOrd8* and C57BL/6N mice at the different flash intensities and ages were compared by applying a two-way ANOVA with a Sidak's multiple



comparison test. The software used for this purpose was the GraphPad Prism 8 Software. Between 12 and 14 eyes per group were analyzed and significant differences were established when P-values were inferior than 0.05.

## **1.6. AOxNPs synthesis and administration**

Antioxidant nanoparticles were prepared by the Pharmacokinetic Nanoparticles group led by Dr. Puentes at Vall d'Hebron Research Institute. Nanoparticles were purified by centrifugation, resuspended in an aqueous solution of 10 mM TMAOH and stored at 4°C until their use. Its surface charge (Z-potential) was characterized in a Zetasizer (Malvern Panalytical).

AOxNPs were used for in vitro testing (detailed in section MM.3, page 53) and in vivo experiments. For the in vivo animal experimentation, AOxNPs were administered to C57BL/6N and *DKOrd8* mice through both intravitreal and topical administration. For each delivery route, AOxNPs were prepared accordingly.

### **1.6.1 Biodistribution experiments**

The biodistribution experiments consisted in the comparison of intravitreal and topical administration of AOxNPs in C57BL/6N mice, to evaluate the efficiency of both delivery routes.

#### **1.6.1.1. Intravitreal injection**

For intravitreal injection, AOxNPs at 10 mM were conjugated with murine serum albumin to stabilize the solution and avoid nanoparticles aggregation once injected into the vitreous.

Mice were anesthetized with inhaled 2% isoflurane in an induction chamber and their pupils were dilated with one drop of 1% tropicamide. Each mouse was placed sideways on a heating pad with an anesthetic mask, exposing the eye to inject. A 36-gauge beveled needle assembled to a 10 µl syringe (Nanofil, World Precision Instruments) was inserted in the sclera at approximately 1 mm from the superior limbus and 1.5 µl of AOxNPs at 10 mM were administered. Right after the injection, one drop of tobramycin combined with dexamethasone (Tobradex™ 1 mg/ml + 3 mg/ml, Alcon Laboratories) was applied to the injected eye to prevent infections. The eye fundus was also visualized with the Micron III Imaging platform to corroborate a proper injection. The eyes in which the lens appeared punctured or some hemorrhage had occurred were discarded.

### 1.6.1.2. Topical administration

For topical administration, a specific solution of AOxNPs was prepared to facilitate a longer presence in the surface of the cornea after the application of a drop, increasing the absorption period.

Mice were slightly anesthetized with inhaled 2% isoflurane to guarantee the correct absorption of the treatment. Once anesthetized, 5  $\mu$ l of AOxNPs at 10 mM were placed on the surface of the cornea using a micropipette. Mice received the same treatment in both eyes to avoid cross-contamination.

### **1.6.2. Treatment of the DKOrd8 model**

The therapeutic efficacy of AOxNPs through topical administration was evaluated in DKOrd8 mice. Mice were randomly distributed into treatment or placebo groups and topical administration was performed as explained above: mice were slightly anesthetized and one drop of the correspondent formulation was applied to each eye. Mice in the treatment group received AOxNPs at 10 mM; whereas mice in the placebo group received a formulation without AOxNPs.

## **2. Post-mortem animal experimentation**

### **2.1. Tissue processing and histology**

For histological evaluation, mice were anesthetized with an intraperitoneal administration of ketamine:xylazine (1:0.3 ml) (Ketolar 50 mg/ml, Pfizer and Xilagesic 2%, Laboratorios Calier). Next, they were transcardially perfused first with 1X phosphate-buffered saline (PBS) to remove blood, and second with a 4% paraformaldehyde (PFA) (Formaldehyde aqueous solution 37%, Panreac) flush to fixate the tissues. A stitch was performed in the upper part of each eye, to enable the anatomical identification of the superior and inferior retina before the eyes were enucleated. Following enucleation, the eyes were fixed with PFA 4% at RT during 4 hours and were dehydrated and embedded in paraffin blocks. The embedded eyes were sectioned along the inferior-superior axis with a microtome making slices of 4  $\mu\text{m}$  of thickness. The resulting slides were stored at 4°C until further use.

#### **2.1.1. Hematoxylin and eosin staining**

Central retina sections were deparaffinized by heating the slides at 65°C during 1 hour. The slides were rehydrated in a graded ethanol series and washed with dH<sub>2</sub>O. They were fixed and permeabilized with ice-cold methanol/acetic solution (95:5 v/v) and washed with H<sub>2</sub>O. Following permeabilization, the slides were stained with hematoxylin (Química Clínica Aplicada. Ref. 995960) for 2 minutes, and with eosin (Alfa Aesar GmbH & Co. Ref. B24535) for 1 minute. Next, they were dehydrated in a graded ethanol series and immersed in xylene for 3 minutes. Eventually, they were mounted with DPX (Sigma. Ref. 06522) and covered with a coverslip before being visualized in a bright field Olympus BX61 microscope.

#### **2.1.2. Immunofluorescence in paraffin-embedded slides**

Central retina sections were deparaffinized by heating the slides at 65°C during 1 hour, rehydrated in a graded ethanol series and washed with dH<sub>2</sub>O. Afterwards, they were fixed and permeabilized with ice-cold methanol/acetic solution (95:5 v/v) and washed 3-4 times with PBS 1X. Heat-induced antigen retrieval was performed in a pressure cooker. Briefly, slides were immersed in citrate buffer pH 6 (1.92 g citric acid (anhydrous) and 0.5 ml Tween-20 for 1 liter of buffer) in a closed metal box and the pressure cooker was filled with dH<sub>2</sub>O. Samples were

incubated for 4 minutes once the cooker reached full pressure. After, the cooker was depressurized and the slides were cooled down allowing the antigenic site to re-form after the exposure to high temperatures. Samples were afterwards blocked for 1 hour at RT with 3% Bovine Serum Albumin (BSA, Sigma. Ref. A7906) and/or 1% Normal Goat Serum (NGS, Sigma. Ref. G9023) in PBS 1X with slight variations depending on the antibody used. After blocking, primary antibodies were diluted as shown in table MM.2 and incubated overnight at 4°C. The following day, the slides were washed 3 times during 10 minutes with PBS 1X and incubated 1 hour at RT with the secondary antibody. Slides were washed 4 more times with PBS 1X before mounting them with mounting medium containing DAPI (4',6-diamidino-2-phenylindole) (Fluoroshield, Sigma. Ref F6057). The slides were visualized and imaged in the Olympus Confocal Microscope (FluoView ASW 1.4; Olympus).

**Table MM.2. List of antibodies used.**

| <b>Primary antibodies</b> |                                 |                                  |                 |                                      |
|---------------------------|---------------------------------|----------------------------------|-----------------|--------------------------------------|
| <b>Antibody</b>           | <b>Target</b>                   | <b>Host specie</b>               | <b>Dilution</b> | <b>Source &amp; Catalogue number</b> |
| GFAP                      | Müller glia                     | Rabbit                           | 1:250           | Abcam, ab7260                        |
| IBA1                      | Microglia cells                 | Rabbit                           | 1:100           | Wako, 019-19741                      |
| RPE65 3D9                 | RPE cells                       | Mouse                            | 1:150           | Santa Cruz, sc-73616                 |
| 8OHdG                     | DNA                             | Mouse                            | 1:75            | Abcam, ab62623                       |
| Lectin – FITC conjugated  | Endothelial cells and microglia | Lycopersicon esculentum (Tomato) | 1:100           | Sigma, L0401                         |
| Opsin                     | Cone photoreceptors             | Rabbit                           | 1:100           | Antibodies online, ABIN350673        |
| Rhodopsin                 | Rod photoreceptors              | Mouse                            | 1:250           | Sigma, O4886                         |
| Synaptophysin SP15        | Pre-synaptic vesicles           | Mouse                            | 1:100           | Millipore, MAB329C                   |
| Recoverin                 | Photoreceptors                  | Rabbit                           | 1:250           | Millipore, AB5585                    |
| Calbindin                 | Horizontal cells                | Mouse                            | 1:50            | Swant, 300                           |

## Secondary antibodies

| Antibody            | Target      | Host specie | Dilution | Source & Catalogue number |
|---------------------|-------------|-------------|----------|---------------------------|
| Alexa Fluor IgG 488 | Anti-rabbit | Goat        | 1:500    | ThermoFisher, A11008      |
| Alexa Fluor IgG 488 | Anti-mouse  | Goat        | 1:500    | ThermoFisher, A11029      |
| Alexa Fluor IgG 568 | Anti-rabbit | Goat        | 1:500    | ThermoFisher, A11036      |
| Alexa Fluor IgG 568 | Anti-mouse  | Goat        | 1:500    | ThermoFisher, A11004      |

### 2.1.3. Immunofluorescence in flat-mounted RPE and retina

Mice were euthanized with inhaled CO<sub>2</sub> and eyes were immediately enucleated and fixated with 4% PFA for 1 hour at RT. Next, the eyes were washed with PBS 1X and dissected under the stereomicroscope in ice-cold PBS 1X. The anterior segment of the eye was cut through the limbus, and the cornea, iris and lens were all removed. Retina was separated from the RPE-choroid-sclera complex and both parts were flattened by making four radial cuts as shown in figure MM.3.

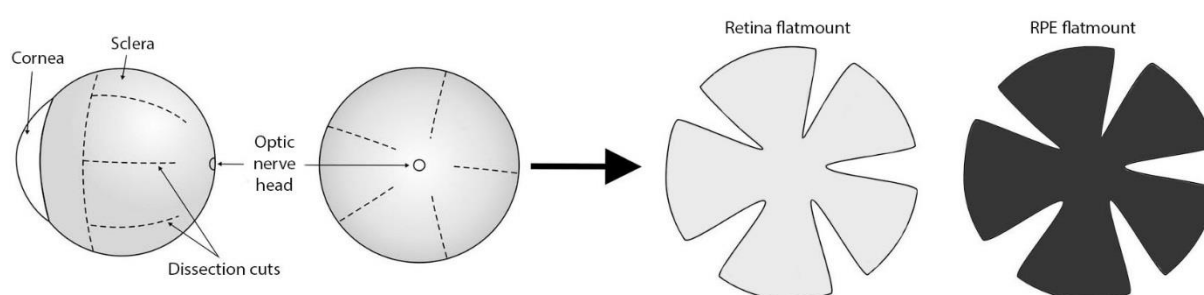


**Figure MM.3. Representative diagram of the eye dissection and the RPE/retina flatmounting.** After getting rid of the anterior segment of the eye, the neural retina on one hand, and the posterior pole on the other, are separated and cut to flatten the complex. Modified from Pijanka et al. 2014

RPE and retinal flatmounts were placed in a 48-well plate with PBS 1X. Retinal flatmounts were fixed again with methanol:acetic acid (95:5) at -20°C for 2 minutes and washed afterwards twice

with PBS 1X. Following fixation, both RPE and retinal flatmounts were blocked with 3% BSA and 0.3% Triton X-100 (Sigma, Ref. T8787) in PBS 1X for 1 hour at RT with gentle shaking. Once the samples were blocked, they were incubated with primary antibodies overnight at 4°C (Table MM.3). The following day, samples were washed three times with 0.3% Triton X-100 in PBS 1X with gentle shaking. The secondary antibody was incubated for 1 hour at RT and flatmounts were washed again three times. RPE flatmounts were mounted so that RPE stayed upwards. Regarding retinal flatmounts, the ganglion cell layer was placed upwards. Both samples were mounted using a mounting medium containing DAPI, and covered with a coverslip before their visualization under the confocal microscope (FluoView ASW 1.4, Olympus). The images taken were further used to quantify Iba1 positive cells using the Cell Counter plugin in ImageJ software.

For RPE flatmounts, all Iba1 positive cells per flatmount were counted. In flatmounted retinas, Iba1 positive cells from four different regions were counted. Statistical analyses in both cases were performed by applying a one-way ANOVA with a Tukey's multiple comparison test. Significance differences were established when P-values were inferior than 0.05.

**Table MM.3. List of antibodies used for the flatmounts.** References of each antibody are specified in table MM.2

|                          | Primary antibody and dilution | Secondary antibody and dilution |
|--------------------------|-------------------------------|---------------------------------|
| <b>RPE flatmounts</b>    | Iba1 (rb) (1:150)             | Anti-rb 488 (1:300)             |
|                          | RPE65 (m) (1:150)             | Anti-m 568 (1:300)              |
| <b>Retina flatmounts</b> | Iba1 (rb) (1:300)             | Anti-rb 488 (1:400)             |

## **2.2. Gene expression analysis**

The expression profile of *DKOrd8* mice was studied with a microarray analysis. This technique is based on the detection of fluorescence intensity emitted by cDNA fluorescently labelled after the hybridization to a probe sequence (Churchill 2002). In a microarray, thousands of specific probes are attached to a chip allowing the study of the whole genome expression profile.

### **2.2.1. RNA extraction**

The first step of the procedure was the RNA extraction. For that purpose, mice were euthanized with inhaled CO<sub>2</sub> and eyes were immediately enucleated and kept in *RNAlater*<sup>™</sup> Stabilization Solution (AM7020, Invitrogen, ThermoFisher Inc.) before being dissected under the stereomicroscope. The posterior pole of the eye (retina + RPE + choroid + sclera) was obtained by cutting the anterior segment through the limbus and removing the cornea, iris and lens. Once obtained, it was transferred into a microcentrifuge tube containing 140 µl of TRI Reagent<sup>™</sup> (T9424, Sigma-Aldrich), frozen in liquid nitrogen and stored at -80°C until RNA extraction.

Total RNA was isolated from the posterior pole using the PureLink RNA Mini Kit (Ref. number 12183018A, ThermoFisher Inc.), following manufacturer's instructions. The quality of the isolated RNA was later measured by capillary electrophoresis (Bioanalyzer 2100, Agilent).

### **2.2.2. Microarrays**

Microarrays service was carried out by the High Technology Unit (UAT) at Vall d'Hebron Research Institute, using a GeneTitan System (Affymetrix, Thermo Fisher Scientific). A plate containing 24 Clariom S arrays was used for this particular experiment. These arrays provide an accurate measurement of the mouse transcriptome at a gene-level by using probes covering more than 20.000 well-annotated genes, distributed through constitutive exons.

Briefly, 180 ng of total RNA from each sample were used as starting material. Single stranded-cDNA suitable for labelling was generated from total RNA using the WT Plus Reagent Kit (Thermo Fisher Scientific), according to the manufacturer's instructions. After, purified sense-strand cDNA was fragmented, labelled and hybridized to the arrays using the GeneTitan Hybridization, Wash and Stain Kit for WT Plates (Thermo Fisher Scientific). The plate was loaded into the GeneTitan and, after array scanning, raw data quality control was performed to check the performance of the whole processing.

### **2.2.3. Bioinformatic analyses**

After the quality control, a complete bioinformatic analysis was performed at the Statistics and Bioinformatics Unit (UEB) of the Vall d'Hebron Research Institute. The selection of differentially expressed genes was based on a linear model analysis with empirical Bayes modification for the variance estimates. P-values were adjusted to obtain stronger control over the false discovery rate (FDR). All the analyses were performed using the R version 3.5.3 software and Bioconductor libraries.

The analysis of biological significance was based on an enrichment analysis against the Gene Ontology database (GO, The Gene Ontology Consortium, 2019). The resulting data was also analyzed with Cytoscape software (Cytoscape Consortium, 2019).

## **2.3. ICP-MS analysis**

Biodistribution of the antioxidant component in wt mice was evaluated through Inductively Coupled Plasma Mass Spectrometry (ICP-MS), a type of mass spectrometry capable of detecting metals at concentrations as low as one part per quadrillion (ppq,  $10^{15}$ ). This precise detection is achieved by ionizing the sample with inductively coupled plasma and then by using a mass spectrometer to separate and quantify those ions.

### **2.3.1. Tissue obtainment**

Mice were euthanized with inhaled CO<sub>2</sub> and the eyes, the liver and the brain from each of them were collected. Livers and brains were weighted and kept at -80°C until further analyses. Eyes were fixed with 4% PFA for 30 minutes at RT before dissecting their different components. The ocular components analyzed were (i) the cornea and the iris (referred to as anterior pole), (ii) the lens, (iii) the retina and (iv) the posterior pole, which contained the retinal pigment epithelium, the choroid and the sclera. All the eye components were also weighted with a high precision scale before storing them at -80°C.



### **2.3.2. Tissue digestion and ICP-MS analysis**

Tissue digestion and ICP-MS analyses were carried out in collaboration with Dr. Puntès lab at the Catalan Institute of Nanoscience and Nanomaterials (ICN2). In brief, samples were diluted with an aqueous solution of HNO<sub>3</sub> 2% w/w (Trace Metal Basis; Sigma) and analyzed for the antioxidant compound concentration by ICP-MS (Agilent Technologies 7500ce; Agilent Tech.).

### **3. Cell culture**

#### **3.1. Cell maintenance**

ARPE19 (Adult Retinal Pigment Epithelial cell line 19) cells were used in all experiments. ARPE19 is an immortalized cell line derived from human RPE, from a 19-years old male donor. This line was given to us from Dr. Pedraz group, at University of the Basque Country. Cells were maintained in Dulbecco's Modified Eagle Medium/Nutrient Mixture F12 (DMEM/F12) supplemented with GlutaMAX™ (Gibco, ThermoFisher Inc. Ref. 10565018). This basal medium was supplemented with 10% of Fetal Bovine Serum (FBS) (Gibco, ThermoFisher Inc. Ref. 10270) and with the antibiotics streptomycin and penicillin (Gibco, ThermoFisher Inc. Ref. 15140122). Basal medium with all the complements is further referred to as complete medium. Complete medium was changed twice a week and the subculture was performed every week once the cells reached confluence in 75 cm<sup>2</sup> flasks. In brief, cells were washed once with PBS 1X and after that 3 ml of trypsin (Gibco, ThermoFisher Inc. Ref. 15400054) were added. Cells were incubated 2 minutes at 37°C until they were detached. Next, 6 ml of complete medium were added to inactivate the trypsin. After trypsin inactivation, the cellular suspension was transferred into a 15 ml tube and centrifuged for 5 minutes at 1200 rpm. Once the cells precipitated, the medium was removed and the cells were resuspended in new complete medium. Cell counting was performed with the Neubauer Chamber, and 500.000 or 1 million cells were seeded in the new flask. Cells were maintained in the incubator at 37°C with 5% CO<sub>2</sub>.

#### **3.2. Cell viability assay**

Cell viability was assessed through an MTT assay in ARPE19 cells treated with CeO<sub>2</sub>NPs at different concentrations. For all the in vitro experiments, AOxNPs were synthesized as explained previously in section MM.1.6 (page 44) and the 10 mM aqueous solution of AOxNPs in TMAOH was used as stock solution.

The MTT assay is a colorimetric assay based on the metabolic reduction of tetrazolium dye 3-(4,5-dimethylthiazol-2-yl)-2,5-diphenyltetrazolium bromide (MTT) into its insoluble form called formazan, which has a purple color. It can be used to assess cytotoxicity, as the number of alive cells is directly proportional to the coloring of the well.

For this purpose, 80.000 cells/ml were seeded in 24-well plates in complete medium. 36 hours after seeding, cells were washed with PBS 1X and then AOxNPs were added into each well at the final concentrations of 10 nM, 50 nM, 100 nM or 500 nM. Cells were incubated with the AOxNPs treatment (in DMEM-F12 + 10% FBS) for 24 or 48 hours and cell viability was measured afterwards through the MTT assay. After the different periods of incubation, 100 µl of MTT solution (VWR, LLC. Ref. 10005-370) were added per well and cells were incubated for 4 hours. The medium was then removed and 300 µl of Dimethyl Sulfoxide (DMSO, Sigma. Ref. D8418) were added into each well to dissolve the formazan crystals. Absorbance was measured in a plate reader at the emission wavelength of 590 nm.

ARPE19 cells with no treatment were used as a control of viability and cells treated with 40% DMSO were used as a negative control or as a control for cell death. The effect of AOxNPs in the viability of ARPE19 cells was measured dividing the corrected absorbance (or OD, for optical density) of our samples ( $OD_{590}(\text{sample}) - OD_{590}(\text{negative control})$ ) by the absorbance of the viability control ( $OD_{590}(\text{viability control}) - OD_{590}(\text{negative control})$ ) and expressed as a percentage.

$$\text{Cell viability} = \frac{OD_{590}(\text{sample}) - OD_{590}(\text{negative control})}{OD_{590}(\text{viability control}) - OD_{590}(\text{negative control})} \times 100$$

A total of three independent experiments with 4 replicates per condition were performed and analyzed, giving a total of 12 data sets per condition. Viability was compared between all the different groups by applying a one-way ANOVA with a Dunnet's multiple comparison test, using the GraphPad Prism 8 software. Statistical differences were established when P-values were inferior than 0.05.

### 3.3. Intracellular ROS measurement

The antioxidant capacity of AOxNPs was assessed in ARPE19 cells with induced oxidative stress using the 2',7'-dichlorodihydrofluorescein diacetate (H<sub>2</sub>DCFDA) probe (ThermoFisher. Ref. D399). This probe is a chemically reduced form of fluorescein, which upon cleavage of the acetate groups by intracellular esterases and oxidation, is converted into the highly fluorescent 2',7'-dichlorofluorescein (DCF) (Figure MM.4). It is used to detect the generation of reactive oxygen species (ROS) in cells, as an increase of intracellular ROS is traduced into an increase in the amount of fluorescence emitted.

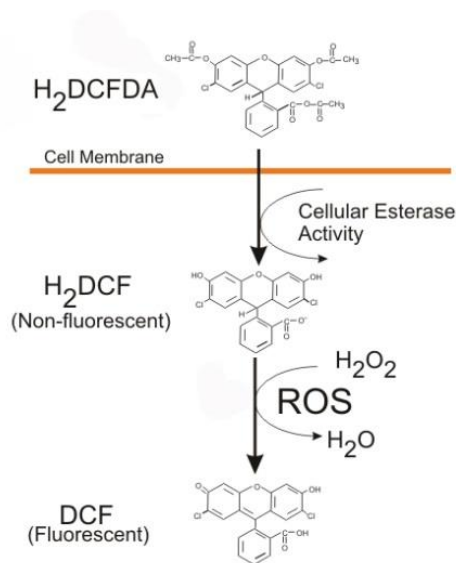


**Figure MM.4. DCF fluorescent formation.** The cell-permeant H<sub>2</sub>DCFDA diffuses passively into cells and is retained at the intracellular level after cleavage by esterases. Upon oxidation by ROS, the resulting non-fluorescent H<sub>2</sub>DCF is converted to the highly fluorescent DCF. Image from Held 2015.

For this purpose, 80.000 cells/ml were seeded into 24-well plates in complete medium. After 36 hours, cells were washed with PBS 1X and a pretreatment with AOxNPs was added into each well at final concentrations that ranged from 1 nM to 500 nM. After a 24 hours incubation, the H<sub>2</sub>DCFDA assay was performed.

Cells were washed once with PBS 1X to eliminate the excess of AOxNPs, and in parallel, the H<sub>2</sub>DCFDA probe was prepared at 10 μM in DMEM-F12 + 0.5% FBS. Once the cells were washed and the probe prepared, 500 μl of the probe were added into each well and plates were incubated at 37°C for 30 minutes. From this point, the following steps of the procedure were performed in the dark to avoid photo-oxidation.

After the incubation, oxidative stress was induced with different oxidizing agents depending on the experiment. The three agents used were (i) hydrogen peroxide (H<sub>2</sub>O<sub>2</sub>) at 300 μM, (ii) antimycin A at 50 μM and (iii) *tert*-Butyl hydroperoxide (tBH) at 250 μM (tBH 70% aq. Sol. AlfaAesar, ThermoFisher Inc. Ref. A13926). Once added into the correspondent well, they were

incubated for 1 hour at 37°C. Afterwards, cells were washed once with PBS 1X, and 200 µl of cell lysis buffer (20 mM Tris-HCL, 150 mM NaCl, 1 mM EDTA and 1% Triton X-100) were added into each well and incubated for 5 minutes at RT. After homogenizing the lysate, 50 µl from each well were transferred into a 96-well black microplate and fluorescence was immediately read with a spectrofluorometer (Appliskan, ThermoFisher) at an excitation and emission wavelengths of 485/20 nm and 528/20 nm respectively.

ARPE19 cells with no induction of oxidative stress were used as a control for basal levels of oxidative stress and cells not treated with H<sub>2</sub>DCFDA were used as blank. The effect of AOxNPs was measured dividing the corrected fluorescence intensity (FI) of our samples (FI<sub>(sample)</sub> – FI<sub>(blank)</sub>) by the intensity of the control (FI<sub>(control)</sub> – FI<sub>(blank)</sub>). A total of three independent experiments with 4 replicates per condition were performed and analyzed, giving a total of 12 data sets per condition. Statistical analyses were performed by applying a one-way ANOVA with a Dunnet's multiple comparison test, using the GraphPad Prism 8 software. Significant differences were established when P-values were inferior than 0.05.

### **3.4. Gene expression analyses**

Gene expression changes in AOxNPs-treated ARPE19 cells after inducing oxidative stress were evaluated through quantitative PCR. This technique allows for the measurement of the amount of copies of a RNA transcript of a specific gene which is present in a sample after the amplification of this transcript. Therefore, gene expression differences can be evaluated.

#### **3.4.1. RNA extraction and retrotranscription**

In brief, 100.000 cells/well were seeded in 12-well plates with complete medium. After 36 hours, cells were washed once with PBS 1X, a pretreatment with AOxNPs was added at the final concentrations of 50 nM and 500 nM, and cells were incubated overnight. The following day, oxidative stress was induced by incubating cells with tBH at 250 µM for 4 hours. Next, cells were washed with PBS 1X and 200 µl of TRI Reagent were added into each well. Cells were scrapped, transferred into a microcentrifuge tube, frozen in liquid nitrogen and stored at -80°C until RNA extraction.

For RNA extraction, samples were incubated for 5 minutes at RT to disrupt all the RNA-protein complexes and 0.2 ml of chloroform per ml of Trizol used were added. Samples were vortexed during 30 seconds and incubated 3 minutes at RT to allow phase separation. Next, samples were centrifuged at 12.000 *g* for 15 minutes at 4°C, the aqueous phase was transferred into a new tube, and 0.5 ml of isopropanol per ml of Trizol used were added. Samples were then mixed and incubated at RT for 10 minutes before being centrifuged at 16.000 *g* at 4°C for 20 minutes. Later, the supernatant was removed and the pellet containing the RNA was washed with 200 µl of ethanol 75%. Samples were centrifuged at 7500 *g* for 10 minutes at 4°C, the supernatant was discarded and the pellet was air-dried before being resuspended in 20 µl of RNase-free water. The quality and quantity of the RNA was determined by running an agarose gel and taking spectrophotometric readings (Nanodrop™, Thermo Scientific).

RNA was treated with DNase I (Invitrogen Ref. 18068015) to remove any remaining DNA. Once the RNA was DNAsed, cDNA was synthesized from 2 µg of purified RNA using the High-Capacity cDNA Reverse Transcription Kit (Applied Biosystems Ref. 4368814) and oligo(dT)<sub>18</sub> primers (Thermo Scientific, Ref. SO132) following manufacturer's instructions.

### **3.4.2. Quantitative Polymerase Chain Reaction (qPCR)**

Quantitative PCR was performed on the resulting cDNA using the LightCycler™ 480 SYBR Green I Master kit (Roche, Ref. 04887352001) and the LightCycler™ 480 Instrument (Roche). In brief, cDNA from each sample was diluted 1:10 and mixed with the Green I Master buffer, which contained a FastStart Taq DNA polymerase, reaction buffer, dNTPs SYBR Green I dye and MgCl<sub>2</sub>. Specific primers were also added to the reaction. Three separate experiments were analyzed, with six replicates performed for each sample, giving a total of eighteen data sets.

The expression of the targeted genes was normalized to the housekeeping gene GAPDH. Sequences of primers used in this assay are listed below.

**Table MM.4. Primers used for in vitro gene expression analyses**

| <b><i>SOD2</i> primers</b> |                              |
|----------------------------|------------------------------|
| Forward                    | 5'- GTAGCACCAGCACTAGCAG -'3  |
| Reverse                    | 5'- CGTTGATGTGAGGTTCCAGG -'3 |

| <b><i>Nrf2</i> primers</b> |                              |
|----------------------------|------------------------------|
| Forward                    | 5'- AGCACATCCAGTCAGAAACC -'3 |
| Reverse                    | 5'- CGTAGCCGAAGAAACCTCA -'3  |

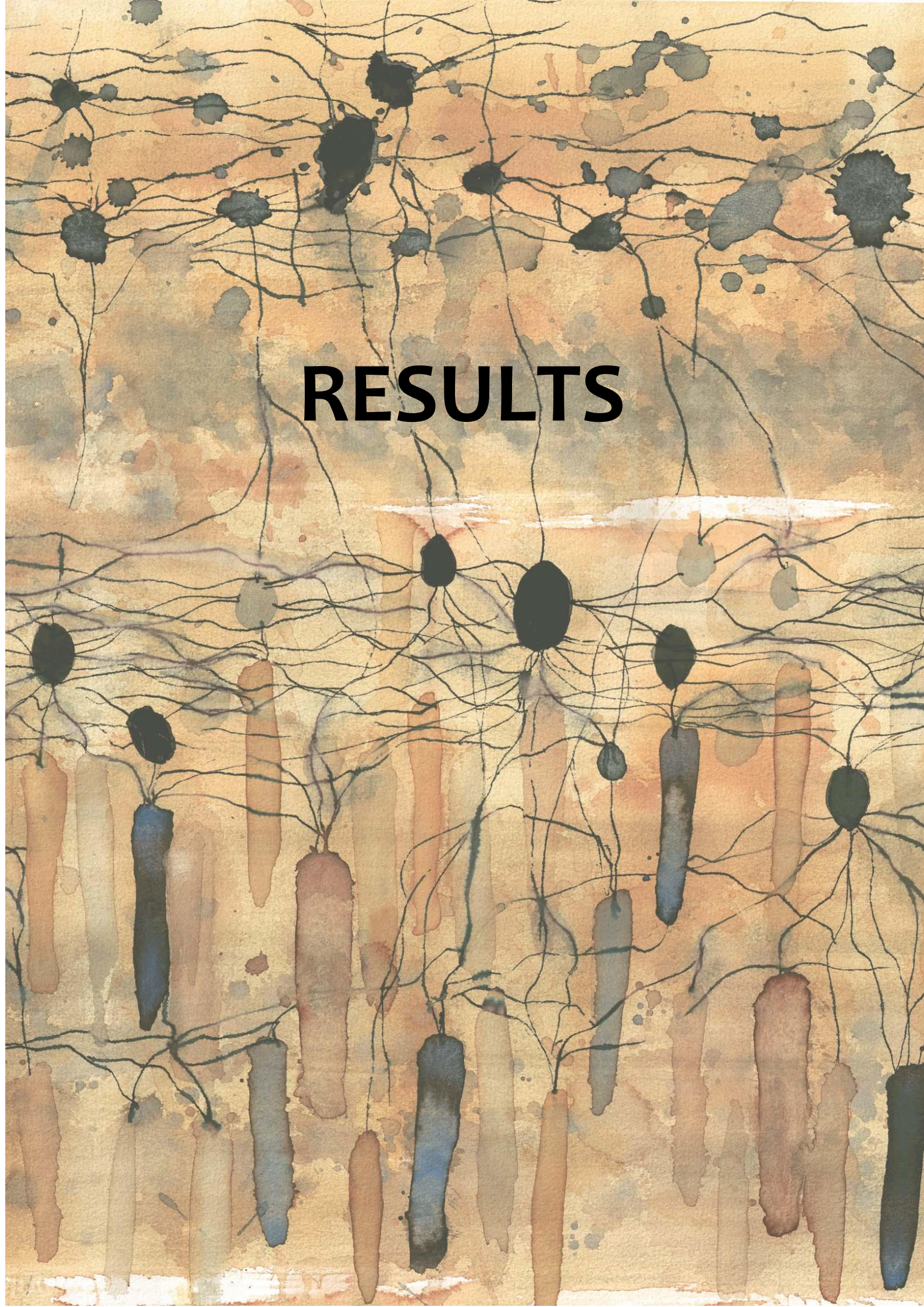
| <b><i>NOX4</i> primers</b> |                                |
|----------------------------|--------------------------------|
| Forward                    | 5'- AGTTTTGGCAAGAGAACAGACC -'3 |
| Reverse                    | 5'- TCCACCGAGGACGTCCTATAA -'3  |

| <b><i>HO1</i> primers</b> |                               |
|---------------------------|-------------------------------|
| Forward                   | 5'- TCAGGCAGAGGGTGATAGAAG -'3 |
| Reverse                   | 5'- TTGGTGTCATGGGTCAGC -'3    |

| <b><i>GAPDH</i> primers</b> |                               |
|-----------------------------|-------------------------------|
| Forward                     | 5'- GGTATCGTGGAAGGACTCATG -'3 |
| Reverse                     | 5'- GTAGAGGCAGGGATGATGTTC -'3 |

The background is an abstract watercolor composition. It features a dense network of thin, black, branching lines that resemble a neural network or a complex web. These lines are set against a wash of warm, earthy colors, including shades of tan, beige, and light brown. Interspersed among the lines are various organic, blotchy shapes in darker tones, such as deep blue, charcoal, and dark brown. Some of these shapes are elongated and vertical, while others are more rounded or irregular. The overall effect is one of intricate, organic complexity.

# RESULTS





## Chapter 1. Generation and characterization of the DKOrd8 mouse

---

The first goal of this thesis was the obtainment of a reliable model mimicking the aged-related macular degeneration (AMD) phenotype in humans. For that purpose, we aimed to generate the *Ccl2*<sup>-/-</sup>; *Cx3cr1*<sup>-/-</sup>; *Crb1*<sup>rd8/rd8</sup> mouse model, which has already been described to recapitulate certain features of AMD. Once generated, we aimed to characterize it through in vivo and post-mortem assessments to corroborate its phenotype and acquire a deeper knowledge of their pathogenic characteristics.



## 1. The DKOrd8 mouse is generated by crossing three different mouse strains

In the last years, the double knockout mouse for *Ccl2* and *Cx3cr1* genes together with the presence of the *rd8* mutation in the *Crb1* gene, has gained importance as a model for dry AMD thanks to the early onset of certain AMD-like features. Until now, these mice had only been generated and used by Tuo et al. and although partially characterized by them, a better understanding of their phenotype is needed to develop and test new therapies for AMD.

As these mice are not commercially available, we planned to generate our own *Ccl2*<sup>-/-</sup>; *Cx3cr1*<sup>-/-</sup>; *Crb1*<sup>rd8/rd8</sup> mice colony, further referred to as DKOrd8, starting from the *Ccl2* and *Cx3cr1* single knockout mice and the C57BL/6N mice with the *Crb1*<sup>rd8/rd8</sup> mutation.

Four couples of *Cx3cr1* knockout mice [B6.129P-*Cx3cr1*<sup>tm1Litt/J</sup>] were handed over to us by a researcher of our center. We genotyped them for *Cx3cr1* to confirm that all mice were homozygous for the mutant form of the allele (Figure R.1A). Although these mice were supposed to have a 6J background (characterized by the absence of the *rd8* mutation), we also genotyped them for the *rd8* mutation in the *Crb1* gene to make sure the genetic background was 6J. Nonetheless, by DNA sequencing, we found out that these mice had the *rd8* mutation in homozygosis (Figure R.2). Further inquiries let us know that the original *Cx3cr1*<sup>-/-</sup> mice sent to The Jackson Laboratory repository had a mixed 6N and 6J genetic background.

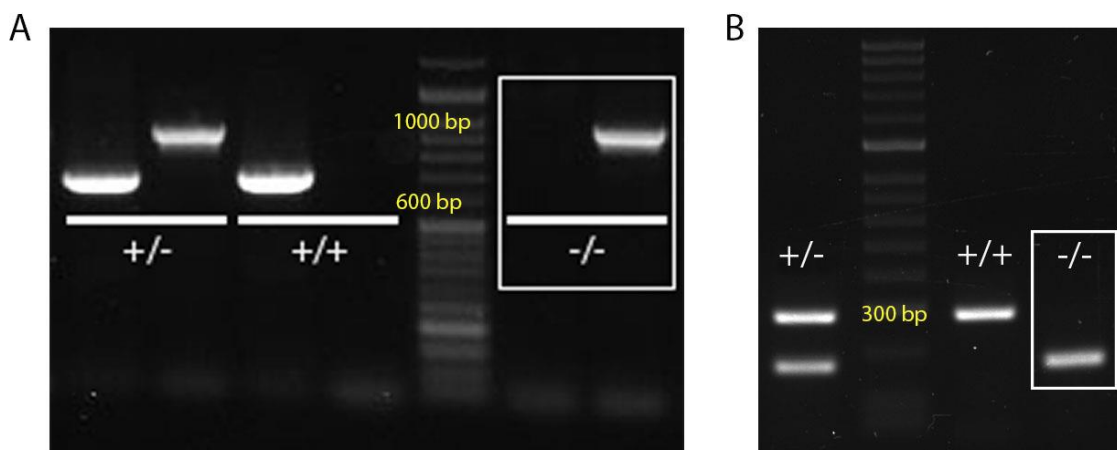


**Figure R.1. Genotyping of *Cx3cr1* and *Ccl2* genes.** (A) Representative image of an agarose gel showing the PCR product of heterozygote (+/-), homozygote for the wild type allele (+/+) and homozygote for the mutant allele (-/-) mice. *Cx3cr1* PCR yielded a wildtype band of 689 bp and a mutant band of 937 bp. (B) Representative image of an agarose gel showing the PCR product of heterozygote (+/-), homozygote for the wild type allele (+/+) and homozygote for the mutant allele (-/-) mice. *Ccl2* PCR yielded a wild type band of 287 bp and a mutant band of 179 bp.

Regarding *Ccl2*<sup>-/-</sup> mice, three females knockout for *Ccl2* [B6.129S4-*Ccl2*<sup>tm1Ro1</sup>/J] were purchased directly at The Jackson Laboratory. Upon their arrival, we genotyped them for *Ccl2*, confirming the presence of the mutant allele in homozygosity (Figure R.1 B); and for the *rd8* mutation, which was not present. We also genotyped them for *Nnt*, a single nucleotide polymorphism (SNP) marker that distinguishes the C57BL/6J and C57BL/6N substrains. All three mice presented the mutant allele in homozygosity, confirming the 6J background (data not shown).

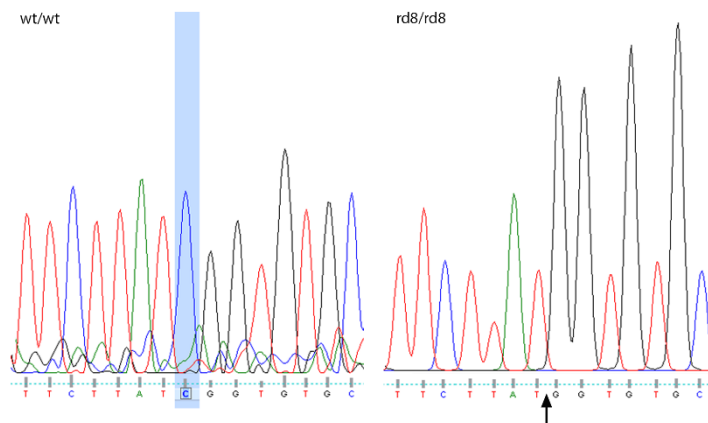


**Figure R.2. Genotyping of *rd8* allele.** Representative images of the sequences of a wt/wt mouse, without the *rd8* point mutation; and an *rd8/rd8* mouse, with a deletion in the cytosine (arrow) in the nucleotide 3.481 of the *Crb1* gene.

The C57BL/6N mice, also referred to as 6N mice, were directly purchased at Charles River Laboratories Inc. and we confirmed the presence of the *rd8* mutation in homozygosity by sequencing.

Once we had genotyped all the founders of the future colony, we started the crosses to obtain our *Ccl2*<sup>-/-</sup>; *Cx3cr1*<sup>-/-</sup>; *Crb1*<sup>rd8/rd8</sup> mice. First, we crossed *Ccl2*<sup>-/-</sup> females with C57BL/6N males (with the *rd8* mutation in homozygosity) to obtain mice with the mutant *Ccl2* and *Crb1* alleles in heterozygosity (*Ccl2*<sup>+/-</sup>; *Crb1*<sup>+/rd8</sup>) (Figure R.3). At eight weeks of age, we intercrossed these mice to obtain *Ccl2*<sup>-/-</sup>; *Crb1*<sup>rd8/rd8</sup> mice. We genotyped all the progeny and among the 92 pups obtained, a total of 8 were *Ccl2*<sup>-/-</sup>; *Crb1*<sup>rd8/rd8</sup>: 5 males and 3 females. We crossed these mice with *Cx3cr1*<sup>-/-</sup>; *Crb1*<sup>rd8/rd8</sup> mice to obtain animals with mutant *Ccl2* and *Cx3cr1* alleles in heterozygosity and the mutant *Crb1* allele in homozygosity. Once confirmed this genotype, we intercrossed *Ccl2*<sup>+/-</sup>; *Cx3cr1*<sup>+/-</sup>; *Crb1*<sup>rd8/rd8</sup> mice to finally obtain the triple knockout mice *Ccl2*<sup>-/-</sup>; *Cx3cr1*<sup>-/-</sup>; *Crb1*<sup>rd8/rd8</sup>, referred to as DKOrd8 mice. In that case, among the 71 pups obtained, 5 had the *Ccl2*<sup>-/-</sup>; *Cx3cr1*<sup>-/-</sup>; *Crb1*<sup>rd8/rd8</sup> genotype: 3 females and 2 males. We used these mice to amplify the number of *Ccl2*<sup>-/-</sup>; *Cx3cr1*<sup>-/-</sup>; *Crb1*<sup>rd8/rd8</sup> mice and settle the colony.

Thus, 12 months after the establishment of the first crosses, we successfully generated the DKOrd8 mouse.

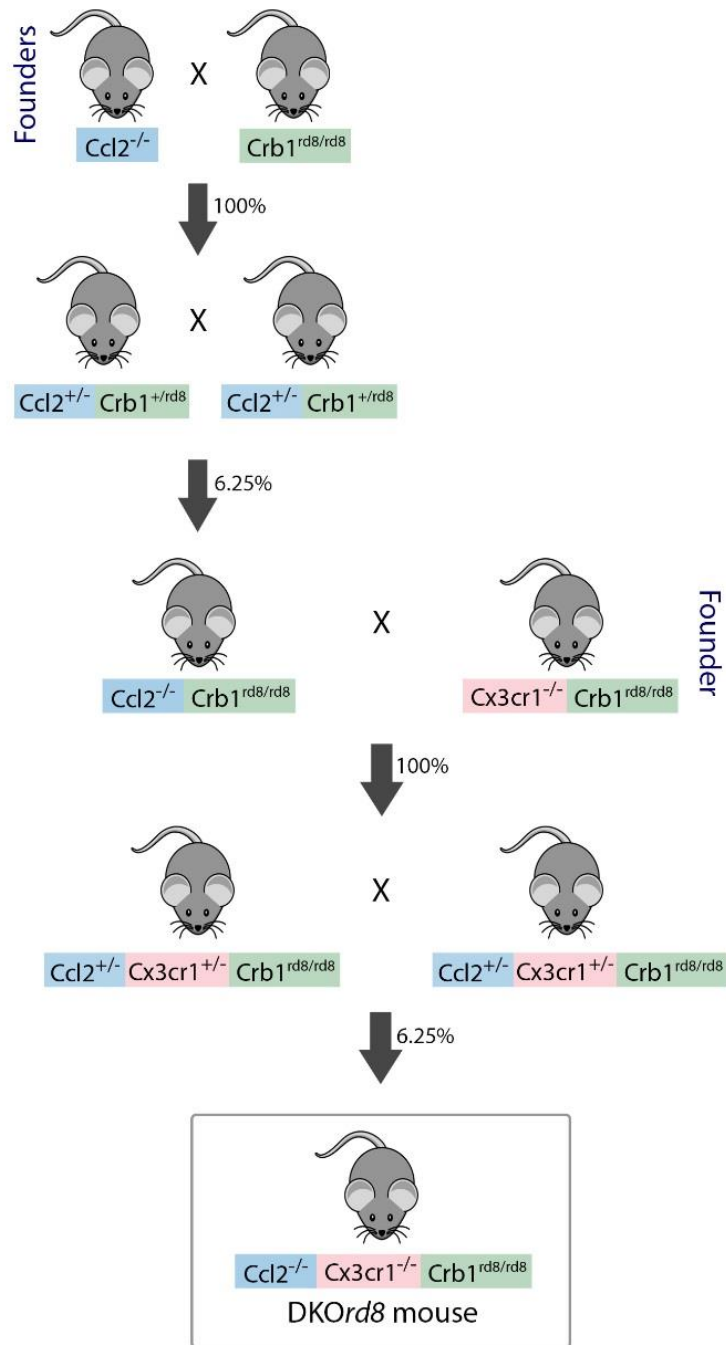


**Figure R.3. Diagram of the DKOrd8 mouse generation.**  $Ccl2^{-/-}$ ,  $Crb1^{rd8/rd8}$  and  $Cx3cr1^{-/-}$  mice were used for the generation of the DKOrd8 mouse. In brief,  $Ccl2^{-/-}$  mice were crossed with  $Crb1^{rd8/rd8}$ . The  $Ccl2^{+/-}$ ;  $Crb1^{+/rd8}$  obtained were intercrossed to produce  $Ccl2^{-/-}$ ;  $Crb1^{rd8/rd8}$  mice. The later were then crossed with  $Cx3cr1^{-/-}$  mice to generate  $Ccl2^{-/-}$ ;  $Crb1^{rd8/rd8}$ ;  $Cx3cr1^{-/-}$  mice that were again intercrossed to finally obtain the DKOrd8 mouse model. Percentages refer to the proportion of animals with that particular phenotype obtained after each crossing.

## 2. The *DKOrd8* mouse presents early eye fundus alterations and a progressive thinning of the inferior retina

To evaluate the phenotype of the recently generated *DKOrd8* colony and validate our mice as a model for dry AMD, we followed up 47 *DKOrd8* and 25 C57BL/6N mice as wild type control for nine months. During that period, we performed different in vivo assays, including the visualization of the eye fundus and optical coherence tomography of the retina.

The first in vivo assay performed in *DKOrd8* mice was the eye fundus imaging or funduscopy. This quick, non-invasive and reliable technique allows for the observation of the eye fundus and the monitoring of certain retinal conditions. Using the Micron III retinal-imaging microscope, we evaluated the retina of the same mice from 1 to 9 months of age.

At one month of age, we observed the presence of several bright spots in the inferior hemisphere of the *DKOrd8* mice eyes, more predominant in the nasal quadrant (Figure R.4). At three months, these spots appeared enlarged and less intense. The brightness of the spots kept decreasing upon ageing as well as the number of spots observed. At 9 months of age, the spots had declined and presented a more yellowish appearance. On the contrary, we did not observe abnormalities in C57BL/6N mice eyes' fundus at any of the ages analyzed.

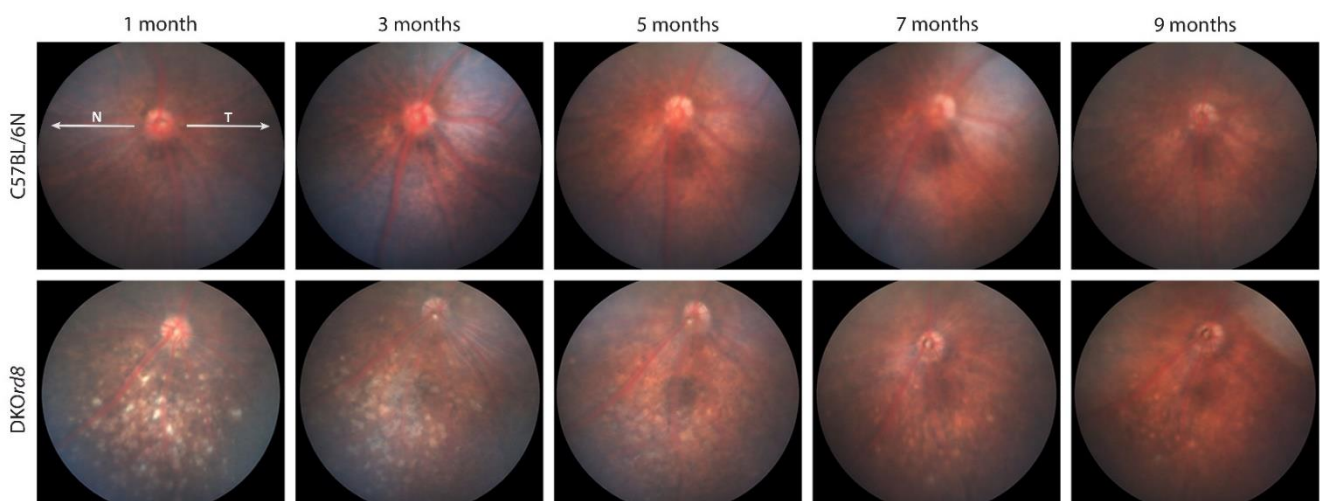


**Figure R.4.** In vivo assessment of retinal status in *DKOrd8* and C57BL/6N mice with funduscopy. Eye fundus images of the inferior hemisphere of the left eye of *DKOrd8* and C57BL/6N mice taken at 1, 3, 5, 7 and 9 months of age. Arrows indicate the temporal (T) and nasal (N) parts of the eye.

To determine in which retinal layer were located these spots, we performed Optical Coherence Tomography (OCT). This non-invasive technique offers an *in vivo* cross-sectional view of the retina and of all its layers allowing the study of the different layers separately. We evaluated periodically the same mice with an image-guided OCT scan attached to the Micron III platform.

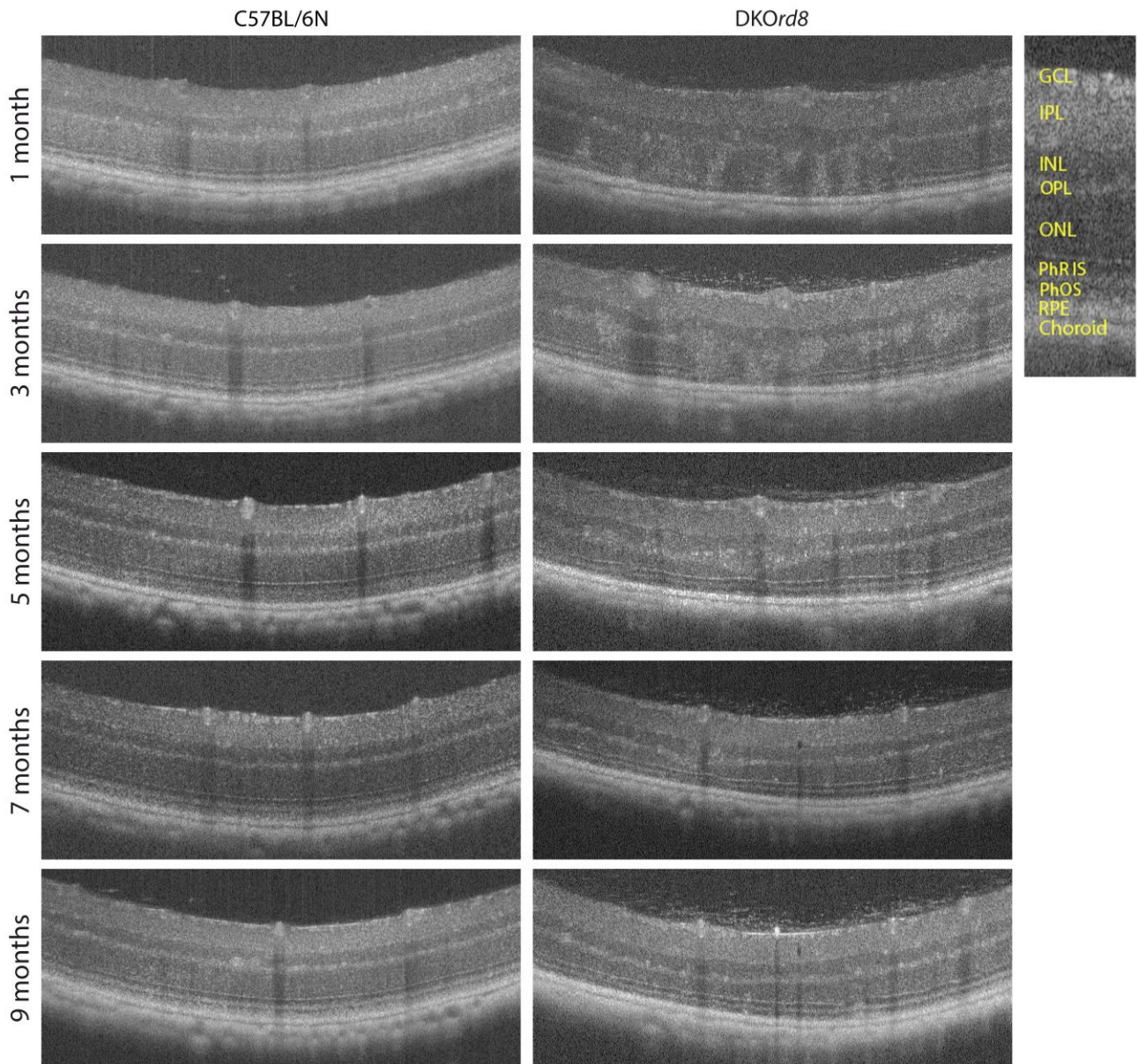


**Figure R.5. OCT evaluation of the retina status in DKOrd8 and C57BL/6N mice.** OCT imaging performed in the inferior retina of the same mice shown in Figure R.4, at 1, 3, 5, 7 and 9 months of age. GCL, ganglion cell layer; IPL, inner plexiform layer; INL, inner nuclear layer; OPL, outer plexiform layer; ONL, outer nuclear layer; PhRIS, photoreceptor inner segments; PhOS photoreceptor outer segments; RPE, retinal pigment epithelium.



At one month of age, we observed numerous hyper-reflective areas located in the outer nuclear layer of *DKOrd8* mice (Figure R.5). Most of them expanded from the OPL through the ONL and the photoreceptor inner and outer segments layer, without disrupting the retinal pigment epithelium. At 3 months, these areas were bigger and mostly confined in the photoreceptor nuclear layer and the inner and outer segments layer, although they also disrupted the OPL and reached the INL. At 5 months, all these focal areas had disappeared and we observed an enlargement of the OPL and a thinning of the ONL thickness. This decrease in the ONL thickness, was more prominent at 7 and 9 months of age, although the rest of the layers seemed to maintain its structure. *C57BL/6N* mice followed-up at the same time did not present any alteration in their retinal layers.

To corroborate this decrease in the thickness of the ONL in *DKOrd8* mice, we quantified and compared all the retinal layers and total retina thickness of *DKOrd8* and *C57BL/6N* mice at all the specified ages. At three months of age, *DKOrd8* mice already presented a significantly thinner ONL in comparison to age-matched *C57BL/6N* mice (Figure R.6). This decreased number of photoreceptors in the *DKOrd8* retinas was either significant in the rest of the ages analyzed, confirming that *DKOrd8* mice retinas had a lower number of photoreceptors.

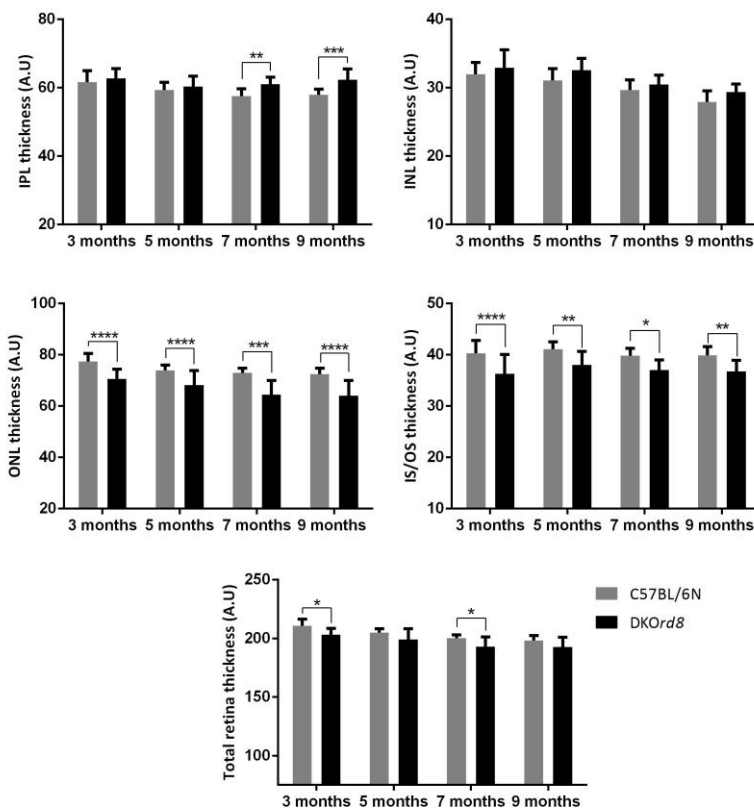


**Figure R.6. Quantification of the retinal layers.** Thickness quantification of the different retinal layers from images obtained by OCT, expressed with Arbitrary Units (A.U). Graphs show thickness mean  $\pm$  Standard Deviation (SD) of inner plexiform layer (IPL), inner nuclear layer (INL), outer nuclear layer (ONL), inner and outer segments photoreceptors' layer (IS/OS) and total retina. Statistical analyses were performed by applying a two-way ANOVA with Sidak's multiple comparison test; \* $p \leq 0.05$ ; \*\* $p \leq 0.01$ ; \*\*\* $p \leq 0.001$ ; \*\*\*\* $p \leq 0.0001$  (n=26 eyes for *DKOrd8*; n=16 eyes for *C57BL/6N*).

Furthermore, *DKOrd8* retinas presented shorter inner and outer photoreceptor segments compared to C57BL/6N mice at all ages. No significant differences were observed in the thickness of the INL. Regarding the IPL, we did not observe differences at three and five months, but at seven months its thickness was greater in *DKOrd8* retinas, which increased even more at nine months.

Overall, total retina thickness was reduced in *DKOrd8* mice, although this decrease was not as severe as the one observed in the ONL and IS/OS layers separately.

When looking into the progression of the different retinal layer thicknesses from 3 to 9 months, we observed an age-dependent thickness reduction of the inner and outer nuclear layers and total retina (Figure R.7). While the observed decrease in the INL and total retina thicknesses was similar in both *DKOrd8* and C57BL/6N mice, the thickness of the ONL in *DKOrd8* mice experienced a greater decrease (9,5%) in contrast with the C57BL/6N mice (6,2%). Inner and outer photoreceptor segment length, despite of being shorter in *DKOrd8* mice, was maintained upon ageing. Therefore, we could confirm that photoreceptors were the main cell type affected in our *DKOrd8* model.

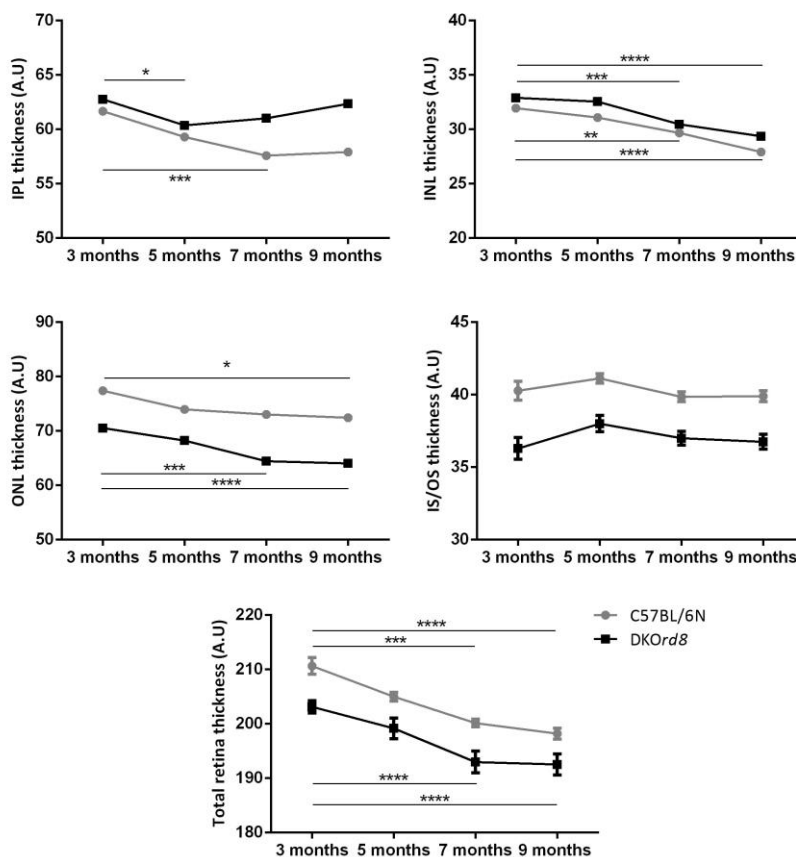


**Figure R.7. Progression of retinal thickness.** Progression of the thickness of each retinal layer from 3 to 9 months of age, expressed in arbitrary units (A.U). Graphs show thickness mean  $\pm$  Standard Error of the Mean (SEM) of inner plexiform layer (IPL), inner nuclear layer (INL), outer nuclear layer (ONL), inner and outer segments photoreceptors' layer (IS/OS) and total retina. Statistical analyses were performed by applying a two-way ANOVA with Sidak's multiple comparison test; \* $p \leq 0.05$ ; \*\* $p \leq 0.01$ ; \*\*\* $p \leq 0.001$ ; \*\*\*\* $p \leq 0.0001$  ( $n=26$  eyes for *DKOrd8* and  $n=16$  eyes for C57BL/6N).

Regarding the IPL thickness, this retinal layer suffered an age-dependent decrease in C57BL/6N mice from 3 to 7 months, which was maintained by 9 months of age. On the contrary, DKOrd8 mice experienced an initial thinning but from 5 months on, its thickness slightly increased.

It is important to emphasize that the presence of the hyper-reflective areas and alterations in the thickness of the different layers of DKOrd8 mice were strictly restricted in the inferior retina. OCT imaging of the superior retina did not show alterations at any of the ages analyzed (Figure R.8) and DKOrd8 mice had a similar retinal thickness as C57BL/6N age-matched mice (data not shown).

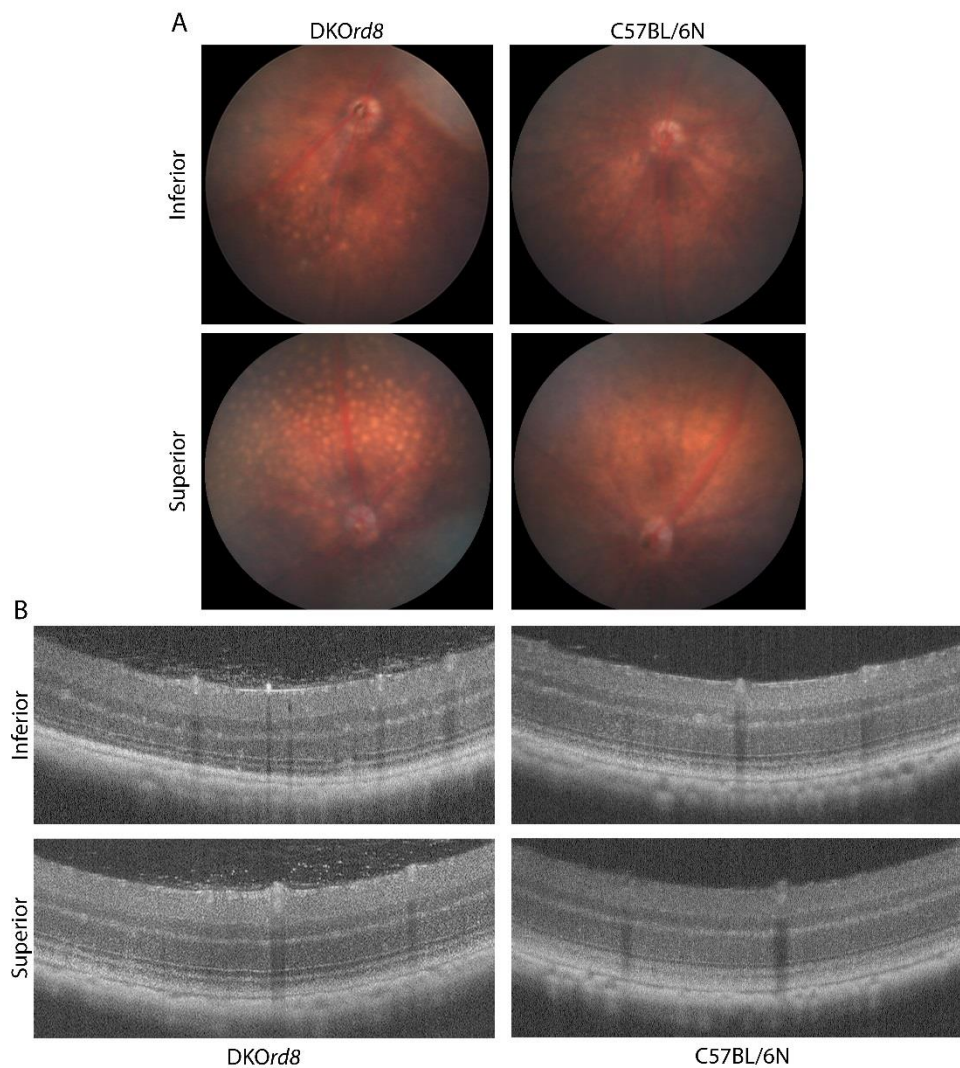


**Figure R.8. Comparison of the inferior and superior hemisphere of DKOrd8 and C57BL/6N mice eyes. (A)** Eye fundus images of DKOrd8 and C57BL/6N mice at 9 months. DKOrd8 mice present an increased number of drusen-like deposits in the inferior and superior retina. **(B)** OCT imaging comparing the superior and the inferior eye hemisphere at 9 months of age. Retinal thickness was maintained in the superior part of the retina but not in the inferior part.

At nine months however, we did observe a higher presence of the drusen-like yellowish spots in the superior retina of *DKOrd8* mice, which has also been reported in other models.

In summary, *DKOrd8* mice (i) showed alterations in their eye fundus already at one month of age, (ii) had a thinner outer nuclear layer, (iii) presented shorter inner and outer photoreceptor segments and (iv) experienced a greater decrease in the ONL thickness only in the inferior retina.

### **3. Retinal function alterations arise in young *DKOrd8* mice and are maintained upon ageing**

Retinal function is usually evaluated in humans through electroretinography (ERG) to obtain an objective measure of the visual loss associated to a retinal pathology. Retinal function of rodents can be evaluated with the same technique. ERG measures the electrical response of all retinal cells in response to a light stimulus, usually applied at increasing intensities. Low light intensities are useful to observe a predominant response of rods whereas high intensities show a mixed response of rods and cones. Therefore, it is important to cover a wide range of intensities to completely evaluate the response of the retina.

During the characterization of the *DKOrd8* model, we aimed to evaluate whether these mice presented any abnormality in their retinal function. For that purpose, we performed Ganzfeld ERG in dark-adapted *DKOrd8* and C57BL/6N mice from three to nine months of age, recording the electrical response of their retinas after light stimuli at intensities ranging from -1.7 to 1.6 log cd·s/m<sup>2</sup>, and chose a mild (-0.2 log cd·s/m<sup>2</sup>) and a high (1 log cd·s/m<sup>2</sup>) intensity to represent the observed results.

At three months of age, *DKOrd8* mice presented a significant decrease in the a-wave amplitude (derived from photoreceptors activity) compared to C57BL/6N mice when stimulated with both mild (6N mean=71.87 μV vs. *DKOrd8* mean=45.7 μV) and high (6N mean=145.4 μV vs. *DKOrd8* mean=108.6 μV) intensities (Figure R.9). The b-wave amplitude (derived mainly from bipolar cells), as well as the implicit times to both a and b waves, were not altered. A decreased a-wave amplitude was also observed in the succeeding recordings (five, seven and nine months) although it did not worsen with ageing.

Differences in the a-wave implicit time appeared at 7 months. At that age, the a-wave implicit time was higher in *DKOrd8* mice after a 1 log cd-s/m<sup>2</sup> stimulation, indicating a delayed a-wave and therefore, a slower photoreceptor response. This delayed response was maintained up to nine months, in this case observed after both mild and high stimulations.

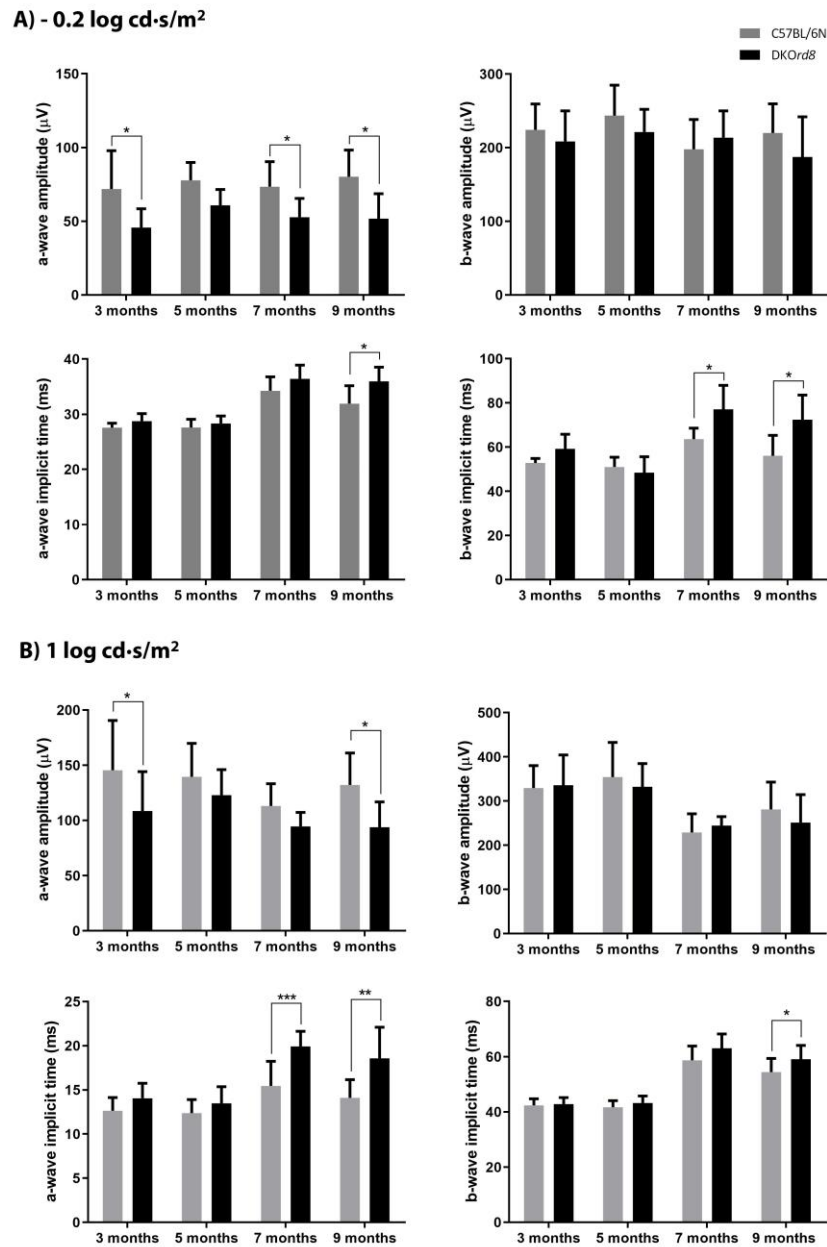


**Figure R.9. Electrophysiological response of *DKOrd8* and *C57BL/6N* mice.** Analyses of the a-wave amplitude, a-wave implicit time, b-wave amplitude and b-wave implicit time after light stimuli of (A) -0.2 log cd-s/m<sup>2</sup> and (B) 1 log cd-s/m<sup>2</sup> showed as mean±SD. Two-way ANOVA with Sidak's multiple comparison test; \*p≤0.05; \*\*p≤0.01;\*\*\*p≤0.001 (n=12 eyes per group). Amplitude expressed in microvolts (µV) and implicit time in milliseconds (ms).

Over the nine months of evaluation, no differences were observed in the b-wave amplitude in *DKOrd8* mice at any of the tested light intensities. In correlation with the delayed a-wave, we also observed a delayed b-wave response in older *DKOrd8* mice, striking at 7 months. Figure R.10 shows representative ERG responses of both *DKOrd8* and 6N mice at the different ages analyzed.

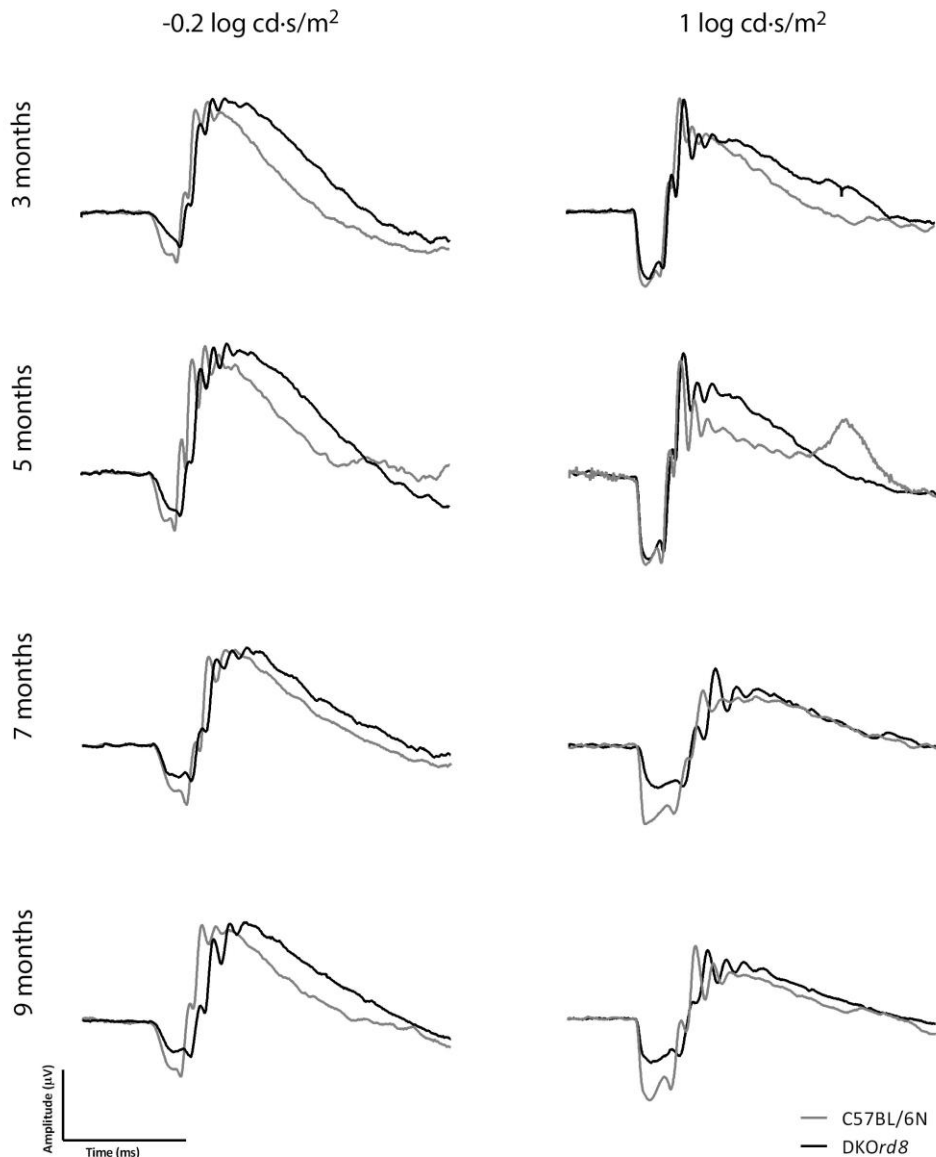


**Figure R.10. Representative ERG waveforms of *DKOrd8* and C57BL/6N mice.** ERG waveforms after a light stimulus of  $-0.2 \log \text{cd}\cdot\text{s}/\text{m}^2$  and  $1 \log \text{cd}\cdot\text{s}/\text{m}^2$  in *DKOrd8* and C57BL/6N mice at 3, 5, 7 and 9 months of age. The lower intensity produces a modest response, with a shorter a-wave whereas the high intensity produces a full response, also with a shorter a-wave. *DKOrd8* mice present a smaller a-wave and a delayed response upon ageing.

During the ERG recording, low amplitude oscillating waves, known as Oscillatory Potentials (OPs), can be observed on the rising phase of the b-wave. This group of wavelets reflect the activity of amacrine cells and are usually evaluated as the summation of the different peaks observed.

The analyses of the OPs revealed decreased amplitude in *DKOrd8* mice only at mild intensities, observed at 3, 7 and 9 months (Figure R.11). Both 6N and *DKOrd8* mice suffered an important decrease in the amplitude of their OPs at 7 and 9 months after a high stimulation, but this decrease was no different between groups. What *DKOrd8* mice did present was an increase in their OPs implicit time from 7 months on, which was more significant when stimulated at 1 log cd·s/m<sup>2</sup>, thus, indicating a delayed response. This correlated with the increased a-wave implicit time observed at the same intensity.

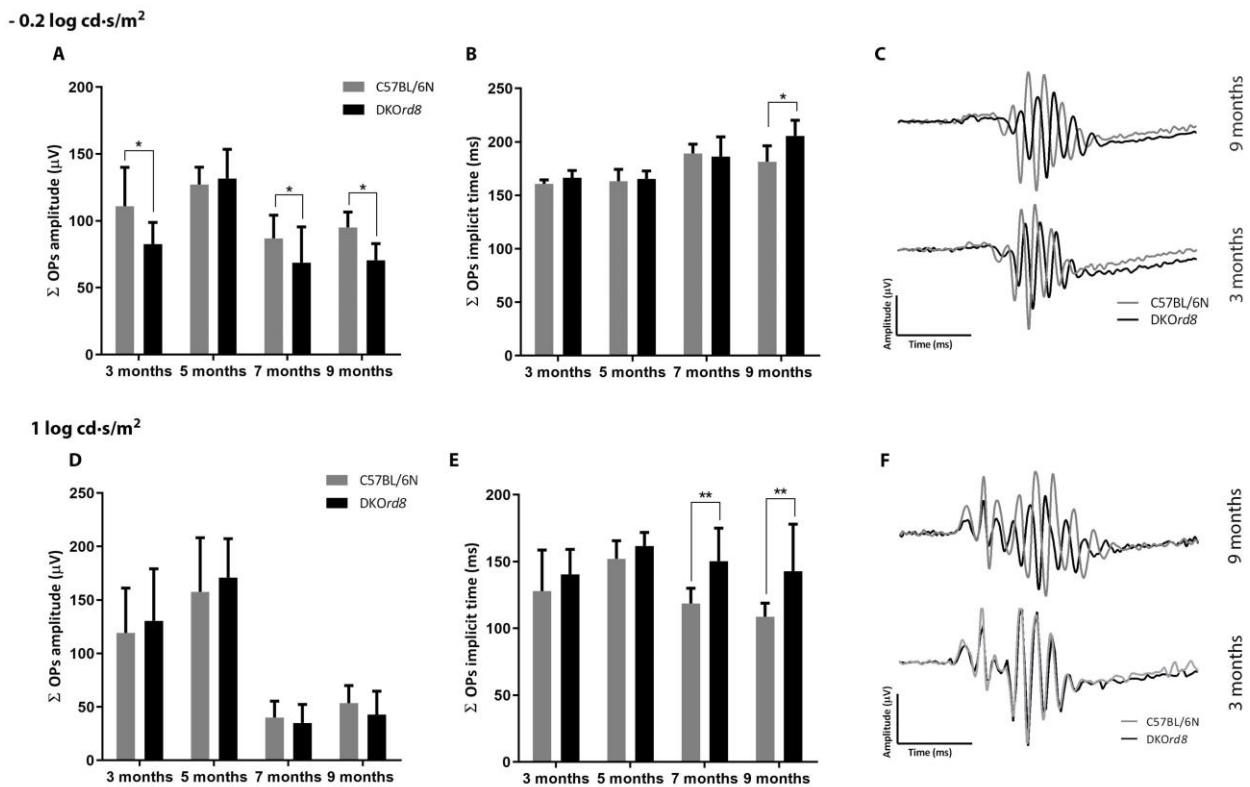


**Figure R.11. Oscillatory potentials (OPs) evaluation of *DKOrd8* and C57BL/6N mice.** Assessment of the OPs generated after a -0.2 log cd·s/m<sup>2</sup> (A, B, C) and 1 log cd·s/m<sup>2</sup> light stimulus (D, E, F). **(A, B)** Summation of OPs amplitude and implicit time at -0.2 log cd·s/m<sup>2</sup> intensity. *DKOrd8* mice presented decreased amplitude of OPs at 3, 7 and 9 months and a delayed response at 9 months. **(C)** Representative OPs waveform at 3 and 9 months showed reduced amplitude at 3 months and a delayed response at 9 months. **(D, E)** Summation of OPs amplitude and implicit time at 1 log cd·s/m<sup>2</sup> intensity. No significant changes observed in the OPs amplitude at a high stimulation. At 9 months, implicit time appears delayed in *DKOrd8* mice compared to 6N. **(F)** Representative OPs waveform showed no differences between groups at 3 months and a delayed response at 9 months. Two-way ANOVA with Bonferroni's multiple comparison test; \*p<0.05; \*\*p<0.01 (n=12 eyes per group).

In summary, *DKOrd8* mice presented a decreased photoreceptor function, seen as (i) lower a-wave amplitude, which was maintained over time; and (ii) a delayed retinal response upon ageing, observed as longer implicit times to a-wave, b-wave and OPs.

#### **4. *DKOrd8* mice present an age-dependent increase of microglia in the subretinal space**

The *Cx3cr1*<sup>-/-</sup> founder mice used to obtain our *DKOrd8* mouse model were generated by inserting a green fluorescent protein (*GFP*) reporter gene in the *Cx3cr1* locus (Jung et al. 2000). *Cx3cr1* is constitutively expressed in mouse retinal microglia. Therefore, the insertion of *GFP* under the control of *Cx3cr1* promoter allows for the easy visualization of *Cx3cr1* expression pattern and consequently, microglia distribution.

Taking advantage of the easy access to the retina through the visualization of the eye fundus, and the fluorescent modality of Micron III retinal-imaging microscope, we aimed to evaluate *in vivo* microglia distribution with the observation of GFP-expressing cells.

At one month of age, GFP expression in *DKOrd8* mice eyes was distributed homogeneously all over the retina, with a slight increase in the inferior retina and around the optic nerve (Figure R.12). From three months on, a higher amount of GFP-expressing cells were accumulated in the inferior retina, correlating with the areas where the fundus spots seen with the bright field imaging were localized. This same pattern was observed in mice analyzed at 5, 7 and 9 months of age, showing the accumulation of microglia in the focal retinal lesions.

From 5 months on, eye fundus images also presented a higher green background. It is known that lipofuscin accumulates in RPE cells with ageing and that its emission spectrum is localized around 500 nm, like the GFP wavelength (Xu et al. 2008). Knowing that *DKOrd8* mice also have higher amounts of A2E, the main component of lipofuscin (Tuo et al. 2007), we could correlate this increased green background with an accumulation of lipofuscin in RPE cells.



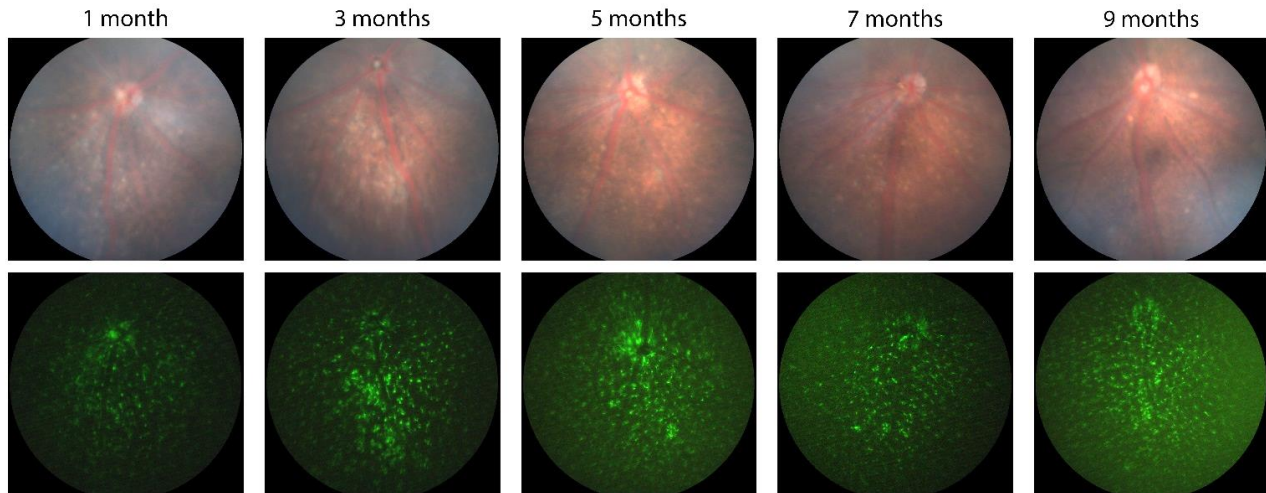


**Figure R.12. Fluorescent funduscopy evaluation of DKOrd8 mice.** Eye fundus of DKOrd8 mice imaged in bright field modality (above images) and with a green fluorescent filter at 1, 3, 5, 7 and 9 months of age (bottom images). Increased expression of GFP in the inferior retina, where fundus spots with bright field imaging are also localized, and increased autofluorescence from 5 months on.

To better characterize microglia distribution in DKOrd8 mice retinas, we performed post-mortem evaluations. It has been reported in both *Cx3cr1* and *Ccl2* single knockout mice that they experience an accumulation of subretinal microglia with ageing. However, this phenotypic characteristic has not been assessed in DKOrd8 mice yet.

Thus, we quantified the number of microglial cells in retinal and RPE flatmounts through immunostaining with the microglia marker Iba1 (Ionized calcium-Binding Adapter molecule 1). RPE flatmounts allowed for the evaluation of subretinal microglia, whereas with retinal flatmounts we could evaluate the infiltration of these cells in the inner layers of the retina.

Through the immunostaining of RPE flatmounts, we observed subretinal microglia above the RPE monolayer, the later stained with the specific marker for RPE cells RPE65 (Figure R.13 D). Interestingly, the number of subretinal microglia was similar during the first seven months of age, with no significant differences, but at 9 months, the amount of Iba1 positive cells experienced a significant 3-fold increase (Figure R.13C).

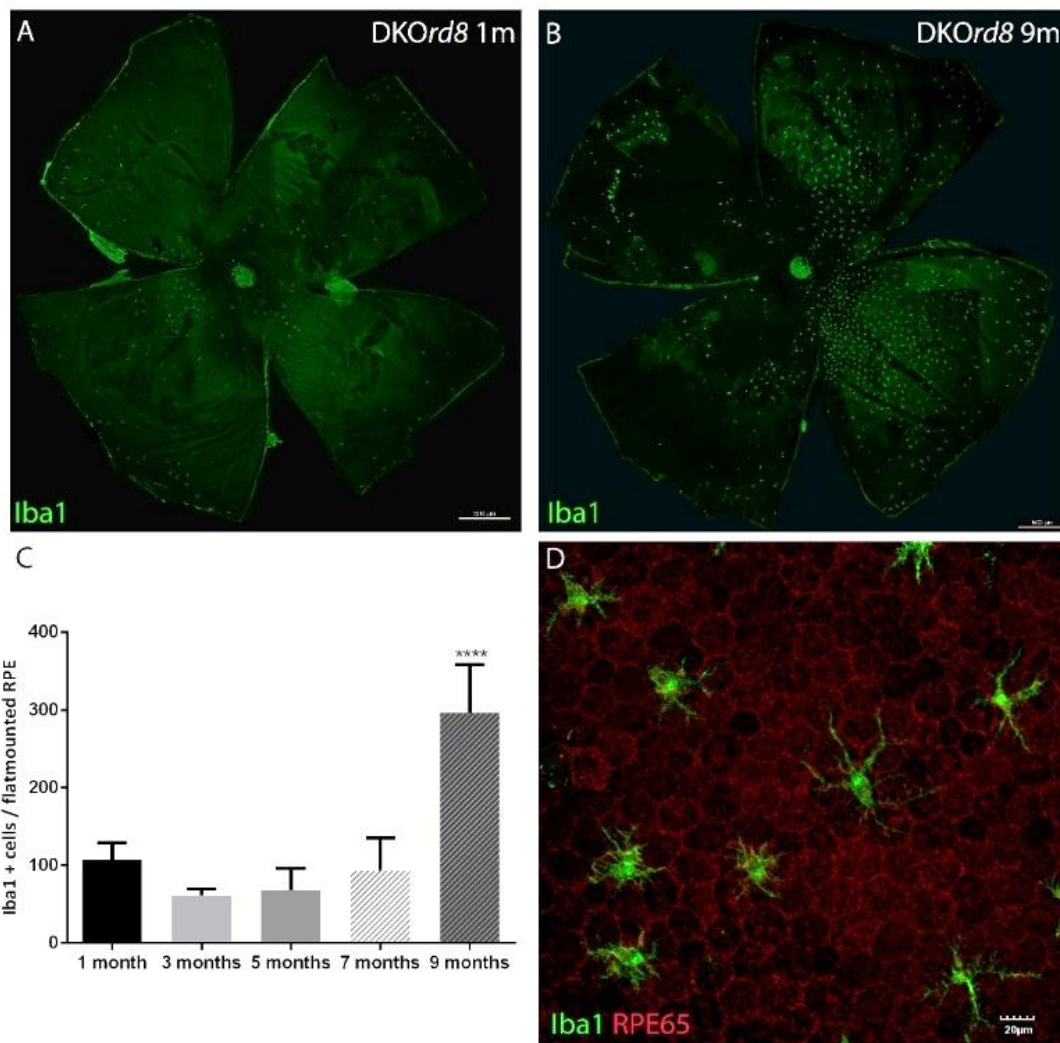


**Figure R.13. Microglia quantification in RPE flatmounts.** Representative images of RPE flatmounts of DKOrd8 mice at (A) 1 month and (B) 9 months of age, immunostained with Iba1 antibody. (C) Quantification of Iba1 positive cells in RPE flatmounts. Graph shows mean±SD; statistical analysis was performed applying a one-way ANOVA test with Tukey's multiple comparison test; \*\*\*p<0.001; n=6-8 eyes/group. (D) RPE flatmount stained with the microglia marker Iba1 and the RPE marker RPE65, showing tight junctions between the RPE cells and the microglia above them.

In contrast, the number of microglial cells in the inner retina was similar in all samples analyzed over several months (Figure R.14), and the rise in the amount of subretinal microglial cells observed at 9 months was not observed in the inner retina.

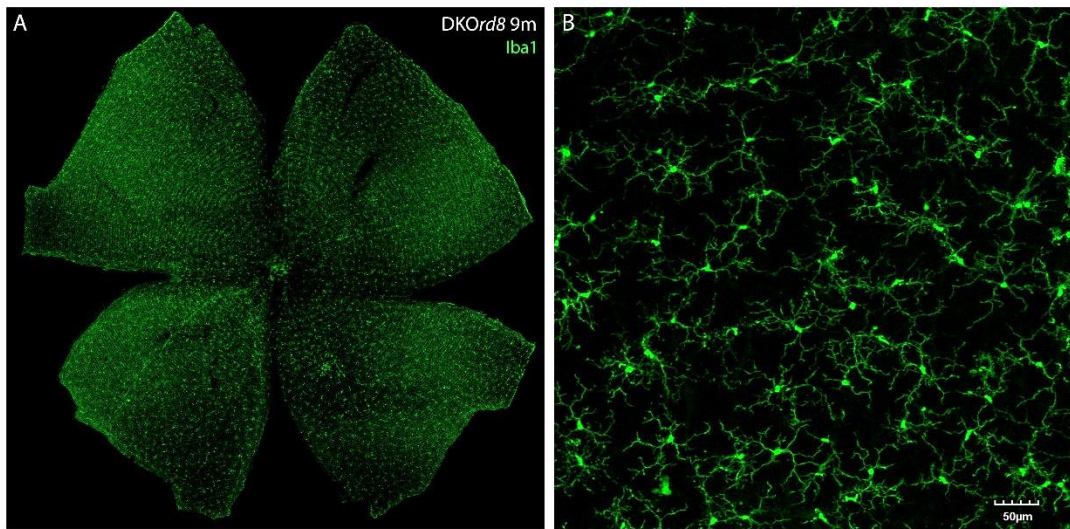


**Figure R.14. Microglia quantification in retinal flatmounts.** (A) Representative image of a flatmounted retina of a DKOrd8 mouse at 9 months of age. (B) Magnification of the retinal flatmount, where microglial cells positive for Iba1 can be observed. (C) Quantification of Iba1 positive cells in retinal flatmounts. Graph shows mean±SD; statistical analysis performed applying a one-way ANOVA test with Tukey's multiple comparison test; n=6-8 eyes/group.

## **5. *DKOrd8* retinas present focal lesions with disruption of the photoreceptors layer**

To evaluate the histopathology and progression of the lesions observed by OCT and confirm their localization in the different retinal layers, we performed a post-mortem histological evaluation. *DKOrd8* mice were euthanized at different time points (from one to nine months of age) and their eyes were removed and processed for histological evaluation.

Hematoxylin and eosin staining of *DKOrd8* and 6N mice eyes gave us a first and general overview of their retinal architecture. Although we had previously observed some abnormalities in *DKOrd8* retinas at 1 month of age through OCT, we did not find any major histological alterations in the eyes analyzed at that age (Figure R.15 A).

We did observe a mislocalization of photoreceptor nuclei in 3-months old *DKOrd8* retinas. Nuclei aggregations moved from the ONL towards the INL, disrupting the OPL, where synaptic connections between photoreceptors and bipolar cells take place. This disruption led to a focal loss of photoreceptors, as observed in 5-months old *DKOrd8* retinas. Further progression of these focal alterations resulted in a decrease of the ONL thickness, observed in 9-months old retinas. In contrast, we did not identify any alteration in C57BL/6N mice retinas at any of the ages analyzed.

Moreover, *DKOrd8* mice presented an increased thickness of the inner plexiform layer at 9 months of age, as determined by the quantitative analysis of the retinal layers from the OCT images. Regarding the GCL, we did not observe any alteration in that layer at any time point.

*DKOrd8* mice have been reported to exhibit RPE damage (Chan et al. 2008), although in an age-dependent manner and beginning at 8 months of age (Luhmann et al. 2012). In our case, we did not observe any alteration until 9 months. At that age, RPE cells presented an increased number of vacuoles (Figure R.15 B), which have been associated with atrophic cells in other mouse models with an AMD-like phenotype (Huang et al. 2017). Furthermore, photoreceptor segments looked shorter and less dense in *DKOrd8* mice, even if they were partially detached because of the post-mortem processing of the tissue.

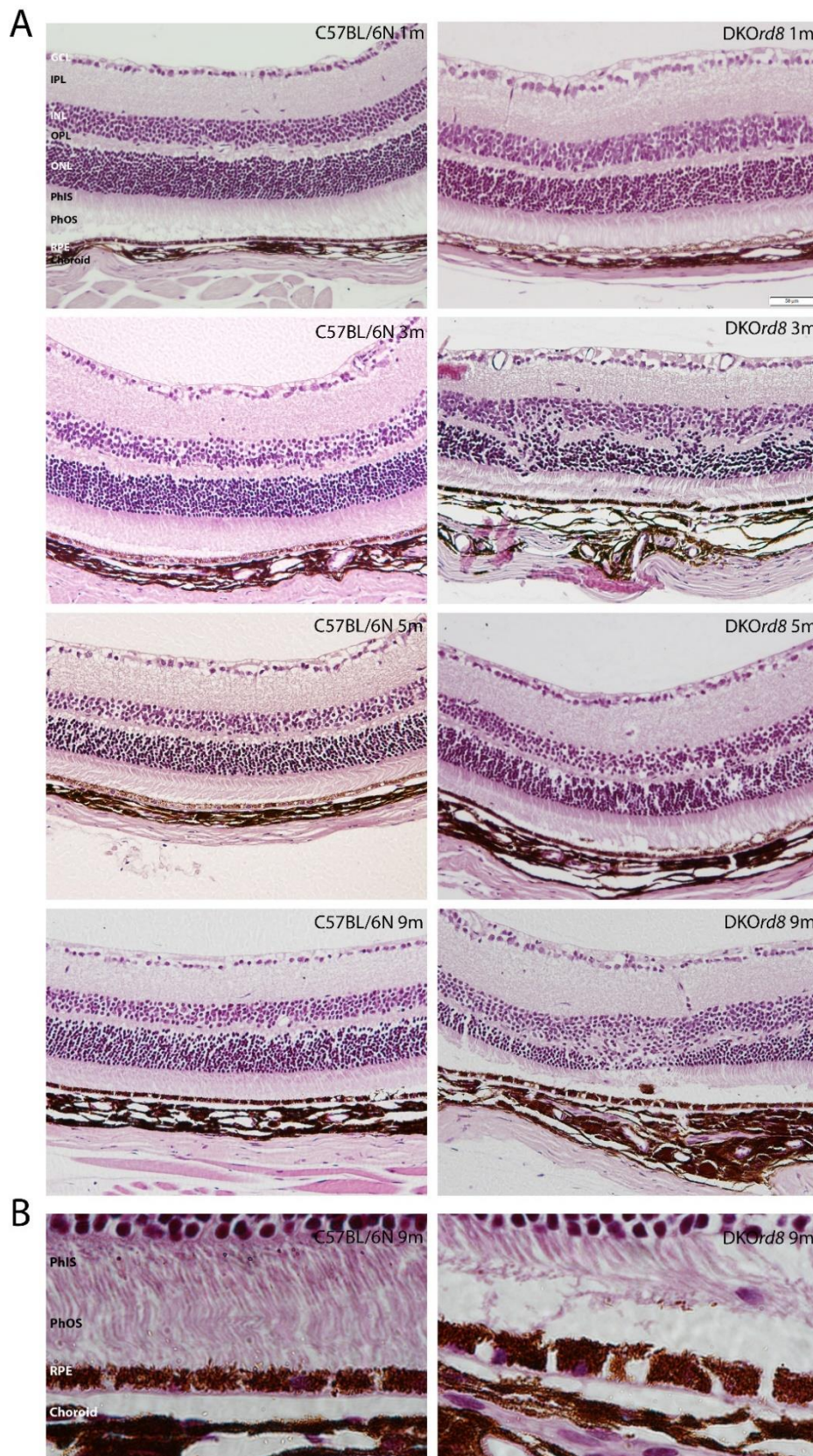


**Figure R.15. Histological evaluation of DKOrd8 and 6N mice eye sections. (A)** Hematoxylin and eosin staining of DKOrd8 and 6N mice eyes from 1 to 9 months of age. Images show the retina, with its different layers, RPE, and choroid. Abnormalities in the ONL and OPL can be observed. **(B)** Magnification of the RPE layer of 9 months old mice showing the increased vacuolization of these cells in DKOrd8 mice, indicative of atrophy and shorter photoreceptor inner (PhIS) and outer segments (PhOS).

We further evaluated the focal disruption of photoreceptors by immunofluorescence, through which we analyzed the expression of synaptophysin, recoverin and calbindin in 3-months old retinas. Synaptophysin is an integral membrane protein of the synaptic vesicles, expressed in the inner and outer plexiform layers of mice retinas, where synapses occur (Dan et al. 2008). Recoverin is a protein expressed by rod photoreceptors, which is involved in the recovery phase of visual excitation (Sampath et al. 2005), whereas calbindin is a calcium-binding protein, which is used as the main marker for horizontal cells.

As shown in figure R.16, 6N wild type mice expressed synaptophysin mainly in the OPL and in the INL, and recoverin in the photoreceptor nuclei. Calbindin was expressed by horizontal cells throughout all the INL. In contrast, *DKOrd8* mice retinas presented areas where photoreceptor

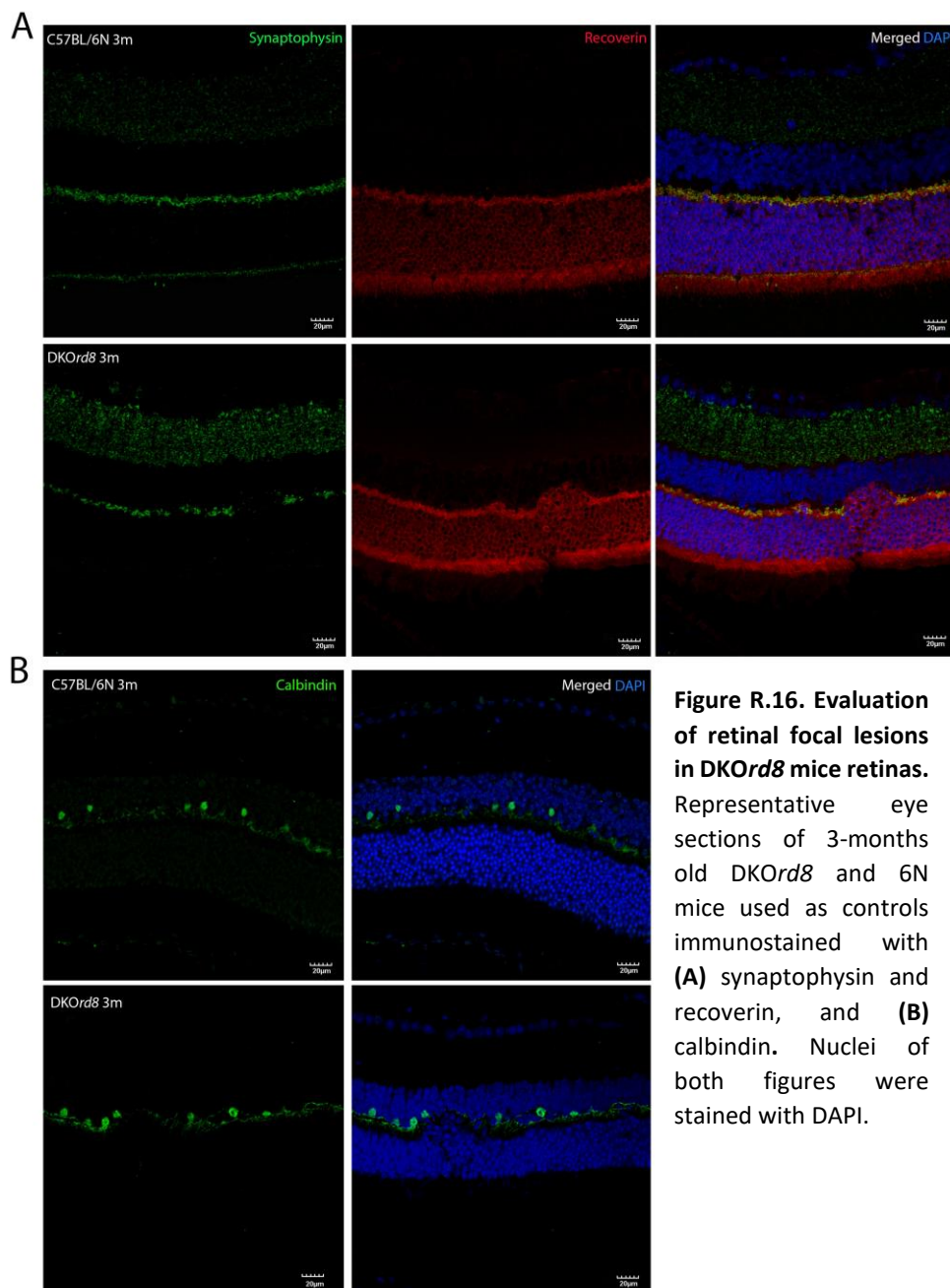


**Figure R.16. Evaluation of retinal focal lesions in *DKOrd8* mice retinas.** Representative eye sections of 3-months old *DKOrd8* and 6N mice used as controls immunostained with (A) synaptophysin and recoverin, and (B) calbindin. Nuclei of both figures were stained with DAPI.

nuclei protruded into the INL. These areas expressed recoverin but lacked the expression of synaptophysin (Figure R.16 A) and calbindin (Figure R.16, B), confirming that the mislocalization of photoreceptors disrupted the OPL and altered synaptic connections in these areas.

Given these alterations in the photoreceptors layer, we also evaluated the expression of the photoreceptors pigments opsin and rhodopsin, expressed by cones and rods respectively. Zhang et al. had already described a reduction of cones but not of rods in 1-month old *DKOrd8* mice retinas (J. Zhang et al. 2013). In our case, we did not observe significant differences in rhodopsin expression in 3-months old *DKOrd8* mice compared to 6N mice (Figure R.17). Regarding opsin immunostaining, *DKOrd8* retinas did present a reduced expression of this protein in the photoreceptors outer segments layer.

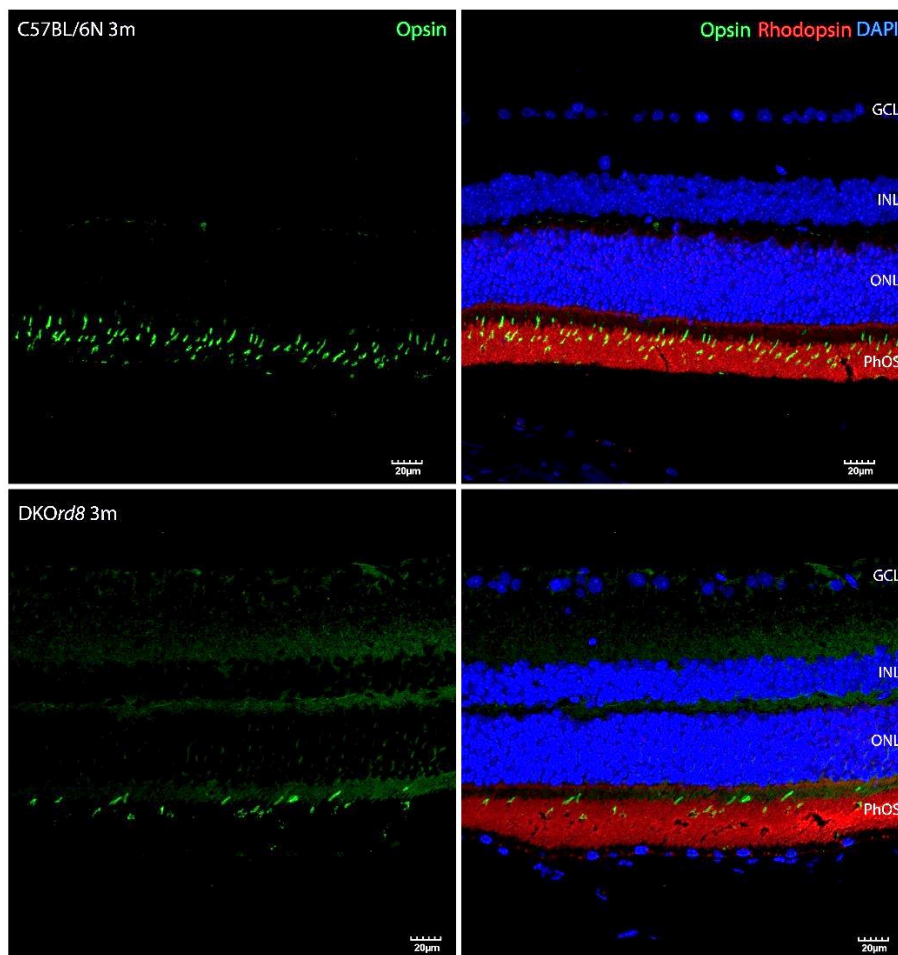


**Figure R.17. Evaluation of photoreceptors pigments in *DKOrd8* mice.** Representative eye sections of 3-month old *DKOrd8* and 6N mice (used as wild type control) immunostained with rhodopsin and opsin, whose expression is limited to the photoreceptor segments. Nuclei were stained with DAPI.

Taken together, *DKOrd8* mice retinas presented (i) a mislocalization of photoreceptors nuclei, which moved towards the INL disrupting the outer plexiform layer and altering synaptic connectivity on those areas, (ii) a progressive thinning of the ONL, (iii) atrophy of RPE cells, and (iv) a decreased expression of the cone's photopigment opsin.

## **6. *DKOrd8* retinas present an increased gliosis, microglia infiltration and oxidative stress**

Continuing with the histopathological evaluation of *DKOrd8* retinas, we analyzed reactive gliosis through glial fibrillary acidic protein (GFAP) immunostaining. GFAP is an intermediate filament protein poorly expressed in normal conditions by Müller glia. Its expression greatly increases in response to stress, injury or neurodegeneration (Verardo et al. 2008). It has been described that 3-months old *DKOrd8* mice present increased levels of GFAP with a pronounced localization in the focal retinal lesions (Zhou et al. 2011). To have a complete evaluation of GFAP expression, we immunostained *DKOrd8* and 6N mice retinas from 1 to 9 months of age.

Compared to C57BL/6N mice, GFAP expression was highly increased in *DKOrd8* mice retinas, and this increased expression was already observed in 1-month old *DKOrd8* mice (Figure R.18). While the expression in 6N retinas was restricted to the GCL, GFAP expression in *DKOrd8* was distributed across the retina, from the GCL to the OPL. At three months, GFAP was still expressed throughout the retina and in the focal lesions with photoreceptors disruption. At 5 and 9 months, GFAP expression appeared slightly decreased compared to 1 or 3 months, but it was still present in the OPL. Although not shown, GFAP expression in 6N retinas and during the rest of the months analyzed remained restricted to the GCL.

These same sections were also stained with RPE65, an enzyme expressed by RPE cells, to evaluate the state of this layer or any possible disruption. We observed a continuous expression of RPE65 throughout the entire RPE layer throughout all the months assessed.

Therefore, *DKOrd8* mice retinas presented (i) an increased gliosis at already 1 month of age, which was maintained during all the months evaluated, and (ii) a preservation of the RPE layer structure.



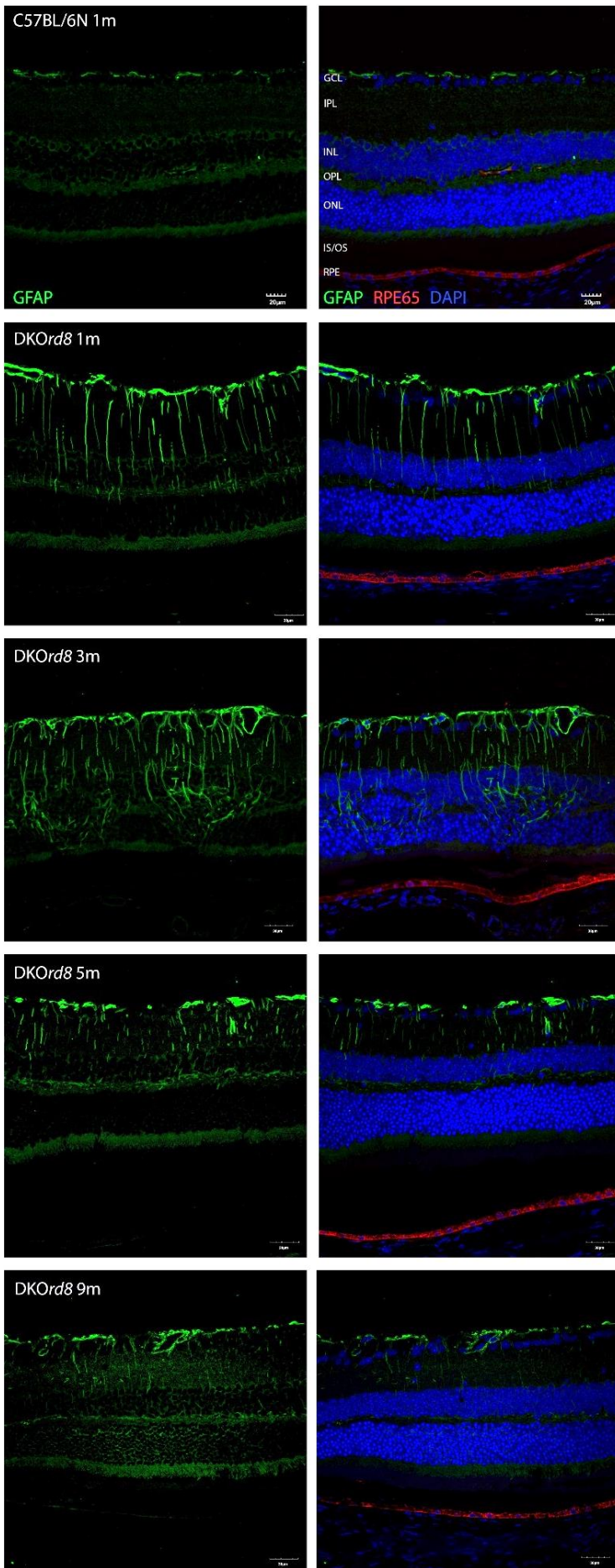


**Figure R.18. Evaluation of retinal gliosis in *DKOrd8* mice.** Representative eye sections of *DKOrd8* mice from 1 to 9 months of age and a 1-month old C57BL/6N mouse, immunostained with GFAP and RPE65. Nuclei stained with DAPI.

Previous histological characterization of *DKOrd8* mice revealed that microglia is recruited to the early retinal lesions (Luhmann et al. 2012). Through the eye fundus imaging, we had already observed in vivo an accumulation of microglia in the focal retinal lesions. To corroborate this finding in histological sections, we stained 3-months old *DKOrd8* and 6N retinas with lectin, a marker for microvasculature and macrophages and microglial cells.

The histopathological evaluation of the immunostained retinas revealed that the focal lesions in the ONL presented an increased expression of lectin, as several lectin positive cells were observed in the areas with mislocalization of photoreceptor nuclei (Figure R.19). This was also observed with Iba1 staining (data not shown), confirming the infiltration of the microglia in the focal retinal lesions.

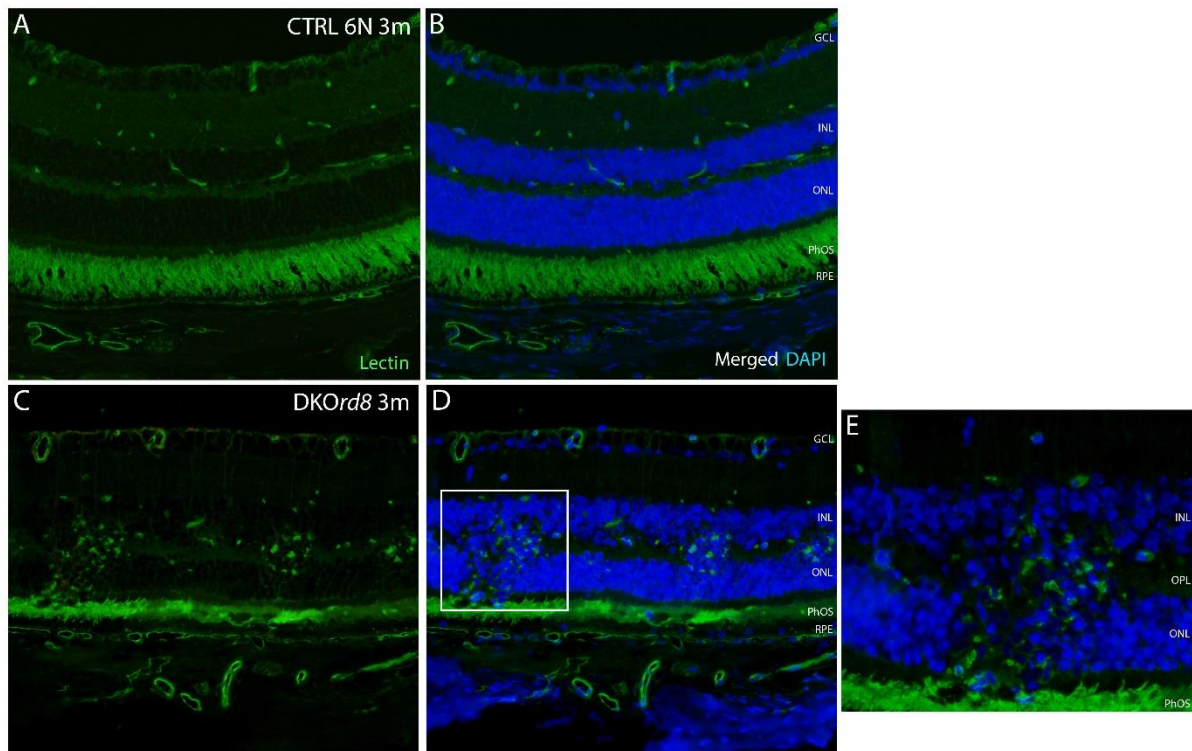


**Figure R.19. Evaluation of microglia infiltration in focal retinal lesions. (A, B)** Eye sections of 3-months old 6N mice used as wild type control and **(C, D)** *DKOrd8* mice. Immunostaining shows microvasculature and microglial cells, with an increased expression in focal retinal lesions. **(E)** Magnification of a *DKOrd8* focal retinal lesion, showing the inner nuclear layer (INL), outer plexiform layer (OPL) and outer nuclear layer (ONL).

Although the increased oxidative stress is the main inducer of the AMD phenotype in humans, its role in the onset of the phenotype of *DKOrd8* mice is not clear yet. For that purpose, we evaluated oxidative stress in 3-month old *DKOrd8* retinas through 8-Oxo-2'-deoxyguanosine (8-OHdG) immunostaining. 8-OHdG is one of the major products of DNA oxidation and a marker of oxidative stress. Immunofluorescence staining revealed that *DKOrd8* retinas presented increased levels of 8-OHdG in all the nuclear layers in comparison to 6N mice (Figure R.20).

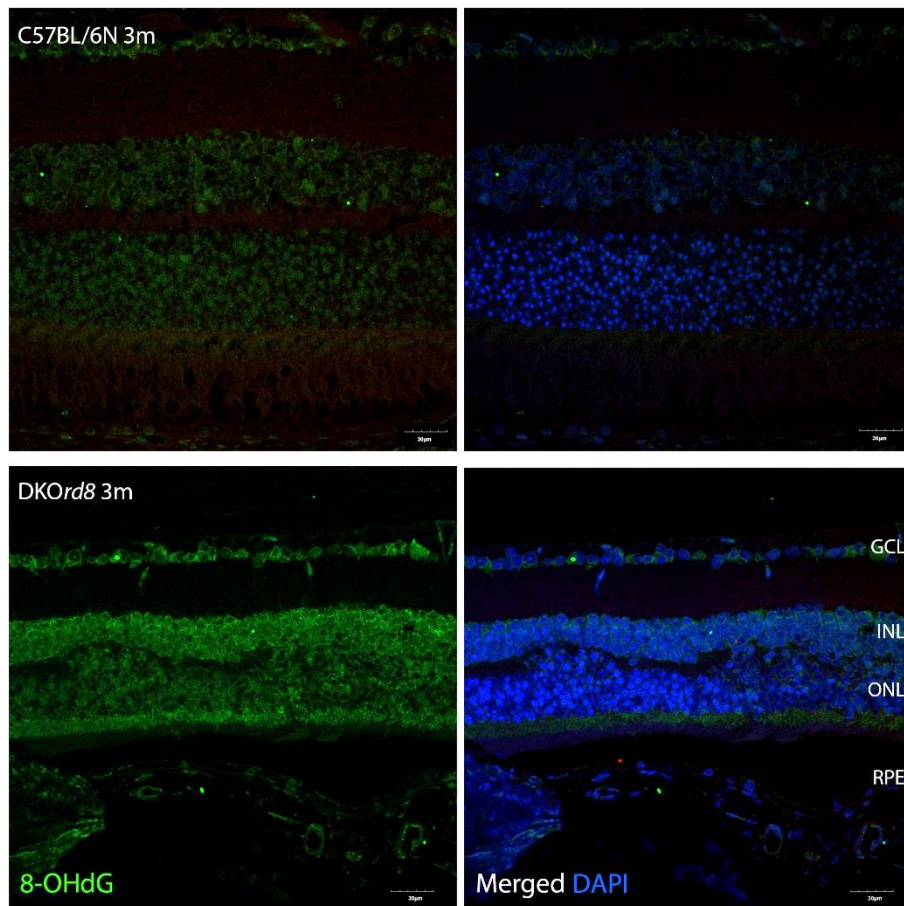


**Figure R.20. Evaluation of oxidative stress in *DKOrd8* mice retinas.** Images of 3-months old mice eye sections immunostained with 8-OHdG, marker of oxidative stress. Increased expression in the nuclear layers of *DKOrd8* mice, compared to 6N mice.

## 7. *DKOrd8* mice eyes present an altered gene expression pattern

To have a better understanding of the phenotype of *DKOrd8* model, we analyzed the gene expression profile of their retinas and posterior pole with a cDNA microarray, comparing the expression of 3-months old *DKOrd8* and C57BL/6N mice. We chose 3 months old mice because at that age they already displayed most of the phenotypical key features of the model. Moreover, it is still an early age, which becomes useful when using murine models for the study of a disease and the application of therapies.

After running the microarrays, the resulting data underwent a quality control to check if all the genes were suitable for a differential expression analysis. After that, data was normalized and filtered to make all the samples comparable as well as to remove technical biases. A total of 8 *DKOrd8* and 8 6N mice were used to perform the gene expression comparison. However, after normalizing the data and performing a principal component analysis, two *DKOrd8* samples were discarded as they did not appear grouped with the rest of the *DKOrd8* in the sample distribution plot (data not shown).

Data filtering helped us to select the 7105 genes to be included in the differential expression analysis. From all those genes, *DKOrd8* mice presented 1245 genes downregulated and 354 upregulated compared to the 6N mice, with an absolute log<sub>2</sub> fold change equal or greater than 0.05 and an adjusted P value below 0.01. With a restricted absolute fold change value of 1, the number of genes differentially expressed were reduced to 422 downregulated and 69 upregulated (Figure R.21).

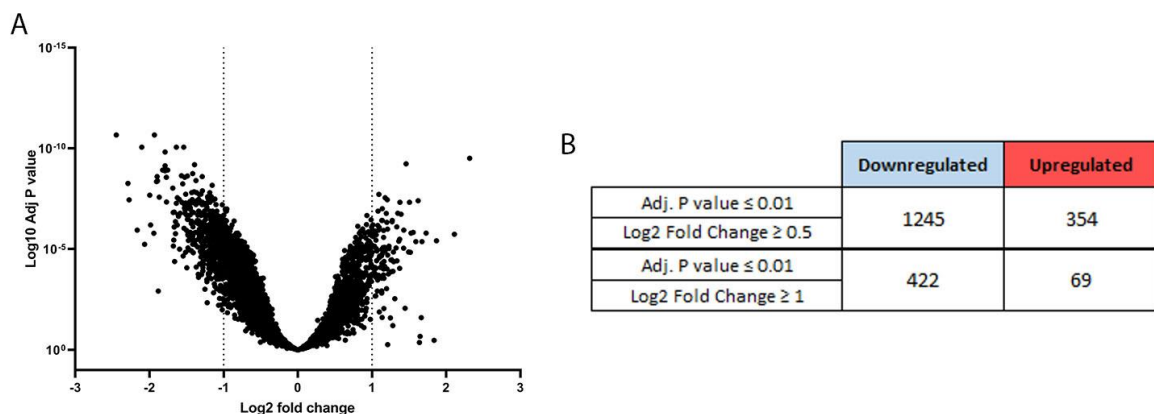


**Figure R.21. Differential gene expression in *DKOrd8* mice.** *DKOrd8* mice present an increased number of genes downregulated in comparison to 6N mice. **(A)** Volcano plot showing all the genes included in the differential expression analysis, with dotted lines indicating an absolute fold change of 1. **(B)** Table indicating the exact number of genes up and downregulated.

These were the genes represented in a heatmap (Figure R.22), which allowed for the visualization of differences in the expression pattern of *DKOrd8* mice compared to 6N mice. The samples analyzed showed a considerably homogeneous expression pattern within their group, with a greater number of genes downregulated (blue colored) in *DKOrd8* mice compared to 6N.

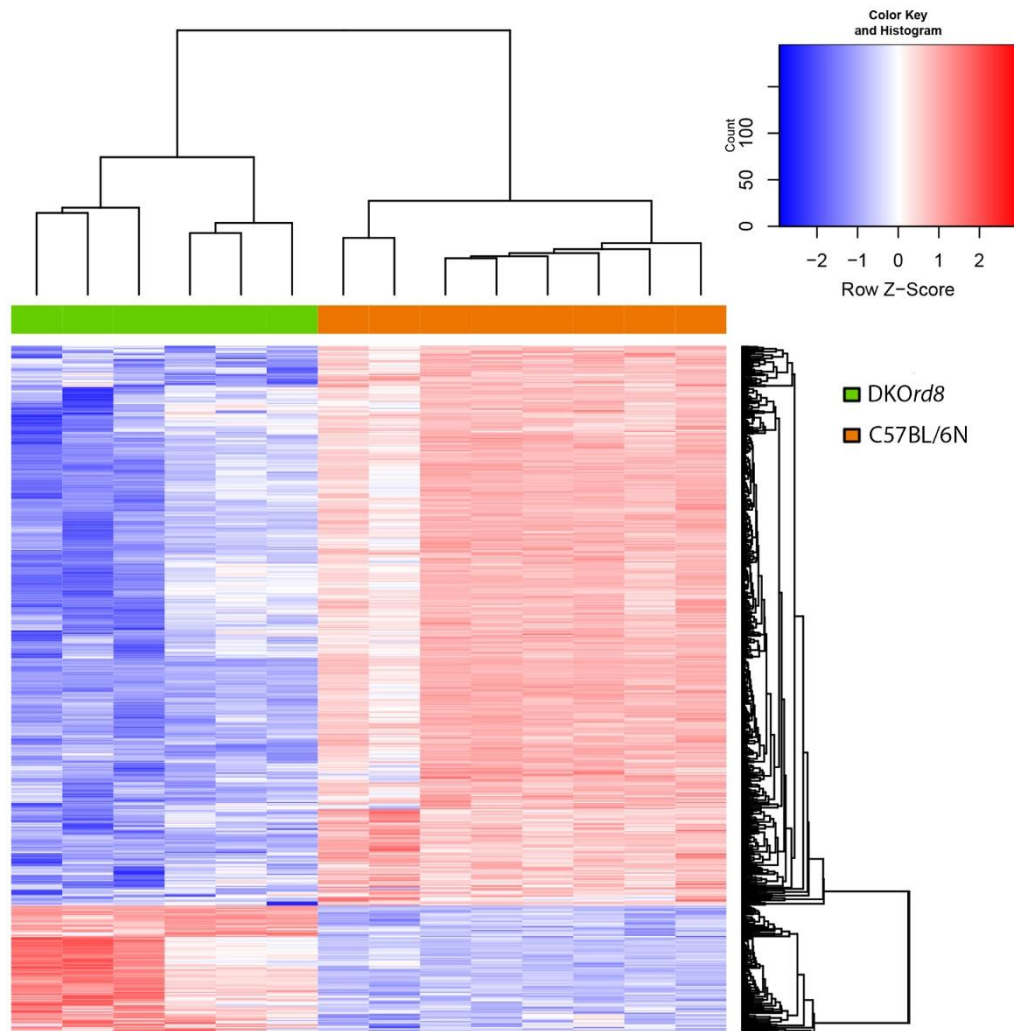


**Figure R.22. Heatmap comparing the expression pattern of 3-months old *DKOrd8* and 6N mice.** A total of 8 6N and 6 *DKOrd8* mice were analyzed in the heatmap, where the expression of 491 genes is shown. The relative expression of each gene is represented, with downregulated genes showed in blue colors and upregulated genes in red.

To elucidate the gene expression changes implicated in the phenotype of the *DKOrd8* mouse model, we identified the genes selected for the heatmap ( $\log_2$  fold change  $\geq 1$  and adjusted P value  $\leq 0.01$ ) and categorized them according to their function. Table R.1 and R.2 summarize relevant genes which were found differentially expressed in *DKOrd8* mice, both up and downregulated. These genes were related with oxidative stress, neuronal function, cell death,

senescence, immune response and cell cycle; categories that have been associated with AMD pathogenesis and progression.

In the oxidative stress category, a great number of the downregulated genes were directly related with the mitochondrial electron transport chain (mETC), responsible for ATP synthesis and major generator of radical oxygen species. Transcription factor *Nrf2*, the major regulator of the cellular antioxidant response, was also downregulated in *DKOrd8* mice eyes, as well as the antioxidant enzyme *SOD3*.

Several genes related with neuronal function, including the GABA receptor *Gabra1* or *Impg2*, responsible for photoreceptor's outer segments maintenance, were also downregulated.

*DKOrd8* mice also presented a downregulation in several genes related to autophagy such as *Atg4b* and *Tmem59*. *Mtor*, an integrator of metabolic signaling pathways and regulator of autophagy was also downregulated.

**Table R.1. List of relevant genes upregulated in *DKOrd8* mice.**

| Gene Symbol                      | Name                                | logFC | adj.P.Val | Function                    |
|----------------------------------|-------------------------------------|-------|-----------|-----------------------------|
| <b>Oxidative Stress</b>          |                                     |       |           |                             |
| <i>Txndc11</i>                   | Thioredoxin Domain Containing 11    | 1,374 | 8,97E-05  | Redox regulator             |
| <b>Neuronal Function</b>         |                                     |       |           |                             |
| <i>Id2</i>                       | Inhibitor Of DNA Binding 2          | 1,192 | 1,68E-07  | Retinogenesis regulator     |
| <b>Cell death and senescence</b> |                                     |       |           |                             |
| <i>Gas2</i>                      | Growth Arrest Specific 2            | 1,256 | 3,45E-05  | Apoptosis                   |
| <i>Mrp120</i>                    | Mitochondrial Ribosomal Protein L20 | 1,002 | 1,43E-05  | Genomic instability         |
| <b>Immune response</b>           |                                     |       |           |                             |
| <i>Ccr1</i>                      | C-C Motif Chemokine Receptor 1      | 1,675 | 4,20E-06  | Inflammation                |
| <i>Ccl2</i>                      | C-C Motif Chemokine Ligand 2 (MCP1) | 1,527 | 1,60E-06  | Inflammation                |
| <i>Il18</i>                      | Interleukin 18                      | 0,962 | 3,95E-06  | Inflammation                |
| <i>Cd302</i>                     | CD302 Molecule                      | 0,930 | 2,70E-05  | Cell adhesion and migration |
| <i>Cd46</i>                      | CD46 Molecule                       | 0,841 | 2,20E-04  | Complement system           |
| <i>Il9</i>                       | Interleukin 9                       | 0,793 | 7,37E-04  | Inflammation                |
| <b>Cell cycle</b>                |                                     |       |           |                             |
| <i>Stag1</i>                     | Stromal Antigen 1                   | 1,102 | 2,16E-05  | Chromosomal architecture    |

Genes related to apoptosis, senescence and cell cycle also appeared downregulated in *DKOrd8* mice eyes. In comparison, most of the differentially expressed genes related with the immune system were upregulated. The chemokine receptor *Ccr1* and the ligand *Ccl2* (transcribed in *DKOrd8* mice but not translated) were upregulated, indicating the abnormal chemokine signaling in this model as well as some interleukins and genes related with the complement

system. A relevant gene related with the immune response we found downregulated was NF- $\kappa$ B, associated with microglia activation and retinal degeneration (Wu et al. 2002).

**Table R.2. List of relevant genes downregulated in DKOrd8 mice**

| Gene Symbol                      | Name  | logFC  | adj.P.Val | Function                               |
|----------------------------------|---|--------|-----------|--|
| <b>Oxidative Stress</b>          |   |        |           |  |
| <i>Ndufs7</i>                    | NADH:Ubiquinone Oxidoreductase Core Subunit S7          | -1,940 | 1,61E-06  | Mitochondrial electron transport chain |
| <i>Oxa1l</i>                     | Mitochondrial Inner Membrane Protein                    | -1,609 | 2,36E-07  | Mitochondrial electron transport chain |
| <i>Atp5g1</i>                    | ATP Synthase Membrane Subunit C Locus 1                 | -1,321 | 5,37E-05  | Mitochondrial electron transport chain |
| <i>Sdhb</i>                      | Succinate Dehydrogenase Complex Flavoprotein Subunit D  | -1,305 | 2,41E-05  | Mitochondrial electron transport chain |
| <i>Cox6a1</i>                    | Cytochrome C Oxidase Subunit 6A1                        | -0,927 | 9,09E-04  | Mitochondrial electron transport chain |
| <i>Mdh2</i>                      | Malate Dehydrogenase 2                                  | -1,985 | 6,29E-07  | Mitochondrial metabolism               |
| <i>Gstt3</i>                     | Glutathione S-Transferase Theta 3                       | -1,148 | 8,32E-06  | Detox enzyme                           |
| <i>Nrf2</i>                      | Nuclear Factor, Erythroid 2 Like 2                      | -1,125 | 5,19E-04  | Antioxidant transcription factor       |
| <i>Sod3</i>                      | Superoxide Dismutase 3                                  | -0,792 | 4,13E-04  | Detox enzyme                           |
| <i>Hif3a</i>                     | Hypoxia Inducible Factor 3 Subunit Alpha                | -0,791 | 3,81E-04  | Hypoxia-induced transcription factor   |
| <b>Neuronal Function</b>         |   |        |           |  |
| <i>Gabra1</i>                    | GABA Receptor Alpha 1 Subunit                           | -1,586 | 1,63E-07  | GABA receptor                          |
| <i>Gfra1</i>                     | GDNF Family Receptor Alpha 1                            | -1,550 | 5,72E-09  | Neurotrophic receptor                  |
| <i>Syng1</i>                     | Synaptogyrin 3  | -1,477 | 3,37E-07  | Neurotransmission                      |
| <i>Impg2</i>                     | Interphotoreceptor Matrix Proteoglycan 2                | -1,393 | 6,39E-10  | PhOS maintenance                       |
| <i>Aplp1</i>                     | Amyloid Beta Precursor Like Protein 1                   | -1,363 | 1,56E-08  | Neurotransmission                      |
| <i>Cdh13</i>                     | Cadherin 13   | -1,126 | 3,16E-05  | Axone growth regulator                 |
| <i>Casp6</i>                     | Caspase 6   | -1,011 | 2,50E-06  | Axone maintenance                      |
| <i>Nos1</i>                      | Nitric Oxide Synthase 1                                 | -0,965 | 8,32E-06  | Neurotransmission                      |
| <b>Cell death and senescence</b> |   |        |           |  |
| <i>Tmem59</i>                    | Transmembrane Protein 59                                | -2,448 | 2,15E-11  | Autophagy regulator                    |
| <i>Gadd45g</i>                   | Growth Arrest And DNA Damage Inducible Gamma            | -2,065 | 5,72E-06  | Apoptosis regulator                    |
| <i>Atg4b</i>                     | Autophagy Related 4B Cysteine Peptidase                 | -1,101 | 5,91E-07  | Autophagy                              |
| <i>Mtor</i>                      | Mammalian Target Of Rapamycin                           | -1,077 | 3,22E-06  | Autophagy regulator                    |
| <i>Terf2ip</i>                   | Telomeric Repeat-Binding Factor 2-Interacting Protein 1 | -2,103 | 8,63E-11  | Telomere regulation                    |
| <i>Myc</i>                       | MYC Proto-Oncogene                                      | -1,496 | 8,29E-05  | Transcription regulator                |
| <b>Immune response</b>           |   |        |           |  |
| <i>Nf-<math>\kappa</math>B1</i>  | Nuclear Factor Kappa B Subunit 1                        | -1,127 | 4,34E-05  | Cellular response to stress            |
| <b>Cell cycle</b>                |   |        |           |  |
| <i>Cdc23</i>                     | Cell division cycle                                     | -1,904 | 4,40E-09  | DNA replication                        |
| <i>Usp11</i>                     | Ubiquitin Specific Peptidase 11                         | -1,268 | 1,35E-07  | Epigenetic modifications               |
| <i>Pold2</i>                     | DNA Polymerase Delta 2, Accessory Subunit               | -1,166 | 2,97E-07  | DNA repair                             |
| <i>Cdkn1a</i>                    | Cyclin Dependent Kinase Inhibitor 1A                    | -1,093 | 9,20E-04  | Cell cycle checkpoint                  |

Moreover, we also detected some genes that have been associated with AMD although some of them still do not have a defined function (Table R.3). From all them, *Timp3* was the most relevant one, as variants in this gene have been associated with an increased risk of AMD in humans (Fritsche et al. 2016).

**Table R.3. List of genes associated with AMD**

| Gene Symbol                | Name                              | logFC  | adj.P.Val | Function                |
|----------------------------|-----------------------------------|--------|-----------|-------------------------|
| <b>Genes downregulated</b> |                                   |        |           |                         |
| <i>Timp3</i>               | TIMP Metallopeptidase Inhibitor 3 | -1,432 | 4,05E-07  | Bruch's membrane marker |
| <i>Ctsb</i>                | Cathepsin B                       | -0,991 | 6,16E-07  | Redox metabolism        |
| <b>Genes upregulated</b>   |                                   |        |           |                         |
| <i>Omd</i>                 | Osteomodulin                      | 1,870  | 3,84E-06  | AMD related gene        |
| <i>Tnmd</i>                | Tenomodulin                       | 1,372  | 3,17E-06  | AMD candidate gene      |
| <i>Crygb</i>               | Crystallin Gamma B                | 1,154  | 1,89E-04  | RPE marker              |
| <i>Mmp11</i>               | Matrix Metallopeptidase 11        | 0,815  | 1,23E-05  | Bruch's membrane marker |

To gain insight into the biological function of the genes differentially expressed in *DKOrd8* retinas, we performed analyses of biological significance based on enrichment analyses in the Gene Ontology (GO) database. The goal of these analyses is to determine whether a group of genes are more often associated to certain biological functions than what would be expected in a random set of genes.

Interestingly, we found that most of the GO terms significantly enriched among all the downregulated genes fitted into categories related to neuronal regulation, regulation of synapses and regulation of transferase activity, indicating an abnormal function of retinal neurons. Figure R.23 shows the three GO terms with a higher gene ratio in each category, being neurogenesis the GO term with a higher ratio. Among the upregulated genes, only a few GO terms were significantly enriched, which fitted into the striated muscle organization category.

In summary, the expression pattern of *DKOrd8* mice presented a major gene downregulation when compared to 6N mice. We observed a differential expression of genes related with the mitochondrial electron transport chain, neuronal function, immune regulation, autophagy or apoptosis, categories related to AMD. Furthermore, regarding gene enrichment analyses, *DKOrd8* mice presented a major alteration of neuronal function and regulation, indicating the abnormal functioning of the retina.



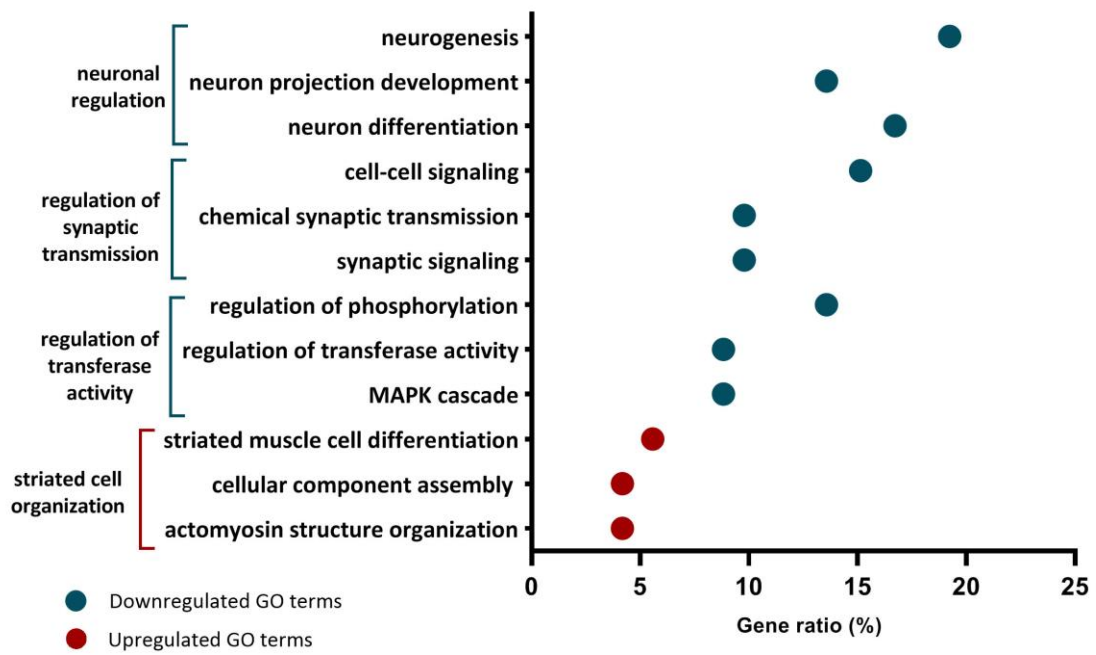


**Figure R.23. Gene enrichment analysis.** Graph showing the main biological functions over-represented in the gene enrichment analysis, with the three GO terms with higher gene ratio. Downregulated GO terms are shown in blue and upregulated in red.

## Chapter 2. Evaluation of AOxNPs for the treatment of age-related macular degeneration

---

The second main aim of this thesis was the development of a novel therapy to treat age-related macular degeneration. Given the role oxidative stress plays in the onset and progression of AMD and the beneficial effects CeO<sub>2</sub>NPs have shown in murine models with severe retinal degeneration, we intended to use antioxidant nanoparticles as a treatment for AMD.

To ensure the efficacy and safety of the treatment, several preliminary studies were performed including (i) *in vitro* assays to discard any cytotoxic effect of our AOxNPs and to ensure their antioxidant effect in RPE cell cultures; and (ii) biodistribution studies to evaluate the capacity of AOxNPs to reach the retina and RPE after their administration. After that, the *DKOrd8* mouse model, which was already generated and characterized, was used to test the efficacy of AOxNPs treatment in attenuating or reverting the pathological phenotype of the model.



## 1. Evaluation of AOxNPs safety and efficacy in vitro

The first aim in the development of an effective therapy to treat AMD was the evaluation in vitro of our AOxNPs in order to discard any cytotoxic effect and to corroborate their antioxidant activity. For all experiments, AOxNPs were freshly synthesized and each batch was characterized to ensure a correct size and charge of the nanoparticles.

### 1.1. AOxNPs are non-toxic in ARPE19 cell cultures

A large number of in vitro studies about the cytotoxic effects of AOxNPs have been published, showing a non-toxic effect in different ocular cell types, including photoreceptors precursor cells and human lens epithelial cells (Chen et al. 2006; Pierscionek et al. 2010). However, these results should be taken cautiously given the different synthesis protocols used in each study and therefore, the different properties they can present (Casals et al. 2017).

We evaluated the cytotoxic effect of our freshly generated AOxNPs by assessing the viability of RPE-derived ARPE19 cells with an MTT assay. ARPE19 cells were exposed to AOxNPs at increasing concentrations (10 nM, 50 nM, 100 nM and 500 nM) during 24 or 48 hours before evaluating their viability. Interestingly, we did not observe any significant reduction in cell viability at any of the tested concentrations (Figure R.24). Hence, the exposure to AOxNPs for 24 and 48 hours did not produce any cytotoxic effect in ARPE19 cells.

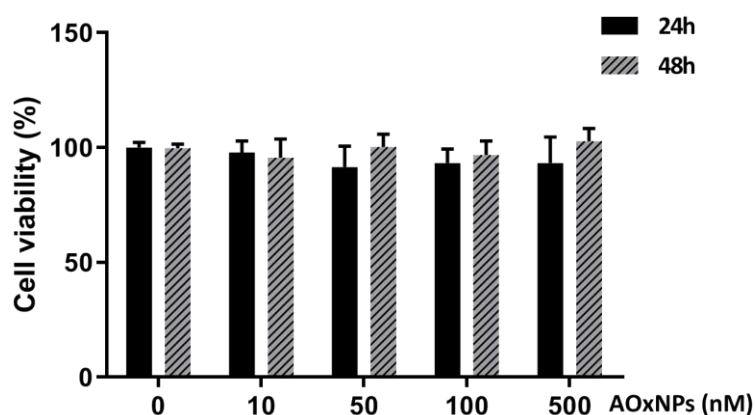


**Figure R.24. Evaluation of the cytotoxic effect of AOxNPs.** Viability of ARPE19 cells after a 24 or 48 hours treatment with AOxNPs at increasing concentrations. No differences are observed between groups. Graph shows mean $\pm$ SD of three experiments with four replicates per condition.

## 1.2. AOxNPs scavenge intracellular ROS and induce SOD2 upregulation

CeO<sub>2</sub>NPs are known for their strong antioxidant potential and have a proven capacity to reduce intracellular ROS levels in numerous cell types, including leukocytes, cardiomyocytes, spinal cord neurons and retinal neurons (Celardo et al. 2011; Niu et al. 2011; Das et al. 2007; Chen et al. 2006).

To corroborate the capacity in our AOxNPs, we measured the levels of ROS in ARPE19 cells with the H<sub>2</sub>DCFDA probe. ARPE19 cells were pre-treated with AOxNPs at increasing concentrations (from 1 mM to 500 mM) for 24 hours to allow the internalization of the nanoparticles. Afterwards, oxidative stress was induced with H<sub>2</sub>O<sub>2</sub> for 1 hour. The H<sub>2</sub>O<sub>2</sub> induction alone produced a 5-fold rise of ROS levels (Figure R.25 A), which significantly decreased in cells pre-treated with AOxNPs. This reduction was concentration-dependent and reached a plateau at 20 mM, as higher concentrations of AOxNPs did not cause a higher reduction of ROS levels. Moreover, we also observed that a pre-treatment with AOxNPs in cells without induction of oxidative stress did not cause any change in ROS levels.

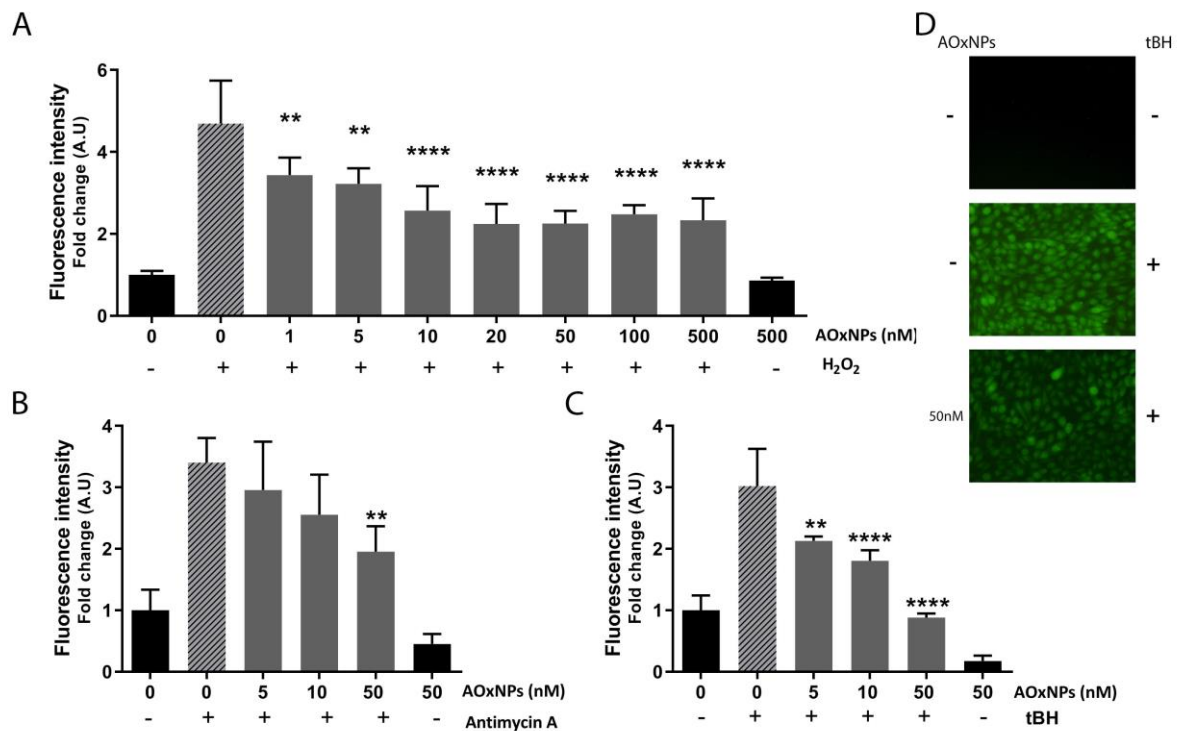


**Figure R.25. Antioxidant capacity of AOxNPs in in vitro cultures.** Dose-dependent reduction of intracellular ROS levels in ARPE19 cells treated with AOxNPs for 24h before inducing oxidative stress with **(A)** H<sub>2</sub>O<sub>2</sub>, **(B)** antimycin A and **(C)** tBH. All graphs show mean±SD of three experiments with four replicates per condition. Significant differences analysed by applying a one-way ANOVA with a Dunnet's multiple comparison test. \*\*p<0.01, \*\*\*p<0.001, \*\*\*\*p<0.0001. **(D)** Representative images of ARPE19 cells, where the fluorescence emitted by intracellular ROS levels can be observed.

Despite the achievement of reproducible results, H<sub>2</sub>O<sub>2</sub> is unstable and suffers photo-oxidation, which increases the variability between replicates. To corroborate the effect observed, we repeated the experiment inducing oxidative stress with two other oxidant agents: antimycin A and tBH. Antimycin A binds to cytochrome c reductase disrupting the electron transport chain and resulting in the formation of toxic radical oxygen species (Dairaku et al. 2004). tBH is a membrane-permeable organic peroxide that reduces the activity of glutathione peroxidase inducing oxidation (Slyshenkov et al. 2002). The two agents are widely used as free radical inducers in in vitro assays.

Both antimycin A and tBH produced a similar increase of ROS levels (Figure R.25 B, C). We observed again a concentration-dependent reduction of ROS levels in cells treated with AOxNPs, with a better outcome when using tBH as oxidizing agent. Interestingly, in that case the pre-treatment with AOxNPs at 50 nM was able to reduce ROS to basal levels and the AOxNPs treatment alone was also able to reduce ROS below the basal levels.

Cerium oxide nanoparticles act themselves as catalysts, having a biological activity similar to SOD2 or catalase (Das et al. 2013). However, it is not clear whether they could also scavenge ROS indirectly by modifying the expression of oxidative stress-related genes. We evaluated the antioxidant capacity of our AOxNPs by quantitative PCR in ARPE19 cells pre-treated with AOxNPs during 24 hours after a 4-hour induction of oxidative stress with tBH.

First, we evaluated *SOD2* expression. *SOD2* is located in the mitochondria and transforms toxic superoxide into hydrogen peroxide and diatomic oxygen, which allows to clear mitochondrial ROS, conferring protection against cell death (Korsvik et al. 2007).

The treatment with AOxNPs alone did not produce changes in *SOD2* expression (Figure R.26). However, the induction of oxidative stress caused almost a 3-fold increase in its expression. Interestingly, AOxNPs-treated cells with induced oxidative stress experienced a higher increase

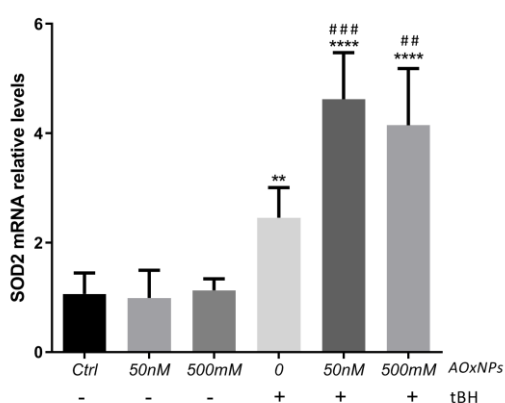


**Figure R.26. Changes in *SOD2* expression after AOxNPs treatment.** Increased expression of *SOD2* in ARPE19 cells that have been previously treated with AOxNPs. Graph shows mRNA levels normalized to GAPDH of three experiments with 6-8 replicates per condition. Statistical analyses done applying a one-way ANOVA with Dunnet's multiple comparison test. \* shows statistical differences with Ctrl. # shows statistical differences with the 0 AOxNPs bar.

in the expression of *SOD2*. AOxNPs were able to upregulate *SOD2* expression in conditions of induced oxidative stress, which increased the cellular antioxidant response.

Besides *SOD2*, we also evaluated the expression of *Nrf2*. This transcription factor is a key antioxidant regulator as it induces the expression of over 250 genes, including ROS-neutralizing enzymes or molecular chaperones among many others (Nakagami 2016). Despite its importance in oxidative stress, we did not observe an upregulation of *Nrf2* upon induction with tBH. We did see a slightly significant reduction of *Nrf2* expression in cells treated with 500 nM AOxNPs (Figure R.27 A).

NADPH oxidase 4 (NOX4) is a key enzyme of the ROS generation system. Upon induction of oxidative stress, we observed a decrease in its expression, with no significance differences in AOxNPs pre-treated cells (Figure R.27 B).

Another relevant gene in the oxidative stress response is heme oxygenase 1 (HO1): an enzyme that catalyzes the degradation of heme and whose expression is induced by oxidative stress under regulation of *Nrf2*. The induction of oxidative stress through tBH produced a high increase in the expression of HO1. AOxNPs treatment slightly reduced this upregulation although it was not significant (Figure R.27 C).

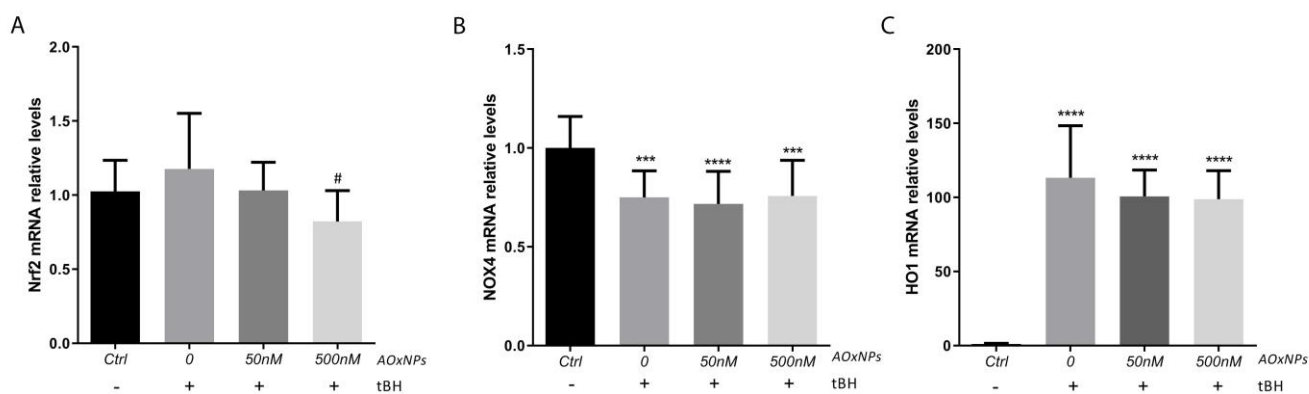


**Figure R.27. Changes in mRNA levels of genes related with the oxidative stress response.** Relative expression of (A) *Nrf2*, (B) *Nox4* and (C) HO1 genes. All data has been normalized to *Gapdh* and is shown as the mean $\pm$ SD of three experiments with 6-8 replicates per condition. Statistical analyses done applying a one-way ANOVA with Dunnet's multiple comparison test. \* shows statistical differences with Ctrl. # shows statistical differences with the 0 AOxNPs bar. #p<0.1, \*\*\*p<0.001, \*\*\*\*p<0.0001.

Overall, AOxNPs showed a consistent capacity of reducing ROS levels in vitro after an oxidative stress induction. Furthermore, although they were able to induce *SOD2* upregulation in stress conditions, the secondary effect of AOxNPs in modulating antioxidant-related gene expression needs to be further explored.

## **2. Biodistribution of AOxNPs**

The potential of CeO<sub>2</sub>NPs as a therapy for retinal degenerative pathologies has been tested *in vivo* in the *tubby* and *Vldlr*<sup>-/-</sup> mice models and in the light-damaged rat model, but in all cases it was tested through an intravitreal administration route. Given the associated complications this route of administration presents, the topical delivery is contemplated as a more convenient option.

Cerium distribution and permanence in rat eyes have been evaluated after an intravitreal injection, and the findings indicated high levels of cerium even 120 days after the injection (Wong et al. 2013). However, the efficacy of a topical administration has never been assessed. In fact, it is not known whether an antioxidant compound could cross the cornea and diffuse to the posterior part of the eye.

### **2.1. The antioxidant compound reaches mice retina after topical administration**

To elucidate whether the antioxidant compound could reach the retina and posterior pole of the eye after topical administration, we performed a biodistribution assay in C57BL/6N mice which received AOxNPs at 10 mM via either intravitreal or topical administration. For intravitreal administration, we injected 1.5 µl of AOxNPs solution, whereas for topical administration a 5 µl drop was applied in the anterior surface of the eye. Mice were euthanized 24 hours after administration, and eyes were enucleated and dissected to quantify through ICP-MS the amount of the antioxidant (AOx) compound present in the different parts of the eye, as well as in the liver and brain.

We detected 59% of all AOx administered in the eyes of mice receiving intravitreal administration versus a 10.1% in those eyes receiving the treatment topically. AOx was homogeneously distributed in the different parts of the eye after a topical administration. For instance, the amount of AOx detected in the anterior pole was 1.7% of the total administered and in the lens, we detected a 2.3%. Strikingly, the amount detected in the retina and in the posterior pole was 2.1% of total AOx administered (Table R.4). With intravitreal injection, AOx was preferentially retained in the retina (21.6% of the total AOx administered), but it was also present in the rest of eye parts. Surprisingly, the anterior pole retained 14% of all AOx administered in the vitreous cavity.



**Table R.4. Percentage of AOx detected in different tissues after diverse administration routes and schedules**

|                 | Delivery route | Ant. pole | Lens | Retina | Post. pole | Liver | Brain | Total        | Dose administered |
|-----------------|----------------|-----------|------|--------|------------|-------|-------|--------------|-------------------|
| <b>24 hours</b> | IV injection   | 14%       | 9.8% | 21.6%  | 11.4%      | 1 %   | 1.2%  | <b>59%</b>   | 2 µg              |
|                 | Topical        | 1.7%      | 2.3% | 2.1%   | 2.1%       | 1.1%  | 0.8%  | <b>10.1%</b> | 8.6 µg            |
| <b>7 days</b>   | Topical        | 1.7%      | 0.7% | 0.6%   | 0.8%       | 0.8%  | 1%    | <b>5.6%</b>  | 60.2 µg           |

As expected, the total amount of AOx detected with a single topical administration was considerably lower than with an intravitreal injection. Nevertheless, the concentration of AOx that reached the different parts of the eye with a single topical administration was about half of the reached with intravitreal injection, proving the efficiency of AOxNPs topical delivery (Figure R.28, orange and grey bars).

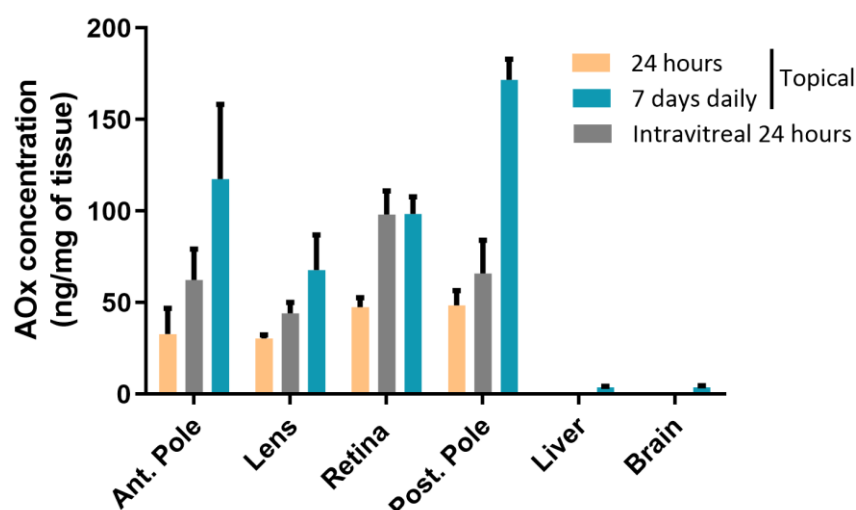


**Figure R.28. AOx concentration in different tissues after ocular administration.** Concentration of AOx after intravitreal or topical administration in the different parts of the eye, the liver and the brain. Graph shows mean±SD, n=3-4.

Knowing that topical administration is less efficient than intravitreal injection, a topical treatment will need a sustained delivery to reach an equal concentration in the retina than the concentration obtained after an intravitreal injection. To assess the number of topical administrations needed to achieve a similar concentration than with a single intravitreal injection, we applied AOxNPs 10 mM daily to 6N mice for one week.

After a week of topical daily administration, AOx concentration in the retina was about 100 ng/ml (Figure R.28, blue bar), the same concentration achieved with a single intravitreal injection. In contrast, AOx accumulated in all parts of the eye at a higher concentration than with a single intravitreal injection, preferentially in the posterior pole. Overall, the amount of AOx detected after a one-week administration was much lower than the total amount of AOx administered ( $6.48 \pm 1.5\%$  of total AOx administered,  $n=4$ ), indicating a high clearance rate.

Regarding extraocular tissues, a small amount of AOx was detected in the liver and brain with the different administrations routes and schedules. Nevertheless, the concentration per mg of tissue was very low, even negligible in some of the samples. Hence, we proved topical administration to be an effective delivery route for AOxNPs.

### **3. Evaluation of AOxNPs topical treatment efficacy in DKOrd8 mice**

The DKOrd8 mouse model has already been used to test different therapies, including the oral supplementation of antioxidants or the intravitreal injection of the neuroprotective factors PEDF and PDGF (Tuo et al. 2009; Ramkumar et al. 2013a; Wang et al. 2013; Wang et al. 2014). These therapies slowed the progression of focal retinal lesions and decreased the expression of inflammatory factors. Furthermore, it has been demonstrated that an intravitreal injection of CeO<sub>2</sub>NPs is able to reduce photoreceptors death in murine models with severe photoreceptor degeneration (Cai et al. 2012; Wong et al. 2015). Despite that, the effect of an antioxidant therapy locally delivered in the eye has not been assessed in the DKOrd8 mouse yet.

Once confirmed AOxNPs efficacy and safety in vitro, and their capacity to reach mice retinas after a topical administration, we aimed to evaluate AOxNPs efficacy as an antioxidant treatment in the DKOrd8 mouse model.

Mice were randomly distributed to receive either AOxNPs or vehicle in both eyes following a daily administration schedule during two months. We started the topical administration in 1-month old DKOrd8 mice and evaluated the efficacy of the therapy when they reached 3 months of age with in vivo and post-mortem assessments. We considered 3 months an adequate age to evaluate the effect of the treatment as DKOrd8 mice already display several phenotypic AMD-like features at that age.

#### **3.1. Retinal thinning is partially prevented with AOxNPs treatment**

The in vivo characterization of DKOrd8 mice through optical coherence tomography (OCT) revealed a main affectation in the photoreceptor layers, with a progressive thinning of the outer nuclear layer and shorter photoreceptor segments.

To evaluate the effect of AOxNPs in the preservation of retinal thickness and architecture, we performed OCT imaging comparing AOxNPs-treated and vehicle-treated DKOrd8 mice together with age-matched 6N mice as controls. We observed focal retinal lesions in DKOrd8 mice but with no important differences between AOxNPs or vehicle treatment (Figure R.29 A).

Upon quantification of the different retinal layers after the treatment, we did observe differences between groups, with a greater significance in the ONL. This layer was a 3% thicker

in *DKOrd8* mice that had received AOxNPs compared to the vehicle-treated mice (Figure R.29 B). Although it was still thinner than the ONL of 6N mice, AOxNPs slowed the progressive thinning observed in this layer.

As observed in the phenotypical characterization, IPL thickness was greater in *DKOrd8* mice, but there were no significant differences between AOxNPs and vehicle-treated mice. AOxNPs treatment did not cause any differences neither in photoreceptors inner and outer segments nor in the inner nuclear layer.

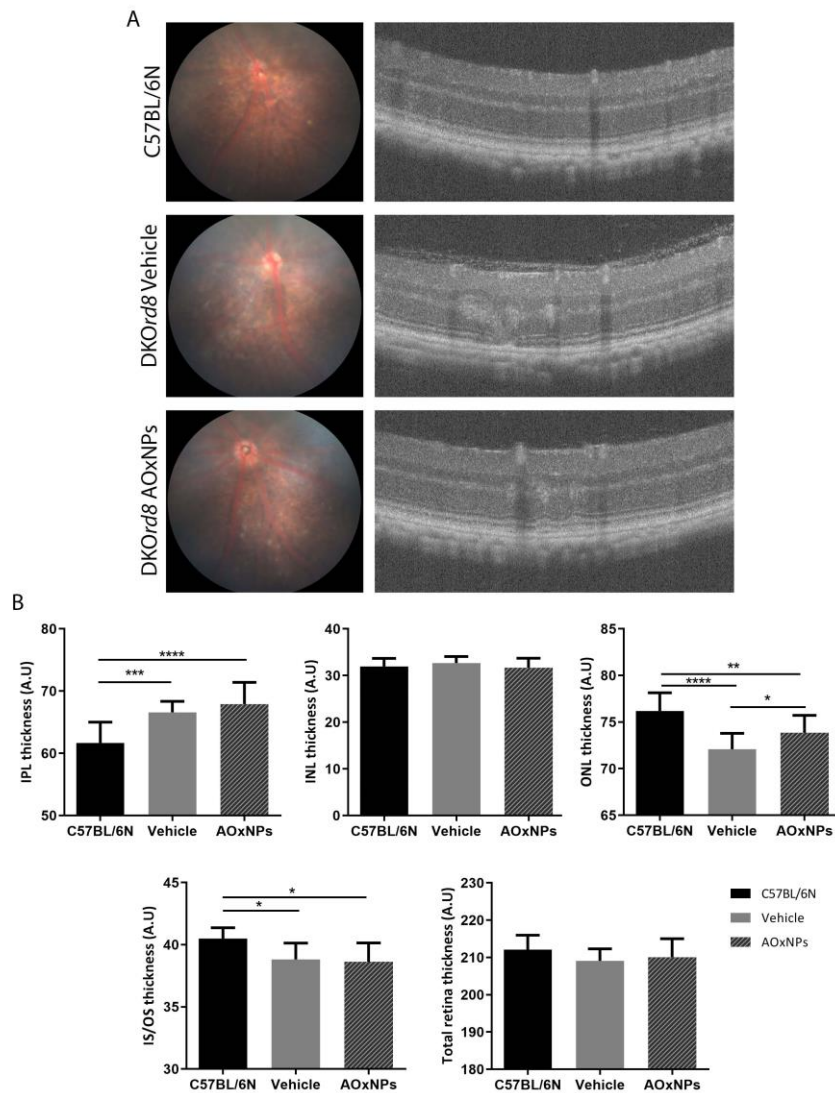


**Figure R.29. Evaluation of the retinal status and quantification of the different retinal layers. (A)** Funduscopy and OCT images of *DKOrd8* mice after a 2-months treatment with AOxNPs or vehicle, and 6N mice which were used as wild type control. **(B)** Quantification of the retina layers of the same groups using the OCT images. Graphs show the average thickness±SD of inner plexiform layer (IPL), inner nuclear layer (INL), outer nuclear layer (ONL), inner and outer segments photoreceptors' layer and total retinal in arbitrary units (A.U). Statistical analyses were performed by applying a one-way ANOVA with Tukey's multiple comparison test. \* $p < 0.05$ , \*\* $p < 0.01$ , \*\*\* $p < 0.001$ , \*\*\*\* $p < 0.0001$  n=15-20 retinas per group.

We also evaluated the preservation of retinal thickness and architecture through histological evaluation without observing any alteration in mice receiving AOxNPs daily for two months (data not shown).

### 3.2. AOxNPs treatment does not ameliorate retinal function in *DKOrd8* mice

During the characterization of the *DKOrd8* mouse model, we evaluated retinal function through electroretinography and reported a reduced function of photoreceptors in 3-months old mice, observed as decreased a-wave amplitude.

Following the analysis of AOxNPs effect in *DKOrd8* mice, we evaluated through ERG the capacity of AOxNPs to improve retinal function after a two-month treatment. For that purpose, we applied light stimuli at increasing intensities to dark-adapted *DKOrd8* mice eyes, receiving either AOxNPs or vehicle, and recorded their retinal responses. Again, we only represent the results after a mild ( $-0.2 \log \text{cd}\cdot\text{s}/\text{m}^2$ ) and a high ( $1 \log \text{cd}\cdot\text{s}/\text{m}^2$ ) light stimulations (Figure R.30).

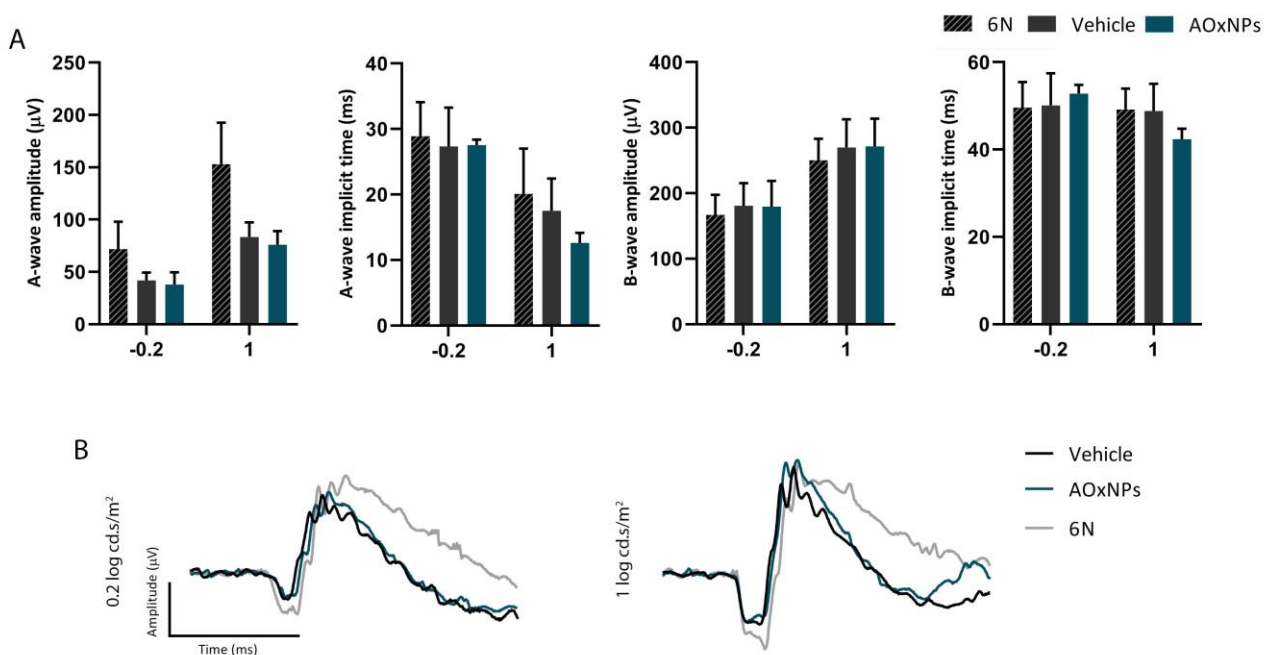


**Figure R.30. Electoretinographic responses of *DKOrd8* mice after AOxNPs treatment. (A)** Analyses of the a-wave amplitude, a-wave implicit time, b-wave amplitude, and b-wave implicit time after a light stimulus of  $-0.2 \log \text{cd}\cdot\text{s}/\text{m}^2$  and  $1 \log \text{cd}\cdot\text{s}/\text{m}^2$ . Two-way ANOVA with Sidak's multiple comparison test; \* $p \leq 0.01$ ; \*\* $p \leq 0.01$ ; \*\*\* $p \leq 0.001$  ( $n=12$  eyes per group). **(B)** Representative ERG wave forms after a light stimulus of  $-0.2 \log \text{cd}\cdot\text{s}/\text{m}^2$  and  $1 \log \text{cd}\cdot\text{s}/\text{m}^2$  in *DKOrd8* and C57BL/6N mice after the two-month treatment.

After the analyses of the recordings, we did not observe any differences in AOxNPs-treated compared to vehicle-treated *DKOrd8* mice at any of the tested intensities. Although the a-wave of *DKOrd8* mice presented decreased amplitude compared to 6N mice, the a-wave and b-wave amplitudes as well as implicit times to both waves were similar between the two *DKOrd8* groups. Therefore, the preservation of the outer nuclear layer thickness previously observed through OCT was not translated into an improvement in the visual function.

### **3.3. AOxNPs reduce microglia infiltration in *DKOrd8* mice retinas**

The characterization of *DKOrd8* mice revealed an accumulation of microglial cells in the focal retinal lesions as well as an age-dependent increase of subretinal microglia. To evaluate whether AOxNPs could have an effect in the increased microglia recruitment and migration observed in this model, we assessed quantitatively the number of microglial cells in the subretinal space and the inner retina after the two-month treatment. RPE flatmounts stained with Iba1 were used to quantify subretinal microglia, and retinal flatmounts to quantify inner retinal microglia.

*DKOrd8* mice treated with AOxNPs presented a reduced number of microglia cells both in the subretinal space (Figure R.31 B) and the inner retina (Figure R.31 D), compared to vehicle-treated mice. In fact, the number of subretinal microglial cells in AOxNPs-treated mice was slightly lower than in C57BL/6N mice, although not significant. Interestingly, we also observed an increased number of microglia in the inner retina of *DKOrd8* mice compared to 6N mice that was significantly reduced with the AOxNPs treatment.

Taken together, AOxNPs treatment reduced microglia recruitment in the subretinal space and infiltration in the inner retina of *DKOrd8* mice.

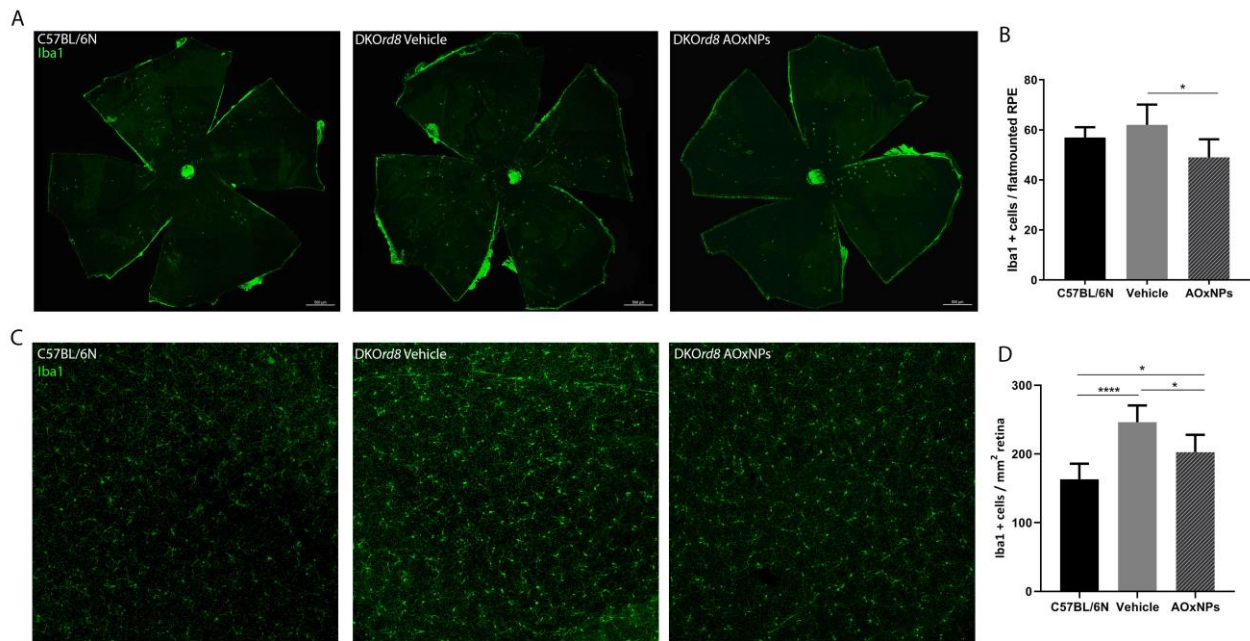


**Figure R.31. Microglia quantification in RPE and retinal flatmounts. (A)** Representative images of RPE flatmounts of DKOrd8 mice after the 2-months treatment and immunostained with Iba1. **(B)** Quantification of Iba1 positive cells in the whole RPE flatmount. **(C)** Representative images of retinal flatmounts after the two-month treatment and immunostained with Iba1. **(D)** Quantification of Iba1 positive cells in retinal flatmounts. Images from four different areas were quantified. Both graphs show mean±SD. Statistical analysis performed applying a one-way ANOVA test with Tukey’s multiple comparison test; \*p<0.05; \*\*\*\*p<0.0001; n=6-8 eyes/group.

### 3.4. AOxNPs topical treatment reverts the altered gene expression pattern of DKOrd8 mice

We also evaluated the efficacy of AOxNPs as a treatment for AMD through a gene expression profile analysis. After the two-month treatment of DKOrd8 mice with topical delivery, we removed their eyes and used the retina and posterior pole to perform a cDNA microarray.

As previously explained in the section of model characterization, the resulting data of the microarray underwent a quality control and was normalized and filtered to make all the genes comparable. In this case, from the total 8 samples of AOxNPs-treated mice, one was removed from further analyses, as it did not fit in the sample distribution plot (data not shown).

We have previously described the altered expression profile of 3-months old DKOrd8 mice compared to 6N mice, with a total of 422 genes downregulated and 69 upregulated with a log2 fold change ≥ 1 and an adjusted P value ≤ 0.01. After the AOxNPs treatment, mice were also 3 months old so data was comparable.

After the treatment, the differential expressed genes of treated *DKOrd8* mice compared to non-treated had changed; 471 genes were upregulated and 73 were downregulated, with an absolute log<sub>2</sub> fold change  $\geq 1$  and an adjusted P value of 0.01 (Figure R.32 B).

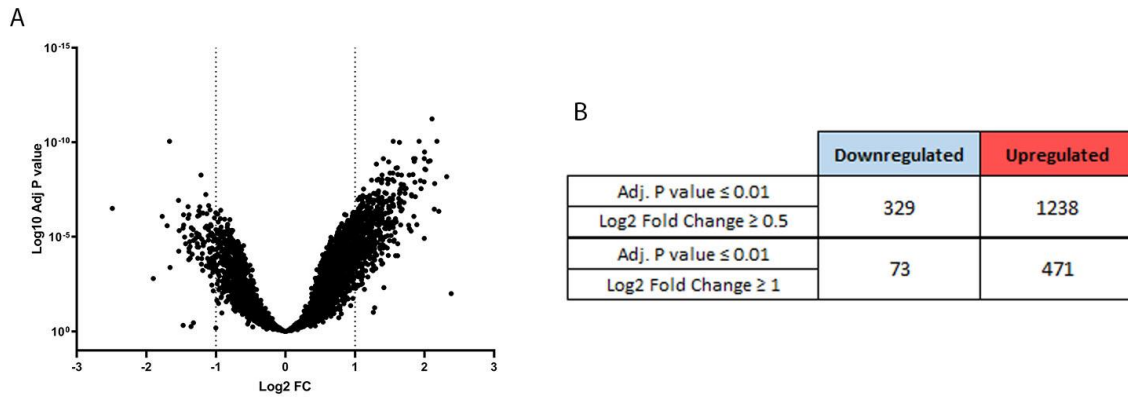


**Figure R.32. Differential gene expression in *DKOrd8* mice after the AOxNPs treatment.** *DKOrd8* mice treated with AOxNPs present an increased number of genes upregulated in comparison to non-treated *DKOrd8* mice. **(A)** Volcano plot showing all the genes included in the differential expression analysis, with dotted lines indicating an absolute fold change of 1. **(B)** Table indicating the exact number of genes up and downregulated in AOxNPs-treated mice.

The differential expression of the selected genes was represented in a heatmap (Figure R.33). This graph shows the changes in the expression pattern of AOxNPs-treated mice, with the majority of the genes that appeared downregulated in non-treated *DKOrd8* mice being upregulated after the treatment and vice versa. Surprisingly, the expression pattern of AOxNPs-treated mice closely resembled 6N mice pattern; with only 13 genes differentially expressed (10 upregulated and 3 downregulated) between these two groups.



Thus, the topical treatment with AOxNPs during two months was able to revert the altered expression pattern of *DKOrd8* mice, approaching it to the wild type 6N mice pattern.

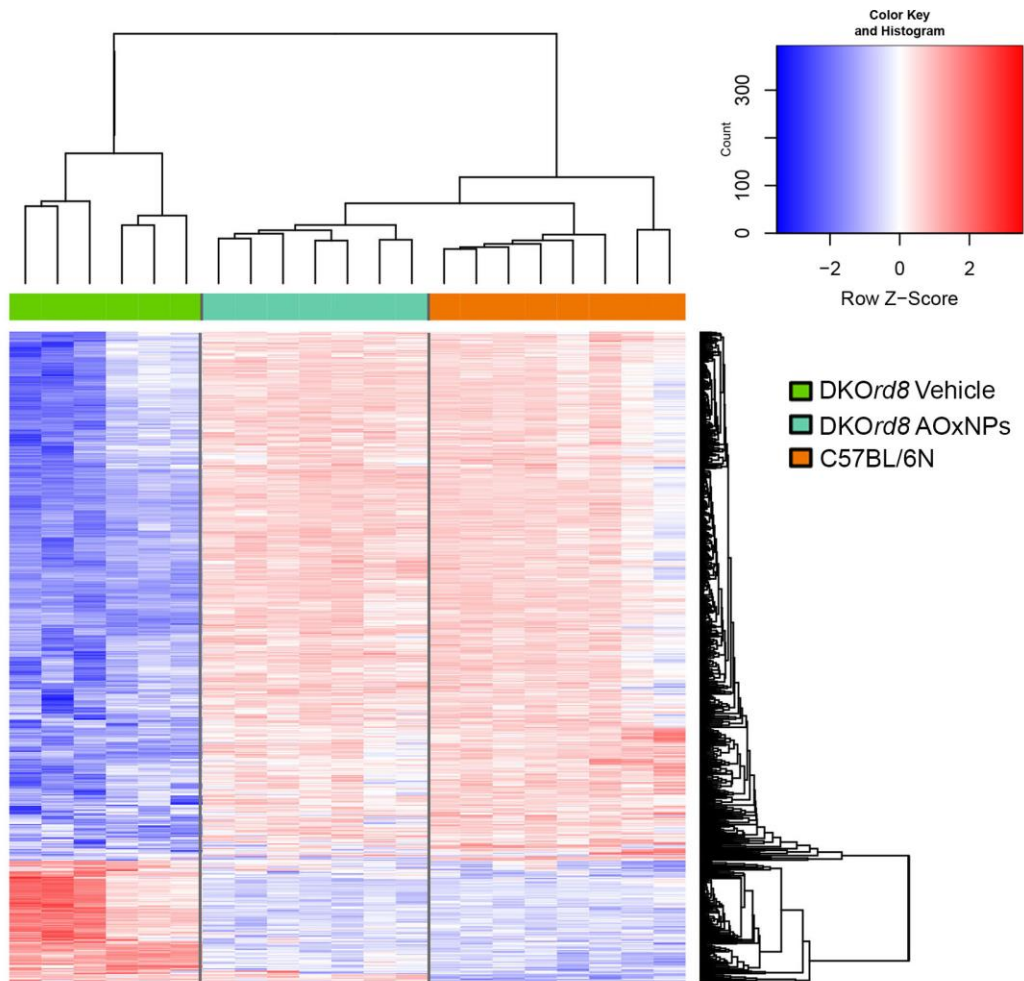


**Figure R.33. Heatmap comparing the expression pattern of *DKOrd8* mice after the treatment with AOxNPs.** Comparison of the expression pattern of *DKOrd8* mice after receiving a 2-months topical treatment (*DKOrd8* AOxNPs), with *DKOrd8* mice receiving placebo (*DKOrd8* Vehicle) and 6N mice used as wild type control (C57BL/6N). The relative expression of 491 genes is represented, with downregulated genes showed in blue and upregulated genes in red.

Interestingly, most of the genes whose expression was altered in *DKOrd8* mice experienced an up or downregulation with the AOxNPs treatment, returning to 6N levels. From the 491 genes differentially expressed in the *DKOrd8* model, 379 appeared also differentially expressed in AOxNPs-treated mice. In all cases, returning to the expression levels of 6N mice (Figure R.34).

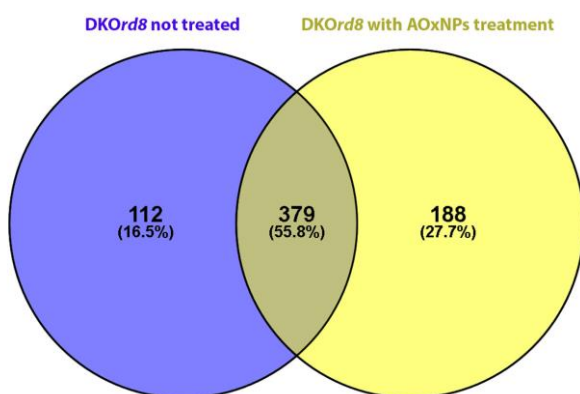


**Figure R.34. AOxNPs-treated mice share most of the differentially expressed genes.** Venn diagram showing differentially expressed in *DKOrd8* in comparison to 6N (blue); and in AOxNPs-treated mice in comparison to vehicle treated (yellow). The 379 genes shared between comparisons correspond to altered genes in *DKOrd8* mice whose expression return to 6N levels after the AOxNPs treatment.

As performed previously in the characterization of the model, we identified and categorized the genes represented in the heatmap according to their involvement in processes of oxidative stress, neuronal function, cell death, senescence, immune response and cell cycle.

All the genes related with the mitochondrial electron transport chain that were found downregulated in *DKOrd8* mice were upregulated after the treatment, returning to 6N levels.

**Table R.5. List of relevant downregulated genes in *DKOrd8* mice after AOxNPs treatment**

| Gene Symbol                      | Name   | logFC  | adj.P.Val | Function                    |
|----------------------------------|--|--------|-----------|-----------------------------|
| <b>Oxidative Stress</b>          |  |        |           |                             |
| <i>Txndc11</i>                   | Thioredoxin Domain Containing 11                 | -1,369 | 1,31E-04  | Redox regulator             |
| <i>Mrps36</i>                    | Mitochondrial Ribosomal Protein S36              | -1,104 | 2,19E-07  | Mitochondrial function      |
| <b>Neuronal function</b>         |  |        |           |                             |
| <i>Homer1</i>                    | Homer Scaffold Protein 1                         | -1,110 | 8,90E-06  | Postsynaptic density        |
| <i>Id2</i>                       | Inhibitor Of DNA Binding 2                       | -0,818 | 2,83E-05  | Neurogenesis regulator      |
| <b>Cell death and senescence</b> |  |        |           |                             |
| <i>Gas2</i>                      | Growth Arrest Specific 2                         | -1,377 | 1,78E-05  | Apoptosis                   |
| <i>Pdcd10</i>                    | Programmed Cell Death 10                         | -0,968 | 4,41E-06  | Apoptosis                   |
| <i>Mrpl20</i>                    | Mitochondrial Ribosomal Protein L20              | -0,851 | 1,28E-04  | Genomic Inestability        |
| <b>Immune response</b>           |  |        |           |                             |
| <i>Cd302</i>                     | CD302 Molecule                                   | -1,053 | 9,09E-06  | Cell adhesion and migration |
| <i>Il18</i>                      | Interleukin 18                                   | -0,973 | 4,91E-06  | Inflammation                |
| <i>Cd46</i>                      | CD46 Molecule                                    | -0,882 | 1,83E-04  | Complement system           |
| <b>Cell cycle</b>                |  |        |           |                             |
| <i>Zfp326</i>                    | Zinc Finger Protein 326                          | -1,347 | 8,10E-06  | Transcription and splicing  |
| <i>Pms1</i>                      | PMS1 Homolog 1, Mismatch Repair System Component | -1,294 | 1,24E-05  | DNA repair                  |
| <i>Stag1</i>                     | Stromal Antigen 1                                | -1,242 | 7,47E-06  | Chromatid cohesion          |

This same pattern was observed for *Nrf2* and *SOD3* expression and for most of the genes included in the other categories (Tables R.5 and R.6).

**Table R.6. List of relevant upregulated genes in DKOrd8 mice after AOxNPs treatment**

| Gene Symbol                      | Name  | logFC | adj.P.Val | Function                               |
|----------------------------------|---|-------|-----------|--|
| <b>Oxidative Stress</b>          |   |       |           |  |
| <i>Ndufs7</i>                    | NADH:Ubiquinone Oxidoreductase Core Subunit 7                       | 2,206 | 4,44E-07  | Mitochondrial electron transport chain |
| <i>Oxa1l</i>                     | Oxidase Assembly 1-Like Protein                                     | 1,817 | 6,87E-08  | Mitochondrial electron transport chain |
| <i>Cyp4f13</i>                   | Cytochrome P450 Family 4 Subfamily F Member 3                       | 1,551 | 1,94E-07  | Mitochondrial electron transport chain |
| <i>Sdha</i>                      | Succinate Dehydrogenase Complex Flavoprotein Subunit A              | 1,479 | 1,32E-06  | Mitochondrial electron transport chain |
| <i>Cox6a1</i>                    | Cytochrome C Oxidase Subunit 6A1                                    | 1,045 | 3,65E-04  | Mitochondrial electron transport chain |
| <i>Mdh2</i>                      | Malate Dehydrogenase 2  | 2,140 | 3,42E-07  | Mitochondrial metabolism               |
| <i>Fam213a</i>                   | Peroxisredoxin Like 2A  | 1,617 | 4,99E-09  | Antioxidant                            |
| <i>Atp5g1</i>                    | ATP Synthase Membrane Subunit C Locus 1                             | 1,408 | 3,84E-05  | Mitochondrial metabolism               |
| <i>Gstt3</i>                     | Glutathione S-Transferase Theta 3                                   | 1,392 | 1,06E-06  | Detox enzyme                           |
| <i>Nrf2</i>                      | Nuclear Factor, Erythroid 2 Like 2 (Nrf2)                           | 1,246 | 2,45E-04  | Antioxidant transcription factor       |
| <i>Sod3</i>                      | Superoxide Dismutase 3  | 1,182 | 6,46E-06  | Detox enzyme                           |
| <i>Tigar</i>                     | TP53 Induced Glycolysis Regulatory Phosphatase                      | 1,154 | 2,25E-06  | Antioxidant protection                 |
| <b>Neuronal function</b>         |   |       |           |  |
| <i>Gabra1</i>                    | Gamma-Aminobutyric Acid Type A Receptor Alpha1 Subunit              | 1,634 | 1,59E-07  | GABA receptor                          |
| <i>Syng13</i>                    | Synaptogyrin 3  | 1,556 | 2,40E-07  | Neurotransmission                      |
| <i>Gfra1</i>                     | GDNF Family Receptor Alpha 1  | 1,539 | 9,22E-09  | Neurotrophic receptor                  |
| <i>Impg2</i>                     | Interphotoreceptor Matrix Proteoglycan 2                            | 1,408 | 7,24E-10  | PhOS maintenance                       |
| <i>Rdh12</i>                     | Retinol Dehydrogenase 12  | 1,308 | 1,41E-09  | PhR detoxification                     |
| <i>Cdh13</i>                     | Cadherin 13   | 1,275 | 1,10E-05  | Axon growth regulator                  |
| <i>Nrl</i>                       | Neural Retina Leucine Zipper  | 1,245 | 2,19E-06  | Photoreceptors function regulator      |
| <i>Aplp1</i>                     | Amyloid Beta Precursor Like Protein 1                               | 1,143 | 2,44E-07  | Neurotransmission                      |
| <i>Casp6</i>                     | Caspase 6   | 1,043 | 2,40E-06  | Axons maintenance                      |
| <b>Cell death and senescence</b> |   |       |           |  |
| <i>Tmem59</i>                    | Transmembrane Protein 59  | 2,693 | 5,79E-12  | Autophagy regulator                    |
| <i>Terf2ip</i>                   | TERF2 Interacting Protein   | 2,000 | 3,23E-10  | Telomere regulation                    |
| <i>Gadd45g</i>                   | Growth Arrest And DNA Damage Inducible Gamma                        | 1,996 | 1,19E-05  | Apoptosis regulator                    |
| <i>Tbc1d17</i>                   | TBC1 Domain Family Member 17  | 1,772 | 2,40E-06  | Autophagy regulator                    |
| <i>Dad1</i>                      | Defender Against Cell Death 1                                       | 1,434 | 5,51E-07  | Apoptosis regulator                    |
| <i>Bag6</i>                      | BCL2 Associated Athanogene 6  | 1,341 | 8,87E-09  | Apoptosis regulator                    |
| <i>Atg4b</i>                     | Autophagy Related 4B Cysteine Peptidase                             | 1,153 | 4,60E-07  | Autophagy regulator                    |
| <i>Mtor</i>                      | Mammalian Target Of Rapamycin                                       | 1,082 | 4,20E-06  | Autophagy regulator                    |
| <b>Immune response</b>           |   |       |           |  |
| <i>Cd59a</i>                     | CD59 Antigen  | 1,941 | 1,06E-08  | Complement system                      |
| <i>Sike1</i>                     | Suppressor Of IKBKE 1   | 1,640 | 1,00E-10  | Inflammation regulator                 |
| <i>Ikkg</i>                      | Inhibitor Of Nuclear Factor Kappa B Kinase Regulatory Subunit Gamma | 1,372 | 1,09E-08  | NF-KB inhibitor                        |
| <i>Ccl27a</i>                    | C-C Motif Chemokine Ligand 27                                       | 1,272 | 6,38E-06  | Immune response regulator              |
| <b>Cell cycle</b>                |   |       |           |  |
| <i>Cdc23</i>                     | Cell division cycle 23  | 2,016 | 2,81E-09  | DNA replication - cell cycle           |
| <i>Pold2</i>                     | DNA Polymerase Delta 2, Accessory Subunit                           | 1,277 | 1,22E-07  | DNA repair                             |
| <i>Usp11</i>                     | Ubiquitin Specific Peptidase 11                                     | 1,234 | 2,83E-07  | Epigenetic modifications               |

Some genes that were upregulated in the DKOrd8 model maintained that upregulation after the treatment (112 genes, showed in Figure R.34). This was the case of the cytokine-related genes *Ccr1* and *Ccl2*, the immune response regulator *NF-kB*, or the cell cycle regulator *Cdkn1a*. In these genes, the treatment with AOxNPs did not cause any changes in their expression.

Other genes not differentially expressed in the DKOrd8 model experienced a change in their expression after the AOxNPs treatment. This was the case of 188 genes (Figure R.34), which

included *Fam312a* and *Tigar*, genes involved in mitochondrial trafficking and in the protection of DNA damage by ROS respectively. The expression of *Nrl* and *Homer1* genes, which are related to photoreceptor and synaptic function, were also altered; as well as the expression of *Dad1* and *Bag6* genes, related with apoptosis, among many others.

Again, we looked into the genes associated with AMD that were differentially expressed in the *DKOrd8* model. After the AOxNPs treatment, most of them returned to 6N levels of expression (Table R.7).

**Table R.7. List of genes associated with AMD**

| Gene Symbol                | Name                                | logFC  | adj.P.Val | Function                   |
|----------------------------|-------------------------------------|--------|-----------|----------------------------|
| <b>Genes upregulated</b>   |                                     |        |           |                            |
| <i>Timp3</i>               | TIMP Metallopeptidase Inhibitor 3   | 1,374  | 1,01E-06  | Bruch's membrane marker    |
| <i>Ctsb</i>                | Cathepsin B                         | 1,039  | 4,79E-07  | Involved in APP processing |
| <b>Genes downregulated</b> |                                     |        |           |                            |
| <i>Omd</i>                 | Osteomodulin                        | -1,390 | 1,61E-04  | MD related gene            |
| <i>Mrpl20</i>              | Mitochondrial Ribosomal Protein L20 | -0,851 | 1,28E-04  | Bruch's membrane marker    |
| <i>Crygb</i>               | Crystallin Gamma B                  | -1,109 | 3,93E-04  | RPE marker                 |

We also performed analyses of biological significance to gain insight into the biological function of all the genes differentially expressed after the AOxNPs treatment. Interestingly, the GO terms with higher ratio fitted into the ATP metabolic process, directly related with the mitochondrial electron transport chain, where ATP is produced. The other GO terms with higher ratio were related with the cellular catabolism and ribonucleoprotein complex, involved in processing RNA transcripts. Among the downregulated genes, only a few GO terms were significantly enriched, which fitted into the RNA localization category.

Overall, AOxNPs topical treatment was able to revert the altered gene expression pattern of *DKOrd8* mice. Most differentially expressed genes in the model returned to 6N levels after the treatment, with very few differences between treated and 6N mice. Moreover, gene enrichment analyses showed major differences in the ATP metabolic process, directly related to the production of ATP in the mETC and therefore, to oxidative stress.

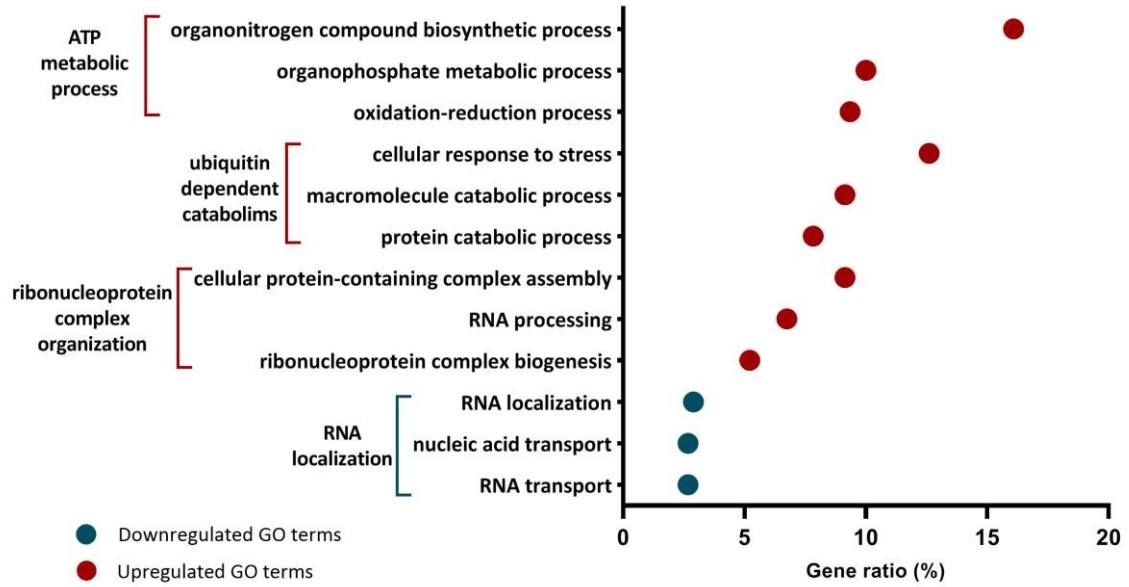


**Figure R.35. Gene enrichment analysis.** Graph showing the main biological functions over-represented in the gene enrichment analysis, with the three GO terms with higher gene ratio. Downregulated GO terms are shown in blue and upregulated in red.

The background is an abstract watercolor composition. It features a dense network of thin, black, branching lines that resemble a neural network or a complex web. Interspersed among these lines are numerous dark, irregular spots and blotches in shades of black, dark grey, and charcoal. The overall color palette is dominated by warm, earthy tones such as ochre, tan, and light brown, with some cooler, muted blue-grey washes. The texture appears soft and layered, characteristic of watercolor painting on paper. The word "DISCUSSION" is centered in the upper half of the image.

# DISCUSSION



The efforts invested in the last decade in the study of AMD have granted a deeper knowledge of its pathogenesis and a better understanding of its associated risk factors, essential for the study of new treatments. Nevertheless, to this day, no effective therapy to revert or stop the progression of AMD has been developed.

With this in mind, we generated a reliable mouse model that mimics certain features of AMD and proved the beneficial effect of AOxNPs, administered as topical eye drops, in improving the pathological characteristics of the model.

## **1. The use of murine models to study AMD**

### **1.1. Limitations of mice to model AMD**

The development of effective treatments for AMD, as happens in other complex degenerative diseases, remains challenging mainly because of the lack of models recapitulating the totality of alterations that compose the phenotype of the disease.

All the murine models developed for the study of AMD have helped to gain insight into the contribution of different pathological mechanisms such as genetic polymorphisms, oxidative stress, lipid metabolism and dysregulation of the complement or chemokine pathways. Mouse models have been able to recreate many of the histological features of AMD including the thickening of Bruch's membrane, the development of drusen-like deposits in the subretinal space, the atrophy of photoreceptors and RPE, and the accumulation of lipofuscin, complement proteins and microglial cells (Pennesi et al. 2012). However, all these models do not recapitulate the totality of the features, and if so, they do it at a very advanced age, which hinders their use in the search of effective treatments. In this regard, the *DKOrd8* model constitutes an improvement, as it is the only AMD model that starts presenting phenotypic alterations already at one month of age and develops all the features mentioned above before the 9 months.

Another significant limitation of murine models is their lack of macula, which has been postulated as one of the reasons why mice do not recapitulate the complex evolution of AMD (Marmorstein and Marmorstein 2007). A few studies have tried to localize a macula-like region in murine retinas. In all cases, a higher density of photoreceptors in the central retina compared to the peripheral retina has been observed. But quantitatively, this central-peripheral density difference in mice is considerably lower than the macula-retina difference in humans (Carter-



Dawson et al. 1979; Jeon et al. 1998; Volland et al. 2015). Moreover, in contrast to the human macula, mice central retina is mainly composed of rods, with only 2.2% of cones. Despite this, the density of photoreceptors is 3 to 4 times greater in mice retinas than in the human macula. As a higher photoreceptor density implies a greater phagocytic load on the RPE, murine RPE cells have more photoreceptor outer segments (PhOS) to degrade and are likely to be more susceptible to inefficiencies in this process. Overall, the phagocytic load per RPE murine cell is considered to be more than double than the load of RPE cells in the human macula (Volland et al. 2015).

These existing variations in the density and composition of photoreceptors between mouse and human retinas should be considered when using mice as models. The same consideration applies for the increased phagocytic load of RPE cells in mice, which in fact, could be a reliable feature to study the role of RPE in AMD.

In the seeking of reliable models, a postulated alternative is the dog. Canine retinas also present a higher photoreceptor density than human retinas. But unlike mice, dogs possess an increased number of cone photoreceptors in their central retina, constituting a fovea-like area (Mowat et al. 2008; Beltran et al. 2014). Moreover, an increasing number of naturally occurring genetic mutations associated with retinal degeneration in humans have also been observed in dogs (Miyadera et al. 2012; Miyadera 2018). In fact, some of these genetic mutations cause a progressive retinal degeneration starting in the fovea-like area of dogs' retina (Beltran et al. 2006). Hence, the dog is proving to be a valuable large animal model for the preclinical testing of novel therapeutic approaches. It could be of great use as an intermediate model to translate the effects observed in mice to human trials.

## 1.2. The importance of the genetic background

The *Ccl2*<sup>-/-</sup>; *Cx3cr1*<sup>-/-</sup> mouse model, developed initially by Tuo et al., was the first model recapitulating most of the AMD-like features at an early age, starting already at one month. Nevertheless, finding the presence of the *Crb1*<sup>rd8/rd8</sup> mutation in those mice some years later defined the genetic background to be of great importance in the manifestation of the phenotype; as *Ccl2*<sup>-/-</sup>; *Cx3cr1*<sup>-/-</sup> mice generated in a 6J background did not present the severe features observed in mice with 6N background (Raoul et al. 2010; Vessey et al. 2012).

The *Crb1*<sup>rd8/rd8</sup> mutation, present in all the vendor lines of C57BL/6N mice, causes some retinal abnormalities with a penetrance around 10 to 15%, although with variations between vendors (Mattapallil et al. 2012). The main pathological features observed are the presence of small multifocal lesions in the retina observed in the histological evaluation as retinal folds, located predominantly in the inferior nasal eye fundus; and a slow photoreceptor degeneration (Moore et al. 2018). Despite that, affected *rd8* mice maintain their retinal function even at advanced ages (9 months), with ERG responses comparable to other wild type mice (Saul et al. 2017; Aleman et al. 2011). The *rd8* mutation alone is necessary but not sufficient for the development of these features. Other mouse lines with different genetic origins (Balb/c and 129S2/Sv) carrying the *rd8* mutation did not manifest retinal lesions in the inferior retina (Luhmann et al. 2015), highlighting how genetic background differences can influence on the manifestation of these retinal abnormalities.

For the generation of our DKO*rd8* mice, the backgrounds of the founder mice were 6J for the *Ccl2*<sup>-/-</sup> mice, a mixed 6J and 6N for the *Cx3cr1*<sup>-/-</sup> mice, and 6N for the C57BL/6N mice, resulting in a mouse with a mixed background, with a higher contribution of the 6N. For that reason, we chose 6N mice as wild type controls in all our experiments. Therefore, we could differentiate the pathological features caused by the combination of both *Ccl2* and *Cx3cr1* inactivation from the ones caused by the *rd8* mutation and the genetic background.

In either case, given the variability implicit in the genetic background, we performed two backcrosses of our DKO*rd8* mice with 6N mice to homogenize the genetic background of our model (Figure D.1). Each backcross took around 10 months to be performed. As a result, we could not include the characterization of the backcrossed mice in this thesis and used the ones obtained after the first generation, taking in consideration the variations that might be implied due to background differences.

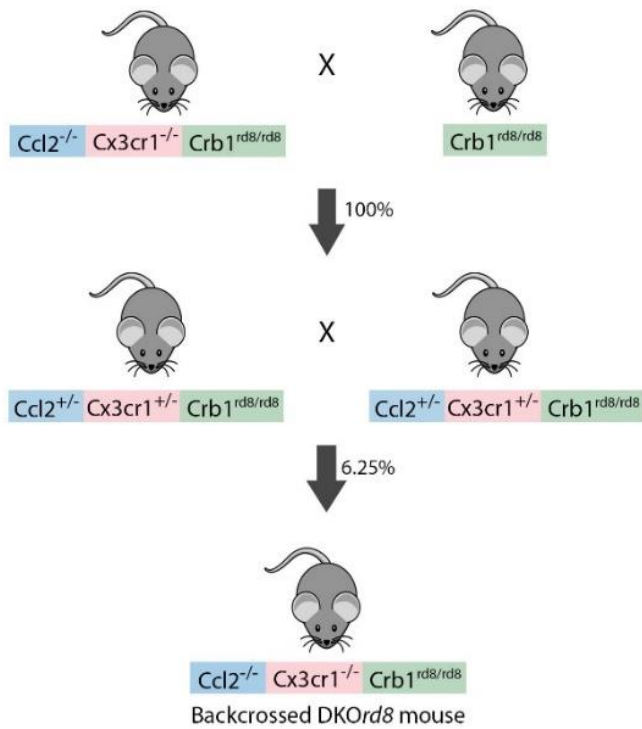


**Figure D.1. Scheme followed for the generation of a backcross.** The initial DKOrd8 mice ( $Ccl2^{-/-}; Cx3cr1^{-/-}; Crb1^{rd8/rd8}$ ) were crossed with 6N mice ( $Crb1^{rd8/rd8}$ ). The mice obtained, heterozygous for  $Ccl2$  and  $Cx3cr1$  and homozygous mutant for  $Crb1$ , were intercrossed. After genotyping all the progeny, the pups with the three mutations in homozygosis ( $Ccl2^{-/-}; Cx3cr1^{-/-}; Crb1^{rd8/rd8}$ ) were maintained as the first backcrossed mice. This same scheme was followed again to generate the second backcross.

## 2. A close look into the pathological features of the *DKOrd8* mice

### 2.1. Location of the retinal lesions

*DKOrd8* mice are known to present early lesions in the inferior retina, starting in the outer nuclear layer, which enlarge with ageing leading to photoreceptor degeneration (Zhou et al. 2011). During the characterization of our *DKOrd8* mice, we corroborated this phenotype by observing the presence of retinal spots in the inferior hemisphere of their eye fundus already at one month of age.

Curiously, the localization of the retinal lesions of our *DKOrd8* mice (predominantly in the inferior nasal quadrant) was the same described in 6N mice. In our case, however, the 25 wild type 6N mice followed up did not present any abnormality in their eye fundus, highlighting the existing differences in penetrance and vendor lines (Mattapallil et al. 2012).

The reason why these lesions are restricted to the inferior retina has not been elucidated. *DKOrd8* mice raised in complete darkness since birth, showed the same inferior localization of the lesions at 8 weeks of age (Luhmann et al. 2012), supporting that the manifestation of these lesions is not light-dependent. This same pattern has also been observed in the *Crb1*<sup>-/-</sup> mice, a model with severe retinal degeneration. *Crb1*<sup>-/-</sup> mice bred in the dark for 6 months suffered the same level of retinal degeneration (predominantly in the inferior temporal quadrant) as mice kept in a 12/12 hour light/darkness cycle (van de Pavert et al. 2007). Retinal lesions of our *DKOrd8* mice started also in the outer nuclear layer (ONL), as previously reported, disrupting the outer plexiform layer (OPL) and reaching the inner nuclear layer (INL). We also observed a progressive degeneration of the ONL, confirmed through quantification of the layers' thickness. However, this degeneration was not as severe as the reported by Zhou et al and Luhmann et al., whose *DKOrd8* mice (originally generated by Tuo et al.) suffered a drastic decrease of retinal thickness by 8 months of age (Figure D.2).

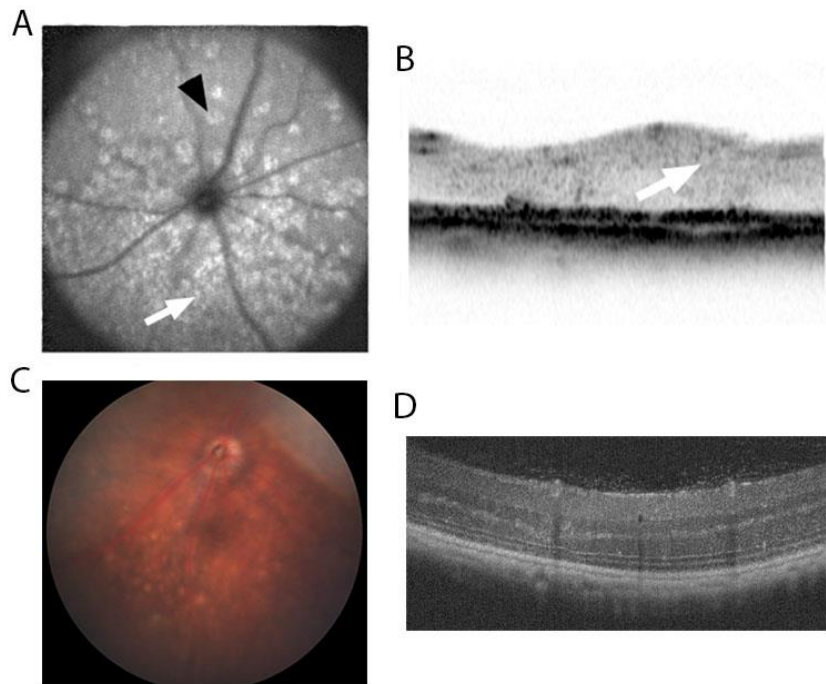


**Figure D.2. In vivo assessment of eye fundus and retinal status of two different lines of DKOrd8 mice.** (A, B) Eye fundus and OCT images from an 8-months old DKOrd8 mice originated by Tuo et al., showing an increased number of fundus spots and severe retinal degeneration with loss of the different layers. Images from Luhmann et al., 2012. (C, D) Eye fundus and OCT images from a 9-months old DKOrd8 mice from the colony we generated and characterized. The outer nuclear layer thickness is decreased but the different retinal layers can be still distinguished.

Considering that both models present the same three mutations in homozygosis, the most plausible explanation of these differences lies in the genetic background. As stated previously, the genetic background has a huge influence in wild type 6N mice, as the *rd8* mutation alone is not sufficient for the development of retinal alterations (Luhmann et al. 2015). In this regard, the characterization of the backcrossed DKOrd8 mice we already obtained should elucidate the precise implications of the background in these differences.

## 2.2. Altered retinal function: age-related or a feature of the model?

DK*Ord8* mice presented a progressive loss of photoreceptors. In accordance with that, ERG recordings reflected an altered activity of these cells observed as decreased a-wave amplitude already at 3 months, which was maintained in succeeding recordings, although with some exceptions.

This is the case of the ERG results from 5-months old mice, where no significant differences between DK*Ord8* and 6N mice were observed neither at mild nor at high light stimulation. These differences are rather explained by the variability of the technique. ERG is a complex and very sensitive technique in which small technical difficulties can imply variations in the recorded response. For this reason, it is important to have a consistent number of animals to corroborate the results. In our case, mice evaluated at the different time points were the same, assuming an identical phenotypic variability and we included a minimum of 12 animals per group to perform the statistical analyses.

Given the progressive thinning observed in the ONL due to a loss of photoreceptors, we expected to see a decline in ERG amplitudes over time. But this was not the case. Although a-wave amplitude was decreased in 9-months old DK*Ord8* mice, it was similar to the 3-months old response. The already reduced function of photoreceptors at 3 months did not deteriorate over time.

Regarding the b-wave amplitude (which mainly reflects the activity of bipolar cells in the INL), we did not observe significant differences between DK*Ord8* and 6N mice at any of the months and intensities analyzed. Thus, the electric transmission from the ONL to the GCL was conserved. What we did observe was a b-wave amplitude decrease from 5 to 7 months only at high light stimulation, and this observation was similar in both DK*Ord8* and 6N mice. ERG studies in aged mice point out a reduced retinal function seen as a decreased b-wave amplitude, striking at 6 months, without observing significant changes in photoreceptors density (Li et al. 2001; Gresh et al. 2003). Other studies in aged models also showed that the implicit time to the b-wave does not change in 12 and 22-months old mice and rats (Nadal-Nicolás et al. 2018). In our model, implicit times to both a and b-waves were increased from 7 months on, indicating a slower response of the retina. Therefore, we suggest that the decreased b-wave amplitude observed from 7 months on was derived from ageing but the increased implicit time was a pathological feature of the model.

The retinal response of *Ccl2*<sup>-/-</sup>; *Cx3cr1*<sup>-/-</sup> mice without the *rd8* mutation has been evaluated by Vessey et al., observing only a decreased amplitude of the OPs in 9 months old mice. Amplitudes

and implicit times to a and b waves were not altered. Those same mice presented an aberrant morphology of amacrine cells (Vessey et al. 2012), the activity of which is reflected in the OPs wavelets (Wachtmeister 1987). Taken together, these results suggested a reduced inner retinal function due to alterations in amacrine cell signaling, not dependent on the *rd8* mutation.

Unlike the *Ccl2*<sup>-/-</sup>; *Cx3cr1*<sup>-/-</sup> mice without the *rd8* mutation, our *Ccl2*<sup>-/-</sup>; *Cx3cr1*<sup>-/-</sup>; *Crb1*<sup>rd8/rd8</sup> mice presented decreased OPs amplitude already at 3 months of age and increased implicit times from 7 months on. Therefore, the presence of the *rd8* mutation in combination with the absence of *Ccl2* and *Cx3cr1* caused a greater impairment in the OPs response.

Despite not evaluating amacrine morphology in our model, histological and immunofluorescence stainings showed that focal retinal lesions of *DKOrd8* mice caused the disruption of the OPL, where synapses between photoreceptors and amacrine, bipolar and horizontal cells occur. In fact, synaptophysin expression in these areas was lost. These mild alterations in the OPL might be the cause of the reduced OPs wavelets. But in any case, this partial affectation in the OPL is not translated into changes on the b-wave amplitude. A more severe damage in the retina is needed to see differences in the ERG response.

### **2.3. Histological alterations and compensative mechanisms**

The histological evaluation performed in our *DKOrd8* mice corroborated the phenotype observed by the in vivo imaging through OCT and helped us to compare it to the previous description of the *DKOrd8* mice generated by Tuo et al. In both cases, retinal lesions were located in the ONL at an early stage and disappeared with time, producing a loss of photoreceptors and a thinning of their nuclear layer.

In our case, we were not able to find major histological changes in the retinas of 1-month old *DKOrd8* mice although we had observed alterations in the ONL through OCT imaging. This lack of major histological alterations could be explained by the fact that the histological evaluation was not performed in a great number of eyes. Nevertheless, we did observe an increased gliosis already in 1-month old *DKOrd8* mice, indicating an activation of Müller glia.

Müller cells act as supportive retinal cells and present a great number of functions: (i) provide metabolic nutrients to the retina, (ii) maintain the ionic and water balance, (iii) protect against oxidative stress increasing the secretion of antioxidants, (iv) release neuroprotective and

vasoactive substances, (v) serve as scaffolds for neurovascular guidance, and (vi) support synaptic activity (Reichenbach and Bringmann 2013). Müller cells are rapidly activated following almost any pathological insult in the retina to protect retinal structure and function. The most prominent feature of this activation, known as reactive gliosis, is the increased expression of intermediate filaments, including GFAP and vimentin, although the purpose of this process remains a matter of concern (Telegina et al. 2018).

The link between reactive gliosis and retinal degeneration is well established. Activation of Müller cells can have an initial positive effect through the secretion of neurotrophic and antioxidant factors (Fu et al. 2015; Lee et al. 2011). But if gliosis persists, Müller cells accelerate neuronal death (Eastlake et al. 2016). In fact, in most models of degenerative retinal diseases, GFAP expression is increased and precedes neuronal apoptosis (Graca et al. 2018). Additionally, studies in mice deficient for GFAP and vimentin have shown a reduced photoreceptors death following induced retinal detachment and a preservation of the ONL thickness (Nakazawa et al. 2007).

Our *DKOrd8* mice exhibited reactive Müller cells at 1 month of age. By 3 months of age, GFAP expression surrounded the focal lesions in the ONL, pointing out the role of Müller cells in the formation of the lesions and posterior loss of photoreceptors. As lesions progressed, GFAP expression was slightly decreased. Nevertheless, gliosis was still present in 9-months old *DKOrd8* mice, which is consistent with studies showing that the GFAP-positive filaments already formed, may remain for many months after the retinal insult or injury (Seoane et al. 1999).

Another histological alteration observed in our *DKOrd8* mice retinas was the decreased expression of opsin in 3-months old mice, which suggested a major affectation of cones in the degenerative process. A reduced expression of opsin was previously observed in 1-month old *DKOrd8* mice (Zhang et al. 2013). Other genetic models with severe retinal degeneration (*RPE65*<sup>-/-</sup> and *Elovl4*<sup>-/-</sup> mice, among others) also showed a preceding affectation of cones and a belated death of rods (Vasireddy et al. 2006; Znoiko et al. 2005).

The reason why cones suffer apoptosis before rods in all those mouse models is not fully understood. In aged humans and patients with early AMD, early cone affectation has been associated with elevated levels of oxidative stress experienced in the macula, where an increased density of these photoreceptors is found (Shelley et al. 2009). But mice present a poor percentage of cones in the central retina. Whether cones are more susceptible than rods to retinal pathological processes should be further assessed. As a start, photopic ERG recordings in



light-adapted *DKOrd8* mice (useful to record only cone responses) could provide additional information about the effect of this loss on retinal function.

Studies in humans presenting advanced AMD have shown an increased thickness of the INL within the areas of geographic atrophy, associated with poor visual acuity. It is hypothesized that changes in the INL thickness associated to photoreceptors degeneration try to compensate this loss, although do not achieve the maintenance of the visual function (Ebner et al. 2016).

*DKOrd8* mice did not present significant changes in the INL thickness compared to 6N mice, but we did observe differences in the IPL thickness. Whereas 6N mice experienced a progressive thinning of this layer, IPL thickness in *DKOrd8* mice suffered an initial decline, but from 5 months on it slightly increased and stabilized. Whether this increase is a compensative response to the greater ONL degeneration observed in the model or the age-related decrease of INL thickness could not be concluded. Changes in this layer in other models for retinal degenerative diseases have not been fully addressed and in AMD patients, IPL thickness is maintained in early and intermediate stages and starts decreasing in advanced AMD (Muftuoglu et al. 2017).

RPE cells are considered to be the first cell type affected in AMD. Their progressive degeneration causes a dysregulation of their many functions inducing the death of photoreceptors. Despite RPE cells from mice have a higher phagocytic load than RPE cells from humans, *DKOrd8* mice did not present alterations in their RPE cells until 9 months. At that age, we observed an increased vacuolization. The presence of vacuoles in RPE cells has been associated with atrophic cells in other mouse models, although in all cases, appeared at a more advanced age (Huang et al. 2017; Muraoka et al. 2018). The earlier alteration of RPE cells in *DKOrd8* mice suggests a greater affectation of these cells than in other models. In line with that, Wang et al showed a higher susceptibility to apoptosis after either inflammatory stimulation or oxidative stress in *DKOrd8* RPE cells compared to RPE cells from 6N mice (Wang et al. 2012).

Taking in consideration these results, the *DKOrd8* mice and primary cultures of their RPE cells could be of great use for understanding the pathological changes undergoing and their implication in the phenotype of *DKOrd8* model.

## 2.4. The role of microglia in retinal degeneration

Microglia plays an important role in the correct function of the retina, taking part in the formation of the retinal-blood barrier, phagocytizing cellular debris and eliminating visual by-products among other functions (Li et al. 2015). Studies depleting microglial cells from the retina showed that the long-term absence of retinal microglia in healthy retinas results in the gradual degeneration of retinal synapses and the deterioration of the ERG response (Wang et al. 2016). In degenerating retinas, microglia also contributes to the survival of retinal neurons and to the maintenance of retinal architecture (Zhao et al. 2015).

During the characterization of the *DKOrd8* model we studied the distribution of retinal microglia in mice retinas. The two main features observed were (i) an accumulation in retinal focal lesions, and (ii) an age-dependent migration and accumulation of microglia in the subretinal space.

Fundus imaging and immunofluorescence staining revealed that microglia accumulated in focal retinal lesions of *DKOrd8* mice although it was not correlated with an increase in the total number of retinal microglia. Other mouse models for retinitis pigmentosa, with severe retinal degeneration, also experience an accumulation of microglia in the degenerative areas. These studies suggest that microglia is recruited to the ONL through chemoattractive signals secreted by stressed photoreceptors to phagocyte the dying ones (Zhao et al. 2015; Zhou et al. 2017). Therefore, we presumed that microglia would be also involved in the progressive loss of photoreceptors of the *DKOrd8* model.

The second feature observed was the age-dependent accumulation of subretinal microglia striking at 9 months of age. This feature has already been described in 14-months old 6N mice but not in aged-matched 6J mice (without the *rd8* mutation) (Aredo et al. 2015; Xu et al. 2008). Regarding *Cx3cr1*<sup>-/-</sup> and *Ccl2*<sup>-/-</sup> single knockout mice, discrepancies succeeded in different studies before noticing that the *rd8* mutation was the determining factor. Some years ago, the importance of the genetic background was not considered as relevant as today. And in most of the studies developed in *Cx3cr1*<sup>-/-</sup> and *Ccl2*<sup>-/-</sup> single knockout mice, the presence or absence of the *rd8* mutation was not specified (Luhmann et al. 2013; Combadière et al. 2007; Chinnery et al. 2012). Microglia accumulation has also been evaluated in *Ccl2*<sup>-/-</sup>; *Cx3cr1*<sup>-/-</sup> mice without the *rd8* mutation and in that case, an increase of subretinal microglia was not observed until 18-months of age (Chen et al. 2013).

The general conclusion extracted from all these studies is that the accumulation of subretinal microglia is an age-dependent feature experienced by 6N and *Ccl2*<sup>-/-</sup>; *Cx3cr1*<sup>-/-</sup> double knockout

mice, appearing at a very advanced age, but that the combination of the three genetic alterations in the *DKOrd8* model accelerate the subretinal accumulation of the microglia.

Another representative feature of AMD observed in *DKOrd8* mice is the presence of yellowish deposits in the eye fundus, referred to as drusen-like deposits, which have been associated with the accumulation of subretinal microglia. We observed an increased number of these deposits in the eye fundus of 9-months old *DKOrd8*, predominantly in the superior hemisphere. Curiously, these deposits are observed in most models mimicking AMD at an advanced age, regardless of the pathway affected.

At this point, we wondered whether the background of those models was influencing the phenotype observed. Surprisingly, we noticed that all the models reported to present drusen-like deposits (see Table I.2) had a C57BL/6 background, without specifying if 6N or 6J in most of the cases. All the genetic models including the *Nrf2*<sup>-/-</sup>, *SOD1*<sup>-/-</sup>, *Cfh*<sup>Y402H</sup>, *ApoE*<sup>-/-</sup> and others, had been generated in C57BL/6 background; and for the induced models, such as the cigarette smoking and the immunized model with CEP, C57BL/6N mice were also used.

The exact mechanism leading to this phenotype will have to be furthered explored, but it seems evident that the presence of drusen-like deposits associated with the accumulation of subretinal microglia is a characteristic dependent on the C57BL/6 background and more probably, on the *rd8* mutation, more than a feature of the model itself.

## 2.5. The gene expression profile as an AMD-like feature

The tools to study complete transcriptomes have experienced great improvements in the last years and a significant reduction of their costs. However, the current knowledge of the transcription profile in the different stages of AMD is still poor.

The first transcriptome studies performed in human ocular tissue addressed the differences in the expression between young and adult retinas and RPE/choroid complexes (Young et al. 2013; Farkas et al. 2013), and between peripheral and macular areas of the retina and the RPE/choroid complexes (Whitmore et al. 2014; Cai et al. 2012; Li et al. 2014). These studies revealed tissue and area-specific molecular signatures in normal human retinas, although they did not focus in pathological processes.

More recently, three large transcriptomic studies in humans comparing normal and AMD retinal tissues have been conducted. These studies pointed chemokine and cytokine signaling and

complement cascade pathways as the most dysregulated (Saddala et al. 2019). Biological processes such as cell communications, cell surface receptor signaling pathways and signal transduction appeared upregulated, whereas pathways associated with synapse development and function were largely downregulated in intermediate AMD (Ratnapriya et al. 2019). Differences in antisense RNA transcripts, which regulate gene expression by blocking the translation of complementary mRNAs, have also been reported in human AMD retinas (Kim et al. 2018).

To have a comprehensive knowledge of the *DKOrd8* model, we performed a transcriptomic analysis with a cDNA microarray and observed a differential expression pattern in *DKOrd8* mice compared to 6N mice, with a greater amount of genes downregulated rather than upregulated.

A limitation of our study is that we included both retinal and RPE/choroid material in the sampling process, which may lead to underrepresentation of retina-specific and RPE/choroid-specific differentially expressed genes. Mouse eyes have a small size, and the amount of RNA that can be extracted is limited, specifically of the RPE/choroid complex. Thus, we decided to include the whole tissue to obtain higher RNA concentrations with a better quality.

One of the cellular functions with a higher number of genes downregulated was the mitochondrial metabolism, with a great representation of genes involved in the mitochondrial electron transport chain (mETC). The mETC is the major source of ROS, which contribute to oxidative stress. Elevated oxidative stress can lead to mitochondrial damage and therefore, to a decreased mitochondrial function (Brown 2018). Mitochondrial dysfunction has been suggested to be a major contributing factor to AMD pathogenesis. Different studies have shown fewer and smaller mitochondria and a decrease content of mETC proteins in the RPE of AMD human donors (Bianchi et al. 2013; Nordgaard et al. 2006; Nordgaard et al. 2008). Furthermore, increased levels of mitochondrial DNA damage have also been found in the RPE but not in the neuroretina of AMD patients with an early disease state (Terluk et al. 2015).

Increasing evidences suggest that aging induces a decline in the cellular antioxidant capacity, causing an impaired induction of antioxidants in response to oxidative stress (Bellezza 2018). *Nrf2*, the transcription factor key regulator of the antioxidant response, is reduced in aged RPE cells (Sachdeva et al. 2014; Zhang et al. 2015) as well as the antioxidant enzyme *SOD3* (He and Tombran-Tink 2010). Interestingly, these two genes were downregulated in *DKOrd8* mice at three months of age, showing an early dysregulation of the antioxidant capacity.

At that age and through immunostaining, we had already observed an increased expression of the oxidative-stress marker 8-OHdG in *DKOrd8* mice retinas. Therefore, the altered expression

of mitochondrial proteins, including the ones of the mETC, oxidative stress regulators, and antioxidant enzymes in the *DKOrd8* mice, could be described as an AMD-like feature of this model.

Interestingly, we also observed the differential expression of genes that have been associated with an increased risk of AMD. This is the case of *TIMP3*, a matrix metalloproteinase inhibitor secreted by RPE and choroidal cells that plays an important role in the control of the extracellular proteolytic activity (Woessner Jr. 2001). Mutations in this gene cause Sorsby fundus dystrophy, a rare degenerative disease of the macula that resembles the neovascular form of AMD (Anand-Apte et al. 2019). Regarding its role in AMD, Wang et al. reported a downregulation of *TIMP3* in the retina of humans with the polymorphism rs5749482, which confers an increased risk of AMD (Strunnikova et al. 2010; Wang et al. 2014).

It is widely established that increased ROS levels lead cells into senescence, which induces the secretion of pro-inflammatory cytokines and chemokines, and regulates autophagy (van Deursen 2014; Kang and Elledge 2016). All these pathways have been associated to AMD pathogenesis, and genes related with all of them were found differentially expressed in *DKOrd8* mice. We also observed a downregulation of genes related with the cell cycle in *DKOrd8* mice. A downregulation of genes related with general transcription have also been found in transcriptomic analyses of human retinas and RPE-choroid-sclera complex of AMD patients (Saddala et al. 2019). In this same study, genes related with the immune response were found upregulated in AMD samples. Similarly, the expression of some genes codifying for chemokines, interleukins and complement proteins was increased in our *DKOrd8* mice, which correlated with the fact that it is a model with a dysregulation in the chemokine pathway.

The enrichment analyses performed on the GO database revealed that most of the downregulated genes fitted into categories related to neuronal regulation and synaptic transmission. Curiously, transcriptome analyses in AMD patients have also shown a downregulation of these categories in patients with intermediate AMD. Furthermore, the  $\gamma$ -aminobutyric acid (GABA) receptor activation pathway was found downregulated too in AMD patients (Ratnapriya et al. 2019; Saddala et al. 2019). In line with that, different subunits of the GABA receptor were also downregulated in our *DKOrd8* mice. Other genes related with neurotransmission, PhOS or axon maintenance such as *Syngn3*, *Aplp1*, *Impg2* or *Casp6* were downregulated in *DKOrd8* mice.

In summary, the gene expression pattern of the *DKOrd8* mice resembled the expression pattern of AMD patients in many ways. And although detailed transcriptomic analyses of AMD patients are still lacking, the *DKOrd8* expression pattern could be considered as an AMD-like characteristic and taken into account when using this model to study the effect of novel therapies.

### 3. Choosing the right therapy for AMD

The search for therapies to revert or stop the progression of AMD has not succeeded yet. Geographic atrophy, the major hallmark of AMD, still does not have an effective treatment. The lack of knowledge about the mechanisms implicated in the onset of the disease, the absence of biomarkers as well as the lack of reliable models have been the major obstacles.

The publication of the AREDS and AREDS2 clinical studies, showing a slower progression of AMD in patients taking an oral supplementation rich in antioxidants (Kassoff et al. 2001; Chew et al. 2014), has been the major outcome until now. This is the only preventive therapy AMD patients can follow. But once the disease progresses, no approved therapy exists. Several clinical trials for geographic atrophy evaluate the effect of drugs targeting the complement cascade, oxidative stress and neuroprotection or the elimination of toxic by-products of the visual cycle (Li et al. 2017). Although most of them have failed in the achievement of the expected outcomes, others are still ongoing. This is the case of brimonidine, an  $\alpha$ -adrenergic receptor agonist with neuroprotective activity that showed beneficial effects in RPE and Müller cells with induced stress (Ramírez et al. 2016). A phase II trial is currently in progress and expected to be completed this year (Clinicaltrials.gov number: NCT02087085).

What is surprising is that given the important role oxidative stress plays in the onset and progression of AMD, only two clinical trials on antioxidant therapies are being held. The antioxidant compound OT-551, a disubstituted hydroxylamine, is being evaluated in a second phase II trial after showing some beneficial effects in the rat model with light-induced retinal degeneration (Tanito et al. 2010) and in a first clinical trial demonstrating the safety of the compound and a significant vision improvement in patients (Wong et al. 2010). The other antioxidant therapy being evaluated in clinical trials is risuteganib, an anti-integrin antibody developed initially to treat diabetic macular edema. As it showed an effect in downregulating oxidative stress, is now being tested in a phase II study with AMD patients (Kuppermann et al. 2016).

Another therapeutic field with promising projection is stem cell-based therapy. Induced pluripotent stem cells (iPSCs) have the potential to be differentiated into photoreceptors and RPE cells and to integrate into a host cell structure to replace or regenerate the lost tissue (Ludwig et al. 2019). Moreover, they present lesser ethical concerns than embryonic stem cells. iPSCs-derived RPE cells have been reported to improve retinal function in retinal degenerative rat and mouse models (Kanemura et al. 2014; Li et al. 2012; Tucker et al. 2011; Riera et al. 2016)

and their use has also been tested in human trials. The first clinical trial using iPSCs-derived RPE cells was performed in 2014 on one patient (Chakradhar 2016). No adverse effects were detected after a year and the patient experienced a stabilization of vision decline. However, the study had to be interrupted for safety concerns, due to the detection of mutations in the second patient's iPSCs (Garber 2015). Currently, three clinical trials using autologous and allogenic iPSC-derived RPE cells to treat AMD are being held (Mandai et al. 2017; Clinicaltrials.gov number: NCT02464956; NCT00874783). Although the future is very promising, long-term studies evaluating immunogenicity and chromosomal instability are still lacking. Moreover, the financial success of these therapies is questioned given the high economic cost of development (Bracha et al. 2017).

In the last years, CeO<sub>2</sub>NPs emerged as a good option to treat AMD due to their high antioxidant capacity. We synthesized AOxNPs of 3nm, discarded any cytotoxic effect in ARPE19 cell cultures and corroborated their antioxidant capacity with in vitro studies. AOxNPs were able to reduce ROS levels in ARPE19 cells after inducing oxidative stress with three different oxidizing agents. Moreover, AOxNPs increased the expression of the enzyme SOD2, reinforcing the antioxidant response of the cell. With this capacity, AOxNPs could prevent the excessive formation of ROS during the visual cycle and their auto-regenerative capacity could extend their efficacy in the targeted tissue. This therapeutic potency has already been demonstrated in several mouse models for degenerative eye diseases, being able to delay photoreceptor death and preserve retinal function (Cai et al. 2012; Wong et al. 2015).

All the models in which antioxidant therapies have been tested suffered a severe and aggressive degeneration, which is not the case of AMD. In AMD, retinal degeneration is progressive and the development of the pathogenic features is not as aggressive as in those models. Therefore, the use of our AOxNPs to reduce oxidative stress in AMD could even present better outcomes than in severe retinal degenerative pathologies.

As stated previously, the use of reliable models is one of the main problems in the translation of therapies from preclinical studies to human trials. In this regard, the characterization of the *DKO<sup>rd8</sup>* we performed placed these mice as an even more reliable model to test new therapies for AMD.



#### **4. Topical delivery as a route of administration to the posterior pole**

Topical delivery with eye drops is the less invasive route of administration for ocular pathologies. It is commonly used in the treatment of pathologies affecting the anterior segment of the eye such as infections, inflammations, elevated intraocular pressure and dry eye. Most eye drop formulations contain small molecular weight drugs with an adequate corneal permeability, allowing the absorption into the anterior chamber. However, their use for pathologies affecting the retina and RPE cells is controversial as the distribution to the posterior part of the eye is hampered by different factors (del Amo et al. 2017; Loftsson and Stefánsson 2017):

- i. Retention time on the ocular surface: topically administered eye drops are rapidly drained from the ocular surface by the lacrimal fluid via the nasolacrimal duct, limiting drug absorption. In addition, the increased tearing following topical application decreases drug concentration (Wong et al. 2019).
- ii. Permeability and transport in the barrier membranes: topical formulations must have an adequate permeability to cross the cornea, conjunctiva and sclera. Transport across the cornea and conjunctiva is limited by the lipophilicity and the size of the compounds (Ramsay et al. 2018). Sclera however, is a more permeable tissue, with a porous membrane that allows the permeation of hydrophilic and large macromolecules (Prausnitz and Noonan 1998).
- iii. Role of flow factors: once inside the eye, a great amount of drug is eliminated via the aqueous humor outflow, which is constantly produced and drained to maintain a correct intraocular pressure. Although the vitreous outflow is lower, drugs can diffuse to the anterior chamber and be eliminated either way by the aqueous humor outflow. The vitreous itself is a negatively charged polymer network that allows the relative unrestricted molecular mobility for small molecules and anionic nanoparticles. However, diffusion of particles above 500 nm or with cationic charge is dramatically restricted (Mains et al. 2012). The penetration of drug molecules into the retina is also hampered by the blood retinal barrier.
- iv. Drug potency and dosing rate: it is evident that the retinal bioavailability is lower after topical administration rather than other administration routes such as intravitreal or subretinal injections. But the concentrations needed for pharmacological activity depend on the compound itself. Highly potent drugs that are active at low

concentrations (preferably in nanomolar range) might be suitable for topical administration.

Another aspect to consider is that ocular pharmacodynamics differs between species. The rodent eye is anatomically dissimilar to the human eye. The distance to the posterior segment is shorter, as well as the volume of the vitreous body, smaller in mice and rats compared to humans as the ratio of the lens to the ocular length is 5-fold greater in mice than in humans (Figure D.3) (Zhou et al. 2007). Moreover, mouse and rat sclera is more permeable than the human sclera (Veleri et al. 2015). For all these reasons, translation from rodent models to humans has to be done cautiously.

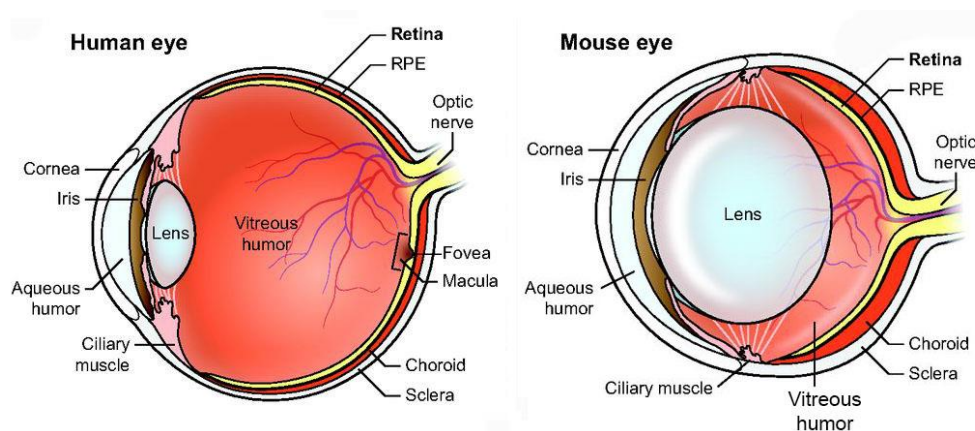


**Figure D.3. Schematic cross-sections of a human and a mouse eye.** The main distinct features are the lack of macula and fovea in the mouse eye and the size of the lens, much larger in the mouse than humans relative to the eye size. Modified from Veleri et al. 2015.

Usually, intravitreal administration is the delivery route chosen for reaching the posterior segment of the eye as the direct injection into the vitreous cavity eliminates part of the barriers mentioned above. In fact, in all the published studies using CeO<sub>2</sub>NPs as a therapy, intravitreal injection has been the chosen administration. But for progressive diseases that need a sustained treatment, it is not the best choice. The risk of complications associated to intravitreal injections increase with recurring administrations (Jager et al. 2004). Hence, topical application is a better choice for progressive degenerative diseases.

There is emerging evidence that several peptides administered in eye drop formulations can reach the murine retina in pharmacological concentrations. Derivatives from the neuroprotective factor PEDF applied once a week for 15 weeks were able to reduce diabetic retinopathy complications in the *Ins2<sup>Akita</sup>* mice (Liu et al. 2012). The neuroprotective glucagon-

like peptide 1 (GLP-1) and a suppressor of cytokine signaling 1 (SOCS1) derived peptide also showed the capacity to prevent neurodegeneration and neuroinflammation respectively in the *db/db* mouse model for diabetic retinopathy (Hernández et al. 2016; Hernández et al. 2019).

Trying to improve topical efficiency, the use of hydrogels has proven to enhance absorption, as they increase the retention period and allow a lateral diffusion through the conjunctiva and sclera, enhancing the bioavailability of the drug (Shikamura et al. 2016).

The formulation of the topical solution is therefore, of great importance to improve the efficiency of the administration. The AOxNPs we used were synthesized in a small size, around 3 nm: similar or even smaller than the peptides reported to be effective for diabetic retinopathy. They were negatively charged, facilitating their transport across the cornea and the vitreous. Moreover, we used a formulation that prolongs the retention in the surface of the cornea and thus, their absorption, increasing the efficiency of topical administration.

With all these characteristics, our AOxNPs administered topically reached the retina and posterior segment of the eye (RPE, choroid and sclera) after a single administration, and with a daily administration during seven days the concentration in the retina was comparable to the one achieved with one intravitreal injection.

## 5. The efficacy of AOxNPs as a treatment for AMD

### 5.1. Reversion of the differential expression pattern

In this thesis we proved the efficacy of a topical treatment with AOxNPs in the *DKOrd8* model. The most evident improvement was the reversion of the altered expression pattern of *DKOrd8* mice. More importantly, we achieved these results with a topical administration sustained for two months; eliminating the need of intravitreal injections and the usual associated complications.

The gene expression pattern of *DKOrd8* mice differed substantially from 6N mice, with a greater number of downregulated genes. Surprisingly, mice treated with AOxNPs experienced a reversion of that expression pattern, resembling the one from 6N mice. The antioxidant capacity of AOxNPs was able to re-establish the expression levels of a great number of genes to wild type levels.

Most of the genes downregulated in *DKOrd8* mice appeared upregulated in AOxNPs-treated mice, reaching the expression levels of 6N mice. This was the case of most of the genes involved with mitochondrial metabolism, neuronal function, cell death, senescence and cell cycle. Although it is unlikely that AOxNPs directly target genes to alter their expression, AOxNPs might indirectly modulate the expression of oxidative stress-related genes by regulating the antioxidant response of the cell through ROS scavenging. In fact, ROS are suggested to be involved in the initiation and progression of inflammatory responses and they also act as second messengers in the intracellular signaling through the post-translational modification of cysteine residues of redox-sensitive proteins that can undergo oxidation (Chelombitko 2018). Therefore, variations in the intracellular ROS levels can produce changes in the expression pattern.

The effect of CeO<sub>2</sub>NPs treatment in the expression of oxidative-stress related genes has been addressed in the *Vldlr*<sup>-/-</sup> mouse model, with severe retinal degeneration (Kyosseva et al. 2013; Cai et al. 2014). Cai et al showed that an intravitreal injection of CeO<sub>2</sub>NPs could upregulate several genes related with oxidative stress that were downregulated in the model, such as the transcription factor *Nrf2* (Cai et al. 2012; Cai et al. 2014) The upregulation of *Nrf2* has also been reported in the streptozotocin-induced type 1 diabetes mouse model receiving intraperitoneal injections of CeO<sub>2</sub>NPs (Khurana et al. 2018). Similarly, *DKOrd8* mice experienced an upregulation of *Nrf2* after the AOxNPs treatment.

We had previously observed an upregulation of *SOD2* in ARPE19 cells treated with AOxNPs after the induction of oxidative stress. Likewise, the AOxNPs treatment in *DKOrd8* mice induced the expression of a superoxide dismutase family enzyme. In this case it was *SOD3*, located in the extracellular matrix, instead of the mitochondrial *SOD2*. Besides *SOD3* and *Nrf2*, *Gstt3*, *Sdha* or *Mdh2*, associated with oxidative stress and the antioxidant response, regained wild type levels after the AOxNPs treatment. Confirming the antioxidant effect of AOxNPs on gene expression, the gene enrichment analysis also showed an upregulation of GO terms related with the ATP metabolic process, directly related with the mitochondrial electron transport chain.

It has also been reported that the intravitreal injection of CeO<sub>2</sub>NPs in *Vldlr*<sup>-/-</sup> mice induced the downregulation of IL7, IL9 and other cytokine-related genes whose expression was increased in the model (Kyosseva et al. 2013). In a similar manner, the genes related with the immune response that were upregulated in the *DKOrd8* model appeared downregulated after the topical AOxNPs treatment.

As previously stated, we hypothesized that the reduction of intracellular ROS levels by AOxNPs could produce changes in the expression pattern, with more probability in genes associated with oxidative stress and inflammation, given that ROS have a higher influence on these processes. But AOxNPs were also able to influence the expression of genes related with neuronal function, autophagy and cell cycle functions.

According to Song et al, CeO<sub>2</sub>NPs exposure in in vitro cultures of endothelial cells and fibroblasts activates the autophagy master regulator, the transcription factor EB (Tfeb), promoting the clearance of lysosomes and enhancing the degradation of the autophagic cargo (Song et al. 2014). In *DKOrd8* mice, we did not observe changes in *Tfeb* expression but we reported an upregulation of several autophagy-related genes that were downregulated in the model. CeO<sub>2</sub>NPs exposure in in vitro neuronal cell cultures has also been reported to induce the expression of genes related to neurological and cell cycle regulation (Lee et al. 2012).

The effect of AOxNPs in the *DKOrd8* model was similar to the one observed in other models treated with other antioxidant nanoparticles, causing an upregulation of the genes related with the antioxidant response and a downregulation of inflammatory-related genes. Overall, the reduction of ROS levels induced by AOxNPs was able to change completely the altered expression pattern of *DKOrd8* mice. Nevertheless, further studies on the exact mechanisms and biological impact of these changes should be addressed.

## 5.2. AOxNPs effect on retinal thickness and microglial activation

The few studies where *DKOrd8* mice have been used to test different therapies conducted an eye fundus evaluation to monitor the effect of the treatment. These studies affirm to observe a stabilization of retinal lesions after nutrient supplementation with antioxidant compounds, the intravitreal administration of an inhibitor of the Wnt pathway or the neuroprotective factors PEDF and PDGF (Ramkumar et al. 2013; Tuo et al. 2015; Wang et al. 2013; Wang et al. 2014). During the characterization of our model, we observed that these lesions tend to decrease upon ageing, as photoreceptors are lost. Therefore, the use of these lesions as a hallmark to establish the efficacy of a treatment is questionable. Rather than the eye fundus evaluation, OCT imaging is becoming the standard technique for the *in vivo* observation of retinal layers and their posterior quantification, as the evaluation of the layers' thickness gives more objective data.

Our evaluation of mice retinas through OCT imaging revealed maintenance of the ONL thickness in treated-mice compared to the non-treated. In other models, CeO<sub>2</sub>NPs treatment showed increased photoreceptors survival through the reduction of ROS levels (Chen et al. 2006, Cai et al. 2012) and decreased apoptosis (Wong et al. 2015). We hypothesize that AOxNPs in the *DKOrd8* mice could have a similar effect. Nevertheless, it should be corroborated with further histological evaluation and analysis of apoptotic markers.

With the evaluation of retinal function, we did not observe differences in AOxNPs-treated mice compared to the not treated. As explained previously, mild changes in the retina are often difficult to observe through ERG recordings. Furthermore, in this case, AOxNPs treatment did not produce the sufficient effect on the ONL to see an improvement in the retinal function.

Another effect of AOxNPs treatment in *DKOrd8* mice was the reduction in the number of microglial cells in the inner retina and subretinal space. Fiorani et al. observed a reduced microglia activation and migration towards the outer nuclear layer in the light-induced retinal damage rat model after a CeO<sub>2</sub>NPs intravitreal injection (Fiorani et al. 2015). We have previously stated that variations in ROS levels can influence the gene expression pattern. Increased ROS levels have also been associated with an increased activation of microglial cells in *in vitro* studies, through the activation of MAPK and NF- $\kappa$ B pathways that induce the secretion of pro-inflammatory cytokines (Ye et al. 2017; Ding et al. 2017). With these results, we suggest that AOxNPs treatment, through the scavenging of ROS, can modulate the activation and migration of microglial cells. Nevertheless, further studies should be conducted to assess the exact pathways involved in this process.

### 5.3. Finding the right dosage

One of the characteristics of CeO<sub>2</sub>NPs is their auto-regenerative capacity, which theoretically, allows them to scavenge ROS for an unlimited time (Heckert et al. 2008). Studies with a single intravitreal injection of CeO<sub>2</sub>NPs rely on this capacity and postulate that a single administration would be enough to revert a pathogenic phenotype. In all these studies, CeO<sub>2</sub>NPs are administrated in the different models before the onset of the retinal degenerative process and the effect of the single intravitreal delivery is evaluated a few weeks after the administration. However, it is not known whether the effects observed are consequence of a maintained antioxidant capacity or if CeO<sub>2</sub>NPs lose their capacity at some point but the effect already caused is enough to improve the altered phenotype in those models.

There is only one study in which CeO<sub>2</sub>NPs were administered when retinal degeneration was already triggered. In that case, a single intravitreal administration slowed down the degenerative process of the light damaged rat model for at least two months and fluorescein-labeled CeO<sub>2</sub>NPs were localized after that time (Tisi et al. 2019). But again, it is not known for how long the auto-regenerative power was maintained in vivo. While cerium has been detected up to 120 days post-injection in rat eyes (Wong et al. 2013), long-term studies correlating the cerium concentration in the tissue and their effect are still lacking.

In our case, we did not have any reference of the effect of AOxNPs after a topical administration, since this delivery route had never been addressed. In a first preliminary study, we treated mice daily for one month (starting at 4 weeks of age until 8 weeks) and performed in vivo and post-mortem studies. However, we did not observe differences in their retinal thickness neither in their retinal function. Regarding the gene expression profile, we just evaluated the expression of some genes related with oxidative stress and the inflammatory response through qPCR without observing significant results. Thus, we decided to extend the treatment until three months of age, an age in which the phenotype of *DKOrd8* mice presented more AMD-like features and was better characterized.

We achieved a reversion of the altered expression profile treating mice daily for two months. Could we have obtained similar results with a more spaced administration? To answer that question it is important to know the concentration of AOx that remained in the ocular tissues after the treatment. Although included in the experimental design, at the time of writing this thesis, we did not have the results of the ICP-MS analyses. To correlate the concentration of AOxNPs that produced those results will be of great importance to design longer studies that resemble the administration pattern AMD patients should follow.

## 6. Future prospects for the management of AMD

The largest part of this thesis has been focused in the obtainment of a reliable murine model mimicking AMD. But the biggest achievement has been the development of an effective antioxidant therapy that with an easy topical administration improved the pathological phenotype of the model previously obtained.

The good results reported in the last years in models for severe retinal degenerative diseases already placed CeO<sub>2</sub>NPs as a good candidate to treat AMD. For the first time, we tested the effect of our AOxNPs, on an AMD-like model, with a more progressive degeneration, obtaining a satisfactory outcome. But before AOxNPs use can be transferred to clinical practice further studies need to be conducted: the mechanisms by which AOxNPs actuate have to be completely understood, the long-term effect of AOxNPs has to be evaluated and biodistribution studies in larger animal models need to be performed.

Until now, the search for AMD therapies has focused in the development of treatments targeting a unique pathway or cell function. The antioxidant capacity of AOxNPs has proven to be very effective in reverting the altered expression profile of *DKOrd8* mice. But for a successful treatment in AMD patients, AOxNPs need to cause greater functional improvements. Although oxidative stress plays an important role, it is increasingly evident that AMD results from the dysregulation of distinct mechanisms and as a complex disease, therapies to treat AMD should lie on the development of combined treatments that could impact on several of these mechanisms.

In any case, the use of AOxNPs point towards a new paradigm for AMD treatment as the formulation of an eye drop solution to be topically applied facilitates their use either alone or in combination with other therapies.





The background is an abstract watercolor composition. It features a dense network of thin, black, branching lines that resemble a neural network or a complex web. These lines are set against a wash of warm, earthy colors, primarily shades of tan, beige, and light brown. Interspersed among the lines are various organic, blotchy shapes in darker tones, including deep blues, greys, and blacks. Some of these shapes are elongated and vertical, while others are more rounded or irregular. The overall effect is one of intricate, organic complexity.

# CONCLUSIONS



About the generation and characterization of the model:

1. The *DKOrd8* mouse model generated mimics several AMD-like features at an early age, although a homogeneous genetic background is required to achieve a complete penetrance.
2. *DKOrd8* mice present alterations in the inferior hemisphere of their eye fundus already at one month of age, with disruption of the photoreceptor layer, an age-dependent decrease of the outer nuclear layer thickness, and shorter photoreceptor inner and outer segments.
3. The alterations in the photoreceptors layer of *DKOrd8* mice are translated into a decreased retinal function, with a lower a-wave amplitude maintained over time and a delayed retinal response upon ageing.
4. *DKOrd8* mice present an age-dependent accumulation of microglia in the subretinal space, a migration of the microglia towards the inner retinal lesions, and increased gliosis in those lesions.
5. The *DKOrd8* mouse model exhibit an altered expression pattern, with an affectation of genes involved with oxidative stress, immune regulation, neuronal function, cell death and senescence.

About the evaluation of AOxNPs as a therapy for AMD:

1. AOxNPs have a reproducible capacity of reducing intracellular ROS levels in in vitro cultures without producing cytotoxicity, and are able to induce the antioxidant response of the cell by upregulating *SOD2* expression.
2. The topical administration of AOxNPs is an efficient delivery route, as AOx is able (i) to reach the retina and the posterior part of the eye after a single administration, and (ii) to achieve a comparable concentration in the retina that the one achieved with intravitreal injection, after a 7-days topical administration.

3. The topical treatment with AOxNPs is effective in improving the phenotypical characteristics of the *DKOrd8* mouse model, as it reverts their altered gene expression profile, reduces microglia infiltration, and prevents the thinning of the outer nuclear layer.

The background is an abstract watercolor composition. It features a dense network of thin, black, branching lines that resemble a neural network or a complex web. These lines are set against a wash of warm, earthy tones, including shades of beige, tan, and light brown. Interspersed among the lines are various organic, blotchy shapes in darker colors, such as deep blue, charcoal grey, and black. Some of these shapes are elongated and vertical, while others are more rounded and irregular. The overall effect is one of intricate, organic complexity.

# REFERENCES



- Aleman, Tomas S., Artur V. Cideciyan, Geoffrey K. Aguirre, Wei Chieh Huang, Cristina L. Mullins, Alejandro J. Roman, Alexander Sumaroka, et al. 2011. "Human CRB1-Associated Retinal Degeneration: Comparison with the rd8 Crb1-Mutant Mouse Model." *Investigative Ophthalmology and Visual Science* 52 (9): 6898–6910. doi:10.1167/iovs.11-7701.
- Al-Zamil, Waseem M, and Sanaa a Yassin. 2017. "Recent Developments in Age-Related Macular Degeneration: A Review." *Clinical Interventions in Aging* 12: 1313–30. doi:10.2147/CIA.S143508.
- Ambati, Jayakrishna, John Atkinson, and Bradley Gelfand. 2013. "Immunology of Age-Related Macular Degeneration." *Immunology Nature Reviews* 13 (9). Nature Publishing Group: 436–51. doi:10.1007/s00347-016-0341-6.
- Anand-Apte, Bela, Jennifer R. Chao, Ruchira Singh, and Heidi Stöhr. 2019. "Sorsby Fundus Dystrophy: Insights from the Past and Looking to the Future." *Journal of Neuroscience Research* 97 (1): 88–97. doi:10.1002/jnr.24317.
- Anderson, Don H., Robert F. Mullins, Gregory S. Hageman, and Lincoln V. Johnson. 2002. "A Role for Local Inflammation in the Formation of Drusen in the Aging Eye." *American Journal of Ophthalmology* 134 (3): 411–31. doi:10.1016/S0002-9394(02)01624-0.
- Aredo, Bogale, Kaiyan Zhang, Xiao Chen, Cynthia Xin-Zhao Wang, Tao Li, and Rafael L Ufret-Vincenty. 2015. "Differences in the Distribution, Phenotype and Gene Expression of Subretinal Microglia/macrophages in C57BL/6N (Crb1rd8/rd8) versus C57BL6/J (Crb1wt/wt) Mice." *Journal of Neuroinflammation* 12 (1): 4–17. doi:10.1186/s12974-014-0221-4.
- Baek, Ahruem, Soojin Yoon, Jean Kim, Yu Mi Baek, Hanna Park, Daehan Lim, Hyewon Chung, and Dong Eun Kim. 2017. "Autophagy and KRT8/keratin 8 Protect Degeneration of Retinal Pigment Epithelium under Oxidative Stress." *Autophagy* 13 (2). Taylor & Francis: 248–63. doi:10.1080/15548627.2016.1256932.
- Beatty, S, Mike Boulton, D Henson, H-H Koh, and Murray I J. 1999. "Macular Pigment and Age-Related Macular Degeneration." *British Journal of Ophthalmology* 83: 867–77.
- Behndig, Anders, Bengt Svensson, Stefan L. Marklund, and Kurt Karlsson. 1998. "Superoxide Dismutase Isoenzymes in the Human Eye." *Investigative Ophthalmology and Visual Science* 39 (3): 471–75.
- Bellezza, Ilaria. 2018. "Oxidative Stress in Age-Related Macular Degeneration: NRF2 as Therapeutic Target." *Frontiers in Pharmacology* 9 (NOV): 1–7. doi:10.3389/fphar.2018.01280.
- Beltran, William a., Artur V. Cideciyan, Karina E. Guziewicz, Simone Iwabe, Malgorzata Swider, Erin M. Scott, Svetlana V. Savina, et al. 2014. "Canine Retina Has a Primate Fovea-like Bouquet of Cone Photoreceptors Which Is Affected by Inherited Macular Degenerations." *PLoS ONE* 9 (3): 11–17. doi:10.1371/journal.pone.0090390.
- Beltran, William a., Pamela Hammond, Gregory M. Acland, and Gustavo D. Aguirre. 2006. "A Frameshift Mutation in RPGR Exon ORF15 Causes Photoreceptor Degeneration and Inner Retina Remodeling in a Model of X-Linked Retinitis Pigmentosa." *Investigative Ophthalmology and Visual Science* 47 (4): 1669–81. doi:10.1167/iovs.05-0845.
- Bergen, Arthur a., Swati Arya, Céline Koster, Matthew G. Pilgrim, Dagmara Wiatrek-Moumoulidis, Peter J. van der Spek, Stefanie M. Hauck, et al. 2019. "On the Origin of Proteins in Human Drusen: The Meet, Greet and Stick Hypothesis." *Progress in Retinal and Eye Research*, no. December. Elsevier: 1–30. doi:10.1016/j.preteyeres.2018.12.003.



- Bianchi, Enrica, Fabio Scarinci, Guido Ripandelli, Janos Feher, Elena Pacella, Giuseppe Magliulo, Corrado Balacco Gabrieli, et al. 2013. "Retinal Pigment Epithelium, Age-Related Macular Degeneration and Neurotrophic Keratouveitis." *International Journal of Molecular Medicine* 31 (1): 232–42. doi:10.3892/ijmm.2012.1164.
- Blasiak, Janusz, Goran Petrovski, Zoltán Veréb, Andrea Facskó, and Kai Kaarniranta. 2014. "Oxidative Stress, Hypoxia, and Autophagy in the Neovascular Processes of Age-Related Macular Degeneration." *BioMed Research International* 2014. doi:10.1155/2014/768026.
- Booij, J. C., D. C. Baas, J. Beisekeeva, T. G.M.F. Gorgels, and a. a.B. Bergen. 2010. "The Dynamic Nature of Bruch's Membrane." *Progress in Retinal and Eye Research* 29 (1). Elsevier Ltd: 1–18. doi:10.1016/j.preteyeres.2009.08.003.
- Boyer, David S., Ursula Schmidt-Erfurth, Menno Van Lookeren Campagne, Erin C. Henry, and Christopher Brittain. 2017. "The Pathophysiology of Geographic Atrophy Secondary to Age-Related Macular Degeneration and the Complement Pathway as a Therapeutic Target." *Retina* 37 (5): 819–35. doi:10.1097/IAE.0000000000001392.
- Bracha, Peter, Nicholas a. Moore, and Thomas a. Ciulla. 2017. "Induced Pluripotent Stem Cell-Based Therapy for Age-Related Macular Degeneration." *Expert Opinion on Biological Therapy* 17 (9). Taylor & Francis: 1113–26. doi:10.1080/14712598.2017.1346079.
- Cai, Hui, Mark a. Fields, Risa Hoshino, and Lucian V. Del Priore. 2012. "Effects of Aging and Anatomic Location on Gene Expression in Human Retina." *Frontiers in Aging Neuroscience* 4 (MAY): 1–20. doi:10.3389/fnagi.2012.00008.
- Cai, Xue, Sudipta Seal, and James F Mcginnis. 2014. "Sustained Inhibition of Neovascularization in Vldlr - /- Mice Following Intravitreal Injection of Cerium Oxide Nanoparticles and the Role of the ASK1-P38 / JNK-NF- K B Pathway." *Biomaterials* 35 (1). Elsevier Ltd: 249–58. doi:10.1016/j.biomaterials.2013.10.022.
- Cai, Xue, Sudipta Seal and James F Mcginnis. 2016. "Non-Toxic Retention of Nanocerium in Murine Eyes." *Molecular Vision* 22 (October): 1176–87.
- Cai, Xue, Steven A Sezate, Sudipta Seal, and James F Mcginnis. 2012. "Sustained Protection against Photoreceptor Degeneration in Tubby Mice by Intravitreal Injection of Nanocerium." *Biomaterials* 33 (34). Elsevier Ltd: 8771–81. doi:10.1016/j.biomaterials.2012.08.030.
- Campbell, Matthew, and Sarah L. Doyle. 2019. "Current Perspectives on Established and Novel Therapies for Pathological Neovascularization in Retinal Disease." *Biochemical Pharmacology* 164 (April). Elsevier: 321–25. doi:10.1016/j.bcp.2019.04.029.
- Cardona, Astrid E., Erik P. Pioro, Margaret E. Sasse, Volodymyr Kostenko, Sandra M. Cardona, Ineke M. Dijkstra, De Ren Huang, et al. 2006. "Control of Microglial Neurotoxicity by the Fractalkine Receptor." *Nature Neuroscience* 9 (7): 917–24. doi:10.1038/nn1715.
- Carter-Dawson, Louvenia D., and Matthew M. Lavail. 1979. "Rods and Cones in the Mouse Retina. I. Structural Analysis Using Light and Electron Microscopy." *Journal of Comparative Neurology* 188 (2): 245–62. doi:10.1002/cne.901880204.
- Casals, Eudald, Muriel F. Gusta, Jordi Piella, Gregori Casals, Wladimiro Jiménez, and Victor Puentes. 2017. "Intrinsic and Extrinsic Properties Affecting Innate Immune Responses to Nanoparticles: The Case of Cerium Oxide." *Frontiers in Immunology* 8 (AUG): 1–7. doi:10.3389/fimmu.2017.00970.

- Cashman, Siobhan M., Akshata Desai, Kashmir Ramo, and Rajendra Kumar-Singh. 2011. "Expression of Complement Component 3 (C3) from an Adenovirus Leads to Pathology in the Murine Retina." *Investigative Ophthalmology and Visual Science* 52 (6): 3436–45. doi:10.1167/iovs.10-6002.
- Caspi, Rachel R. 2006. "Ocular Autoimmunity: The Price of Privilege?" *Immunological Reviews* 213 (1): 23–35. doi:10.1111/j.1600-065X.2006.00439.x.
- Celardo, Ivana, Milena De Nicola, Corrado Mandoli, Jens Z. Pedersen, Enrico Traversa, and Lina Ghibelli. 2011. "Ce3+ Ions Determine Redox-Dependent Anti-Apoptotic Effect of Cerium Oxide Nanoparticles." *ACS Nano* 5 (6): 4537–49. doi:10.1021/nn200126a.
- Chakradhar, Shraddha. 2016. "An Eye to the Future: Researchers Debate Best Path for Stem Cell-Derived Therapies." *Nature Medicine* 22 (2). Nature Publishing Group: 116–19. doi:10.1038/nm0216-116.
- Chan, Chi Chao, Robert J. Ross, Defen Shen, Xiaoyan Ding, Zigurts Majumdar, Christine M. Bojanowski, Min Zhou, Norman Salem, Robert Bonner, and Jingsheng Tuo. 2008. "Ccl2/Cx3cr1-Deficient Mice: An Animal Model for Age-Related Macular Degeneration." *Ophthalmic Research* 40 (3-4): 124–28. doi:10.1159/000119862.
- Charles River, Website. 2019. "C57BL/6 Mouse | Charles River." <https://www.criver.com/products-services/find-model/c57bl6-mouse?region=3661>.
- Chelombitko, M. a. 2018. "Role of Reactive Oxygen Species in Inflammation: A Minireview." *Moscow University Biological Sciences Bulletin* 73 (4): 242–46. doi:10.3103/S009639251804003X.
- Chen, Chunhe, Leopold Adler, Patrice Goletz, Federico Gonzalez-Fernandez, Debra a. Thompson, and Yiannis Koutalos. 2017. "Interphotoreceptor Retinoid-binding Protein Removes All-Trans-Retinol and Retinal from Rod Outer Segments, Preventing Lipofuscin Precursor Formation." *Journal of Biological Chemistry* 292 (47): 19356–65. doi:10.1074/jbc.M117.795187.
- Chen, Junping, Swanand Patil, Sudipta Seal, and James F Mcginnis. 2006. "Rare Earth Nanoparticles Prevent Retinal Degeneration Induced by Intracellular Peroxides." *Nature Nanotechnology* 1: 142–50. doi:10.1038/nnano.2006.91.
- Chen, Mei, Jose R. Hombrebueno, Chang Luo, Rosana Penalva, Jiawu Zhao, Liza Colhoun, Sudha Pirya Soundara Pandi, John V. Forrester, and Heping Xu. 2013. "Age- and Light-Dependent Development of Localised Retinal Atrophy in CCL2-/-CX3CR1GFP/GFP Mice." *PLoS ONE* 8 (4). doi:10.1371/journal.pone.0061381.
- Chen, Mei, Chang Luo, Jiawu Zhao, Gayathri Devarajan, and Heping Xu. 2019. "Immune Regulation in the Aging Retina." *Progress in Retinal and Eye Research* 69 (October 2018). Elsevier: 159–72. doi:10.1016/j.preteyeres.2018.10.003.
- Chen, Ying, Yang Hu, Kangmo Lu, John G. Flannery, and Jian Xing Ma. 2007. "Very Low Density Lipoprotein Receptor, a Negative Regulator of the Wnt Signaling Pathway and Choroidal Neovascularization." *Journal of Biological Chemistry* 282 (47): 34420–28. doi:10.1074/jbc.M611289200.
- Chew, Emily Y., Traci E. Clemons, John Paul SanGiovanni, Ronald P. Danis, Frederick L. Ferris, Michael J. Elman, Andrew N. Antoszyk, et al. 2014. "Secondary Analyses of the Effects of Lutein/zeaxanthin on Age-Related Macular Degeneration Progression AREDS2 Report No. 3." *JAMA Ophthalmology* 132 (2): 142–49. doi:10.1001/jamaophthalmol.2013.7376.
- Chinnery, Holly R., Samuel McLenachan, Timothy Humphries, Jelena M. Kezic, Xiangting Chen, Marc J. Ruitenbergh, and Paul G. McMenamin. 2012. "Accumulation of Murine Subretinal Macrophages:

- Effects of Age, Pigmentation and CX 3CR1." *Neurobiology of Aging* 33 (8). Elsevier Inc.: 1769–76. doi:10.1016/j.neurobiolaging.2011.03.010.
- Churchill, Gary a. 2002. "Fundamentals of Experimental Design for cDNA Microarrays." *Nature Genetics* 32 Suppl (december): 490–95. doi:10.1038/ng1031.
- Cimini, Annamaria, Barbara Dangelo, Soumen Das, Roberta Gentile, Elisabetta Benedetti, Virendra Singh, Antonina Maria Monaco, Sandro Santucci, and Sudipta Seal. 2012. "Antibody-Conjugated PEGylated Cerium Oxide Nanoparticles for Specific Targeting of A $\beta$  Aggregates Modulate Neuronal Survival Pathways." *Acta Biomaterialia* 8 (6). Acta Materialia Inc.: 2056–67. doi:10.1016/j.actbio.2012.01.035.
- Coffey, P. J., C. Gias, C. J. McDermott, P. Lundh, M. C. Pickering, C. Sethi, a. Bird, et al. 2007. "Complement Factor H Deficiency in Aged Mice Causes Retinal Abnormalities and Visual Dysfunction." *Proceedings of the National Academy of Sciences* 104 (42): 16651–56. doi:10.1073/pnas.0705079104.
- Combadière, Christophe, Salomon-Yves Cohen, Laurent Jonet, Philippe Deterre, Charles Feumi, Jean-Claude Jeanny, Sylvain Chemtob, et al. 2007. "CX3CR1-Dependent Subretinal Microglia Cell Accumulation Is Associated with Cardinal Features of Age-Related Macular Degeneration." *Journal of Clinical Investigation* 117 (10): 2920–28. doi:10.1172/jci31692.
- Crabb, J. W., M. Miyagi, X. Gu, K. Shadrach, K. a. West, H. Sakaguchi, M. Kamei, et al. 2002. "Drusen Proteome Analysis: An Approach to the Etiology of Age-Related Macular Degeneration." *Proceedings of the National Academy of Sciences* 99 (23): 14682–87. doi:10.1073/pnas.222551899.
- Curcio, C.A, Millican C.L., Tammy Bailey, and Kruth. 2001. "Accumulation of Cholesterol with Age in Human Bruch's Membrane." *Investigative Ophthalmology and Visual Science* 42 (1): 265–74. <http://0-ovidsp.ovid.com.wam.city.ac.uk/ovidweb.cgi?T=JS&PAGE=reference&D=emed5&NEWS=N&AN=201029004>.
- Curcio, Christine a., and Mark Johnson. 2012. *Structure, Function, and Pathology of Bruch's Membrane. Retina Fifth Edition*. Fifth Edit. Vol. 1. Elsevier Inc. doi:10.1016/B978-1-4557-0737-9.00020-5.
- Dairaku, Naohiro, Katsuaki Kato, Kennichi Honda, Tomoyuki Koike, Katsunori Iijima, Akira Imatani, Hitoshi Sekine, Shuichi Ohara, Hiroshi Matsui, and Tooru Shimosegawa. 2004. "Oligomycin and Antimycin A Prevent Nitric Oxide-Induced Apoptosis by Blocking Cytochrome C Leakage." *Journal of Laboratory and Clinical Medicine* 143 (3): 143–51. doi:10.1016/j.lab.2003.11.003.
- Dan, Chen, Tong Jian-Bin, Wang Hui, Zeng Le-Ping, Zhou Jin, Huang Ju-Fang, and Luo Xue-Gang. 2008. "Synaptophysin Expression in Rat Retina Following Acute High Intraocular Pressure." *Acta Histochemica Et Cytochemica* 41 (6): 173–78. doi:10.1267/ahc.08034.
- Das, Mainak, Swanand Patil, Neelima Bhargava, Jung Fong Kang, Lisa M. Riedel, Sudipta Seal, and James J. Hickman. 2007. "Auto-Catalytic Ceria Nanoparticles Offer Neuroprotection to Adult Rat Spinal Cord Neurons." *Biomaterials* 28 (10): 1918–25. doi:10.1016/j.biomaterials.2006.11.036.
- Das, Soumen, Janet M Dowding, Kathryn E Klump, James F McGinnis, William Self, and Sudipta Seal. 2013. "Cerium Oxide Nanoparticles : Applications and Prospects in Nanomedicine." *Nanomedicine* 8 (9): 1483–1508.
- Del Amo, Eva M., Anna Kaisa Rimpelä, Emma Heikkinen, Otto K. Kari, Eva Ramsay, Tatu Lajunen, Mechthild Schmitt, et al. 2017. "Pharmacokinetic Aspects of Retinal Drug Delivery." *Progress in Retinal and Eye Research* 57: 134–85. doi:10.1016/j.preteyeres.2016.12.001.

- Dillon, Billings, Hockey, DeLaGarza, and Rzigalinski. 2011. "Cerium Oxide Nanoparticles Protect Against MPTP-Induced Dopaminergic Neurodegeneration In A Mouse Model For Parkinson ' S Disease." *NSTI-Nanotech* 3: 451–54.
- Ding, Xinyi, Meng Zhang, Ruiping Gu, Gezhi Xu, and Haixiang Wu. 2017. "Activated Microglia Induce the Production of Reactive Oxygen Species and Promote Apoptosis of Co-Cultured Retinal Microvascular Pericytes." *Graefe's Archive for Clinical and Experimental Ophthalmology* 255 (4). Graefe's Archive for Clinical and Experimental Ophthalmology: 777–88. doi:10.1007/s00417-016-3578-5.
- Dithmar, Stefan, Christine a. Curcio, Ngoc Anh Le, Stephanie Brown, and Hans E. Grossniklaus. 2000. "Ultrastructural Changes in Bruch's Membrane of Apolipoprotein E- Deficient Mice." *Investigative Ophthalmology and Visual Science* 41 (8): 2035–42.
- Djebli, Nassim, Sonia Khier, Florence Griguer, Anne Laure Coutant, Alexandra Tavernier, Gerard Fabre, Caroline Leriche, and David Fabre. 2017. "Ocular Drug Distribution After Topical Administration: Population Pharmacokinetic Model in Rabbits." *European Journal of Drug Metabolism and Pharmacokinetics* 42 (1). Springer International Publishing: 59–68. doi:10.1007/s13318-016-0319-4.
- Dowding, J. M., W. Song, K. Bossy, a. Karakoti, a. Kumar, a. Kim, B. Bossy, et al. 2014. "Cerium Oxide Nanoparticles Protect against A $\beta$ -Induced Mitochondrial Fragmentation and Neuronal Cell Death." *Cell Death and Differentiation* 21 (10). Nature Publishing Group: 1622–32. doi:10.1038/cdd.2014.72.
- Eastlake, K., P. J. Banerjee, A. Angbohang, D. G. Charteris, P. T. Khaw, and G. a. Limb. 2016. "Müller Glia as an Important Source of Cytokines and Inflammatory Factors Present in the Gliotic Retina during Proliferative Vitreoretinopathy." *Glia* 64 (4): 495–506. doi:10.1002/glia.22942.
- Ebneter, Andreas, Damian Jaggi, Mathias Abegg, Sebastian Wolf, and Martin S. Zinkernagel. 2016. "Relationship between Presumptive Inner Nuclear Layer Thickness and Geographic Atrophy Progression in Age-Related Macular Degeneration." *Investigative Ophthalmology and Visual Science* 57 (9): OCT299–306. doi:10.1167/iops.15-18865.
- Edwards, Albert O, Robert Ritter, Kenneth J Abel, Alisa Manning, Carolien Panhuysen, and Lindsay a Farrer. 2005. "Complement Factor H Polymorphism and Age-Related Macular Degeneration." *Science (New York, N.Y.)* 308 (5720): 421–24. doi:10.1126/science.1110189.
- Endemann, Gerda, Lawrence W. Stanton, Kip S. Madden, Carmen M. Bryant, R. Tyler White, and Andrew a. Protter. 1993. "CD36 Is a Receptor for Oxidized Low Density Lipoprotein." *Journal of Biological Chemistry* 268 (16): 11811–16.
- Espinosa-Heidmann, Diego G., Ivan J. Suner, Paola Catanuto, Eleut P. Hernandez, Maria E. Marin-Castano, and Scott W. Cousins. 2006. "Cigarette Smoke-Related Oxidants and the Development of Sub-RPE Deposits in an Experimental Animal Model of Dry AMD." *Investigative Ophthalmology and Visual Science* 47 (2): 729–37. doi:10.1167/iops.05-0719.
- Evans, Mark D., Miral Dizdaroglu, and Marcus S. Cooke. 2004. *Oxidative DNA Damage and Disease: Induction, Repair and Significance. Mutation Research - Reviews in Mutation Research*. Vol. 567. doi:10.1016/j.mrrev.2003.11.001.
- Falavarjani, K. Ghasemi, and Q. D. Nguyen. 2013. "Adverse Events and Complications Associated with Intravitreal Injection of Anti-VEGF Agents: A Review of Literature." *Eye* 27 (7). Nature Publishing Group: 787–94. doi:10.1038/eye.2013.107.
- Farkas, Michael H., Gregory R. Grant, Joseph a. White, Maria E. Sousa, Mark B. Consugar, and Eric a. Pierce. 2013. "Transcriptome Analyses of the Human Retina Identify Unprecedented Transcript Diversity

- and 3.5 Mb of Novel Transcribed Sequence via Significant Alternative Splicing and Novel Genes.” *BMC Genomics* 14 (489): 1–14. doi:10.1186/1471-2164-14-486.
- Feng, ChaoYi, Xin Wang, TianJin Liu, Meng Zhang, GeZhi Xu, and YingQin Ni. 2017. “Expression of CCL2 and Its Receptor in Activation and Migration of Microglia and Monocytes Induced by Photoreceptor Apoptosis.” *Molecular Vision* 23 (October): 765–77. <http://www.ncbi.nlm.nih.gov/pubmed/29142497>.
- Fiorani, Lavinia, Maurizio Passacantando, Sandro Santucci, Stefano Di Marco, Silvia Bisti, and Rita Maccarone. 2015. “Cerium Oxide Nanoparticles Reduce Microglial Activation and Neurodegenerative Events in Light Damaged Retina,” 1–18. doi:10.1371/journal.pone.0140387.
- FrishMan, Laura J, and Minhua H. Wang. 2011. “Electroretinogram of Human, Monkey and Mouse.” In *Adler’s Physiology of the Eye*, 11th ed., 480–501.
- Fritsche, Lars G., Wilmar Igl, Jessica N.Cooke Bailey, Felix Grassmann, Sebanti Sengupta, Jennifer L. Bragg-Gresham, Kathryn P. Burdon, et al. 2016. “A Large Genome-Wide Association Study of Age-Related Macular Degeneration Highlights Contributions of Rare and Common Variants.” *Nature Genetics* 48 (2): 134–43. doi:10.1038/ng.3448.
- Fu, Shuhua, Shuqian Dong, Meili Zhu, David M. Sherry, Changyun Wang, Zhipeng You, Jody J. Haigh, and Yun Zheng Le. 2015. “Müller Glia Are a Major Cellular Source of Survival Signals for Retinal Neurons in Diabetes.” *Diabetes* 64 (10): 3554–63. doi:10.2337/db15-0180.
- Galloway, Nicolas Robert, and Winfried Mawutor Kwaku Amoaku. 1999. “Basic Anatomy and Physiology of the Eye.” In *Common Eye Disease and Their Management*, 4:378. London: Springer. doi:10.1097/00006324-192712000-00008.
- Gao, Jianguan, Ruozhou Tom Liu, Sijia Cao, Jing Z. Cui, Aikun Wang, Eleanor To, and Joanne a. Matsubara. 2015. “NLRP3 Inflammasome: Activation and Regulation in Age-Related Macular Degeneration.” *Mediators of Inflammation* 2015. Hindawi Publishing Corporation: 1–11. doi:10.1155/2015/690243.
- Garber, Ken. 2015. “RIKEN Suspends First Clinical Trial Involving Induced Pluripotent Stem Cells.” *Nature Biotechnology* 33 (9). Nature Publishing Group: 890–91. doi:10.1038/nbt0915-890.
- Gouras, Peter, Lena Ivert, Noelle Landauer, Julie A Mattison, Donald K Ingram, and Marha Neuringer. 2008. “Drusenoid Maculopathy in Rhesus Monkeys (Macaca Mulatta): Effects of Age and Gender.” *Graefes Archive for Clinical and Experimental Ophthalmology* 246 (10): 1395–1402. doi:10.1038/mp.2011.182.doi.
- Graca, Anna B., Claire Hippert, and Rachael a. Pearson. 2018. “Müller Glia Reactivity and Development of Gliosis in Response to Pathological Conditions.” *Advances in Experimental Medicine and Biology* 1074: 303–8. doi:10.1007/978-3-319-75402-4\_37.
- Gregg, Ronald G., Maureen a. McCall, and Stephen C. Massey. 2012. “Function and Anatomy of the Mammalian Retina.” In *Retina*, Fifth Edit, 360–400. Elsevier Inc. doi:10.1016/b978-1-4557-0737-9.00015-1.
- Gresh, Jeffrey, Patrice W. Goletz, Rosalie K. Crouch, and Baerbel Rohrer. 2003. “Structure–function Analysis of Rods and Cones in Juvenile, Adult, and Aged C57BL/6 and Balb/c Mice.” *Visual Neuroscience* 20 (2): 211–20. doi:10.1017/s0952523803202108.
- Grossniklaus, Hans E., Eldon E. Geisert, and John M. Nickerson. 2015. “Introduction to the Retina.” In *Progress in Molecular Biology and Translational Science*, 1st ed., 134:383–96. Elsevier Inc. doi:10.1016/bs.pmbts.2015.06.001.

- Guymer, R., P. Luthert, and a. Bird. 1999. "Changes in Bruch's Membrane and Related Structures with Age." *Progress in Retinal and Eye Research* 18 (1): 59–90. doi:10.1016/S1350-9462(98)00012-3.
- Harrison, J. K., Y. Jiang, S. Chen, Y. Xia, D. Maciejewski, R. K. McNamara, W. J. Streit, et al. 1998. "Role of Neuronally Derived Fractalkine in Mediating Interactions between Neurons and CX3CR1-Expressing Microglia." *Proceedings of the National Academy of Sciences* 95 (18): 10896–901. doi:10.1073/pnas.95.18.10896.
- Harry, G. Jean. 2013. "Microglia during Development and Aging." *Pharmacology and Therapeutics* 139 (3). Elsevier B.V.: 313–26. doi:10.1016/j.pharmthera.2013.04.013 Associate Editor: C. Pope.
- He, Yuan, and Joyce Tombran-Tink. 2010. "Mitochondrial Decay and Impairment of Antioxidant Defenses in Aging RPE Cells." In *Retinal Degenerative Diseases, Advances in Experimental Medicine and Biology*, 165–83. doi:10.1007/978-1-4419-1399-9.
- Heckert, Eric G., Ajay S. Karakoti, Sudipta Seal, and William T. Self. 2008. "The Role of Cerium Redox State in the SOD Mimetic Activity of Nanoceria." *Biomaterials* 29 (18): 2705–9. doi:10.1016/j.biomaterials.2008.03.014.
- Heier, Jeffrey S., David M. Brown, Victor Chong, Jean Francois Korobelnik, Peter K. Kaiser, Quan Dong Nguyen, Bernd Kirchhof, et al. 2012. "Intravitreal Aflibercept (VEGF Trap-Eye) in Wet Age-Related Macular Degeneration." *Ophthalmology* 119 (12): 2537–48. doi:10.1016/j.ophtha.2012.09.006.
- Held, Paul. 2015. "An Introduction to Reactive Oxygen Species Measurement of ROS in Cells." *TechNote*, 1–21. doi:10.1017/CBO9781107415324.004.
- Hernández, Cristina, Patricia Bogdanov, Lidia Corraliza, Marta García-Ramírez, Cristina Solà-Adell, José a. Arranz, Ana I. Arroba, Angela M. Valverde, and Rafael Simó. 2016. "Topical Administration of GLP-1 Receptor Agonists Prevents Retinal Neurodegeneration in Experimental Diabetes." *Diabetes* 65 (1): 172–87. doi:10.2337/db15-0443.
- Hernández, Cristina, Patricia Bogdanov, Carmen Gómez-Guerrero, Joel Sampedro, Cristina Solà-Adell, Carmen Espejo, Marta García-Ramírez, Ignacio Prieto, Jesús Egido, and Rafael Simó. 2019. "SOCS1-Derived Peptide Administered by Eye Drops Prevents Retinal Neuroinflammation and Vascular Leakage in Experimental Diabetes." *International Journal of Molecular Sciences* 20 (15): 3615. doi:10.3390/ijms20153615.
- Himawan, Erico, Per Ekström, Matej Buzgo, Pieter Gaillard, Einar Stefánsson, Valeria Marigo, Thorsteinn Loftsson, and François Paquet-Durand. 2019. "Drug Delivery to Retinal Photoreceptors." *Drug Discovery Today*, 1–7. doi:10.1016/j.drudis.2019.03.004.
- Hollyfield, Joe G., Vera L. Bonilha, Mary E. Rayborn, Xiaoping Yang, Karen G. Shadrach, Liang Lu, Rafael L. Ufret, Robert G. Salomon, and Victor L. Perez. 2008. "Oxidative Damage-Induced Inflammation Initiates Age-Related Macular Degeneration." *Nature Medicine* 14 (2): 194–98. doi:10.1038/nm1709.
- Holz, Frank G., Srinivas R. Sadda, Brandon Busbee, Emily Y. Chew, Paul Mitchell, Adnan Tufail, Christopher Brittain, et al. 2018. "Efficacy and Safety of Lampalizumab for Geographic Atrophy due to Age-Related Macular Degeneration: Chroma and Spectri Phase 3 Randomized Clinical Trials." *JAMA Ophthalmology* 136 (6): 666–77. doi:10.1001/jamaophthalmol.2018.1544.
- Huang, Hu, Ying Liu, Lei Wang, and Wen Li. 2017. "Age-Related Macular Degeneration Phenotypes Are Associated with Increased Tumor Necrosis-Alpha and Subretinal Immune Cells in Aged Cxcr5 Knockout Mice." *PLoS ONE* 12 (3): 1–23. doi:10.1371/journal.pone.0173716.

- Hyttinen, Juha M.T., Janusz Błasiak, Minna Niittykoski, Kati Kinnunen, Anu Kauppinen, Antero Salminen, and Kai Kaarniranta. 2017. "DNA Damage Response and Autophagy in the Degeneration of Retinal Pigment Epithelial cells—Implications for Age-Related Macular Degeneration (AMD)." *Ageing Research Reviews* 36. Elsevier B.V.: 64–77. doi:10.1016/j.arr.2017.03.006.
- Imamura, Y., S. Noda, K. Hashizume, K. Shinoda, M. Yamaguchi, S. Uchiyama, T. Shimizu, Y. Mizushima, T. Shirasawa, and K. Tsubota. 2006. "Drusen, Choroidal Neovascularization, and Retinal Pigment Epithelium Dysfunction in SOD1-Deficient Mice: A Model of Age-Related Macular Degeneration." *Proceedings of the National Academy of Sciences* 103 (30): 11282–87. doi:10.1073/pnas.0602131103.
- Inan, Sibel, Ersan Cetinkaya, Resat Duman, Ismet Dogan, and Umit Übeyt Inan. 2019. "Quality of Life among Patients with Age-Related Severe Macular Degeneration Assessed Using the NEI-VFQ, HADS-A, HADS-D and SF-36 Tests. A Cross-Sectional Study." *Sao Paulo Medical Journal* 137 (1): 25–32. doi:10.1590/1516-3180.2018.0195071218.
- Isas, J. Mario, Volker Luibl, Lincoln V. Johnson, Rakez Kaye, Ronald Wetzel, Charles G. Glabe, Ralf Langen, and Jeannie Chen. 2010. "Soluble and Mature Amyloid Fibrils in Drusen Deposits." *Investigative Ophthalmology and Visual Science* 51 (3): 1304–10. doi:10.1167/iops.09-4207.
- Jager, Rama D., William F Mieler, and Joan W Miller. 2008. "Age-Related Macular Degeneration." *The New England Journal of Medicine* 385 (24): 2606–17.
- Jager, Rama D., Lloyd Paul Aiello, Samir C. Patel, and Emmett T. Cunningham. 2004. "Risks of Intravitreal Injection: A Comprehensive Review." *Retina* 24 (5): 676–98. doi:10.1097/00006982-200410000-00002.
- Jeon, Chang Jin, Enrica Strettoi, and Richard H. Masland. 1998. "The Major Cell Populations of the Mouse Retina." *Journal of Neuroscience* 18 (21): 8936–46.
- Jung, S, J Aliberti, P Graemmel, M J Sunshine, G W Kreutzberg, A Sher, and D R Littman. 2000. "Analysis of Fractalkine Receptor CX(3)CR1 Function by Targeted Deletion and Green Fluorescent Protein Reporter Gene Insertion." *Molecular and Cellular Biology* 20 (11): 4106–14. doi:10.1128/MCB.20.11.4106-4114.2000.Updated.
- Justilien, Verline, Ji Jing Pang, Kutralanathan Renganathan, Xianquan Zhan, John W. Crabb, Ra Kim So, Janet R. Sparrow, William W. Hauswirth, and Alfred S. Lewin. 2007. "SOD2 Knockdown Mouse Model of Early AMD." *Investigative Ophthalmology and Visual Science* 48 (10): 4407–20. doi:10.1167/iops.07-0432.
- Kaarniranta, Kai, Debasish Sinha, Janusz Blasiak, Anu Kauppinen, Zoltán Veréb, Antero Salminen, Michael E. Boulton, and Goran Petrovski. 2013. "Autophagy and Heterophagy Dysregulation Leads to Retinal Pigment Epithelium Dysfunction and Development of Age-Related Macular Degeneration." *Autophagy* 9 (7): 973–84. doi:10.4161/auto.24546.
- Kabasawa, Sho, Keisuke Mori, Kuniko Horie-Inoue, Peter L. Gehlbach, Satoshi Inoue, Takuya Awata, Shigehiro Katayama, and Shin Yoneya. 2011. "Associations of Cigarette Smoking but Not Serum Fatty Acids with Age-Related Macular Degeneration in a Japanese Population." *Ophthalmology* 118 (6). Elsevier Inc.: 1082–88. doi:10.1016/j.ophtha.2010.10.012.
- Kaneko, Hiroki, Sami Dridi, Valeria Tarallo, Bradley D. Gelfand, Benjamin J. Fowler, Won Gil Cho, Mark E. Kleinman, et al. 2011. "DICER1 Deficit Induces Alu RNA Toxicity in Age-Related Macular Degeneration." *Nature* 471 (7338): 325–32. doi:10.1038/nature09830.

- Kanemura, Hoshimi, Masahiro J. Go, Masayuki Shikamura, Naoki Nishishita, Noriko Sakai, Hiroyuki Kamao, Michiko Mandai, Chikako Morinaga, Masayo Takahashi, and Shin Kawamata. 2014. "Tumorigenicity Studies of Induced Pluripotent Stem Cell (iPSC)-Derived Retinal Pigment Epithelium (RPE) for the Treatment of Age-Related Macular Degeneration." *PLoS ONE* 9 (1): 1–11. doi:10.1371/journal.pone.0085336.
- Kang, Chanhee, and Stephen J. Elledge. 2016. "How Autophagy Both Activates and Inhibits Cellular Senescence." *Autophagy* 12 (5). Taylor & Francis: 898–99. doi:10.1080/15548627.2015.1121361.
- Karakoti, Ajay, Sanjay Singh, Janet M. Dowding, Sudipta Seal, and William T. Self. 2009. "Redox-Active Radical Scavenging Nanomaterials." *Chemical Society Reviews* 39 (11): 4422–32. doi:10.1039/b919677n.
- Kassoff, a., J. Kassoff, J. Buehler, M. Eglow, F. Kaufman, M. Mehu, S. Kieval, et al. 2001. "A Randomized, Placebo-Controlled, Clinical Trial of High-Dose Supplementation with Vitamins C and E, Beta Carotene, and Zinc for Age-Related Macular Degeneration and Vision Loss: AREDS Report No. 8." *Archives of Ophthalmology* 119 (10): 1417–36. doi:10.1001/archophth.119.10.1417.
- Kaszubski, Patrik, Tal Ben Ami, Celine Saade, and R. Theodore Smith. 2016. "Geographic Atrophy and Choroidal Neovascularization in the Same Eye." *Ophthalmic Research* 55 (4): 185–93. doi:10.1002/cncr.27633.Percutaneous.
- Khurana, Amit, Sravani Tekula, and Chandraiah Godugu. 2018. "Nanoceria Suppresses Multiple Low Doses of Streptozotocin-Induced Type 1 Diabetes by Inhibition of Nrf2/NF-κB Pathway and Reduction of Apoptosis." *Nanomedicine* 13 (15): 1905–22. doi:10.2217/nnm-2018-0085.
- Kim, Chi Kyung, Taeho Kim, In Young Choi, Min Soh, Dohoung Kim, Young Ju Kim, Hyunduk Jang, et al. 2012. "Ceria Nanoparticles That Can Protect against Ischemic Stroke." *Angewandte Chemie - International Edition* 51 (44): 11039–43. doi:10.1002/anie.201203780.
- Kim, Eun Ji, Gregory R. Grant, Anita S. Bowman, Naqi Haider, Harini V. Gudiseva, and Venkata Ramana Murthy Chavali. 2018. "Complete Transcriptome Profiling of Normal and Age-Related Macular Degeneration Eye Tissues Reveals Dysregulation of Anti-Sense Transcription." *Scientific Reports* 8 (1). Springer US: 1–13. doi:10.1038/s41598-018-21104-7.
- Klein, Robert J, Caroline Zeiss, Emily Y Chew, Jen-Yue Tsai, Richard S Sackler, Chad Haynes, Alice K Henning, et al. 2005. "Complement Factor H Polymorphism in Age-Related Macular Degeneration." *Science (New York, N.Y.)* 308 (5720): 385–89. doi:10.1126/science.1109557.
- Kliffen, M., E. Lutgens, M. J.a.P. Daemen, E. D. De Muinck, C. M. Mooy, and P. T.V.M. De Jong. 2000. "The APO\*E3-Leiden Mouse as an Animal Model for Basal Lamina Deposit." *British Journal of Ophthalmology* 84 (12): 1415–19. doi:10.1136/bjo.84.12.1415.
- Kolb, Helga. 2013. "Simple Anatomy of the Retina by Helga Kolb." *The Organization of the Retina and Visual System*.
- Korsvik, Cassandra, Swanand Patil, Sudipta Seal, and William T. Self. 2007. "Superoxide Dismutase Mimetic Properties Exhibited by Vacancy Engineered Ceria Nanoparticles." *Chemical Communications*, no. 10: 1056–58. doi:10.1039/b615134e.
- Kumar-Singh, Rajendra. 2019. "The Role of Complement Membrane Attack Complex in Dry and Wet AMD - From Hypothesis to Clinical Trials." *Experimental Eye Research* 184 (February). Elsevier: 266–77. doi:10.1016/j.exer.2019.05.006.



- Kuppermann, Baruch D, David S Boyer, Peter K Kaiser, Jeffrey S Heier, Peter A Campochiaro, Hugo Quiroz-Mercado, Julia Kornfield, et al. 2016. "Topline Results from Prospective, Double-Masked, Placebo Controlled Phase 2 Clinical Study Evaluating Luminata(R) (ALG-1001) in Patients with Symptomatic Focal Vitreomacular Adhesion." In *Investigative Ophthalmology & Visual Science*. Vol. 57. [Association for Research in Vision and Ophthalmology, etc.]. <https://iovs.arvojournals.org/article.aspx?articleid=2560367&resultClick=1>.
- Kur, Joanna, Eric a. Newman, and Tailoi Chan-Ling. 2012. "Cellular and Physiological Mechanisms Underlying Blood Flow Regulation in the Retina and Choroid in Health and Disease." *Progress in Retinal and Eye Research* 31 (5). Elsevier Ltd: 377–406. doi:10.1016/j.preteyeres.2012.04.004.
- Kyosseva, Svetlana V, Lijuan Chen, Sudipta Seal, and James F Mcginnis. 2013. "Nanoceria Inhibit Expression of Genes Associated with Inflammation and Angiogenesis in the Retina of Vldlr Null Mice." *Experimental Eye Research* 116. Elsevier Ltd: 63–74. doi:10.1016/j.exer.2013.08.003.
- Lanzetta, Paolo, and Anat Loewenstein. 2017. "Fundamental Principles of an Anti-VEGF Treatment Regimen: Optimal Application of Intravitreal Anti-vascular Endothelial Growth Factor Therapy of Macular Diseases." *Graefe's Archive for Clinical and Experimental Ophthalmology* 255 (7). Graefe's Archive for Clinical and Experimental Ophthalmology: 1259–73. doi:10.1007/s00417-017-3647-4.
- Lee, Eun Jin, Yerina Ji, Colleen L. Zhu, and Norberto M. Grzywacz. 2011. "Role of Müller Cells in Cone Mosaic Rearrangement in a Rat Model of Retinitis Pigmentosa." *Glia* 59 (7): 1107–17. doi:10.1002/glia.21183.
- Lee, Tin Lap, Joan M. Raitano, Owen M. Rennert, Siu Wai Chan, and Wai Yee Chan. 2012. "Accessing the Genomic Effects of Naked Nanoceria in Murine Neuronal Cells." *Nanomedicine: Nanotechnology, Biology, and Medicine* 8 (5). Elsevier B.V.: 599–608. doi:10.1016/j.nano.2011.08.005.
- Lei, Bo, Gang Yao, Keqing Zhang, Kurt J Hofeldt, and Bo Chang. 2006. "Study of Rod- and Cone-Driven Oscillatory Potentials in Mice." *Investigative Ophthalmology and Visual Science* 47 (6): 2732–38. doi:10.1167/iovs.05-1461.
- Li, Chibo, Ming Cheng, Huijin Yang, Neal S. Peachey, and Muna I. Naash. 2001. "Age-Related Changes in the Mouse Outer Retina." *Optometry and Vision Science* 78 (6): 425–30. doi:10.1097/00006324-200106000-00015.
- Li, Huiling, Sumana R. Chintalapudi, and Monica M. Jablonski. 2017. "Current Drug and Molecular Therapies for the Treatment of Atrophic Age-Related Macular Degeneration: Phase I to Phase III Clinical Development." *Expert Opinion on Investigational Drugs* 26 (10). Taylor & Francis: 1103–14. doi:10.1080/13543784.2017.1369042.
- Li, Lu, Nicole Eter, and Peter Heiduschka. 2015. "The Microglia in Healthy and Diseased Retina." *Experimental Eye Research* 136: 116–30. doi:10.1016/j.exer.2015.04.020.
- Li, Mingyao, Cheng Jia, Krista L. Kazmierkiewicz, Anita S. Bowman, Lifeng Tian, Yichuan Liu, Neel a. Gupta, et al. 2014. "Comprehensive Analysis of Gene Expression in Human Retina and Supporting Tissues." *Human Molecular Genetics* 23 (15): 4001–14. doi:10.1093/hmg/ddu114.
- Li, Yao, Yi Ting Tsai, Chun Wei Hsu, Deniz Erol, Jin Yang, Wen Hsuan Wu, Richard J. Davis, Dieter Egli, and Stephen H. Tsang. 2012. "Long-Term Safety and Efficacy of Human-Induced Pluripotent Stem Cell (iPS) Grafts in a Preclinical Model of Retinitis Pigmentosa." *Molecular Medicine* 18 (9): 1312–19. doi:10.2119/molmed.2012.00242.

- Lim, Laurence S, Paul Mitchell, Johanna M Seddon, Frank G Holz, and Tien Y Wong. 2012. "Age-Related Macular Degeneration." *The Lancet* 379 (9827). Elsevier Ltd: 1728–38. doi:10.1016/S0140-6736(12)60282-7.
- Liu, Chi Hsiu, Zhongxiao Wang, Ye Sun, and Jing Chen. 2017. "Animal Models of Ocular Angiogenesis: From Development to Pathologies." *FASEB Journal* 31 (11): 4665–81. doi:10.1096/fj.201700336R.
- Liu, Jian, David a. Copland, Sofia Theodoropoulou, Hsi An Amy Chiu, Miriam Durazo Barba, Ka Wang Mak, Matthias Mack, Lindsay B. Nicholson, and Andrew D. Dick. 2016. "Impairing Autophagy in Retinal Pigment Epithelium Leads to Inflammasome Activation and Enhanced Macrophage-Mediated Angiogenesis." *Scientific Reports* 6 (October 2015). Nature Publishing Group: 1–15. doi:10.1038/srep20639.
- Liu, Pingfang, and Bruce Demple. 2010. "DNA Repair in Mammalian Mitochondria: Much More than We Thought?" *Environmental and Molecular Mutagenesis* 51 (1): 417–26. doi:10.1002/em.
- Liu, Yanling, Lan Franco Leo, Corban McGregor, Anzor Grivitsvili, Colin J. Barnstable, and Joyce Tombran-Tink. 2012. "Pigment Epithelium-Derived Factor (PEDF) Peptide Eye Drops Reduce Inflammation, Cell Death and Vascular Leakage in Diabetic Retinopathy in Ins2(Akita) Mice." *Molecular Medicine (Cambridge, Mass.)* 18 (6): 1387–1401. doi:10.2119/molmed.2012.00008.
- Loftsson, Thorsteinn, and Einar Stefánsson. 2017. "Cyclodextrins and Topical Drug Delivery to the Anterior and Posterior Segments of the Eye." *International Journal of Pharmaceutics* 531 (2). Elsevier B.V.: 413–23. doi:10.1016/j.ijpharm.2017.04.010.
- Lu, B, B J Rutledge, L Gu, J Fiorillo, N W Lukacs, S L Kunkel, R North, C Gerard, and B J Rollins. 1998. "Abnormalities in Monocyte Recruitment and Cytokine Expression in Monocyte Chemoattractant Protein 1-Deficient Mice." *The Journal of Experimental Medicine* 187 (4): 601–8. doi:10.1084/jem.187.4.601.
- Ludwig, Parker E., S. Caleb Freeman, and Adam C. Janot. 2019. "Novel Stem Cell and Gene Therapy in Diabetic Retinopathy, Age Related Macular Degeneration, and Retinitis Pigmentosa." *International Journal of Retina and Vitreous* 5 (1). BioMed Central: 1–14. doi:10.1186/s40942-019-0158-y.
- Luhmann, Ulrich F O, Livia S. Carvalho, Scott J. Robbie, Jill a. Cowing, Yanai Duran, Peter M G Munro, James W B Bainbridge, and Robin R. Ali. 2013. "Ccl2, Cx3cr1 and Ccl2/Cx3cr1 Chemokine Deficiencies Are Not Sufficient to Cause Age-Related Retinal Degeneration." *Experimental Eye Research* 107: 80–87. doi:10.1016/j.exer.2012.11.015.
- Luhmann, Ulrich F O, Clemens A Lange, Scott Robbie, Peter M G Munro, Jill A Cowing, Hannah E J Armer, Vy Luong, Livia S Carvalho, Robert E Maclaren, et al. 2012. "Differential Modulation of Retinal Degeneration by Ccl2 and Cx3cr1 Chemokine Signalling" 7 (4). doi:10.1371/journal.pone.0035551.
- Luhmann, Ulrich F O, Scott Robbie, Peter M G Munro, Susie E. Barker, Yanai Duran, Vy Luong, Frederick W. Fitzke, James W B Bainbridge, Robin R. Ali, and Robert E. Maclaren. 2009. "The Drusenlike Phenotype in Aging Ccl2-Knockout Mice Is Caused by an Accelerated Accumulation of Swollen Autofluorescent Subretinal Macrophages." *Investigative Ophthalmology and Visual Science* 50 (12): 5934–43. doi:10.1167/iovs.09-3462.
- Luhmann, Ulrich F.O., Livia S. Carvalho, Sophia Martha Kleine Holthaus, Jill a. Cowing, Simon Greenaway, Colin J. Chu, Philipp Herrmann, et al. 2015. "The Severity of Retinal Pathology in Homozygous Crb1rd8/rd8 Mice Is Dependent on Additional Genetic Factors." *Human Molecular Genetics* 24 (1): 128–41. doi:10.1093/hmg/ddu424.

- Luo, Chang, Mei Chen, and Heping Xu. 2011. "Complement Gene Expression and Regulation in Mouse Retina and Retinal Pigment Epithelium/choroid." *Molecular Vision* 17 (September 2010): 1588–97. <http://www.ncbi.nlm.nih.gov/pubmed/21738388>.
- Luster, Andrew D. 1998. "C Hemokines — C Hemotactic C Ytokines T Hat M Ediate I Nflammation." *The New England Journal of Medicine* 338: 436–45. doi:10.1056/NEJM199802123380706.
- Lynn, Savannah a., Eloise Keeling, Rosie Munday, Gagandeep Gabha, Helen Griffiths, Andrew J. Lotery, and J. Arjuna Ratnayaka. 2017. "The Complexities Underlying Age-Related Macular Degeneration: Could Amyloid Beta Play an Important Role?" *Neural Regeneration Research* 12 (4): 538–48. doi:10.4103/1673-5374.205083.
- Ma, Qiang. 2013. "Role of Nrf2 in Oxidative Stress and Toxicity." *Annual Review of Pharmacology and Toxicology* 53 (1): 401–26. doi:10.1146/annurev-pharmtox-011112-140320.
- Ma, Wenxin, and Wai T Wong. 2016. "Aging Changes in Retinal Microglia and Their Relevance to Age-Related Macular Degeneration." In *Retinal Degenerative Diseases*, 73–78. doi:10.1016/c2013-0-06451-1.
- Ma, Wenxin, Lian Zhao, Aurora M. Fontainhas, Robert N. Fariss, and Wai T. Wong. 2009. "Microglia in the Mouse Retina Alter the Structure and Function of Retinal Pigmented Epithelial Cells: A Potential Cellular Interaction Relevant to AMD." *PLoS ONE* 4 (11). doi:10.1371/journal.pone.0007945.
- Mains, Jenifer, and Clive G. Wilson. 2012. "The Vitreous Humor As a Barrier to Nanoparticle Distribution." *Journal of Ocular Pharmacology and Therapeutics* 29 (2): 143–50. doi:10.1089/jop.2012.0138.
- Malek, G, L V Johnson, B E Mace, P Saloupis, D E Schmechel, D W Rickman, and C a Toth. 2005. "Apolipoprotein E Allele-Dependent Pathogenesis.pdf." *Proceedings of the National Academy of Sciences* 102 (33): 11900–905. doi:10.1073/pnas.0503015102.
- Mandai, M., a. Watanabe, Y. Kurimoto, Y. Hiram, C. Morinaga, T. Daimon, M. Fujihara, et al. 2017. "Autologous Induced Stem-Cell-Derived Retinal Cells for Macular Degeneration." *New England Journal of Medicine* 376 (11): 1038–46. doi:10.1056/NEJMoa1608368.
- Marmorstein, Alan D., and Lihua Y. Marmorstein. 2007. "The Challenge of Modeling Macular Degeneration in Mice." *Trends in Genetics* 23 (5): 225–31. doi:10.1016/j.tig.2007.03.001.
- Mattapallil, Mary J., Eric F. Wawrousek, Chi Chao Chan, Hui Zhao, Jayeeta Roychoudhury, Thomas A. Ferguson, and Rachel R. Caspi. 2012. "The Rd8 Mutation of the Crb1 Gene Is Present in Vendor Lines of C57BL/6N Mice and Embryonic Stem Cells, and Confounds Ocular Induced Mutant Phenotypes." *Investigative Ophthalmology & Visual Science* 53 (6): 2921–27. doi:10.1167/iovs.12-9662.
- Mazzoni, Francesca, Hussein Safa, and Silvia C. Finnemann. 2014. "Understanding Photoreceptor Outer Segment Phagocytosis: Use and Utility of RPE Cells in Culture." *Experimental Eye Research* 126: 51–60. doi:10.1016/j.exer.2014.01.010.
- McHarg, Selina, Simon J Clarck, Anthony J Day, and Paul N Bishop. 2015. "Age-Related Macular Degeneration and the Complement System." *Molecular Immunology* 67. Elsevier Ltd: 43–50. doi:10.1016/j.imbio.2011.07.019.
- Mecca, Carmen, Ileana Giambanco, Rosario Donato, and Cataldo Arcuri. 2018. "Microglia and Aging: The Role of the TREM2–DAP12 and CX3CL1–CX3CR1 Axes." *International Journal of Molecular Sciences* 19 (1): 1–27. doi:10.3390/ijms19010318.

- Mehalow, Adrienne K., Shuhei Kameya, Richard S. Smith, Norman L. Hawes, James M. Denegre, James a. Young, Lesley Bechtold, et al. 2003. "CRB1 Is Essential for External Limiting Membrane Integrity and Photoreceptor Morphogenesis in the Mammalian Retina." *Human Molecular Genetics* 12 (17): 2179–89. doi:10.1093/hmg/ddg232.
- Mescher, Anthony L. 2016. *Junqueira's Basic Histology*. 14th ed.
- Miller, Hedva, Benjamin Miller, Tatsuro Ishiboshi, and Stephen J Ryan. 1990. "Pathogenesis of Laser-Induced Choroidal Subretinal Neovascularization." *Investigative Ophthalmology & Visual Science* 31 (5): 899–908.
- Mitra, Rajendra N, Ruijuan Gao, Min Zheng, Ming-jing Wu, Maxim A Voinov, Alex I Smirnov, Tatyana I Smirnova, Kai Wang, Sai Chavala, and Zongchao Han. 2017. "Glycol Chitosan Engineered Autoregenerative Antioxidant Signi Fi Cantly Attenuates Pathological Damages in Models of Age-Related Macular Degeneration." doi:10.1021/acsnano.7b00429.
- Miyadera, Keiko. 2018. "Mapping of Canine Models of Inherited Retinal Diseases." *Advances in Experimental Medicine and Biology* 1074: 257–64. doi:10.1007/978-3-319-75402-4\_31.
- Miyadera, Keiko, Gregory M. Acland, and Gustavo D. Aguirre. 2012. "Genetic and Phenotypic Variations of Inherited Retinal Diseases in Dogs: The Power of within- and across-Breed Studies." *Mammalian Genome* 23 (1-2): 40–61. doi:10.1007/s00335-011-9361-3.
- Moore, Bret A, Michel J Roux, Lionel Sebbag, Ann Cooper, Sydney G Edwards, C Brian, Denise M Imai, et al. 2018. "A Population Study of Common Ocular Abnormalities in C57BL/6N rd8 Mice." *Investigative Ophthalmology & Visual Science* 59: 2252–61.
- Moreira-Neto, Carlos a., Eric M. Moulton, James G. Fujimoto, Nadia K. Waheed, and Daniela Ferrara. 2018. "Choriocapillaris Loss in Advanced Age-Related Macular Degeneration." *Journal of Ophthalmology* 2018: 1–6. doi:10.1155/2018/8125267.
- Mowat, Freya M., Simon M. Petersen-Jones, Helen Williamson, David L. Williams, Philip J. Luthert, Robin R. Ali, and James W. Bainbridge. 2008. "Topographical Characterization of Cone Photoreceptors and the Area Centralis of the Canine Retina." *Molecular Vision* 14 (December): 2518–27.
- Muftuoglu, Ilkay Kilic, Hema L. Ramkumar, Dirk Uwe Bartsch, Amit Meshi, Raouf Gaber, and William R. Freeman. 2017. "Quantitative Analysis of the Inner Retinal Layer Thicknesses in Agerelated Macular Degeneration Using Corrected Optical Coherence Tomography Segmentation." *Retina* 38 (8): 1478–84. doi:10.1097/IAE.0000000000001759.
- Muraoka, Yuki, Yuto Iida, Hanako O. Ikeda, Sachiko Iwai, Masayuki Hata, Takeshi Iwata, Mao Nakayama, et al. 2018. "KUS121, an ATP Regulator, Mitigates Chorioretinal Pathologies in Animal Models of Age-Related Macular Degeneration." *Heliyon* 4 (5). Elsevier Ltd: e00624. doi:10.1016/j.heliyon.2018.e00624.
- Myers, Chelsea E., Barbara E.K. Klein, Ronald Gangnon, Theru a. Sivakumaran, Sudha K. Iyengar, and Ronald Klein. 2014. "Cigarette Smoking and the Natural History of Age-Related Macular Degeneration." *Ophthalmology* 121 (10). Elsevier Inc: 1949–55. doi:10.1016/j.ophtha.2014.04.040.
- Nadal-Nicolás, Francisco M., Manuel Vidal-Sanz, and Marta Agudo-Barriuso. 2018. "The Aging Rat Retina: From Function to Anatomy." *Neurobiology of Aging* 61. Elsevier Inc: 146–68. doi:10.1016/j.neurobiolaging.2017.09.021.
- Nakagami, Yasuhiro. 2016. "Nrf2 Is an Attractive Therapeutic Target for Retinal Diseases." *Oxidative Medicine and Cellular Longevity* 2016: 1–8. doi:10.1155/2016/7469326.

- Nakazawa, Toru, Masumi Takeda, Geoffrey P. Lewis, Kin Sang Cho, Jianwei Jiao, Ulrika Wilhelmsson, Steven K. Fisher, Milos Pekny, Dong F. Chen, and Joan W. Miller. 2007. "Attenuated Glial Reactions and Photoreceptor Degeneration after Retinal Detachment in Mice Deficient in Glial Fibrillary Acidic Protein and Vimentin." *Investigative Ophthalmology and Visual Science* 48 (6): 2760–68. doi:10.1167/iovs.06-1398.
- Naz, Shuguftha, James Beach, Blaze Heckert, Tanuja Tummala, Oleksandra Pashchenko, Tujina Banerjee, and Santimukul Santra. 2017. "Cerium Oxide Nanoparticles: A Radical Approach to Neurodegenerative Disease Treatment." *Nanomedicine*.
- Nita, Malgorzata, Andrzej Grzybowski, Francisco J Ascaso, and Valentín Huerva. 2014. "Age-Related Macular Degeneration in the Aspect of Chronic Low-Grade Inflammation ( Pathophysiological ParaInflammation )." *Mediators of Inflammation* 2014 (930671).
- Niu, Jianli, Kangkai Wang, and Pappachan E Kolattukudy. 2011. "Cerium Oxide Nanoparticles Inhibit Oxidative Stress and Nuclear Factor- $\kappa$ B Activation in H9c2 Cardiomyocytes Exposed to Cigarette Smoke Extract." *The Journal of Pharmacology and Experimental Therapeutics* 338 (1): 53–61. doi:10.1124/jpet.111.179978.
- Nordgaard, Curtis L., Kristin M. Berg, Rebecca J. Kapphahn, Cavan Reilly, Xiao Feng, Timothy W. Olsen, and Deborah a. Ferrington. 2006. "Proteomics of the Retinal Pigment Epithelium Reveals Altered Protein Expression at Progressive Stages of Age-Related Macular Degeneration." *Investigative Ophthalmology and Visual Science* 47 (3): 815–22. doi:10.1167/iovs.05-0976.
- Nordgaard, Curtis L., Pabalu P. Karunadharma, Xiao Feng, Timothy W. Olsen, and Deborah a. Ferrington. 2008. "Mitochondrial Proteomics of the Retinal Pigment Epithelium at Progressive Stages of Age-Related Macular Degeneration." *Investigative Ophthalmology and Visual Science* 49 (7): 2848–55. doi:10.1167/iovs.07-1352.
- Nowak, Jerzy Z. 2014. "AMD - The Retinal Disease With an Unprecised Etiopathogenesis: In Search of Effective Therapeutics." *Polish Pharmaceutical Society* 71 (6): 900–916.
- Nozaki, Miho, Brian J Raisler, Eiji Sakurai, J Vidya Sarma, Scott R Barnum, John D Lambris, Yali Chen, et al. 2006. "Drusen Complement Components C3a and C5a Promote Choroidal Neovascularization." *Proceedings of the National Academy of Sciences of the United States of America* 103 (7): 2328–33. doi:10.1073/pnas.0408835103.
- Peng, Yingqian, Luosheng Tang, and Yedi Zhou. 2017. "Subretinal Injection: A Review on the Novel Route of Therapeutic Delivery for Vitreoretinal Diseases." *Ophthalmic Research* 58 (4): 217–26. doi:10.1159/000479157.
- Pennesi, Mark E., Martha Neuringer, and Robert J. Courtney. 2012. "Animal Models of Age Related Macular Degeneration." *Molecular Aspects of Medicine* 33 (4). Elsevier Ltd: 487–509. doi:10.1016/j.mam.2012.06.003.
- Pennington, Katie L., and Margaret M. DeAngelis. 2016. "Epidemiology of Age-Related Macular Degeneration (AMD): Associations with Cardiovascular Disease Phenotypes and Lipid Factors." *Eye and Vision* 3 (1). Eye and Vision: 1–20. doi:10.1186/s40662-016-0063-5.
- Picard, Emilie, Marianne Houssier, Kim Bujold, Przemyslaw Sapieha, William Lubell, Allison Dorfman, Julie Racine, et al. 2010. "CD36 Plays an Important Role in the Clearance of oxLDL and Associated Age-Dependent Sub-Retinal Deposits." *Aging* 2 (12): 981–89. doi:10.18632/aging.100218.

- Pierscionek, Barbara K., Yuebin Li, Akeel A. Yasseen, Liza M. Colhoun, Ronald A. Schachar, and Wei Chen. 2010. "Nanoceria Have No Genotoxic Effect on Human Lens Epithelial Cells." *Nanotechnology* 21 (3): 1–8. doi:10.1088/0957-4484/21/3/035102.
- Pijanka, Jacek K, Elizabeth Cone-Kimball, Mary E Pease, Ahmed Abass, Thomas Sorensen, Thao D. Nguyen, Harry a. Quigley, and Craig Boote. 2014. "Changes in Scleral Collagen Organization Associated with Murine Chronic Experimental Glaucoma." *Investigative Ophthalmology & Visual Science*. doi:10.1167/iovs.14-15047.
- Pirmohamed, Talib, Janet M. Dowding, Sanjay Singh, Brian Wasserman, Eric Heckert, Ajay S. Karakoti, Jessica E.S. King, Sudipta Seal, and William T. Self. 2010. "Nanoceria Exhibit Redox State-Dependent Catalase Mimetic Activity." *Chemical Communications* 46 (16): 2736–38. doi:10.1039/b922024k.
- Prasad, Tuhina, Ping Zhu, Amrisha Verma, Paramita Chakrabarty, Awilda M. Rosario, Todd E. Golde, and Qihong Li. 2017. "Amyloid B Peptides Overexpression in Retinal Pigment Epithelial Cells via AAV-Mediated Gene Transfer Mimics AMD-like Pathology in Mice." *Scientific Reports* 7 (3222). Springer US: 1–15. doi:10.1038/s41598-017-03397-2.
- Prausnitz, Mark R., and Jeremy S. Noonan. 1998. "Permeability of Cornea, Sclera, and Conjunctiva: A Literature Analysis for Drug Delivery to the Eye." *Journal of Pharmaceutical Sciences* 87 (12): 1479–88. doi:10.1021/js9802594.
- Rai, Uma Do J.P., Simon a. Young, Thilini R. Thrimawithana, Hamdy Abdelkader, Adam W.G. Alani, Barbara Pierscionek, and Raid G. Alany. 2015. "The Suprachoroidal Pathway: A New Drug Delivery Route to the Back of the Eye." *Drug Discovery Today* 20 (4). Elsevier Ltd: 491–95. doi:10.1016/j.drudis.2014.10.010.
- Ramírez, Claudio, Javier Cáceres-del-Carpio, Justin Chu, Joshua Chu, M. Tarek Moustafa, Marilyn Chwa, G. Astrid Limb, Baruch D. Kuppermann, and M. Cristina Kenney. 2016. "Brimonidine Can Prevent In Vitro Hydroquinone Damage on Retinal Pigment Epithelium Cells and Retinal Müller Cells." *Journal of Ocular Pharmacology and Therapeutics* 32 (2): 102–8. doi:10.1089/jop.2015.0083.
- Ramkumar, Hema L, Jingsheng Tuo, De F Shen, Jun Zhang, Xiaoguang Cao, Emily Y Chew, and Chi-chao Chan. 2013a. "Nutrient Supplementation with n3 Polyunsaturated Fatty Acids , Lutein , and Zeaxanthin Decrease A2E Accumulation and VEGF Expression in the Retinas of Ccl2 / Cx3cr1 - Deficient Mice on Crb1 rd8 Background." *The Journal of Nutrition of Nutrition* 143: 1129–35. doi:10.3945/jn.112.169649.1129.
- Ramsay, Eva, Eva M. del Amo, Elisa Toropainen, Unni Tengvall-Unadike, Veli Pekka Ranta, Arto Urtti, and Marika Ruponen. 2018. "Corneal and Conjunctival Drug Permeability: Systematic Comparison and Pharmacokinetic Impact in the Eye." *European Journal of Pharmaceutical Sciences* 119 (April). Elsevier: 83–89. doi:10.1016/j.ejps.2018.03.034.
- Raoul, William, Constance Auvynet, Serge Camelo, Xavier Guillonéau, Charles Feumi, Christophe Combadière, and Florian Sennlaub. 2010. "CCL2/CCR2 and CX3CL1/CX3CR1 Chemokine Axes and Their Possible Involvement in Age-Related Macular Degeneration." *Journal of Neuroinflammation* 7 (87): 1–7. <http://www.jneuroinflammation.com/content/7/1/87> \n <http://0-ovidsp.ovid.com.wam.city.ac.uk/ovidweb.cgi?T=JS&PAGE=reference&D=emed9&NEWS=N&AN=2011011829>.
- Ratnapriya, Rinki, Olukayode a. Sosina, Margaret R. Starostik, Madeline Kwicklis, Rebecca J. Kappahn, Lars G. Fritsche, Ashley Walton, et al. 2019. "Retinal Transcriptome and eQTL Analyses Identify Genes Associated with Age-Related Macular Degeneration." *Nature Genetics* 51 (4): 606–10. doi:10.1038/s41588-019-0351-9.

- Reichenbach, Andreas, and Andreas Bringmann. 2013. "New Functions of Müller Cells." *Glia* 61 (5): 651–78. doi:10.1002/glia.22477.
- Riera, Marina, Laura Fontrodona, Silvia Albert, Diana Mora Ramirez, Anna Seriola, Anna Salas, Yolanda Muñoz, et al. 2016. "Comparative Study of Human Embryonic Stem Cells ( hESC ) and Human Induced Pluripotent Stem Cells ( hiPSC ) as a Treatment for Retinal Dystrophies." *Molecular Therapy* 3 (January): 1–12. doi:10.1038/mtm.2016.10.
- Rofagha, Soraya, Robert B. Bhisitkul, David S. Boyer, Srinivas R. Sadda, and Kang Zhang. 2013. "Seven-Year Outcomes in Ranibizumab-Treated Patients in ANCHOR, MARINA, and HORIZON: A Multicenter Cohort Study (SEVEN-UP)." *Ophthalmology* 120 (11). American Academy of Ophthalmology: 2292–99. doi:10.1016/j.ophtha.2013.03.046.
- Ross, Robert J., Min Zhou, Defen Shen, Robert N. Fariss, Xiaoyan Ding, Christine M. Bojanowski, Jingsheng Tuo, and Chi Chao Chan. 2008. "Immunological Protein Expression Profile in Ccl2/Cx3cr1 Deficient Mice with Lesions Similar to Age-Related Macular Degeneration." *Experimental Eye Research* 86 (4): 675–83. doi:10.1016/j.exer.2008.01.014.
- Rudnicka, Alicja R., Venediktos V. Kapetanakis, Zakariya Jarrar, Andrea K. Wathern, Richard Wormald, Astrid E. Fletcher, Derek G. Cook, and Christopher G. Owen. 2015. "Incidence of Late Stage Age Related Macular Degeneration in American Whites: Systematic Review and Meta-Analysis." *American Journal of Ophthalmology*, no. October 2012. The Authors: 1–9. doi:10.1016/j.ajo.2015.04.003.
- Runkle, E Aaron, and David A Antonetti. 2011. "The Blood-Retinal Barrier: Structure and Functional Significance." In *The Blood-Brain and Other Neural Barriers*, 686:133–48. doi:10.1007/978-1-60761-938-3.
- Saadat, Khandakar, Yusuke Murakami, Xue Tan, Yoko Nomura, Eiichi Okada, Yasuhiro Ikeda, and Yasuo Yanagi. 2014. "Inhibition of Autophagy Induces Retinal Pigment Epithelial Cell Damage by the Lipofuscin Fluorophore A2E." *FEBS Open Bio* 4: 1007–14.
- Sachdeva, Mira M., Marisol Cano, and James T. Handa. 2014. "Nrf2 Signaling Is Impaired in the Aging RPE given an Oxidative Insult." *Experimental Eye Research* 119. Elsevier Ltd: 111–14. doi:10.1016/j.exer.2013.10.024.
- Saddala, Madhu Sudhana, Anton Lennikov, Anthony Mukwaya, Lijuan Fan, Zhengmao Hu, and Hu Huang. 2019. "Transcriptome-Wide Analysis of Differentially Expressed Chemokine Receptors, SNPs, and SSRs in the Age-Related Macular Degeneration." *Human Genomics* 13 (1). Human Genomics: 15. doi:10.1186/s40246-019-0199-1.
- Safaiyan, Shima, Nirmal Kannaiyan, Nicolas Snaidero, Simone Brioschi, Knut Biber, Simon Yona, Aimee L. Edinger, Steffen Jung, Moritz J. Rossner, and Mikael Simons. 2016. "Age-Related Myelin Degradation Burdens the Clearance Function of Microglia during Aging." *Nature Neuroscience* 19 (8): 995–98. doi:10.1038/nn.4325.
- Sampath, Alapakkam P., Katherine J. Strissel, Rajesh Elias, Vadim Y. Arshavsky, James F. McGinnis, Jeannie Chen, Satoru Kawamura, Fred Rieke, and James B. Hurley. 2005. "Recoverin Improves Rod-Mediated Vision by Enhancing Signal Transmission in the Mouse Retina." *Neuron* 46 (3): 413–20. doi:10.1016/j.neuron.2005.04.006.
- Saul, Alan B., Xuezhi Cui, Shanu Markand, and Sylvia B. Smith. 2017. "Detailed Electroretinographic Findings in rd8 Mice." *Documenta Ophthalmologica* 134 (3). Springer Berlin Heidelberg: 195–203. doi:10.1007/s10633-017-9585-y.

- Seddon, Johanna M., D. Scott McLeod, Imran a. Bhutto, Mercedes B. Villalonga, Rachel E. Silver, Adam S. Wenick, Malia M. Edwards, and Gerard a. Luttly. 2016. "Histopathological Insights into Choroidal Vascular Loss in Clinically Documented Cases of Age-Related Macular Degeneration." *JAMA Ophthalmology* 134 (11): 1272–80. doi:10.1001/jamaophthalmol.2016.3519.
- Seoane, Ana, Mónica Espejo, Mercè Pallàs, Eduardo Rodríguez-Farré, Santiago Ambrosio, and Jordi Llorens. 1999. "Degeneration and Gliosis in Rat Retina and Central Nervous System Following 3,3'-Iminodipropionitrile Exposure." *Brain Research* 833 (2): 258–71. doi:10.1016/S0006-8993(99)01552-8.
- Shamsi, Farrukh A, and Mike Boulton. 2001. "Inhibition of RPE Lysosomal and Antioxidant Activity by the Age Pigment Lipofuscin." *Investigative Ophthalmology and Visual Science* 42 (12): 3041–46. <http://0-ovidsp.ovid.com.wam.city.ac.uk/ovidweb.cgi?T=JS&PAGE=reference&D=emed5&NEWS=N&AN=2001393149>.
- Shelley, Elizabeth J., Michele C. Madigan, Riccardo Natoli, Philip L. Penfold, and Jan M. Provis. 2009. "Cone Degeneration in Aging and Age-Related Macular Degeneration." *Archives of Ophthalmology* 127 (4): 483–92. doi:10.1001/archophthalmol.2008.622.
- Shikamura, Yuko, Yoshiko Yamazaki, Toru Matsunaga, Takao Sato, Akira Ohtori, and Kakuji Tojo. 2016. "Hydrogel Ring for Topical Drug Delivery to the Ocular Posterior Segment." *Current Eye Research* 41 (5): 653–61. doi:10.3109/02713683.2015.1050738.
- Skeie, J. M., and R. F. Mullins. 2009. "Macrophages in Neovascular Age-Related Macular Degeneration: Friends or Foes?" *Eye* 23 (4). Nature Publishing Group: 747–55. doi:10.1038/eye.2008.206.
- Slakter, Jason S., and Michael Stur. 2005. "Quality of Life in Patients with Age-Related Macular Degeneration: Impact of the Condition and Benefits of Treatment." *Survey of Ophthalmology* 50 (3): 263–73. doi:10.1016/j.survophthal.2005.02.007.
- Slyshenkov, Vyacheslav S., Anna A. Shevalye, Anton V. Liopo, and Lech Wojtczak. 2002. "Protective Role of L-Methionine against Free Radical Damage of Rat Brain Synaptosomes." *Acta Biochimica Polonica* 49 (4): 907–16.
- Solomon, Sharon D, Kristina B Lindsley, Magdalena G Krzystolik, Satyanarayana S Vedula, and Barbara S Hawkins. 2016. "Intravitreal Bevacizumab Versus Ranibizuman for Treatment of Neovascular Age-Related Macular Degeneration: Findings from a Cochrane Systematic Review." *Ophthalmology* 123 (1): 70–77. doi:10.1002/cncr.27633.Percutaneous.
- Song, Wensi, Seung Soo Lee, Marzia Savini, Lauren Popp, Vicki L. Colvin, and Laura Segatori. 2014. "Ceria Nanoparticles Stabilized by Organic Surface Coatings Activate the Lysosome-Autophagy System and Enhance Autophagic Clearance." *ACS Nano* 8 (10): 10328–42. doi:10.1021/nn505073u.
- Sparrow, J R, D Hicks, and C P Hamel. 2010. "The Retinal Pigment Epithelium in Health and Disease." *Current Molecular Medicine* 10 (9): 802–23. <http://www.ncbi.nlm.nih.gov/pubmed/21091424>.
- Srirangam, Ramesh, Ketan Hippalgaonkar, Bharathi Avula, Ikhlas a. Khan, and Soumyajit Majumdar. 2012. "Evaluation of the Intravenous and Topical Routes for Ocular Delivery of Hesperidin and Hesperetin." *Journal of Ocular Pharmacology and Therapeutics* 28 (6): 618–27. doi:10.1089/jop.2012.0040.
- Strauss, Olaf. 2005. "The Retinal Pigment Epithelium in Visual Function." *Physiological Reviews* 85 (3): 845–81. doi:10.1152/physrev.00021.2004.



- Strunnikova, N. V., a. Maminishkis, J. J. Barb, F. Wang, C. Zhi, Y. Sergeev, W. Chen, et al. 2010. "Transcriptome Analysis and Molecular Signature of Human Retinal Pigment Epithelium." *Human Molecular Genetics* 19 (12): 2468–86. doi:10.1093/hmg/ddq129.
- Swaroop, Anand, Emily Y Chew, Catherine Bowes Rickman, and Gonçalo R Abecasis. 2009. "Unraveling a Multifactorial Late-Onset Disease: From Genetic Susceptibility to Disease Mechanisms for Age-Related Macular Degeneration." *Annual Review of Genomics and Human Genetics* 10: 19–43. doi:10.1146/annurev.genom.9.081307.164350.
- Tanito, Masaki, Feng Li, and Robert E. Anderson. 2010. "Protection of Retinal Pigment Epithelium by OT-551 and Its Metabolite TEMPOL-H against Light-Induced Damage in Rats." *Experimental Eye Research* 91 (1): 111–14. doi:10.1016/j.exer.2010.04.012.
- Tarallo, Valeria, Yoshio Hirano, Bradley D. Gelfand, Sami Dridi, Nagaraj Kerur, Younghee Kim, Won Gil Cho, et al. 2012. "DICER1 Loss and Alu RNA Induce Age-Related Macular Degeneration via the NLRP3 Inflammasome and MyD88." *Cell* 149 (4): 847–59. doi:10.1016/j.cell.2012.03.036.
- Telegina, D. V., O. S. Kozhevnikova, and N. G. Kolosova. 2018. "Changes in Retinal Glial Cells with Age and during Development of Age-Related Macular Degeneration." *Biochemistry (Moscow)* 83 (9): 1009–17. doi:10.1134/S000629791809002X.
- Terluk, Marcia R., Rebecca J. Kappahn, Lauren M. Soukup, Hwee Gong, Christopher Gallardo, Sandra R. Montezuma, and Deborah a. Ferrington. 2015. "Investigating Mitochondria as a Target for Treating Age-Related Macular Degeneration." *Journal of Neuroscience* 35 (18): 7304–11. doi:10.1523/JNEUROSCI.0190-15.2015.
- Teutsch, Steven M, Margaret A McCoy, Brian R Woodbury, and Annalyn Welp. 2017. *Making Eye Health a Population Health Imperative. Optometry and Vision Science.* Vol. 94. doi:10.1097/opx.0000000000001074.
- Tisi, A., M. Passacantando, L. Lozzi, S. Riccitelli, S. Bisti, and R. Maccarone. 2019. "Retinal Long Term Neuroprotection by Cerium Oxide Nanoparticles after an Acute Damage Induced by High Intensity Light Exposure." *Experimental Eye Research* 182 (January). Elsevier: 30–38. doi:10.1016/j.exer.2019.03.003.
- Tobe, T, S Ortega, J D Luna, H Ozaki, N Okamoto, N L Derevjani, S a Vinos, C Basilico, and P a Campochiaro. 1998. "Targeted Disruption of the FGF2 Gene Does Not Prevent Choroidal Neovascularization in a Murine Model." *The American Journal of Pathology* 153 (5). American Society for Investigative Pathology: 1641–46. doi:10.1016/S0002-9440(10)65753-7.
- Tucker, Budd a., In Hyun Park, Sara D. Qi, Henry J. Klassen, Caihui Jiang, Jing Yao, Stephen Redenti, George Q. Daley, and Michael J. Young. 2011. "Transplantation of Adult Mouse iPS Cell-Derived Photoreceptor Precursors Restores Retinal Structure and Function in Degenerative Mice." *PLoS ONE* 6 (4): 1–11. doi:10.1371/journal.pone.0018992.
- Tuo, Jingsheng, Christine M. Bojanowski, Min Zhou, Defen Shen, Robert J. Ross, Kevin L. Rosenberg, D. Joshua Cameron, et al. 2007a. "Murine Ccl2/Cx3cr1 Deficiency Results in Retinal Lesions Mimicking Human Age-Related Macular Degeneration." *Investigative Ophthalmology and Visual Science* 48 (8): 3827–36. doi:10.1167/iovs.07-0051.
- Tuo, Jingsheng, Xiaoguang Cao, Defen Shen, Yujuan Wang, Jun Zhang, Youn Joo Oh, Darwin J Prockop, Chichao Chan, and Chan C.-C. 2012. "Anti-Inflammatory Recombinant TSG-6 Stabilizes the Progression of Focal Retinal Degeneration in a Murine Model." *Journal of Neuroinflammation* 9 (59): 1–8. <http://www.jneuroinflammation.com/content/9/1/59> \nhttp://0-

ovidsp.ovid.com.wam.city.ac.uk/ovidweb.cgi?T=JS&PAGE=reference&D=emed10&NEWS=N&AN=2012299644.

- Tuo, Jingsheng, Robert J Ross, Alexandra A Herzlich, Defen Shen, Xiaoyan Ding, Min Zhou, Steven L Coon, Nahed Hussein, Norman Salem, and Chi-chao Chan. 2009. "A High Omega-3 Fatty Acid Diet Reduces Retinal Lesions in a Murine Model of Macular Degeneration." *The American Journal of Pathology* 175 (2). American Society for Investigative Pathology: 799–807. doi:10.2353/ajpath.2009.090089.
- Tuo, Jingsheng, Yujuan Wang, Rui Cheng, Yichao Li, Mei Chen, Fangfang Qiu, Haohua Qian, et al. 2015. "Wnt Signaling in Age-Related Macular Degeneration: Human Macular Tissue and Mouse Model." *Journal of Translational Medicine* 13 (1). BioMed Central: 330. doi:10.1186/s12967-015-0683-x.
- Ufret-Vincenty, Rafael L., Bogale Aredo, Xinran Liu, Anne McMahon, Peter W. Chen, Hui Sun, Jerry Y. Niederkorn, and Wojciech Kedzierski. 2010. "Transgenic Mice Expressing Variants of Complement Factor H Develop AMD-like Retinal Findings." *Investigative Ophthalmology and Visual Science* 51 (11): 5878–87. doi:10.1167/iovs.09-4457.
- Umeda, Shinsuke, Michihiro T. Suzuki, Haru Okamoto, Fumiko Ono, Atsushi Mizota, Keiji Terao, Yasuhiro Yoshikawa, Yasuhiko Tanaka, and Takeshi Iwata. 2005. "Molecular Composition of Drusen and Possible Involvement of Anti-Retinal Autoimmunity in Two Different Forms of Macular Degeneration in Cynomolgus Monkey (Macaca Fascicularis)." *The FASEB Journal* 19 (12): 1683–85. doi:10.1096/fj.04-3525fje.
- Van de Pavert, Serge A., Alicia Sanz Sanz, Wendy M. Aartsen, Rogier M. Vos, Inge Versteeg, Susanne C. Beck, Jan Klooster, Mathias W. Seeliger, and Jan Wijnholds. 2007. "Crb1 Is a Determinant of Retinal Apical Müller Glia Cell Features." *Glia* 55 (July): 1486–97. doi:10.1002/glia.
- Van Deursen, Jan M. 2014. "The Role of Senescent Cells in Ageing." *Nature* 509 (7501). Nature Publishing Group: 439–46. doi:10.1038/nature13193.
- Van Lookeren Campagne, Menno, Jennifer LeCouter, Brian L Yaspan, and Weilan Ye. 2014. "Mechanisms of Age-Related Macular Degeneration and Therapeutic Opportunities." *The Journal of Pathology* 232 (2): 151–64. doi:10.1002/path.4266.
- Vasireddy, Vidyullatha, Monica M. Jablonski, Md Nawajes a. Mandal, Dorit Raz-Prag, Xiaofei F. Wang, Lesli Nizol, Alessandro Iannaccone, et al. 2006. "Elov14 5-Bp-Deletion Knock-in Mice Develop Progressive Photoreceptor Degeneration." *Investigative Ophthalmology and Visual Science* 47 (10): 4558–68. doi:10.1167/iovs.06-0353.
- Veleri, S., C. H. Lazar, B. Chang, P. a. Sieving, E. Banin, and a. Swaroop. 2015. "Biology and Therapy of Inherited Retinal Degenerative Disease: Insights from Mouse Models." *Disease Models & Mechanisms* 8 (2): 109–29. doi:10.1242/dmm.017913.
- Verardo, Mark R., Geoffrey P. Lewis, Masumi Takeda, Kenneth a. Linberg, Jiyun Byun, Gabriel Luna, Ulrika Wilhelmsson, Milos Pekny, Dong Feng Chen, and Steven K. Fisher. 2008. "Abnormal Reactivity of Müller Cells after Retinal Detachment in Mice Deficient in GFAP and Vimentin." *Investigative Ophthalmology and Visual Science* 49 (8): 3659–65. doi:10.1167/iovs.07-1474.
- Vessey, Kirstan a., Ursula Greferath, Andrew I. Jobling, Joanna a. Phipps, Tracy Ho, Michelle Waugh, and Erica L. Fletcher. 2012. "Ccl2/Cx3cr1 Knockout Mice Have Inner Retinal Dysfunction but Are Not an Accelerated Model of AMD." *Investigative Ophthalmology and Visual Science* 53 (12): 7833–46. doi:10.1167/iovs.12-10650.

- Volland, Stefanie, Julian Esteve-Rudd, Juyea Hoo, Claudine Yee, and David S. Williams. 2015. "A Comparison of Some Organizational Characteristics of the Mouse Central Retina and the Human Macula." *PLoS ONE* 10 (4): 1–13. doi:10.1371/journal.pone.0125631.
- Wachtmeister, Lillemor. 1987. "Basic Research and Clinical Aspects of the Oscillatory Potentials of the Electroretinogram." *Documenta Ophthalmologica* 66 (3): 187–94. doi:10.1007/BF00145232.
- Wang, Gaofeng, Sander R Dubovy, Stephen G Schwartz, Jaclyn L Kovach, Anita Agarwal, William K Scott, Jonathan Haines, and Margaret A Pericak-Vance. 2014. "Genotype at Polymorphism rd5749482 and TIMP3 Expression in AMD." In *Investigative Ophthalmology & Visual Science*, 55:2221–2221. [Association for Research in Vision and Ophthalmology, etc.]. <https://iovs.arvojournals.org/article.aspx?articleid=2267543>.
- Wang, Xu, Lian Zhao, Jun Zhang, Robert N. Fariss, Wenxin Ma, Friedrich Kretschmer, Minhua Wang, et al. 2016. "Requirement for Microglia for the Maintenance of Synaptic Function and Integrity in the Mature Retina." *The Journal of Neuroscience* 36 (9): 2827–42. doi:10.1523/JNEUROSCI.3575-15.2016.
- Wang, Yujuan, Mones S Abu-asab, Cheng-rong Yu, Zhongshu Tang, Defen Shen, Jingsheng Tuo, Xuri Li, and Chi-chao Chan. 2014. "Platelet-Derived Growth Factor ( PDGF ) -C Inhibits Neuroretinal Apoptosis in a Murine Model of Focal Retinal Degeneration." *Laboratory Investigation* 94 (6). Nature Publishing Group: 674–82. doi:10.1038/labinvest.2014.60.
- Wang, Yujuan, Jakub W Hanus, Mones S Abu-asab, Defen Shen, Alexander Ogilvy, Jingxing Ou, Xi K Chu, et al. 2016. "NLRP3 Upregulation in Retinal Pigment Epithelium in Age-Related Macular Degeneration." *International Journal of Molecular Sciences* 17 (73): 1–15. doi:10.3390/ijms17010073.
- Wang, Yujuan, Defen Shen, Vinson M Wang, Cheng-rong Yu Ren-xi Wang, Jingsheng Tuo, and Chi-chao Chan. 2012. "Enhanced Apoptosis in Retinal Pigment Epithelium under Inflammatory Stimuli and Oxidative Stress." *Apoptosis* 17: 1144–55. doi:10.1007/s10495-012-0750-1.
- Wang, Yujuan, Preeti Subramanian, Defen Shen, Jingsheng Tuo, S Patricia Becerra, and Chi-Chao Chan. 2013. "Pigment Epithelium-Derived Factor Reduces Apoptosis and pro-Inflammatory Cytokine Gene Expression in a Murine Model of Focal Retinal Degeneration." *ASN Neuro* 5 (5): 309–19. doi:10.1042/AN20130028.
- Wangsa-Wirawan, Norbert D, and Robert A Linsenmeier. 2003. "Retinal Oxygen. Fundamental and Clinical Aspects." *Acta Ophthalmologica* 94: 547–57. doi:10.1111/j.1755-3768.2016.0085.
- Whitmore, S. Scott, Alex H. Wagner, Adam P. DeLuca, Arlene V. Drack, Edwin M. Stone, Budd a. Tucker, Shemin Zeng, Terry a. Braun, Robert F. Mullins, and Todd E. Scheetz. 2014. "Transcriptomic Analysis across Nasal, Temporal, and Macular Regions of Human Neural Retina and RPE/choroid by RNA-Seq." *Experimental Eye Research* 129. Elsevier Ltd: 93–106. doi:10.1016/j.exer.2014.11.001.
- Willoughby, Colin E., Diego Ponzin, Stefano Ferrari, Aires Lobo, Klara Landau, and Yadollah Omid. 2010. "Anatomy and Physiology of the Human Eye: Effects of Mucopolysaccharidoses Disease on Structure and Function - a Review." *Clinical and Experimental Ophthalmology* 38 (SUPPL. 1): 2–11. doi:10.1111/j.1442-9071.2010.02363.x.
- Woessner Jr., J.Frederick. 2001. "That Impish TIMP: The Tissue Inhibitor of Metalloproteinases-3." *Journal of Clinical Investigation* 108 (6): 799–800. doi:10.1172/JCI200113709.Our.

- Wong, Chee Wai, and Tina T. Wong. 2019. "Posterior Segment Drug Delivery for the Treatment of Exudative Age-Related Macular Degeneration and Diabetic Macular Oedema." *British Journal of Ophthalmology* 313462: 1–5. doi:10.1136/bjophthalmol-2018-313462.
- Wong, Lily L, Suzanne M Hirst, Quentin N Pye, Christopher M Reilly, Sudipta Seal, and James F Mcginnis. 2013. "Catalytic Nanoceria Are Preferentially Retained in the Rat Retina and Are Not Cytotoxic after Intravitreal Injection." *Plos One* 8 (3): 1–10. doi:10.1371/journal.pone.0058431.
- Wong, Lily L, Quentin N Pye, Lijuan Chen, Sudipta Seal, and James F Mcginnis. 2015. "Defining the Catalytic Activity of Nanoceria in the P23H-1 Rat , a Photoreceptor Degeneration Model." *Plos One* 10 (3): 1–17. doi:10.1371/journal.pone.0121977.
- Wong, Wai T., Waynekid Kam, Denise Cunningham, Molly Harrington, Keri Hammel, Catherine B. Meyerle, Catherine Cukras, Emily Y. Chew, Srinivas R. Sadda, and Frederick L. Ferris. 2010. "Treatment of Geographic Atrophy by the Topical Administration of OT-551: Results of a Phase Ii Clinical Trial." *Investigative Ophthalmology and Visual Science* 51 (12): 6131–39. doi:10.1167/iovs.10-5637.
- Wong, Wan Ling, Xinyi Su, Xiang Li, Chui Ming G Cheung, Ronald Klein, Ching Yu Cheng, and Tien Yin Wong. 2014. "Global Prevalence of Age-Related Macular Degeneration and Disease Burden Projection for 2020 and 2040: A Systematic Review and Meta-Analysis." *The Lancet Global Health* 2 (2). Wong et al. Open Access article distributed under the terms of CC BY-NC-ND: e106–16. doi:10.1016/S2214-109X(13)70145-1.
- Wu, Tinghuai, Yueguo Chen, Samuel K.S. Chiang, and Mark O.M. Tso. 2002. "NF-κB Activation in Light-Induced Retinal Degeneration in a Mouse Model." *Investigative Ophthalmology and Visual Science* 43 (9): 2834–40.
- Xiying, Mao, Wu Wenbo, Fang Wangyi, and Liu Qinghuai. 2017. "Association of Apolipoprotein E Polymorphisms with Age-Related Macular Degeneration Subtypes: An Updated Systematic Review and Meta-Analysis." *Archives of Medical Research* 48 (4). Elsevier Inc: 370–77. doi:10.1016/j.arcmed.2017.08.002.
- Xu, Heping, Mei Chen, Ayyakkannu Manivannan, Noemi Lois, and John V. Forrester. 2008. "Age-Dependent Accumulation of Lipofuscin in Perivascular and Subretinal Microglia in Experimental Mice." *Aging Cell* 7 (1): 58–68. doi:10.1111/j.1474-9726.2007.00351.x.
- Yang, Shiqi, Jingke Zhao, and Xiaodong Sun. 2016. "Resistance to Anti-VEGF Therapy in Neovascular Age-Related Macular Degeneration: A Comprehensive Review." *Drug Design, Development and Therapy* 10: 1857–67. doi:10.2147/DDDT.S97653.
- Yaspan, Brian L., David F. Williams, Frank G. Holz, Carl D. Regillo, Zhengrong Li, Amy Dressen, Menno van Lookeren Campagne, et al. 2017. "Targeting Factor D of the Alternative Complement Pathway Reduces Geographic Atrophy Progression Secondary to Age-Related Macular Degeneration." *Science Translational Medicine* 9 (395): eaaf1443. doi:10.1126/scitranslmed.aaf1443.
- Ye, Junli, Zhongxin Jiang, Xuehong Chen, Mengyang Liu, Jing Li, and Na Liu. 2017. "The Role of Autophagy in pro-Inflammatory Responses of Microglia Activation via Mitochondrial Reactive Oxygen Species in Vitro." *Journal of Neurochemistry* 142 (2): 215–30. doi:10.1111/jnc.14042.
- Young, Terri L, Felicia Hawthorne, Sheng Feng, Xiaoyan Luo, Elizabeth St. Germain, Minyue Wang, and Ravikanth Metlapally. 2013. "Whole Genome Expression Profiling of Normal Human Fetal and Adult Ocular Tissues." *Experimental Eye Research*, no. 116: 1–7. doi:10.1038/jid.2014.371.

- Zhang, Hongqiao, Kelvin J.A Davies, and Henry Jay Forman. 2015. "Oxidative Stress Response and Nrf2 Signaling in Aging." *Free Radical Biology Medicine* 88 (0 0): 314–36. doi:10.1016/j.physbeh.2017.03.040.
- Zhang, Jun, Jingsheng Tuo, Xiaoguang Cao, Defen Shen, Wei Ki, and Chi-chao Chan. 2013. "Early Degeneration of Photoreceptor Synapse in Ccl2/Cx3cr1 Deficient Mice on Crb1rd8 Background." *Synapse* 67 (8): 515–31. doi:10.1002/syn.21674.
- Zhao, L., M. K. Zabel, X. Wang, W. Ma, P. Shah, R. N. Fariss, H. Qian, C. N. Parkhurst, W.-B. Gan, and W. T. Wong. 2015. "Microglial Phagocytosis of Living Photoreceptors Contributes to Inherited Retinal Degeneration." *EMBO Molecular Medicine* 7 (9): 1179–97. doi:10.15252/emmm.201505298.
- Zhao, Zhenyang, Yan Chen, Jian Wang, Paul Sternberg, Michael L. Freeman, Hans E. Grossniklaus, and Jiyang Cai. 2011. "Age-Related Retinopathy in NRF2-Deficient Mice." *PLoS ONE* 6 (4): 1–10. doi:10.1371/journal.pone.0019456.
- Zhou, Tian, Zijing Huang, Xiaowei Sun, Xiaowei Zhu, Lingli Zhou, Mei Li, Bing Cheng, Xialin Liu, and Chang He. 2017. "Microglia Polarization with M1/M2 Phenotype Changes in rd1 Mouse Model of Retinal Degeneration." *Frontiers in Neuroanatomy* 11 (September): 1–11. doi:10.3389/fnana.2017.00077.
- Zhou, Xiangtian, Weiwei Wang, Fan Lu, Songnian Hu, Liqin Jiang, Dongsheng Yan, Xiaowei Zhang, Xiaomin Yu, Jun Yu, and Jia Qu. 2007. "A Comparative Gene Expression Profile of the Whole Eye from Human, Mouse, and Guinea Pig." *Molecular Vision* 13 (May 2014): 2214–21.
- Zhou, Xiaohong, Lily L Wong, Ajay S Karakoti, Sudipta Seal, and James F Mcginnis. 2011. "Nanoceria Inhibit the Development and Promote the Regression of Pathologic Retinal Neovascularization in the Vldlr Knockout Mouse." *Plos One* 6 (2): 1–10. doi:10.1371/journal.pone.0016733.
- Zhou, Yongdong, Kristopher G. Sheets, Eric J. Knott, Cornelius E. Regan, Jingsheng Tuo, Chi Chao Chan, William C. Gordon, and Nicolas G. Bazan. 2011. "Cellular and 3D Optical Coherence Tomography Assessment during the Initiation and Progression of Retinal Degeneration in the Ccl2/Cx3cr1-Deficient Mouse." *Experimental Eye Research* 93 (5). Elsevier Ltd: 636–48. doi:10.1016/j.exer.2011.07.017.
- Znoiko, Sergey L., Baerbel Rohrer, Kangmo Lu, Heather R. Lohr, Rosalie K. Crouch, and Jian Xing Ma. 2005. "Downregulation of Cone-Specific Gene Expression and Degeneration of Cone Photoreceptors in the Rpe65<sup>-/-</sup> Mouse at Early Ages." *Investigative Ophthalmology and Visual Science* 46 (4): 1473–79. doi:10.1167/iovs.04-0653.